THE CHARACTERIZATION AND FABRICATION OF POLY (3,4-ETHYLENEDIOXYTHIOPHENE) ENZYME BASED BIOSENSORS

by

Sarah Anne Spanninga

A dissertation submitted in partial fulfillment
of the requirements for the degree of
Doctor of Philosophy
(Macromolecular Science and Engineering)
in The University of Michigan
2010

Doctoral Committee:

Professor Zhan Chen, Co-Chair
Adjunct Professor David C. Martin, Co-Chair
Associate Professor Jinsang Kim
Associate Professor Joerg Lahann

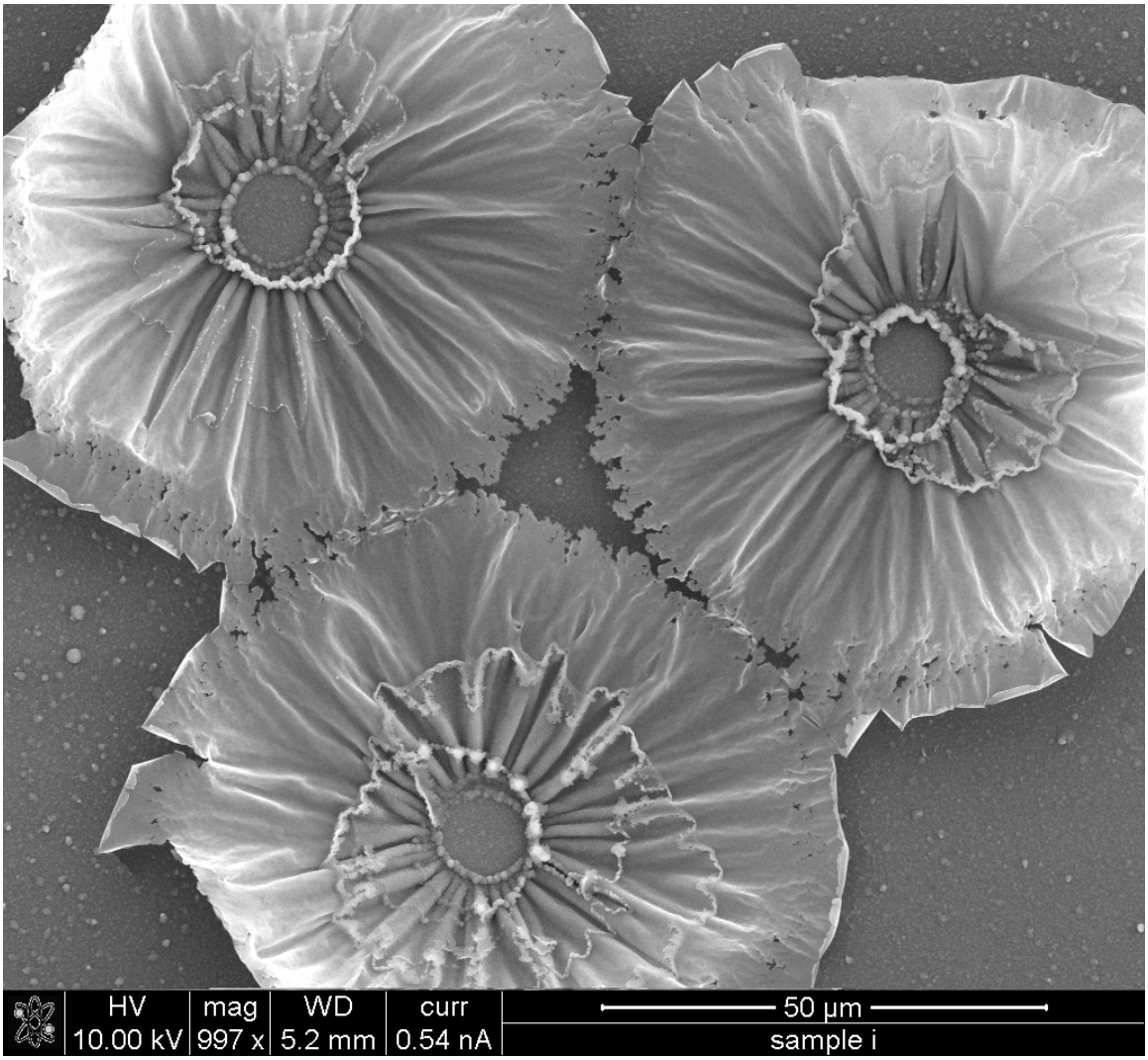
HV
10.00 kV
mag
997 x
WD
5.2 mm
curr
0.54 nA
50 µm
sample i

2010

To Mom, Dad, R.J., Dutch, and Anne

ACKNOWLEDGEMENTS

The research contained in this dissertation could have never been completed without the guidance of my advisors, Professor Zhan Chen and Professor David C. Martin. I would like to thank Dr. Martin for all his guidance on all materials science issues and Dr. Chen for his guidance on sum frequency generation vibrational spectroscopy.

I wish to thank Professor Jinsang Kim and Professor Joerg Lahann for serving on my doctoral committee and providing valuable comments and suggestions. I would also like to thank Dr. Kai Sun and Dr. Haiping Sun at the University of Michigan Electron Microbeam Analysis Laboratory (EMAL) for helping me with X-ray photoelectron spectroscopy. Additional thanks go to Dr. Peter Moran for his guidance and wisdom thourghout my Masters research and the Michigan Technological University Materials Science and Engineering Department for providing my with a solid materials science foundation on which to build upon.

I would also like to thank all of the past and present members of the Martin and Chen Labs which have contributed in some way to the completion of this work through their support and friendship. Additional thanks to Nonna Hamilton and the students of Macromolecular Science and Engineering for their support and encouragement as well.

I would to also like to acknowledge the MURI: Bio-Integrated Structural and Neural Prosthetic Materials for Dr. David C. Martin, the NSF Career Award for Dr. Zhan

Chen, the department of Chemistry at the University of Michigan for the teaching support, and the Rackham REA fellowship for their financial support.

Finally, but not the least, I would like to thank my family, Russ, Carol, and R.J. Spanninga (Dutch too), and Kaajal-Raj (Anne) Juggernauth who have been with me and encouraging me through all eight years of graduate school, two theseses, and two defenses.

TABLE OF CONTENTS

LIST OF FIGURES

LIST OF TABLES

CHAPTER 1

INTRODUCTION

1.1 Introduction

The goal of this work is to characterize and fabricate an enzyme based biosensor using the conductive polymer, poly (3,4-ethylenedioxythiophene) (PEDOT). To begin to accomplish this goal, PEDOT was first characterized before the biosensor was fabricated. Characterization involved the use of sum frequency generation vibrational spectroscopy (SFG), X-ray photoelectron spectroscopy (XPS), electrochemical impedance spectroscopy (EIS), and cyclic voltommetry (CV). The highly surface sensitive technique sum frequency generation vibrational spectroscopy was used to deduce the chemical functional group orientation found in the commercially available version of PEDOT: poly (sodium 4-styrenesulfonate) (PSSNa). Surface chemical composition and the driving forces underlying PEDOT counter-ion incorporation during electrochemical polymerization were then studied utilizing X-ray photoelectron spectroscopy. These studies were carried out in the hopes of further understanding PEDOT counter-ion incorporation for both small anions and poly-anions, so the mechanism for enzyme physical enzyme entrapment during electrochemical polymerization of PEDOT could be better understood. Finally enzyme based PEDOT biosensors were fabricated and characterized.

1.2 Poly (3,4-ethylenedioxythiophene)

Poly(3,4-ethylenedioxythiophene) (PEDOT), Figure 1.1, is a highly conductive, π conjugated polymer that can be polymerized by either oxidative chemical polymerization, organic chemical vapor deposited[1], or by electrochemical polymerization. Conductivity in polymers is a result of an extended, delocalized π bond structure. The conjugation of alternating single and double bonds is the cause for the delocalized structure found in the conducting polymers.[2,3] Due to its high conductivity of ~300 S/cm, PEDOT has been used in anti-static coatings, organic light emitting devices[4], solar cells[5], and batteries.[6] By utilizing its electronic and ionic conductivity, superior thermal[7] and chemical stability[8,9] properties PEDOT has been found to be a more successful biological tissue interfacing agent[10,11] than polypyrrole.[12-15]

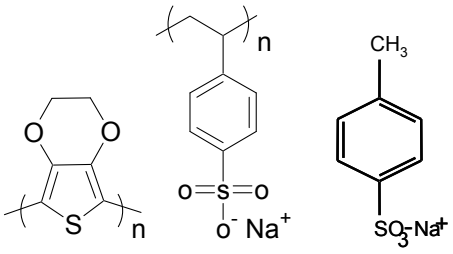

Figure 1.1 (Left) Poly(3,4-ethylenedioxythiophene) (PEDOT), (Center) Poly(sodium 4-styrenesulfonate) (PSSNa), and (Right) Sodium p- toluenesulfonate (TosNa)

As previously stated PEDOT can be polymerized using multiple different ways, but for the purposes of this work, electrochemical polymerization has been used to synthesize PEDOT unless otherwise mentioned. PEDOT electrochemical polymerization on the anode electrode occurs as follows[2]:

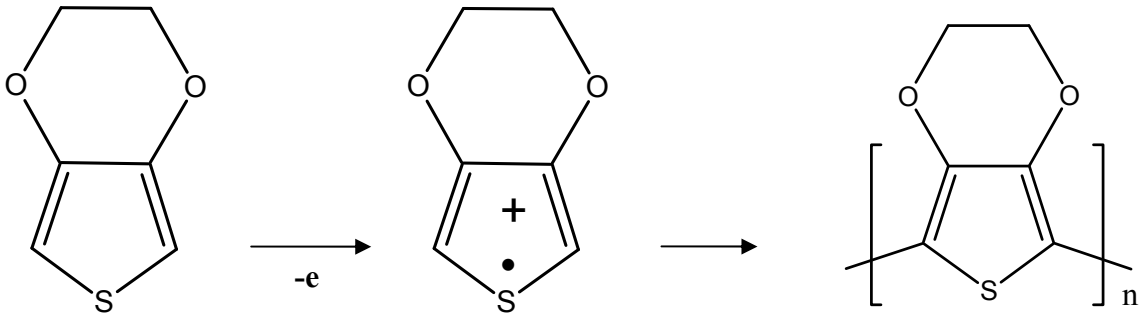

Figure 1.2 Electrochemical polymerization mechanism of poly (3,4-ethylenedioxythiophene) (PEDOT)

PEDOT, like other conductive polymers such as polypyrrole (PPy) and polythiophene, has a positive charge on roughly every third repeating unit[16] in its oxidative state, thus conductivity is produced through hole transport. Because, there is a positive charge present; a counter-ion is used to neutralize the over all charge. In the case of polymers in the reduced state, the polymer is neutral and is non-conductive.[2] Though PEDOT is best know for its electrical conductivity, it is also ionically as depicted in Figure 1.3 below.

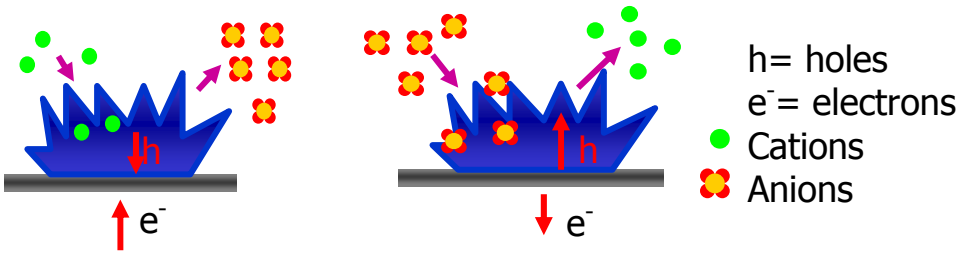

Figure 1.3 Diagram of PEDOT ionic conductivity

PEDOT characterization has centered on the use of X-ray Photoelectron Spectroscopy (XPS)[16-27], Fourier Transform Infrared Spectroscopy (FTIR)[28-31],

Raman[28,32] and UV-Visible Spectroscopy[9,16,28] for chemical composition information. Scanning Electron Microscopy (SEM)[25,33-35] and Atomic Force Microscopy (AFM), have been used to study the surface morphology. X-ray Diffraction (XRD) and even some Transmission Electron Microscopy (TEM)[34] have been utilized for studying the packing/ crystal structure determination.[36,37] PEDOT electrochemical and electrical properties have been probed with Electrochemical Impedance Spectroscopy (EIS), Cyclic Voltammetry (CV), and conductivity measurements.[4,8,9,16,25,38] Valence structural information has been obtained using Ultraviolet Photoelectron Spectroscopy (UPS) to study the valence band structures of PEDOT.[27]

1.3 Sum Frequency Generation

1.3.1 Introduction

Sum frequency generation vibrational spectroscopy is a surface characterization technique which is sensitive to surface and interfacial chemical functional groups and their respective orientation. This technique is an optical, non-vacuum technique, which provides the opportunity to study samples *in situ*, as long as the sample is accessible to light. SFG uses two pulsed lasers, a visible (532 nm) and frequency tunable infrared laser, that are overlapped both spatially and temporally on a sample to create a sum frequency signal. The sum frequency signal, ω_{SF}, is the sum of the infrared and visible frequencies, $\omega_{IR}+\omega_{Vis}$. The sum frequency signal will be enhanced if the IR frequency is scanned over the sample's vibrational resonance. In terms of the vibrational and electronic states, the IR beam raises the vibrational state from the ground to an excited state (Figure 1.4). The visible beam further excites the sample and raises the energy level

to a virtual electronic state. The sum frequency signal is generated by the relaxation of the sample from the virtual electronic state back to the ground electronic and vibrational states. By plotting SFG Intensity versus ω_{IR}, a vibrational spectrum of the sample's surface composition is able to be detected.

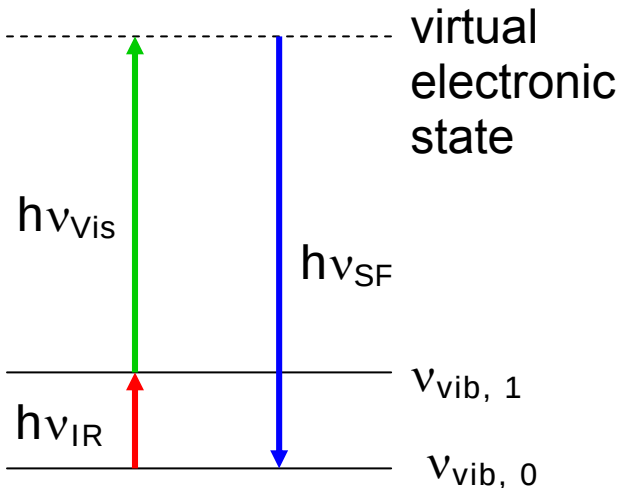

Figure 1.4 Diagram of a SFG transition, which can be regarded as a combination of IR and Raman transitions.

1.3.2 Theory

When light is introduced to a material, the electric field of the light wave induces a polarization of the molecules. The resulting polarization, P (oscillating dipoles per unit volume), is related to the electric field of the input light and is the sum of the electric dipoles following the electric dipole approximation[39]

$$P = \varepsilon_o \chi^{(1)} E$$

where ε_o is the vacuum permittivity, $\chi^{(1)}$ is the first order, or linear, susceptibility, and E is the electric field. In the case of light produced by lasers, the resulting electric field is of sufficient strength that it is comparable to the field experienced by the electrons in the

molecule. When this occurs the non-linearity increases and the second and third order terms become significant[39,40]

$$P= P^{(1)} + P^{(2)} + P^{(3)}+\ldots= \varepsilon_o(\chi^{(1)}E + \chi^{(2)}E^2 + \chi^{(3)}E^3+\ldots)$$

where $\chi^{(2)}$ and $\chi^{(3)}$ are the second and third order non-linear susceptibilities with $\chi^{(2)}$ and $\chi^{(3)}$ being third and fourth ranked tensors respectively. Higher order terms can be ignored when the electric field is weak, so the polarization becomes proportional to the linear susceptibility. Since SFG is a laser technique, the electric fields are not weak and therefore the higher order terms do apply. When $\chi^{(1)}$ becomes small and the $\chi^{(2)}$ dominates, like in SFG, the behavior is considered non-linear. The relationship between the polarization and the frequency dependence on the electric field for two light waves mixed in a media for SFG is as follows:

$$P^{(2)} = \varepsilon_o\chi^{(2)} (½ E_1E_2\cos(\omega_1+\omega_2)t)$$

where ω_1 and E_1 and ω_2 and E_2 are the frequencies and amplitudes of the two input beams of light in a material. Since the two beams of light utilized in SFG are a tunable infrared and visible beam, the polarization equation can be rewritten as[39]:

$$P^{(2)}_{SF} \alpha \varepsilon_o\chi^{(2)}E_{vis}E_{IR}$$

The light beams are temporarily and spatially overlapped onto the material's surface in a SFG experiment as depicted in Figure 1.5.

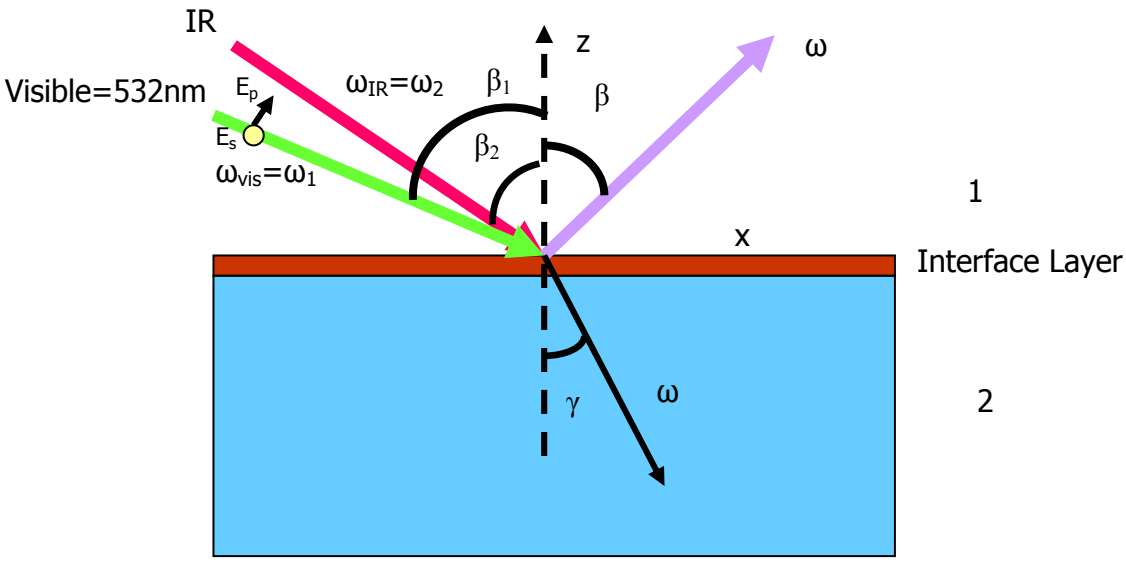

Figure 1.5 Diagram of SFG experimental geometry

Taking into account the different media refractive indices at input visible, input IR, and output sum frequency beams and applying the phase matching conditions (i.e. applying the conservation of momentum parallel to the interface), the following condition is found.[39]

$$n_{SF}\omega_{SF}\sin\beta_{SF} = n_{vis}\omega_{vis}\sin\beta_{vis} \pm n_{IR}\omega_{IR}\sin\beta_{IR}$$

or

$$n_{SF}k_{SF}\beta_{SF} = n_{vis}k_{vis}\beta_{vis} \pm n_{IR}k_{IR}\sin\beta_{IR}$$

where n is the refractive index of the material which the light propagates, ω is the frequency, β is the angle to the surface normal of each beam, and k is ω/c, where c is the speed of light. A positive sign is used when the two beams are arriving in the same x direction (co-propagating) and negative sign is used when the beams are arriving from opposite directions (counter-propagating).

The intensity of the sum frequency output can be related to the intensities of the input beams by[39,41,42]:

$$I(\omega) = \frac{8\pi^3\omega^3 \sec^2\beta}{c^3 n(\omega)n(\omega_1)n(\omega_2)}\left|\chi^{(2)}_{eff}\right|^2 I_1(\omega_1)I_2(\omega_2)$$

where n is the refractive index of the media at a frequency, β is the reflection angle of the sum frequency field, $\chi^{(2)}_{eff}$ is the effective second order non-linear susceptibility, and $I(\omega_1)$ and $I(\omega_2)$ are the two input beam intensities.

A distinct advantage of SFG is its unique monolayer surface sensitivity. In all systems, including centrosymmetric systems, $\chi^{(2)}_{ijk} = -\chi^{(2)}_{-i-j-k}$ with a sign change due to the inversion operation because it is a third rank tensor where ijk are laboratory coordinates. In media with inversion symmetry, $\chi^{(2)}_{ijk} = \chi^{(2)}_{-i-j-k}$, therefore $\chi^{(2)}_{ijk} = \chi^{(2)}_{-i-j-k} = -\chi^{(2)}_{-i-j-k} = 0$ resulting in no signal. When the inversion symmetry is broken, as in monolayers or at interfaces, there can be non-zero components possible resulting in SFG signal.[39]

The $\chi^{(2)}_{eff}$ is composed of the non-linear susceptibility in the lab coordinate system, $\chi^{(2)}_{xyz}$, and the Fresnel coefficient.[39,41]

$$\chi^{(2)}_{eff} = [\hat{e}(\omega)\cdot L(\omega)]\cdot\chi^{(2)}\colon [L(\omega_1)\cdot\hat{e}(\omega_1)][L(\omega_2)\cdot\hat{e}(\omega_2)]$$

where $\hat{e}(\Omega)$ is the unit polarization vector and $L(\Omega)$ is the Fresnel factor at frequency ω. $\chi^{(2)}_{eff}$ in the lab coordinate system has 27 components. When the surface does not have any chirality and is azimuthally isotropic, only seven non-vanishing components exist. These components are $\chi_{xxz} = \chi_{yyz}$, $\chi_{xzx} = \chi_{yzy}$, $\chi_{zxx} = \chi_{zyy}$, and χ_{zzz}, where z is along the interface normal, x is in the incident plane, and y is coming out of the page (Figure 1.5) in the laboratory coordinate system. They are related to the $\chi^{(2)}_{eff}$ components probed by

different polarization combinations of the input and ouput beams, such as of ssp (s polarized sum frequency output, s polarized visible, and p polarized IR), sps, pss, and ppp. Now by combining the χ components with the Frensel coefficients, the following $\chi^{(2)}_{eff}$ can be found[41,42]:

$$\chi^{(2)}_{eff,\,ssp} = L_{yy}(\omega_{SF})L_{yy}(\omega_1)L_{zz}(\omega_2)\sin\beta_2\chi_{yyz}$$

$$\chi^{(2)}_{eff,\,sps} = L_{yy}(\omega_{SF})L_{zz}(\omega_1)L_{yy}(\omega_2)\sin\beta_1\chi_{yzy}$$

$$\chi^{(2)}_{eff,\,pss} = L_{zz}(\omega_{SF})L_{yy}(\omega_1)L_{yy}(\omega_2)\sin\beta_{SF}\chi_{xyy}$$

$$\chi^{(2)}_{eff,\,ppp} = -L_{xx}(\omega_{SF})L_{xx}(\omega_1)L_{zz}(\omega_2)\cos\beta_{SF}\cos\beta_1\sin\beta_2\chi_{xxz} -$$

$$L_{xx}(\omega_{SF})L_{zz}(\omega_1)L_{xx}(\omega_2)\cos\beta_{SF}\sin\beta_1\cos\beta_2\chi_{xzx} +$$

$$L_{zz}(\omega_{SF})L_{xx}(\omega_1)L_{xx}(\omega_2)\sin\beta_{SF}\cos\beta_1\cos\beta_2\chi_{zxx} +$$

$$L_{zz}(\omega_{SF})L_{zz}(\omega_1)L_{zz}(\omega_2)\sin\beta_{SF}\sin\beta_1\sin\beta_2\chi_{zzz}$$

where the Fresnel coefficients are as follows:

$$L_{xx}(\Omega) = \frac{2n_1(\Omega)\cos\gamma}{n_1(\Omega)\cos\gamma + n_2(\Omega)\cos\beta},$$

$$L_{yy}(\Omega) = \frac{2n_1(\Omega)\cos\beta}{n_1(\Omega)\cos\beta + n_2(\Omega)\cos\gamma},$$

$$L_{zz}(\Omega) = \frac{2n_2(\Omega)\cos\beta}{n_1(\Omega)\cos\gamma + n_2(\Omega)\cos\beta}\left(\frac{n_1(\Omega)}{n'(\Omega)}\right)^2$$

where β is the incidence angle of the beam under consideration, $n'(\Omega)$ is the refractive index of the interfacial layer, and γ is the refracted angle [$n_1(\Omega)\sin\beta = n_2(\Omega)\sin\gamma$]. $\chi^{(2)}$ can be related to the molecular nonlinear polarizability, $\alpha^{(2)}$ by using the following equation:

$$\chi^{(2)}_{ijk} = N_s \sum_{lmn} \left\langle (\hat{\mathbf{i}}\cdot\hat{\xi})(\hat{\mathbf{j}}\cdot\hat{\eta})(\hat{\mathbf{k}}\cdot\hat{\zeta}) \right\rangle \alpha^{(2)}_{lmn}$$

where Ns is the surface density of the molecules and (i,j,k) and (ξ,η,ζ) are the unit vectors along the lab and molecular coordinate systems respectively. This equation relates the $\chi^{(2)}$ tensor to the $\alpha^{(2)}$ tensor through a coordinate transformation averaged over the molecular orientational distribution.

When the infrared frequency (ω_2) is near the vibrational resonance $\alpha^{(2)}$ and $\chi^{(2)}$ are written as[39,41]:

$$\alpha^{(2)} = \alpha_{NR}^{(2)} + \sum_q \frac{\alpha_q}{\omega_2 - \omega_q + i\Gamma_q}$$

and

$$\chi^{(2)} = \chi_{NR}^{(2)} + \sum_q \frac{\chi_q}{\omega_2 - \omega_q + i\Gamma_q}$$

where $\chi_{NR}^{(2)}$ is the non-resonant signal contribution, α_q and χ_q are the signal strength, ω_q is the oscillator frequency, and Γ_q is the damping constant of the qth vibrational mode, respectively.

The orientation of specific chemical functional groups on the surface can be determined if $(\alpha_q^{(2)})_{\xi\eta\zeta}$ is known. $\alpha_q^{(2)}$ can be obtained by IR and Raman measurements. This is because the product of the IR dipole derivative and the Raman polarizability tensor of the vibrational mode q is directly proportional to $\alpha_q^{(2)}$ seen in SFG.

$$\alpha_R^{(2)} \propto \frac{\partial \mu_{IR}}{\partial Q} \frac{\partial \alpha_{Raman}}{\partial Q}.$$

Thus in order to have SFG signal the vibrational mode must be both IR and Raman active.

In order to deduce the functional group orientation, the SFG signal must be spectrally fit first. As mentioned before the SFG signal follows[41,42]:

$$I(\omega_{SF}) \propto \left|\chi^{(2)}\right|^2 = \left|\chi_{NR} + \sum_q \frac{A_q}{\omega_{IR} - \omega_q + i\Gamma_q}\right|^2$$

where $\chi_{NR}^{(2)}$ is the non-resonant signal contribution, A_q is the oscillator strength, ω_q is the oscillator frequency, and Γ_q is the damping constant of the qth vibrational mode, respectively. Therefore the SFG has a maximum intensity when $\omega_q = \omega_{IR}$. Since SFG is a coherent process, the intensity generated is affected by the coverage, average orientation, and orientation distribution of all the functional groups inside the optical field. The orientation of specific chemical functional groups on the surface can be determined by utilizing the properties of polarized light, using different polarization combinations of the input beams and output beam, and by relating the surface second-order non-linear susceptibility in the lab coordinate system to the hyperpolarizibility in the molecular coordinate system as previously explained.[40-44]

1.3.3 SFG Experimental Set-Up

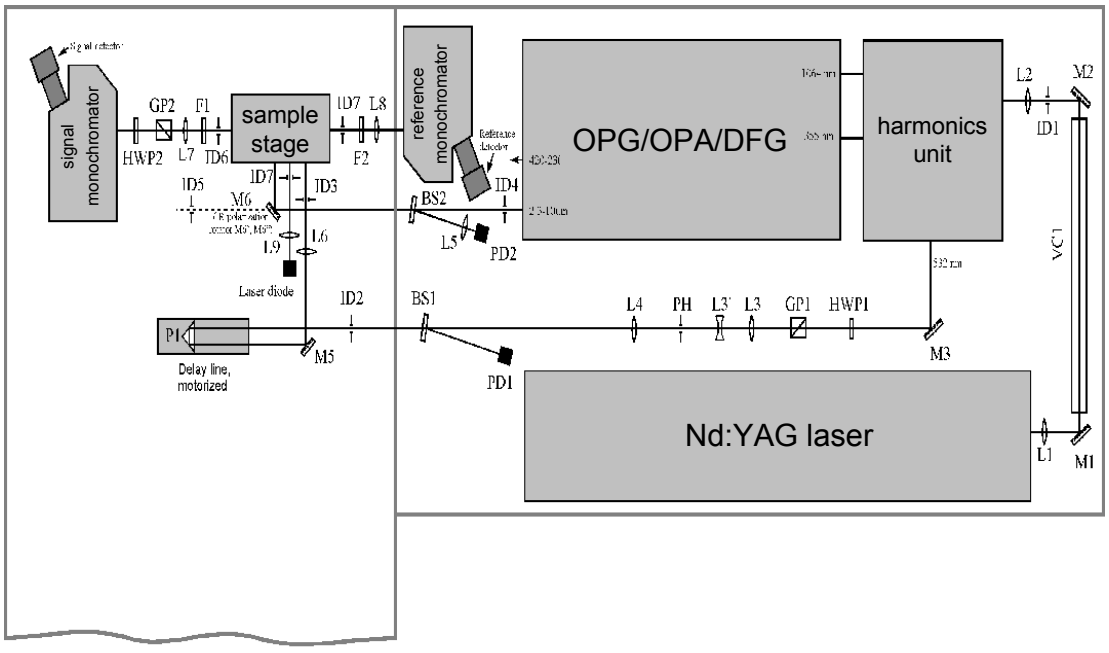

Figure 1.6 Layout of the EKSPLA SFG System

The SFG system employed for this research was custom designed by EKSPLA. Both the infrared and visible beams originate from a pico-second Nd:YAG laser (Figure 1.6). The laser produces a fundamental 1064 nm output with a 20 ps pulsewidth and 20 Hz repetition rate. One part of the output is then frequency doubled into a 532 nm visible beam using K*DP nonlinear crystals and the other fundamental portion, along with some 532 nm contributions, is frequency tripled into a 355 nm beam in the harmonics unit. The optical parametric generation (OPG)/ optical parametric amplification (OPA) and difference frequency generation (DFG) units are based on LBO and $AgGaS_2$ crystals produce the tunable infrared beam from 1000 to 4300 cm^{-1} (2.3-10μm) from the input 1064 nm and 355 nm beams. The visible and infrared input beams are spatially and temporally overlapped at incident angles of 60° and 54° respectively on the sample with beam diameters of about 0.5 mm. All SFG signals were collected using a photomultiplier tube (PMT).

1.3.4 Experimental Geometries

The experimental geometries used in this research are depicted in Figure 1.7. The materials used to fabricate these substrates are SiO_2 and CaF_2 in order to be both IR and visible transparent in the C-H and C=O ranges respectively.

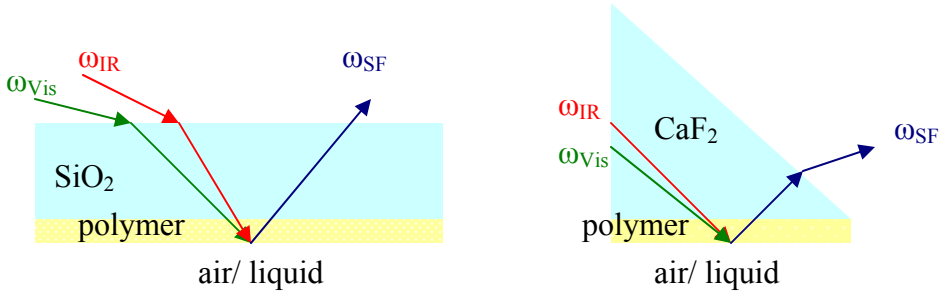

Figure 1.7 SFG Experimental Geometries (left) face-down and (right) prism

The face down geometry allows the IR and visible beams to transmit through the substrate and overlap on the polymer/ air interface. The advantage to this geometry is that the bulk signal, if any, will be minimized because the SFG signal has a shorter coherent length than transmission. The second geometry commonly used is the prism geometry, which can enhance the SFG signal by several orders of magnitude due to the near total internal reflection that occurs.

1.3.5 Previous SFG Research

A significant quantity of SFG studies have centered around simple organic compounds, polymers, adhesion systems, and water molecule research, but in recent years biological components, such as proteins and model lipid bi-layers[45,46] have also been studied. Polymers such as poly(methyl methacrylate) (PMMA)[42,47] and poly(styrene) (PS)[48-50] have been extensively studied and thereby their surface functional group orientations are known. Sum frequency generation data and some orientation

analysis have been performed on various biomolecules such as bovine serum albumin[42,47,51-53], fibrinogen[53-56], factor XII[46,53,57], melittin[58], and tachyplesin I.[59]

1.4 X-ray Photoelectron Spectroscopy

1.4.1 Background

X-ray photoelectron spectroscopy (XPS) or electron spectroscopy for chemical analysis (ESCA), is an ultra-high vacuum, surface sensitive technique. The high surface sensitivity of XPS is in fact its main advantage over other analytical techniques. XPS is typically used to deduce the chemical bonding structures at an interface but, it can also be used for quantitative analysis, and even to determine the electrical characteristics of a material by studying valence region.[60-64]

The origins of X-ray photoelectron spectroscopy date back to the discovery of the photoelectric effect by Hertz in 1887 when using an X-ray source to excite photoemission. Further work was inhibited by World Wars I and II and no further significant progress on this technique was made until Kai Siegbahn et al. developed an iron free double-focusing spectrometer which produced well resolved peaks in the 1950's, thus enabling the present state of XPS or ESCA.[61,62,64] For his work on ESCA, Kai Seigbahn was awarded the Nobel Prize for Physics in 1981.

Rutherford first related the incident x-ray energy to the emitted electron's binding and kinetic energies in 1914 with $E_K = h\nu - E_B$. Later Rutherford's equation was modified to become:

$$E_K = h\nu - E_B - \varphi$$

where an x-ray of known phonon energy, *hv*, is used to eject an electron from a surface atom. The kinetic energy of the ejected electron, E_K, is then measured by the detector and using the equation above, the binding energy, E_B, of the electron in a material is found ultimately resulting in the appearance of a photoelectron line in the spectrum. The binding energy (E_B) of the ejected electron is unique to the atom. The work function, φ, is a function of the spectrometer, which is known for each spectrometer.[61,62]

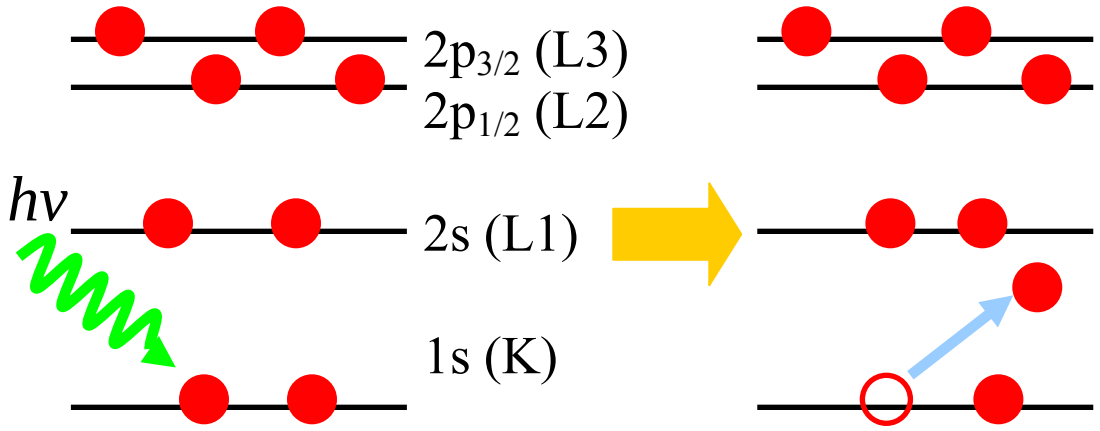

Figure 1.8 Diagram of X-ray photoelectron spectroscopy process

Any atom will eject electrons which have lower binding energies than the x-ray energy. These ejected electrons and their resulting peaks will correspond to the number of occupied energy levels in the atom. XPS utilizes the electron configuration notation in contrast the X-ray notation utilized in Auger spectroscopy (Table 1.1) The intensity of the peak will depend on the probability for electron ejection from each atomic orbital.[63] The surface sensitivity of XPS is the result of the probability of the ejected electron leaving

the surface. Electrons ejected from atomic layers at or near the surface will have a higher probability of leaving the surface than electrons ejected deeper in the material.

XPS uses the detection of an elastically removed photoelectron from the surface to obtain its surface sensitivity. The sampling depth (d) is roughly three times the escape depth ($d=\lambda_{AL}\sin\theta$), where λ_{AL} is the inelastic mean free path and θ is the take off angle to the surface. Where the escape depth is the depth at which an electron can escape from the material without significantly losing energy due to inelastic scattering occurring.[62] About 95% of the signal comes from the sampling depth. For organic molecules: $\lambda_i = B_i E^{1/2}$, where λ_i is the electrons' inelastic mean free path, B_i is 0.087 for organic compounds and E is the energy in eV.[65] For the experimental parameters used here where the detector is 90º to the sample surface (i.e. $\theta = 90º$) and for energies ranging from 164 eV (S 2p) to 530 eV (O 1s), the sampling depth is 3-6 nm.

Core levels, or characteristic elemental regions, are analyzed for peak shifting as a result of specific chemical bonding environments and elemental quantitative information. Core level notation follows nl_j quantum notation, where n is the principle quantum number, l is the orbital angular momentum (l=(n-1)), j is the total angular momentum number (j=(l+s)), and s is the spin angular momentum quantum number (±1/2). Any core spectra taken from non-s levels will exist as a doublet, with a characteristic ratio depending on the atomic subshell, due to spin-orbit coupling (Table 1.2).[62]

n	X-ray notation (Auger)	l	e^- configuration (XPS)	# orbitals	# e^-
1	K	s	1s	1	2
2	L_1, L_2, L_3	s,p	2s, $2p_{1/2}$, $2p_{3/2}$	4	8
3	$M_1 - M_5$	s,p,d	3s, $3p_{1/2}$, $32p_{3/2}$, $3d_{3/2}$, $3d_{5/2}$	9	18
4	N_1-N_7	s,p,d,f	4s-$4f_{7/2}$	16	32

Table 1.1 Auger and XPS notation[62]

Subshell (l)	j value	Area ratio
s	1/2	
p	1/2, 3/2	1:2
d	3/2, 5/2	2:3
f	5/2, 7/2	3:4

Table 1.2 XPS Spin split doublet notation

Though spectral analysis is usually done on the core regions which utilize elastic collisions, inelastic photoemission also occurs resulting in an increase in the spectral background, especially at higher binding energies.[62] This is accentuated when the X-ray source is not monochromatic (one energy), or achromatic, because the Bremsstrahlung radiation given off by the achromatic source causes many excitations to occur thus increasing the spectral background. Other contributions generally found using non-chromated sources include X-ray satellites and X-ray ghost lines.[66] A common phenomenon known as shake-up occurs when an emitted ion is a few eV above ground

state, thus E_K is decreased resulting in a E_B peak at few eV higher than the main peak. In aromatic carbon polymer, this shake-up usually involves the $\pi \rightarrow \pi^*$ transition.[66]

1.4.2 Experimental

A Kratos AXIS Ultra DLD X-Ray Photoelectron Spectrometer (Kratos Analytical Ltd., Manchester, England) with monochromatic aluminum source (Al K_α= 1486.6 eV) at a vacuum pressure of 10^{-8}-10^{-9} torr was used for sample characterization. All surveys utilized a pass energy of 160 eV with a step of 1 eV, while core regions utilized a pass energy of 20 eV with a step of 0.1 eV. All spectra were referenced to the C-C/C-H binding energy set at 285 eV.

XPS peak fitting was carried out using CasaXPS software from Casa Software Ltd. A 70 Guassian/ 30 Lorentzian mixture was used for symmetrical fitting, while a modified Gaussian/Lorentzian asymmetric peak fitting was used to account for charging.

1.5 Electrochemistry: Electrochemical Impedance Spectroscopy (EIS), Cyclic Voltammetry (CV), and Chrono-Amperommetry (CA)

1.5.1 Electrochemical Impedance Spectroscopy

Electrochemical impedance spectroscopy and cyclic voltammetry have been previously used to characterize the electrical and ionic properties of PPy and PEDOT films. PEDOT coatings have been known to lower impedance by as much as 1-2 orders of magnitude in the frequency range of 0.01-100 Hz in comparison to the bare electrode.[11,33,67] EIS measures the current when a single frequency is applied to a film in an ionic solution. The impedance data is comprised of both real (Z_{Re}) and imaginary (Z_{Im})

contributions and differ by the phase angle.[68] The phase angle (φ) is the phase difference between the voltage and current sinusoidal curves and can be used to suggest trends toward either resistance or capacitance. The following equation relates the real and imaginary components of the impedance (Z) as a function of frequency (ω).

$$Z(\omega) = Z_{Re} - jZ_{Im}$$

where Z_{Re} is the resistive portion, Z_{Im} is the capacitive reactance ($X_C = 1/\omega C$), and C is the capacitance.[68] Taking the magnitude of the impedance:

$$|Z|^2 = R^2 + X_C^2 = (Z_{Re})^2 + (Z_{Im})^2$$

with

$$\tan \varphi = Z_{Im}/Z_{Re} = X_C/R$$

Therefore when $\varphi = 0^o$ (0π) , then the system is purely resistive, and when $\varphi = 90^o$ ($\pi/2$), the system is purely capacitive. By utilizing the data yielded by EIS, equivalent circuit models of the system can ultimately be fabricated.[33,68-70]

1.5.2 Cyclic Voltammetry

Cyclic voltammetry is used in the detection of film charge capacity characteristics which is characterized as the area within the curve (Figure 1.9). In addition to film charge capacity information, CV is also used to observe reduction-oxidation reaction potentials, film wear properties (cycles until failure), and in the determination of whether the reactions are reversible, quasi-reversible, or irreversible.[68,71] For this research, CV will be used to characterize the charge capacity of the PEDOT films.

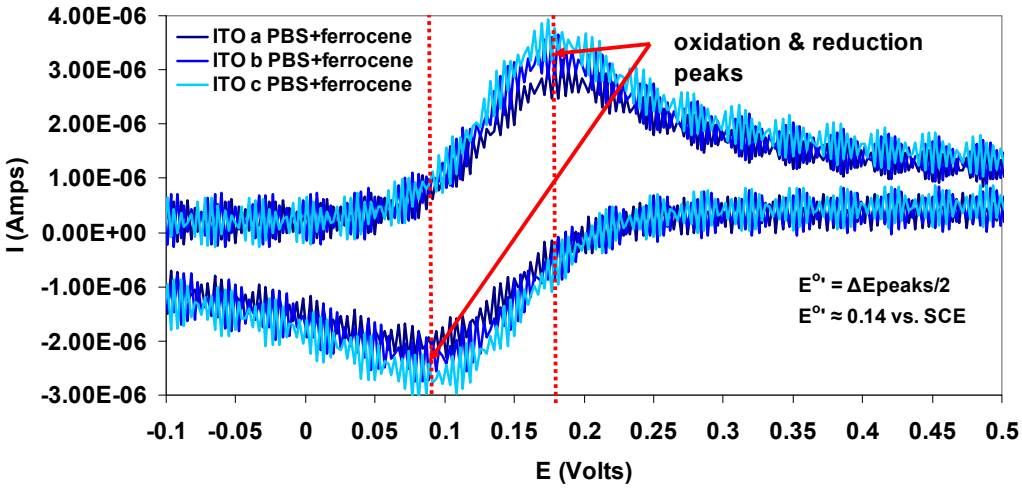

Figure 1.9 An example of a CV curve, ferrocene in phosphate buffer solution using an indium tin oxide working electrode, platinum counter electrode, and a standard calomel electrode (SCE) as the reference electrode

1.5.3 Chrono-Amperometry

Whereas EIS and CV yield characteristic information on the films themselves, chrono-amperometry has been extensively used as the detection method for enzyme based biosensors. Chrono-amperometry is the measurement of current produced from a reaction under the influence of a fixed potential as a function of time.[71] In the case of enzyme based biosensors, the electrons given off during redox reactions taking place within the enzyme are detected or any redox reaction by during chrono-amperometry.

1.5.4 Experimental Set-Up

Electrochemical impedance spectroscopy (EIS) and cyclic voltammetry (CV) were both carried out using an Autolab PGstat 12 Potentiostat/Galvanostat (EcoChemie, Utrect, the Netherlands) with a standard calomel electrode (SCE) as the reference

electrode. The working electrodes used in this research include sputtered Au/Pd barbells (6 mm diameter) on polystyrene coverslips, 90/10 Pt/Ir cochlear ball electrodes (~500 μm diameter), and indium tin oxide (ITO) on glass slides. The counter electrode was a piece of platinum.

1.6 References

1. Lock, J.P.; Im, S.G.; Gleason, K.K. *Macromolecules* **2006**, *39*, 5326.

2. Allcock, H. R.; Lampe, F.W.; Mark, J.E. *Contemporary Polymer Chemistry*; 3rd Ed. Pearson Education, Inc.: Upper Saddle River, New Jersey, 2003.

3. Reichert, W.M. *Indwelling Neural Implants: Strategies for Controlling with the In Vivo Environment;* CRC Press: New York, 2008.

4. Groenendaal, L.; Jonas, F.; Freitag, D.; Pielartzik, H.; Reynolds, J.R. *Adv. Mater.* **2000**, *12*, 481.

5. Na, S.I.; Wang, G.; Kim, S.S.; Kim, T.W.; Oh, S.H.; Yu, B.K.; Lee, T.; Kim, D.Y. *J. Mater. Chem.* **2009**, *19*, 9045.

6. Kiya, Y.; Hutchison, G.R.; Henderson, J.C.; Sarukawa, T.; Hatozaki, O.; Oyama, N.; Abruna, H.D. *Langmuir* **2006**, *22*, 10554.

7. Winter, I.; Reese, C.; Hormes, J; Heywang, G.; Jonas, F. *Chem. Phys.* **1995**, *194*, 207.

8. Dietrich, D.; Heinze, J.; Heywang, G.; Jonas, F. *J. Electroanal. Chem.* **1994**, *369*, 87.

9. Pei, Q.; Zuccarello, G.; Ahlskog, M.; Inganäs, O. *Polymer* **1994**, *35*, 1347.

10. Kim, D.H.; Richardson-Burns, S.M.; Hendricks, J.L.; Sequera, C.; Martin, D.C. *Adv. Funct. Mater.* **2007**, *17*, 79.

11. Richardson-Burns, S.M.; Hendricks, J.L.; Foster, B.; Povlich, L.K.; Kim, D.H.; Martin, D.C. *Biomaterials* **2007**, *28*, 1539.

12. Barisci, J.N.; Hughes, D.; Minett, A.;G.G. Wallace, G.G. *Anal. Chim. Acta* **1998**, *371*, 39.

13. Campbell, T.E.; Hodgson, A.J.;Wallace, G.G. *Electroanalysis* **1999**, *11*, 215.

14. Gooding, J.J.; Wasiowych, C.; Barnett, D.; Hibbert, D.B.; Barisci, J.N.; Wallace, G.G. *Biosens. Bioelectron.* **2004**, *20*, 260.

15. Richardson, R. T.; Thompson, B.; Moulton, S.; Newbold, C.; Lum, M.G.; Cameron, A.; Wallace, G.; Kapsa, R.; Clark, G.; O'Leary, S. *Biomaterials* **2007**, *28*, 513.

16. Zotti, G.; Zecchin, S.; Schiavon, G.; Louwet, F.; Groenendaal, L.; Crispin, X.; Osikowicz, W.; Salaneck, W.R.; Fahlman, M. *Macromolecules* **2003**, *36*, 3337.

17. Crispin, X.; Marciniak, S.; Osikowicz, W.; Zotti, G.;Denier van der Gon, A.W.; Louwet, F.; Fahlman, M.; Groenendaal, L.; De Schryver, F.; Salaneck, W.R. *J. Polym. Sci., Part B: Polym. Phys.* **2003**, *41*, 2561.

18. Denier van der Gon, A.W.; Birgerson, J.; Fahlman, M.; Salaneck, W.R. *Org. Electron.* **2002**, *3*, 111.

19. Greczynski, G.; Kugler, T.; Salaneck, W.R. *Thin Solid Films* **1999**, *354*, 129.

20. Greczynski, G.; Kugler, T.; Keil, M.; Osikowicz, W.; Fahlman, M.; Salaneck, W.R. *J. Electron Spectrosc. Relat. Phenom.* **2001**, *121*,1.

21. Jönsson, S.K.M.; de Jong, M.P.; Groenendaal, L.; Salaneck, W.R.; Fahlman, M. *J. Phys. Chem. B* **2003**, *107*, 10793.

22. Jönsson, S.K.M.; Birgerson, J.; Crispin, X.; Greczynski, G.; Osikowicz, W.; Denier van der Gon, A.W.; Salaneck, W.R.; Fahlman, M. *Synth. Met.* **2003**, *139*, 1.

23. Jönsson, S.K.M.; Salaneck, W.R.; Fahlman, M. *J. Electron Spectrosc. Relat. Phenom.* **2004**, *137-140*, 805.

24. Marciniak, S.; Crispin, X.; Uvdal, K.; Trzcinski, M.; Birgerson, J.; Groenendaal, L.; Louwet, F.; Salaneck, W.R. *Synth. Met.* **2004**, *141*, 67.

25. Spanninga, S.A.; Martin, D.C.; Chen, Z. *J. Phys. Chem. C* **2009**, *113***,** 5585.

26. Tengstedt, C.; Kanciurzewska, A.; de Jong, M.P.; Braun, S.; Salaneck, W.R.; Fahlman, M. *Thin Solid Films* **2006**, *55*, 2085.

27. Xing, K.Z.; Fahlman, M.; Chen, X.W.; Inganäs, O.; Salaneck, W.R. *Synth. Met.* **1997**, *89*, 161.

28. Garreau, S.; Louarn, G.; Buisson, J.P. ; Froyer, G. ; Lefrant, S. *Macromolecules* **1999**, *32*, 6807.

29. Kvarnström, C; Neugebauer, H.; Blomquist, S.; Ahonen, H.J.; Kankare, J.; Ivaska, A. *Electrochimica Acta* **1999**, ***44,*** 2739.

30. Kvarnström, C.; Neugebauer, H.; Ivaska, A.; N.S. Sariciftci, N.S. *J. Mol. Struct.* **2000**, *521*, 271.

31. Mausavi, Z.; Alaviuhkola, T.; Bobacka, J; Latonen, R.-M.; Pursiainen, J.; Ivaska, A.. *Electrochim. Acta* **2008**, *53*, 3755.

32. Winther-Jensen, B.; West, K. *Macromolecules* **2004**, *37*, 4538.

33. Cui, X.; Martin, D.C. *Sens. Actuators, B* **2003**, *89*, 92.

34. Yang, J.; Kim, D.H.; Hendricks, J.H.; Leach, M.; Northey, R.; Martin, D.C. *Acta Biomaterialia* **2005**, *1*, 125.

35. Yang, J.; Lipkim, K.; Martin, D.C. *J. Biomater. Sci. Polymer Edn*., **2007**, *18*, 1075.

36. Aasmundtveit, K.E.; Samuelsen, E.J.; Pattersson, L.A.A.; Inganäs, O.; Johansson, T.; Feidenhans, R. *Syn. Met*. **1999**, *101*, 561.

37. Winther-Jensen, B.; Forsyth, M.; West, K.; Andreasen, J.W.; Bayley, P.; Pas, S.; MacFarlane, D.R. *Polymer* **2008**, *49*, 481.

38. Aubert, P.H.; Groenendaal, L; Louwet, F.; Lutsen, L.; Vanderzande, D.; Zotti, G. *Syn. Met*. **2002**, *126*, 193.

39. Lambert, A.G.; Davies, P.B.; Neivandt, D.J. *Appl. Spectrosc. Rev.* **2005**, *40*, 103.

40. Hirose, C.; Akamatsu, N.; Domen, K. *J. Chem. Phys*. **1992**, *96*, 997.

41. Zhuang, X.; Miranda, P.B.; Kim, D.; Shen, Y.R. *Phys. Rev. B* **1999**, *59*, 12632.

42. Wang, J.; Chen, C.; Buck, S.M.; Chen, Z. *J. Phys. Chem. B* **2001**, *105*, 12118.

43. Hirose, C.; Akamatsu, N.; Domen, K. *Appl. Spectrosc*. **1992**, *46*, 1051.

44. Hirose, C.; Yamamoto, H.; Akamatsu, N.; Domen, K. *J. Phys. Chem.* **1993**, *97*, 10064.

45. Chen, X.; Clarke, M. L.; Wang, J.; Chen, Z. *Int. J. Modern Phys. B* **2005**, *19*, 691.

46. Chen, X.; Tang, H.; Even, M.A.; Wang, J.; Tew, G.N.; Chen, Z. *J. Am. Chem. Soc.* **2006**, *128*, 2711.

47. Wang, J.; Woodcock, S.E.; Buck, S.M.; Chen, C.; Chen, Z. *J. Am. Chem. Soc.* **2001**, *123*, 9470.

48. Briggman, K. A.; Stephenson, J. C.; Wallace, W. E.; Richter, L. J. *J. Phys. Chem. B* **2001**, *105*, 2785.

49. Chen, C.; Wang, J.; Woodcock, S.E.; Chen, Z. *Langmuir* **2002**, *18*, 1302.

50. Gautam, K. S.; Schwab, A. D.; Dhinojwala, A. *Phys. Rev. Lett*. **2000**, *85*, 3854.

51. Pászti, Z.; Wang, J.; Clarke, M.L.; Chen *J. Phys. Chem. B* **2004**, *108*, 7779.

52. Wang, J.; Paszti, Z.; Even, M.A.; Chen, Z. *J. Phys. Chem. B* **2004**, *108*, 3625.

53. Wang, J.; Clarke, M.L.; Chen, X.; Even, M.A.; Johnson, W.C.; Z. Chen, Z. *Surf. Sci.* **2005**, *587*, 1.

54. Clarke, M.L.; Wang, J.; Chen, *Z. J. Phys. Chem. B* **2005**, *109***,** 22027.

55. Wang, J.; Chen, C.; Buck, S.M.; Chen, *Z. J. Phys. Chem. B* **2001**, *105*,12118.

56. Wang, J.; Chen, X.; Clarke, M.L.; Chen, *Z. J. Phys. Chem. B* **2006**, *110*, 5017.

57. Wang, J.; Even, M.A.; Chen, X.; Schmaier, A.H.; Waite, J.H.; Chen, Z. *J. Am. Chem. Soc.* **2003**, *125*, 9914.

58. Chen, X.; Wang, J.; Boughton, A.P.; Kristalyn, C.B.; Chen, *Z. J. Am. Chem. Soc.* **2007**, *129***,** 1420.

59. Chen, X.; Wang, J.; Sniadecki, J.J.; Even, M.A.; *Langmuir* **2005**, *21*, 2662.

60. Beamson, G.; Briggs, D. *High Resolution XPS of Organic Polymers: The Scienta ESCA300 Database*; John Wiley & Sons: New York, New York, 1992.

61. Briggs, D.; Seah, M.P. *Practical Analysis: Volume 1 Auger and X-ray Photoelectron;* 2nd Ed. John Wiley & Sons: New York, 1990.

62. Briggs, D. *Surface analysis of polymers by XPS and static SIMS*; Cambridge University Press: Cambridge, U.K.1998.

63. Brundle, R. C.; Evans Jr., C.A.; Wilson, S. *Encyclopedia of Materials Characterization: Surfaces, Interfaces, Thin Films*; Butterworth-Heinemann, 1992.

64. Siegbahn, K.; Nordling, C.; Fahlman, A.; Nordberg, R.; Hamrin, K.; Hedman, J.; Johansson, G.; Bergmark, T.; Karlsson, S.E.; Lindgren, I.; Lindberg, B. *ESCA: atomic, molecular and solid state structure studied by means of electron spectroscopy.* Uppsala: Uppsala,SWE, 1967.

65. Seah, M.P.; Dench, W.A. *Surf. Int. Sci*.**1979**, *1*, 2.

66. Moulder, J.F.; Stickle, W.R.; Sobol, P.E.;K.D. Bomben, K.D. *Handbook of X-ray photoelectron spectroscopy: A reference book of standard spectra for identification and interpretation of XPS data.* Physical Electronics: Eden Prairie, MN, 1992.

67. Yang, J.Y.; Martin, D.C. *Sens. Actuators, A* **2004**, *113*, 204.

68. Bard, A.J.; Faulkner, L.R. *Electrochemical Methods: Fundamentals and Applications*; 2nd Ed. John Wiley & Sons: New York, 2001.

69. Bhandari, S.; Deepa, M.; Singh, S.; Gupta, G.; Kant, R. *Electrochim. Acta* **2008**, *53*, 3189.

70. Macdonald, J. R. *Impedance spectroscopy: emphasizing solid materials and systems*. John Wiley & Sons: New York, 1987.

71. Brett, C.M.A.; Brett, A.M.O. *Electroanalysis*. Oxford University Press, 1998.

CHAPTER 2

SURFACE ORIENTATION OF PHENYL GROUPS IN POLY (SODIUM 4-STYRENESULFONATE) AND IN POLY (3,4-ETHYLENEDIOXYTHIOPHENE): POLY (SODIUM 4-STYRENESULFONATE) SUSPENSION EXAMINED BY SUM FREQUENCY GENERATION VIBRATIONAL SPECTROSCOPY

2.1 Introduction

As stated previously in chapter 1, poly(3,4-ethylenedioxythiophene) (PEDOT) is a highly conductive, π conjugated polymer. Due to its high conductivity of ~300 S/cm,[1] PEDOT has been used in a variety of applications such as anti-static coatings, organic light emitting devices,[1] solar cells,[2] batteries,[3] and even as a biological tissue interfacing agent.[4,5] The most commonly used form of PEDOT is Baytron P (now known as CLEVIOS P), the commercially available suspension of PEDOT with the poly-anion poly(sodium 4-styrenesulfonate) (PSSNa) in water. PSSNa is the most commonly used poly-anionic counter-ion to PEDOT, but PSS itself is also used for its charged polyelectrolyte properties.[6] The PEDOT within Baytron P is chemically polymerized in the presence of a PSSNa aqueous bath.[1] The resulting polymer has a characteristic blue-black color that can be spin coated for application purposes.

Even though a variety of characterization techniques have been used to examine PEDOT[7-20], the molecular surface structure such as surface functional group orientation

has not been studied. Many PEDOT properties are mediated by its surface or interfacial structures. This chapter seeks to investigate the surface functional group orientation of Baytron P, providing a base for future examinations on buried interfacial structure of Baytron P and its relation to the conductivity of the polymer. In order to study the functional group orientation, the surface characterization technique, Sum Frequency Generation (SFG) vibrational spectroscopy, will be utilized.

As an optical and non-vacuum technique, SFG provides the opportunity to study samples in situ, as long as the sample is accessible to light. SFG has been proven very insightful in studying surfaces and interfaces especially in determining the functional group orientation of polymer surfaces and interfaces.[21-49] A distinct advantage of SFG is its unique monolayer surface sensitivity.[21-49] As introduced in chapter 1, the orientation of specific chemical functional groups on the surface can be determined by utilizing the properties of polarized light, e.g., different polarization combinations of the input beams and output beam, and by relating the surface second-order non-linear susceptibility in the lab coordinate system to the hyperpolarizability in the molecular coordinate system.[50-53]

Baytron P contains a significant amount of PSS, therefore in this study PSS was used as a reference comparison to Baytron P. In this chapter, the orientation of the phenyl group on a PSSNa surface was first determined. In the past, the orientation of phenyl groups on polystyrene (PS) surface has been investigated using SFG spectra collected.[18,54,55] The difference between the phenyl groups in PSSNa and PS is that PSSNa has a para-substituted ring, while PS has a mono-substituted ring. Therefore a method was applied to study para-substituted phenyl groups in order to determine their

orientation on the PSSNa surface. After the PSSNa surface was analyzed, the PSS phenyl ring orientation on the Baytron P surface was determined.

2.2 Experimental

2.2.1 Materials

The Baytron P, or CLEVIOS P, sample with 1:2.5 poly (3,4-ethylenedioxythiophene) (PEDOT):poly(sodium 4-styrenesulfonate) (PSSNa) was obtained from H. C. Starck. Poly(sodium 4-styrenesulfonate) (PSSNa) was purchased from Acros Organics. Polymer films were spin coated from 2 wt % solutions of PSSNa/de-ionized water solution and Baytron P on calcium fluoride at 2500 rpm and 4200 rpm, respectively.

2.2.2 Sum Frequency Generation (SFG) vibrational spectroscopy

The SFG set-up,[44,45] SFG theory,[21-49] and SFG experimental geometry[49] have been presented previously and will not be repeated here. In this research, a face down geometry was utilized, allowing the frequency tunable infrared and 532 nm visible input beams to both spatially and temporally overlap at the polymer/air interface after traveling through the calcium fluoride substrates at angles (vs. surface normal) of 54º and 60º respectively. The beam diameters were around 500 μm. SFG spectra were collected using ssp (s-polarized sum frequency output, s-polarized visible, and p-polarized IR input) and sps polarization combinations. All data were normalized by the input IR and visible intensities. The vibrational frequency was calibrated using a poly(methyl methacrylate) reference. While the IR energy used was around 200 μJ, the visible energies employed were varied based upon the sample probed. The PSSNa samples utilized visible energies

around 100 μJ, while the energy was reduced to 50 μJ, to minimize degradation from the Baytron P.

2.3 Results and Discussion

2.3.1 General discussion of SFG spectra

SFG spectra were collected from surfaces of spin coated PSSNa and Baytron P samples. The detailed spectral analysis will be presented later. First the aromatic C-H vibrational modes of PSSNa will be discussed. As discussed previously, the phenyl group in PS is a mono-substituted aromatic ring. There are five normal modes for the aromatic C-H stretching vibrations for such a phenyl group,[58,59] as depicted in Figure 2.1. The symmetry of a phenyl group belongs to a C_{2v} point group, thus all the five modes are both IR and Raman active. Only when a vibrational mode is both IR and Raman active, can it be detected in SFG; therefore all these five modes are SFG active.

The SFG hyperpolarizability tensor, β, can be described as a tensor product of the IR transition dipole moment and the Raman polarizability tensor,

$$\beta_{lmn,q} \propto \frac{\partial \alpha_{lm}}{\partial Q_q} \frac{\partial \mu_n}{\partial Q_q}$$

where l, m, and n are the molecular coordinates, $\frac{\partial \alpha_{lm}}{\partial Q_q}$ and $\frac{\partial \mu_n}{\partial Q_q}$ are components of the Raman polarizability and IR dipole moment derivatives with respect to the normal mode coordinate of the q^{th} vibrational mode, respectively. A vibrational mode with both strong IR and Raman signals may lead to a strong SFG signal. For the five modes depicted in Figure 2.1, the ν_2 and ν_{7a} modes are able to have both a large IR transition dipole moment

and Raman polarizability, therefore they may also have strong SFG signals (this also depends on the beam polarization combinations used to collect the signal).

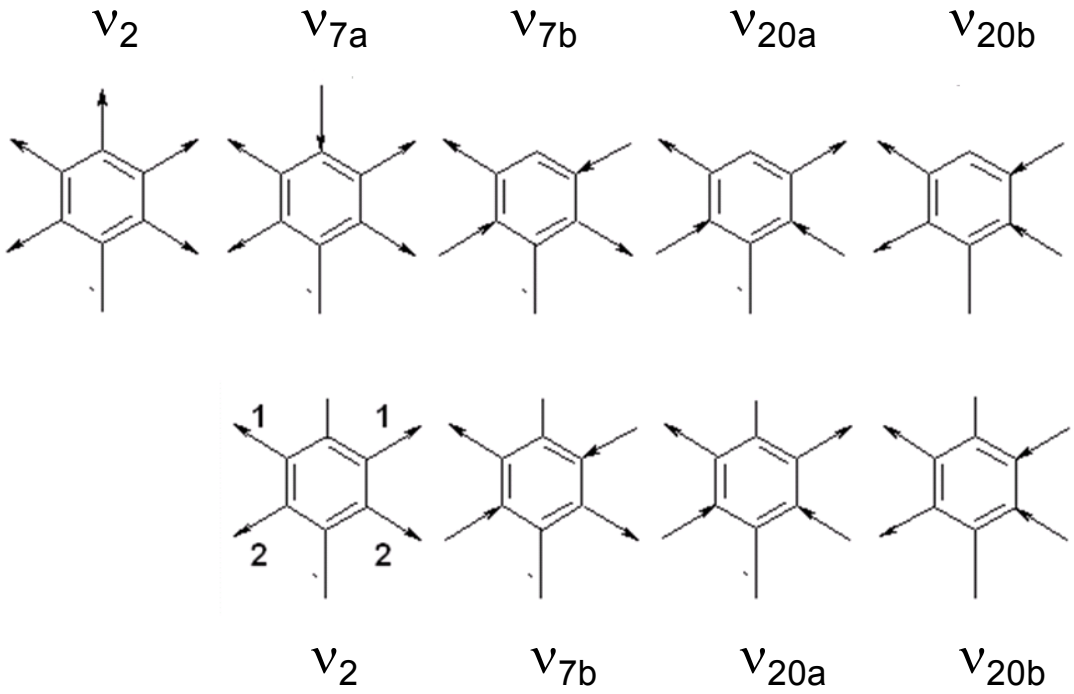

Figure 2.1 The five normal modes of the C-H stretching vibrations for a mono-substituted phenyl ring (top) and the four normal modes for a para-substituted phenyl ring (bottom).

Clearly the SFG activity for the ν_{7b} mode depends on the "unequal" IR dipole transition moment derivatives of the C-H bonds at the ortho and meta positions from the mono-substituted position. If these two positions are the same, then this mode is IR forbidden. If these two positions are not drastically different (e.g., for PS), then it may generate a weak IR signal, leading to a weak SFG signal as well. The SFG activities for the ν_{20a} and ν_{20b} modes depend on the "unequal" C-H bond Raman polarizability derivatives at the ortho and meta positions with respect to the mono-substituted position. Similarly, if these two positions are not drastically different, these two modes will

generate weak Raman signals resulting in weak SFG signals. According to this analysis, the ν_2 and ν_{7a} modes would dominate the SFG spectra collected from the PS surface.

Differing from the PS mono-substituted phenyl group, the PSSNa aromatic ring is para-substituted. Because the two substitutions are not the same, the group (we will still call it phenyl) still has C_{2v} symmetry. For the PSSNa phenyl group, the two PS modes ν_2 and ν_{7a} become the same (Figure 2.1). This new mode is called ν_2. It is both IR and Raman active because of the hetero-substitution, creating "unequal" positions in the carbon 1 and carbon 2 within the group (Figure 2.1). The ν_2 and ν_{7b} modes are IR active because of the hetero-substitution. Since ν_2 mode can have a stronger Raman signal than ν_{7b} mode, the ν_2 mode may lead to a stronger SFG signal. Similar to the ν_{20a} and ν_{20b} modes in PS, the PSSNa intensities must also depend on how strongly the hetero-substitution affects the Raman C-H bond polarizabilities at the carbon 1 and carbon 2 positions.

Figure 2.2 shows PSSNa and Baytron P SFG spectra collected using the ssp and sps polarization combinations. Such SFG spectra were fitted using the following equation:

$$\chi_{eff}^{(2)} = \chi_{nr} + \sum \frac{A_q}{\omega_{IR} - \omega_q + i\Gamma_q}$$

where $\chi_{eff}^{(2)}$ is the effective second-order nonlinear susceptibility, $\chi_{nr}^{(2)}$ is the nonresonant background and A_q, ω_q, and Γ_q are the strength, resonant frequency and damping coefficient (width) for the vibrational mode q. The SFG spectral assignment and fitting results are shown in Table 2.1. The peak assignment was based on the previous SFG study focusing on the polar orientation of the benzoate derivative counter ions bound to a

surfactant monolayer,[58] and the comprehensive reference book about IR and Raman peak assignment of benzene derivatives.[56,57] Indeed, the signal from the ν_2 mode in the ssp spectrum is the strongest, while the intensities of ν_{7b}, ν_{20a}, and ν_{20b} modes are relatively weak and become more prominent only in the sps spectra.

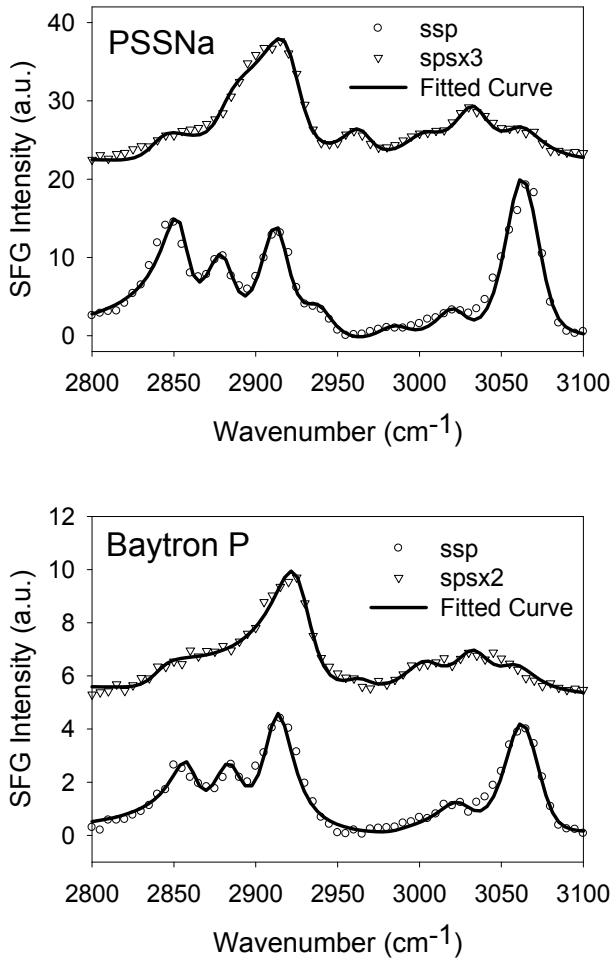

Figure 2.2 The (top) PSSNa and (bottom) Baytron P SFG spectra in ssp and sps.

Sample	ω_q (cm^{-1})	A_q		Γ_q (cm^{-1})	Assignment
		ssp	sps		
PSSNa	2855	23±1	-11±1	10	CH_2 ss
	2881	26±1	-10±1	12	CH_3 ss
	2895	14±1	—	15	unassigned
	2913	38±1	—	12	CH_2 Fermi
	2922	—	27±1	12	CH_2 as
	2938	15±1		12	CH_3 Fermi
	2965	—	9±1	12	CH_3 as
	3005	—	8±1	15	Combination
	3021	21±2	—	15	ν_{20b}
	3030	-6±1	18±1	15	ν_{7b}
	3060	73±2	12±1	15	ν_2
	3076	-30±1	—	15	ν_{20a}
Baytron P	2840	—	-5±1	10	Combination
	2860	9±1	—	10	CH_2 ss
	2885	13±1	—	12	CH_3 ss
	2895	-10±1	—	15	unassigned
	2913	23±1	—	12	CH_2 Fermi
	2927	—	19±1	15	CH_2 as
	2965	—	3±1	12	CH_3 as
	3005	—	7±1	15	Combination
	3025	12±1	—	15	ν_{20b}
	3034	-2±1	10±1	15	ν_{7b}
	3060	34±1	7±1	15	ν_2

	3076	-15±1	—	15	ν_{20a}

Table 2.1 PSSNa and Baytron P fitting where 'ss' is symmetric stretching, 'as' is anti-symmetric stretching, and Fermi denotes Fermi resonance.

2.3.2 Phenyl group orientation order on the two sample surfaces

To determine the phenyl group orientation information on a surface, it is necessary to know the relationship between the surface effective second-order nonlinear susceptibility ($\chi_{eff}^{(2)}$) and the molecular hyperpolarizability (β). The $\chi_{eff}^{(2)}$, especially the ratio between certain $\chi_{eff}^{(2)}$ components can be measured in SFG experiments using different input and output beam polarization combinations. The hyperpolarizability components of the para-substituted phenyl groups can be calculated. The $\chi_{eff}^{(2)}$ is related to the hyperpolarizability through orientation angles of the surface functional groups; therefore orientation information can be deduced.

As discussed above, for a para-substituted phenyl ring, a local C_{2v} symmetry can be adopted for analysis. It is reasonable to assume that both the sample surfaces are azimuthally isotropic and thus we only need to consider the tilt angle and the twist angle of the phenyl ring to determine the orientation. Figure 2.3 shows the schematic describing the laboratory-fixed and the molecule-fixed coordinates for a phenyl group adopting the C_{2v} symmetry. The molecule-fixed coordinate system is defined as an (a, b, c) system. The "c" axis is in the same direction as the principal axis in C_{2v} symmetry; the "a" axis is perpendicular to the "c" axis and is in the phenyl plane; the "b" axis is orthogonal to the phenyl plane. The laboratory-fixed coordinate system is defined as an (X, Y, Z) system. The tilt angle, θ, is defined as the angle between the Z-axis (which is the surface normal)

and the c-axis of the phenyl group. The twist angle, ϕ, is defined as the rotation angle of the phenyl plane with respect to the c-axis.

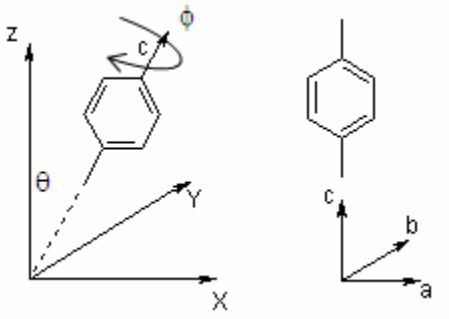

Figure 2.3 The schematics show the laboratory-fixed coordinate system (left) and the molecule-fixed coordinate system (right) for a para-substituted phenyl group, respectively.

Based upon the local C_{2v} symmetry for the para-substituted phenyl rings, we know that ν_2 and ν_{20a} modes belong to the A_1 irreducible representation, which has three non-zero molecular hyperpolarizability components: β_{aac}, β_{bbc}, and β_{ccc}. The ν_{7b} and ν_{20b} modes belong to the B_1 irreducible representation, which has two non-zero molecular hyperpolarizabilities, $\beta_{aca} = \beta_{caa}$. The relations between the second order nonlinear susceptibility components and various hyperpolarizability components for different modes are:[49-51]

For A_1:

$$\chi_{yyz,A1} = \frac{N_s}{8}[\beta_{aac,A1}\cos\theta(3+\cos 2\theta - 2\sin^2\theta\cos 2\phi) + \beta_{bbc,A1}\cos\theta(3+\cos 2\theta + 2\sin^2\theta\cos 2\phi) + \beta_{ccc,A1}(\cos\theta - \cos 3\theta)]$$

$$\chi_{yzy,A1} = \frac{N_s}{16}[-\beta_{aac,A1}(\cos\theta - \cos 3\theta)(1+\cos 2\phi) - \beta_{bbc,A1}(\cos\theta - \cos 3\theta)(1-\cos 2\phi) + 2\beta_{ccc,A1}(\cos\theta - \cos 3\theta)]$$

For B_1:

$$\chi_{yyz,B1} = -\frac{N_s}{8}\beta_{aca,B1}(\cos\theta - \cos 3\theta)(1+\cos 2\phi)$$

$$\chi_{yzy,B1} = \frac{N_s}{8}\beta_{aca,B1}[4\cos\theta - (\cos\theta - \cos 3\theta)(1+\cos 2\phi)]$$

As mentioned above, the second order nonlinear optical susceptibility components, especially their ratios, can be measured in the SFG experiment. In order to deduce the tilt and twist angles, the relative hyperpolarizablity tensor component ratios, shown above, should be known. For the PSSNa para-substituted phenyl ring, the ν_2 and ν_{7b} modes were focused upon. The bond-additivity approach was applied to evaluate the following relative hyperpolarizablity tensor component ratios.[50-52,58]

For para-substituted phenyl ring:

$$\frac{\beta_{ccc,\nu 2}}{\beta_{aac,\nu 2}} = 0.69\,,\ \frac{\beta_{bbc,\nu 2}}{\beta_{aac,\nu 2}} = 0.04\,,\ \frac{\beta_{aca,\nu 7b}}{\beta_{aac,\nu 2}} = 0.47\,.$$

By combining the measured SFG spectra and the above deduced ratios, the tilt and twist angles can be determined. The different ratios will be used to cross check the accuracy of the deduced orientation angles.

The para-substituted phenyl group tilt and twist angles at the PSSNa and Baytron P interfaces were estimated by inputting these deduced values into the above equations to relate χ and β. For the para-substitued phenyl ring:

$$\frac{\chi_{yyz,\nu 2}}{\chi_{yzy,\nu 2}} = \frac{25.4\cos\theta - \cos 3\theta - 11.3\cos\theta\sin^2\theta\cos 2\phi}{(\cos\theta - \cos 3\theta)(1 - 2.82\cos 2\phi)}$$

$$\frac{\chi_{yyz,\nu 7b}}{\chi_{yzy,\nu 7b}} = \frac{(\cos 3\theta - \cos\theta)(1+\cos 2\phi)}{4\cos\theta - (\cos\theta - \cos 3\theta)(1+\cos 2\phi)}$$

$$\frac{\chi_{yyz,\nu 7b}}{\chi_{yyz,\nu 2}} = \frac{(\cos 3\theta - \cos\theta)(1+\cos 2\phi)}{9.20\cos\theta - 0.36\cos 3\theta - 4.08\cos\theta\sin^2\theta\cos 2\phi}$$

$$\frac{\chi_{yzy,\nu 7b}}{\chi_{yzy,\nu 2}} = \frac{4\cos\theta - (\cos\theta - \cos 3\theta)(1+\cos 2\phi)}{(\cos\theta - \cos 3\theta)(0.36 - 1.02\cos 2\phi)}$$

By combining any of the two equations among the above four equations, both the tilt angle and twist angle can be deduced. A tilt angle assuming an isotropic distribution of the twist angle was also determined. The results for the PSSNa and Baytron P phenyl groups are shown in Table 2.2 and Table 2.4 respectively.

Tilt angle (°)	Twist angle (°)	Sources
51	52	$\chi_{yyz,\nu 2} / \chi_{yzy,\nu 2}$, $\chi_{yyz,\nu 7b} / \chi_{yzy,\nu 7b}$
48	61	$\chi_{yyz,\nu 2} / \chi_{yzy,\nu 2}$, $\chi_{yzy,\nu 7b} / \chi_{yzy,\nu 2}$
48	64	$\chi_{yyz,\nu 7b} / \chi_{yzy,\nu 7b}$, $\chi_{yzy,\nu 7b} / \chi_{yzy,\nu 2}$
43	58	$\chi_{yyz,\nu 7b} / \chi_{yyz,\nu 2}$, $\chi_{yzy,\nu 7b} / \chi_{yzy,\nu 2}$
47.5±5.3	58.8±8.2	----------

Table 2.2 The deduced tilt and twist angles of the PSSNa surface phenyl groups.

Tilt angle (°)	Sources
Out of range, near 90°[35]	$\chi_{yyz,\nu 2} / \chi_{yzy,\nu 2}$
32	$\chi_{yyz,\nu 7b} / \chi_{yzy,\nu 7b}$
25	$\chi_{yyz,\nu 7b} / \chi_{yyz,\nu 2}$
63	$\chi_{yzy,\nu 7b} / \chi_{yzy,\nu 2}$

Table 2.3 The deduced tilt angle of PSSNa surface phenyl groups supposing an isotropic twist.

Tilt angle (°)	Twist angle (°)	Sources
50	62	$\chi_{yyz,\nu 2} / \chi_{yzy,\nu 2}$, $\chi_{yyz,\nu 7b} / \chi_{yzy,\nu 7b}$
49	66	$\chi_{yyz,\nu 2} / \chi_{yzy,\nu 2}$, $\chi_{yzy,\nu 7b} / \chi_{yzy,\nu 2}$
49	68	$\chi_{yyz,\nu 7b} / \chi_{yzy,\nu 7b}$, $\chi_{yzy,\nu 7b} / \chi_{yzy,\nu 2}$
45	65	$\chi_{yyz,\nu 7b} / \chi_{yyz,\nu 2}$, $\chi_{yzy,\nu 7b} / \chi_{yzy,\nu 2}$
48.2±3.6	65.2±4	----------

Table 2.4 The deduced tilt and twist angles of Baytron P surface phenyl groups.

Tilt angle (°)	Source
Out of range, near 90°[11]	$\chi_{yyz,\nu 2} / \chi_{yzy,\nu 2}$
26	$\chi_{yyz,\nu 7b} / \chi_{yzy,\nu 7b}$
21	$\chi_{yyz,\nu 7b} / \chi_{yyz,\nu 2}$
54	$\chi_{yzy,\nu 7b} / \chi_{yzy,\nu 2}$

Table 2.5 The deduced tilt angle of the Baytron P surface phenyl groups supposing an isotropic twist.

When using the different equation combinations, the resulting tilt and twist angles were not found to be very different, indicating that the deduced angles are reliable. For example, the PSSNa phenyl group tilt angle was determined to be 51, 48, 48, 43 degrees, which were not very different from each other. Table 2.2 shows the average tilt and twist angles for PSSNa phenyl groups are 47.5°±5.3° and 58.8°±8.2°, respectively. However, the tilt angles deduced assuming an isotropic (or random) distribution of the twist angle using different combinations of the two equations are quite different, as shown in Table

2.3. Clearly, the PSSNa phenyl groups do not have an isotropic twist angle distribution. It appears that the PSSNa phenyl groups adopt a specific orientation with certain tilt and twist angles.

The average tilt and twist angles of PSSNa component within Baytron P were also determined. Again tilt and twist angle results, Table 2.4, do not differ significantly. The average tilt and twist angles are 48.2°±3.6° and 65.2°±4.0°, respectively. Both the PSSNa and Baytron P results are depicted in Figure 2.4 below. The phenyl tilt angle of PSSNa within Baytron P is similar to that of pure PSSNa on a surface, but the twist angle is slightly different, possibly due to the interactions between the PSS and PEDOT in Baytron P. Similarily to the PSSNa situation, the Baytron P phenyl tilt angles were found to be very different using different combinations of the two equations and assuming an isotropic or random distribution of the twist angle (Table 2.5), indicating that the PSSNa phenyl groups within Baytron P on the surface do not have an isotropic twist angle.

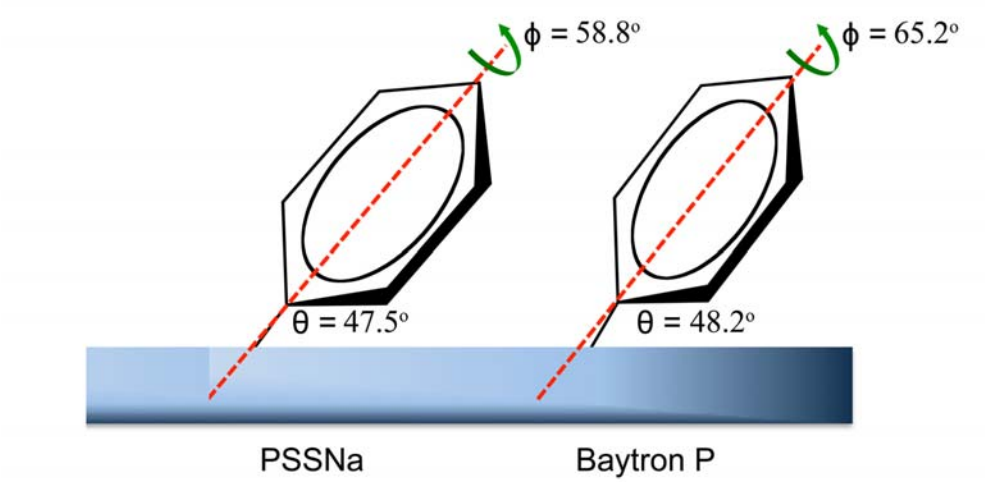

Figure 2.4 A schematic showing the PSSNa and Baytron P tilt and twist angle results.

2.4 Conclusions

SFG was applied to deduce phenyl group orientation for PSSNa and Baytron P surfaces. For the PSSNa para-substituted phenyl ring, a tilt angle of 47.5°±5.3° and a twist angle of 58.8°±8.2° were found. The Baytron P phenyl tilt and twist angles, 48.2°±3.6° and 65.2°±4.0° respectively, were also found indicating that the orientations were not very different. The similarity in both the tilt and twist angles was to be expected because a significant portion of the Baytron P signal likely resulted from the excess PSSNa (1 PEDOT: 2.5 PSSNa) present. Some differences between PSSNa and Baytron P twist angle values could be attributed to the fact that some of PSSNa in Baytron P interacts electrostatically with PEDOT, affecting the phenyl ring orientation.

2.5 References

1. Groenendaal, L.; Jonas, F.; Freitag, D.; Pielartzik, H.; Reynolds, J.R. *Adv. Mater.* **2000**, *12*, 481.

2. Greczynski, G.; Kugler, T.; Salaneck, W.R. *Thin Solid Films* **1999**, *354*, 129.

3. Greczynski, G.; Kugler, T.; Keil, M.; Osikowicz, W.; Fahlman, M.; Salaneck, W.R. *J. Electron Spectrosc. Relat. Phenom*. **2001**, *121*,1.

4. Spanninga, S.A.; Martin, D.C.; Chen, Z. *J. Phys. Chem. C* **2009**, *113*, 5585.

5. Zotti, G.; Zecchin, S.; Schiavon, G.; Louwet, F.; Groenendaal, L.; Crispin, X.; Osikowicz, W.; Salaneck, W.R.; Fahlman, M. *Macromolecules* **2003**, *36*, 3337.

6. Garreau, S.; Louarn, G.; Buisson, J.P. ; Froyer, G. ; Lefrant, S. *Macromolecules* **1999**, *32*, 6807.

7. Kvarnström, C; Neugebauer, H.; Blomquist, S.; Ahonen, H.J.; Kankare, J.; Ivaska, A. *Electrochimica Acta* **1999**, ***44,*** 2739.

8. Kvarnström, C.; Neugebauer, H.; Ivaska, A.; N.S. Sariciftci, N.S. *J. Mol. Struct.* **2000**, *521*, 271.

9. Mausavi, Z.; Alaviuhkola, T.; Bobacka, J; Latonen, R.-M.; Pursiainen, J.; Ivaska, A.. *Electrochim. Acta* **2008**, *53*, 3755.

10. Winther-Jensen, B.; West, K. *Macromolecules* **2004**, *37*, 4538.

11. Pei, Q.; Zuccarello, G.; Ahlskog, M.; Inganäs, O. *Polymer* **1994**, *35*, 1347.

12. Cui, X.; Martin, D.C. *Sens. Actuators, B* **2003**, *89*, 92.

13. Yang, J.; Kim, D.H.; Hendricks, J.H.; Leach, M.; Northey, R.; Martin, D.C. *Acta Biomaterialia* **2005**, *1*, 125.

14. Yang, J.; Lipkim, K.; Martin, D.C. *J. Biomater. Sci. Polymer Edn*., **2007**, *18*, 1075.

15. Winther-Jensen, B.; Forsyth, M.; West, K.; Andreasen, J.W.; Bayley, P.; Pas, S.; MacFarlane, D.R. *Polymer* **2008**, *49*, 481.

16. Dietrich, D.; Heinze, J.; Heywang, G.; Jonas, F. *J. Electroanal. Chem*. **1994**, *369*, 87.

17. Briggman, K. A.; Stephenson, J. C.; Wallace, W. E.; Richter, L. J. *J. Phys. Chem. B* **2001**, *105*, 2785.

18. Chen, C.; Wang, J.; Woodcock, S.E.; Chen, Z. *Langmuir* **2002**, *18*, 1302.

19. Chen, C.; Wang, J.; Even, M.A.; Chen, Z. *Macromolecules* **2002**, *35*, 8093.

20. Gautam, K. S.; Schwab, A. D.; Dhinojwala, A. *Phys. Rev. Lett*. **2000**, *85*, 3854.

21. Shen, Y.R.; Ostroverkhov, V. *Chem. Rev*. **2006**, *106*, 1140.

22. Eisenthal, K. B. *Chem. Rev.* **1996**, *96*, 1343.

23. Bain, C. D. *J. Chem. Soc. Faraday. Trans.* **1995**, *91*,1281.

24. Richmond, G.L. *Annu. Rev. Phys. Chem.* **2001**, *52*, 357.

25. Tadjeddine, A.; Peremans, A. *Surf. Sci.* **1996**, *368*, 377.

26. Shultz, M.J.; Schnitzer, C.; Simonelli, D.; Baldelli, S. *Inter. Rev. Phys. Chem.* **2000,** *19*, 123.

27. Williams, C. T.; Beattie, D. A. *Surf. Sci.* **2002,** *500*, 545.

28. Perry, A.; Neipert, C.; Space, B.; Moore, P. B. *Chem. Rev.* **2006**, *106*, 1234.

29. Shi, Q.; Ye, S.; Kristalyn, C.; Su, Y.; Jiang, Z.; Chen, Z. *Langmuir* **2008**, *24* 7939.

30. Ye, S.; McClelland, A.; Majumdar, P.; Stafslien, S. J.; Daniels, J.; Chisholm, B.; Chen, Z. *Langmuir* **2008**, *24* 9686.

31. Chen, Z.; Shen, Y. R.; Somorjai, G. A. *Ann. Rev. Phys. Chem.* **2002,** *53*, 437.

32. Chen, Z. *Poly. Inter.* **2006,** *56*, 577.

33. Zhang, D.; Ward, R. S.; Shen, Y.R.; Somorjai, G. A. *J. Phys. Chem. B* **1997**, *101*, 9060.

34. Li, G.; Shen, Y.; Morita, S.; Nishida, T.; Osawa, M. *J. Am. Chem. Soc.* **2004**, *126*, 12198.

35. Clarke, M. L.; Wang, J.; Chen, Z. *Anal. Chem.* **2003**, *75*, 3275.

36. Clarke, M.L.; Wang, J.; Chen, Z. *J. Phys. Chem. B* **2005**, *109*, 22027.

37. Rangwalla, H.; Schwab, A. D.; Yurdumakan, B.; Yablon, D. G.; Yeganeh, M. S.; Dhinojwala, A. *Langmuir* **2004**, *20*, 8625.

38. Yang, C. S. C.; Wilson, P. T.; Richter, L. J. *Macromolecules* **2004**, *37*, 7742.

39. Chen, C.Y.; Wang, J.; Chen, Z. *Langmuir* **2004**, *20*, 10186.

40. Shi, Q.; Ye, S.; Spanninga, S. A.; Su, Y.; Jiang, Z.; Chen, Z. *Soft Matter* **2009**, *5*, 3487.

41. Chen, X.; Clarke, M. L.; Wang, J.; Chen, Z. *Int. J. Mod. Phys. B* **2005**, *19*, 691.

42. Lambert, A. G.; Davies, P. B.; Neivandt, D. J. *Appl. Spectrosc. Rev.* **2005**, *40*, 103.

43. Casford, M. T. L.; Davies, P. B. *J. Phys. Chem. B* **2008**, *112*, 2616.

44. Wang, J.; Paszti, Z.; Even, M. A.; Chen, Z. *J. Am. Chem. Soc.* **2002**, *124*, 7016.

45. Wang, J.; Woodcock, S. E.; Buck, S. M.; Chen, C. Chen, Z. *J. Am. Chem. Soc.* **2001**, *123* 9470.

46. McGall, S. J.; Davies, P.B.; Neivandt, D. J.; *J. Phys. Chem. B* **2004**, *108*, 16030.

47. Gautam, K. S.; Schwab A. D.; Dhinojwala, A.; Zhang, D.; Dougal, S. M.; Yeganeh, M. S. *Phys. Rev. Letts.* **2000**, *85,* 3854.

48. Wilson, P. T.; Briggman, K. A.; Wallace, W. E.; Stephenson, J. C.; Richter, L. J. *Appl. Phys. Lett.* **2002,** *80*, 3084.

49. Chen, C. Y.; Wang, J.; Even, M. A.; Chen, Z. *Macromolecules* **2002**, *35*, 8093.

50. Hirose, C.; Akamatsu, N.; Domen, K. *Appl. Spectrosc*. **1992**, *46*, 1051.

51. Hirose, C.; Akamatsu, N.; Domen, K. *J. Chem. Phys*. **1992**, *96*, 997.

52. Hirose, C.; Yamamoto, H.; Akamatsu, N.; Domen, K. *J. Phys. Chem.* **1993**, *97*, 10064.

53. Zhuang, X.; Miranda, P.B.; Kim, D.; Shen, Y.R. *Phys. Rev. B* **1999**, *59*, 12632.

54. Gautam, K. S.; Schwab, A. D.; Dhinojwala, A. *Phys. Rev. Lett*. **2000**, *85*, 3854.

55. Briggman, K. A.; Stephenson, J. C.; Wallace, W. E.; Richter, L. J. *J. Phys. Chem. B* **2001**, *105*, 2785.

56. Varsanyi, G. Vibrational spectra of benzene derivatives; Academic Press: New York and London, 1969.

57. Varsanyi, G. Assignments for Vibrational Spectra of Seven Hundred Benzene Derivatives, Vol. 1; Halsted Press: New York, 1974.

58. Duffy, D. C.; Davies, P. B.; Bain, C. D. *J. Phys. Chem*. **1995**, *99*, 15241.

CHAPTER 3

X-RAY PHOTOELECTRON SPECTROSCOPY STUDY OF COUNTER-ION INCORPORATION IN POLY(3,4-ETHYLENEDIOXYTHIOPHENE) (PEDOT)

3.1 Introduction

PEDOT is a highly conductive polymer. PEDOT conductivity varies with the type of polymerization and dopants used, for example conductivities of ~300 S/cm[1] and ~100 S/cm[13] have been found for the chemically polymerized and organic chemical vapor deposited versions respectively. For electrochemical polymerization, PEDOT can also be doped with other counter-ions.[1,14] The incorporation of counter-ions into PEDOT affects both the polymer surface morphology and electrical properties of the PEDOT polymer film. Therefore, studying the process of counter-ion incorporation can greatly improve basic understanding of these film properties. Of particular interest is the electrochemical polymerization of 3,4-ethylenedioxythiophene (EDOT) in phosphate buffer solution (PBS). PBS is a common biological buffer, and is required for the incorporation of biological components for applications such as biosensors[8-12] and implant coatings.[2] Understanding PEDOT counter-ion incorporation in PBS is therefore a prerequisite for the incorporation of biological components into PEDOT.

The counter-ions used in this research include the poly-anion poly(sodium 4-styrenesulfonate) (PSSNa), lithium perchlorate ($LiClO_4$), sodium chloride (NaCl),

sodium phosphate monobasic monohydrate (NaH_2PO_4 H_2O), and ions in phosphate buffer solution (PBS) (including KH_2PO_4, NaCl, and Na_2HPO_4). X-ray photoelectron spectroscopy (XPS) is an ultra-high vacuum, surface sensitive technique[15-18] which was used to investigate the differences in binding energy as a result of different counter-ion incorporation. Electrochemical impedance spectroscopy, cyclic voltammetry, and scanning electron microscopy were used to supplement the XPS study. Impedance spectroscopy and cyclic voltammetry were used to characterize the film's electrical properties, while scanning electron microscopy was used to investigate the resulting morphology.

Previous XPS studies have been used to deduce how chemical bonding in PEDOT was affected by the presence of various counter-ions. The majority of XPS characterization has been completed on commercially available PEDOT-PSS (Baytron P), which is used extensively in organic electronic devices.[1] The characteristic regions normally used for analysis are the carbon (C 1s), oxygen (O 1s), and sulfur (S 2p) regions.

Initial XPS studies on PEDOT focused on the effect of different dopants on the PEDOT binding energy in an effort to deduce how the counter-ion bound to PEDOT. Chemically polymerized PEDOT, via iron(III) tris-p-toluene sulfonate, was found to have a peak at 289.8 eV in the C 1s region, at 538.4 eV in the O 1s region, and at 168.2 eV in the S 2p region.[19] The PEDOT was then doped with the large polymeric anion PSS^- or the small anion tosylate (p-methyl benzyl sulfonate) (TsO^-). Xing et al. found that the use of counter-ions resulted in PEDOT in the oxidized state, broadening the C 1s peaks. Based upon peak placement, they also found that there could be twice the quantity of

PSS^- present in comparison to TsO^-, which could suggest that the dopant used will affect device performance.

Greczynski et al. examined the effect of counter-ions on PEDOT by studying the dopants poly(4-styrenesulfonic acid) (PSSH) and $PSS^- Na^+$.[20,21] The S 2p spectrum is complicated by the presence of positively charged PEDOT ($PEDOT^+$) which manifests itself in an asymmetric tail at higher binding energies, a general shift to higher binding energies, and broad binding energy distributions, resulting from a positive charge de-localized over multiple and adjacent rings.[20,21]

Zotti et al. conducted a three part study into the doping relationship of PEDOT with counter-ions. The first portion of the Zotti study focused upon whether the polymeric structure of PSS affected the conductivity of the resulting film by analyzing the sulfonate (PSS) to thiophene ring (PEDOT) ratio ($R_{S/T}$) and comparing it to conductivity measurements. In order to accomplish this, toluenesulfonate was used as a monomeric homologue to PSS^-. The conductivity was found to increase with decreasing $R_{S/T}$. PSS was found to have a larger $R_{S/T}$ value and lower conductivity compared to the toluenesulfonate version. Commercially available PEDOT-PSS was also compared to the electrochemically polymerized version. The electrochemically polymerized PEDOT-PSS was found to contain a greater quantity of PEDOT than the chemically polymerized version.[14]

The second and third portions of the Zotti study focused on how different counter-ions dope PEDOT and how this affects the conductivity. From the peak sizes, the relative quantities of the counter-ions were deduced in the second portion. The PSS counter-ion was found to be present in a greater amount than the TosH counter-ion due to

the fact that only half of the PSS can be used to neutralize the PEDOT charge, while the other half can not be eliminated. In contrast, the amount of TosH utilized is only that which is needed to neutralize the PEDOT.[14,22] PEDOT-TosH was found to have higher conductivity then PEDOT-PSS due to the decrease in electron hopping distance. PSS increases the electron hopping distance leading to a decrease in conductivity. The third portion of the Zotti study assessed the effect of different cation (Na^+ verses H^+) on the poly-anion PSS^- and consequently PEDOT. In terms of conductivity, PSSH was found to be superior to PSS^-Na^+ as well as to dope PEDOT better.[14] The difference in conductivity was a result of an increase the electron hopping distance with sodium, due to its larger size than H^+, thus decreasing the conductivity.

XPS has also been utilized to deduce the chemical binding energies of PEDOT after surface treatments, such as an acid and/or heat treatment of the film.[20,21] The effects of different solvents on PEDOT[23,24] have been studied, as well as PEDOT degradation have also been studied. The degradation studies focused on the atmospheric[22], UV-light[22,25], UV-ozone[26], and electron bombardment degradation mechanisms.[22,27]

In addition to determining information on various counter-ion bonding, surface treatments, and degradation pathways, XPS has also been used to verify the presence of additives within PEDOT or PEDOT derivatives, such as PEDOT/PSS with poly(ethylene glycol)[28], adenosine triphosphate (ATP)[29], gold nanoparticles[30], and PEDOT coated latex spheres.[31] Other studies have focused on PEDOT binding with substrate materials, such as aluminum[32] and indium tin oxide.[33]

This study will build upon previously published work studying the effect of counter-ions on PEDOT. These counter-ions include the poly-anion poly(sodium 4-

styrenesulfonate) (PSSNa), lithium perchlorate ($LiClO_4$), sodium chloride (NaCl), sodium phosphate monobasic monohydrate (NaH_2PO_4 H_2O), and ions present in phosphate buffer solution (PBS). The question of given a mixture of counter-ions which counter-ion(s) will preferentially bind with PEDOT will also be investigated. Understanding if and how counter-ions are incorporated into PEDOT in the presence of PBS is important, for future studies into PEDOT electrochemically polymerized in the presence of mixtures of ions and biological media.

3.2 Experimental Methods

3.2.1 Chemicals

The monomer, 3,4-ethylenedioxythiophene (EDOT), and the commercially available PEDOT-PSS blend (Baytron P) were obtained from H.C. Starck. Lithium perchlorate, sodium chloride, sodium phosphate monobasic monohydrate, poly(4-styrenesulfonic acid), sodium p-toluenesulfonate, and iron (III) chloride were obtained from Sigma-Aldrich. Commercially available ethanol (Pharmco Products Inc.) and poly(sodium 4-styrenesulfonate) (Acros Organics) were obtained. These chemicals were all used as received. Phosphate buffer solution (10x concentration), containing KH_2PO_4, NaCl, and Na_2HPO_4, was obtained from Hyclone and then diluted to a 1x concentration (0.15 M NaCl, 0.0057 M NaH_2PO_4, and 0.001 M KH_2PO_4).

3.2.2 Chemical and Electrochemical Polymerization

The chemical polymerization of PEDOT was carried out in ethanol according to the procedure described by Hong et al..[34] PEDOT electrochemical polymerization was

performed using galvanostatic current from a 0.01M EDOT aqueous solution with various counter-ions. The XPS samples were deposited on Au/Pd sputter-coated barbell shaped electrodes (6 mm diameter) on polystyrene (PS) cover slips at 135 μA for 10 minutes. All samples were either polymerized in de-ionized water or 1x PBS solution with 0.01 M counter-ion concentration present. The samples were then rinsed in de-ionized water to remove excess counter-ion from the surface and allowed to air dry. Additional rinsing was not found to alter the quantity of incorporated counter-ion noticeably. Electrochemical impedance spectroscopy and cyclic voltammetry samples were deposited using a current of 10 μA for 180 seconds on lab fabricated 90/10 platinum/iridium cochlear ball electrodes (diameter = 500 μm). XPS reference samples of PSSH, $LiClO_4$, NaCl, NaH_2PO_4 H_2O, PBS, and Baytron P were deposited from aqueous solution onto Au/Pd barbell electrodes and allowed to air dry. The PSSNa reference samples were used in their powdered form.

3.2.3 X-Ray Photoelectron Spectroscopy

Initial survey scans were run using pass energy of 160 eV, while characteristic region scans of the C 1s, O 1s, S 2p, Cl 2p, and P 2p utilized pass energy of 20 eV with a step 0.1 eV. All spectra were referenced using the C-C/C-H peak at 285 eV.

3.2.4 Electrochemical Impedance Spectroscopy and Cyclic Voltammetry

The impedance range was 1-100,000 Hz while a range of -0.8 V to +1.0 V was used for CV at a scan rate of 0.1 V/s for three cycles.

3.2.5 Scanning Electron Microscopy

SEM samples were deposited following the same procedure as the XPS samples and were then gold coated. A FEI Nova Nanolab Dualbeam Focused Ion Beam and Scanning Electron Microscope was used for imaging with an accelerating voltage of 5 kV.

3.3 Results and Discussion

One of the questions that arises when doping PEDOT is when given a mixture of different ions, which one(s) will act as the counter-ion(s)? A significant portion of the existing XPS studies on PEDOT focus on either chemically produced or electrochemically polymerized PEDOT-PSS due to its extensive use in the organic electronics industry. Other studies have been done using other counter-ions such as perchlorate[14] and tosylate derivatives[14,19,22] as a comparison to PEDOT-PSS in an effort to deduce the electronic structure of PEDOT as a result of incorporating different counter-ions.

This study focused on the counter-ions poly(sodium 4-styrenesulfonate) (PSS), lithium perchlorate ($LiClO_4$), and the ions present in phosphate buffer solution (PBS). The importance of PEDOT-PBS lies in the need to use a phosphate buffer solution environment when incorporating biological molecules into PEDOT. For example, PEDOT can be used as a coating for brain stimulation and recording electrodes.[3,35] Consequently, an understanding of basic counter-ion incorporation must be achieved before the biological incorporated components may be understood.

XPS survey scans for all the samples were taken (not shown) as well as characteristic core region scans. As expected, carbon, oxygen, and sulfur peaks, as well as chlorine and phosphorus where applicable, were present. Interestingly, characteristic nitrogen peaks were also detected in some samples containing PSS. The N 1s appearance was explained by Crispin et al. as being a result of atmospheric ammonia molecules (NH_3) reacting with water and the sulfonic acid group of PSS to form a hydroxide, which further reacts to form ammonium salts. The formation of ammonium salts further induces desulfonation and thus aging of the PSS, which has been known to occur with exposure to light and heat.[22]

3.3.1 Chemically polymerized PEDOT, Baytron P, and electrochemically polymerized PEDOT-PSS

The C 1s, O 1s, and S 2p regions of chemically polymerized PEDOT, the commercially available PEDOT-PSS blend (Baytron P), and electrochemically polymerized PEDOT-PSS are shown in Figure 3.1. Since the chemical polymerization utilized $FeCl_3$ as the oxidizing agent, chlorine ions acted as the counter-ion to the PEDOT[36], this was confirmed with the presence of a Cl 2p doublet ~198.6 eV and 200.2 eV (not shown).

Chemically polymerized PEDOT contains C-C/C-H (285 eV), C-S (285.3 eV) in the α position, C=C-O (286.3 eV) in the β position, and C-O-C (287 eV) bonding in the ethylene bridge, which were in agreement with values previously reported by Jönsson *et al.*[37] and Gelius *et al.*[38] The carbon spectra, in general, also had an asymmetrical tail that resulted from a combination of $\pi \rightarrow \pi^*$ shake up transition[17,31,39] and possibly positively

polarized or charged carbon.[40-42] The PEDOT characteristic C-O-C (533.4 eV) bonding was present in the O 1s region[16] as well as a C-O (532.1 eV) contribution. The PEDOT spin-split sulfur coupling, S $2p_{3/2}$ (164 eV) and S $2p_{1/2}$ (165.1 eV) with a corresponding 1.18 eV separation[43], also had a higher energy broad tail originating from positively charged sulfur within the thiophene ring (delocalization of π electrons).[14,20,21,40] This asymmetric tail was present in all S 2p regions for all combinations of PEDOT-counter-ion.

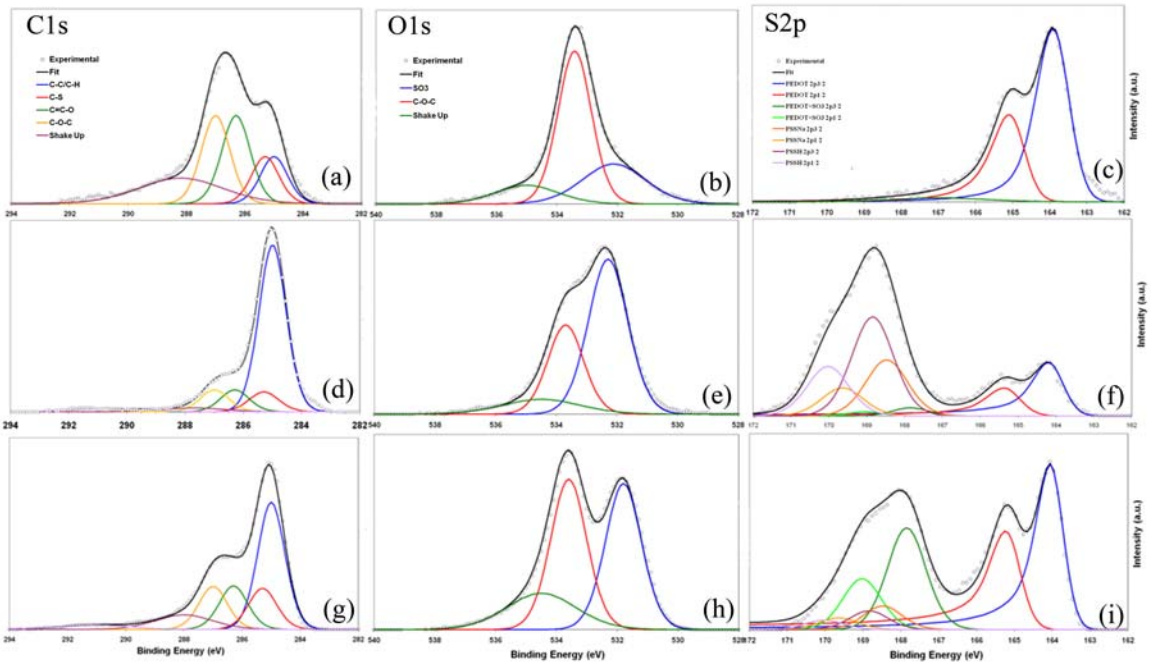

Figure 3.1 C 1s , O1s, and S 2p characteristic regions for chemically polymerized PEDOT (a-c), Baytron P (d-f), and electrochemically polymerized PEDOT-PSS (g-i).

Previous studies have compared electrochemically polymerized PEDOT-PSS and Baytron P (which is known to contain an excess of PSS)[14], as part of this study these samples were analyzed as a comparative basis for other counter-ions. It has been reported that Baytron P contains two PSS based contributions in the form of PSSH and

PSSNa.[20,21] The two PSS contributions usually result from direct PSSNa doping and the dissociation of PSSNa in water taking the proton, H^+, given off by EDOT during polymerization to ultimately act as the counter-ion to PSS forming PSSH.[14] The characteristic S 2p and O 1s binding energies for PSSH and PSSNa vary slightly. In the S 2p region, both PSS types have a sulfur doublet with PSSNa S $2p_{3/2}$ occurring 0.4 eV lower than PSSH and in the O 1s region PSSH has two oxygen contributions (hydroxyl and sulfonic acid), whereas PSSNa only has the sulfonic acid contribution.[20,21] Baytron P was found to have excessive PSS character based on a shift to higher binding energies in the sulfonate region- these peaks shifted towards 168.23 eV (SO_3^- $2p_{3/2}$)[15], the value characteristic of pure PSSNa rather than of PSS bound to PEDOT.[20,21] PSS incorporation also resulted in PEDOT S 2p doublet shift to slightly higher binding energies, likely due to the electronegativity of the oxygen in PSS[44], while the effect of PEDOT on the PSS caused a shift to lower binding energies.[14]

The Baytron P and electrochemically polymerized PEDOT-PSS samples, Figure 3.1, contain C-C/C-H bonds (285 eV) and C-S (285.3 eV) from both PEDOT and PSS, and C=C-O (286.3 eV) and C-O-C (287 eV) from PEDOT. The S 2p peak position for PSS varies depending upon how the PEDOT was deposited. The S 2p binding energy for PSSNa and PSSH was similar to the PSS found in Baytron P (due to the significant excess of PSS), but the binding energy was not the same as PSS in electrochemically polymerized PEDOT-PSS.

The O 1s region, Figure 3.1, contains the C-O-C (PEDOT) and SO_3^- (PSS) contributions. The greater relative intensity of C-O-C bonding in comparison to that of SO_3 bonding indicates that the electrochemically polymerized version of PEDOT-PSS

had a greater relative amount of PEDOT present than in Baytron P. Further indications of PEDOT quantity were observed in the S 2p region where the thiophene to sulfonate signal intensity ratio was much greater than found in Baytron P which was in agreement with Zotti *et al*.[14] In terms of the Baytron P and electrochemically polymerized PEDOT, the amount of PSS present was directly caused by the method of polymerization. PEDOT was polymerized in a bath of excess PSS to create a water soluble suspension, whereas the electrochemically polymerized PEDOT-PSS was a film with no need for excess PSS to create a suspension. The greater the amount of PEDOT in the electrochemical version was a direct result of how it was polymerized.

Ultimately, the addition of PSS, in both Baytron P and electrochemically polymerized PEDOT-PSS, when compared to chemically polymerized PEDOT, resulted in an increase of C-C/C-H bonding in the C 1s, the addition of an SO_3 peak in the O 1s, and for the PEDOT S 2p doublet shift to slightly higher binding energies.

3.3.2 PEDOT-$LiClO_4$

Due to the use of PSS in commercially obtained Baytron P, PSS is probably the most common dopant for PEDOT. One of this study's objectives was to study small anion counter-ions in PBS. Hence another known small anion, lithium perchlorate[14], was utilized for the purpose of comparison to both PSS and PBS. Figure 3.2 displays the C 1s, O 1s, S 2p, and Cl 2p regions for PEDOT-$LiClO_4$. In the C 1s region, C-C/C-H, C-S, C=C-O, and C-O-C peaks were present at 285 eV, 285.3 eV, 286.2 eV and 286.9 eV respectively. The sulfur spin-split peaks from PEDOT occurred at 163.9 eV (S $2p_{3/2}$) and 165.1 eV (S $2p_{1/2}$) with the tail attributed to positively charged sulfur. The Cl 2p range

shows the perchlorate characteristic spin-split peaks at 207.4 eV (Cl $2p_{3/2}$) and 209 eV (Cl $2p_{1/2}$) with a 1.6 eV separation.[43]

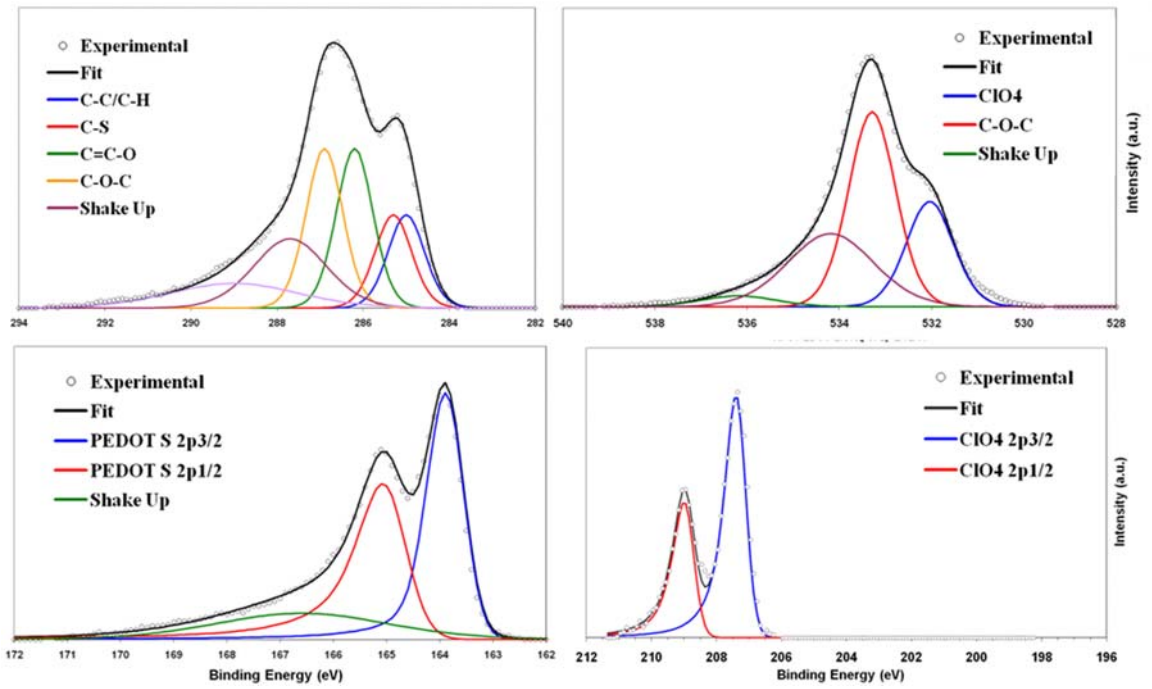

Figure 3.2 C 1s (top left), O1s (top right), S 2p (bottom left), and Cl 2p (bottom right) characteristic regions for PEDOT-$LiClO_4$.

The PEDOT-$LiClO_4$ points of interest lie in the O 1s and Cl 2p characteristic regions. There were two major peaks present in the O 1s region: while one at 533.3 eV is the expected contribution from the PEDOT C-O-C bonding, the other at 531.9 eV, can be attributed to the ClO_4^-counter-ion.[40] When ClO_4^- binds to $PEDOT^+$, it causes the ClO_4^- characteristic oxygen peak to shift from 533.6 eV[45] to a lower energy, at 531.9 eV. The second point of interest was the perchlorate Cl $2p_{3/2}$ appearing at a lower binding energy, 207.9 eV, versus that of lithium perchlorate at ~209 eV[45] again this was the result of PEDOT interactions with the ClO_4^- anion. Similarly to sulfur, chlorine also has an

asymmetric tail toward higher binding energies probably caused by chlorine charging effects as a result of the positively charged sulfur within the thiophene ring.[40]

3.3.3 PEDOT-PBS vs. PEDOT-NaCl vs. PEDOT-NaH_2PO_4

As mentioned above, understanding PEDOT counter-ion incorporation in PBS is a prerequisite for the future incorporation of biological components into PEDOT. Phosphate buffer solution is a common biological buffer used during the incorporation of biological components for applications such as biosensors and implant coatings. PEDOT-PBS was deposited by electrochemically polymerizing EDOT in a bath of 1x phosphate buffer solution (PBS). Ions from the PBS solution (0.001M KH_2PO_4, 0.15M NaCl, and 0.0057M Na_2HPO_4) can act as counter-ions during PEDOT polymerization. The question becomes which of the anion(s), Cl^-, $H_2PO_4^-$, or HPO_4^{2-} present in PBS, act as the counter-ion? To answer this, PEDOT-NaCl and PEDOT-NaH_2PO_4 were also electrochemically polymerized in NaCl and NaH_2PO_4 solutions respectively.

As expected, the C 1s and S 2p regions for PEDOT-PBS, Figure 3.3, only showed PEDOT C-C/C-H (285 eV), C-S (285.3 eV), C=C-O (286.3 eV), C-O-C (287 eV), S $2p_{3/2}$ (163.9 eV) and S $2p_{1/2}$ (165.1 eV) contributions. Similar to PEDOT-$LiClO_4$, the higher energy tail could have been caused by partially charged or positively polarized carbon[40-42] along with $\pi \rightarrow \pi^*$ shake up in the case of PEDOT-PBS, while PEDOT-NaCl and PEDOT-NaH_2PO_4 samples also had an additional chemical oxidation contribution as confirmed by the presence of minute quantities of SO_2 in the S 2p region.

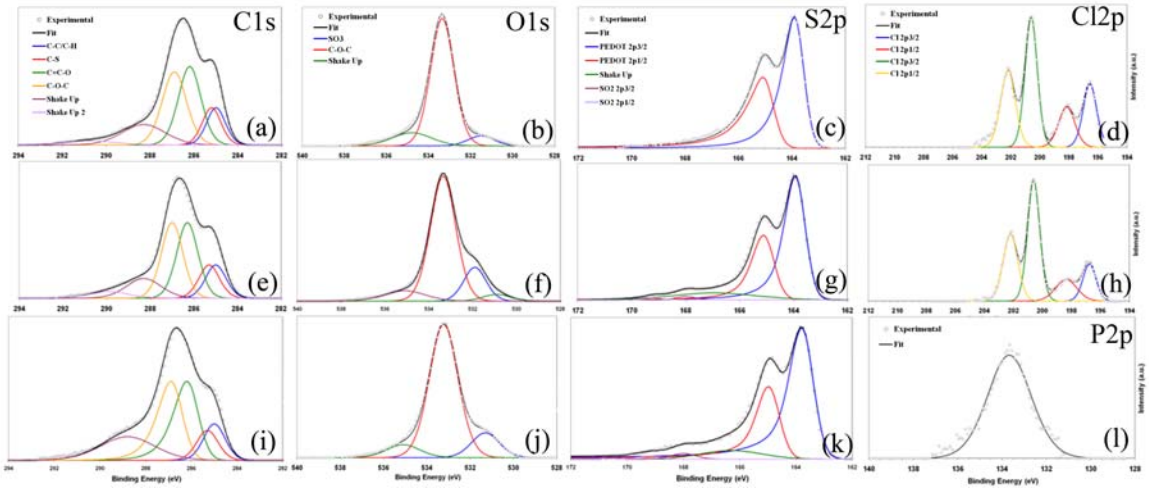

Figure 3.3 C 1s, O1s, S 2p, Cl 2p, and P 2p characteristic regions for PEDOT-PBS (a-d), PEDOT-NaCl (e-h), and PEDOT-NaH_2PO_4 H_2O (i-l) spectra.

The PEDOT-PBS, PEDOT-NaCl, and PEDOT-NaH_2PO_4 O1s regions contained the characteristic PEDOT C-O-C binding energy at 533.4 eV. In addition to the C-O-C peak present, in both the PEDOT-NaCl and PEDOT-NaH_2PO_4 samples another C-O contribution at lower binding energies was also present, Figures 3.3f and 3.3j. In the case of PEDOT-NaH_2PO_4 this contribution was from $H_2PO_4^-$ acting as the counter-ion and sulfon induced by slight oxidation.[25,26,46] Further evidence of phosphate incorporation, in the PEDOT-NaH_2PO_4 sample, came in both the appearance of phosphate in the survey spectrum (not shown) and in the shift in P 2p binding energies from about the 134 eV range to 133.7 eV caused by $H_2PO_4^-$ acting as a counter-ion to PEDOT. The C-O contribution in PEDOT-NaCl was a result of oxygen contamination in NaCl[47] and a sulfon contribution from PEDOT degradation as seen in the S 2p region.[25,26,46]

The appearance of Cl 2p peaks and the lack of significant P 2p in the PEDOT-PBS survey data (not shown) indicated that Cl^- anions were acting as the counter-ion to PEDOT. Characteristic Cl 2p regions from PEDOT-NaCl were used in comparison to the PEDOT-PBS in order to prove that Cl^- acted as the counter-ion. PEDOT-PBS has two Cl 2p doublets at 200.6 eV (Cl $2p_{3/2}$) and 202.2 eV (Cl $2p_{1/2}$) as well as contributions at 196.5 eV (Cl $2p_{3/2}$) and 198.1 eV (Cl $2p_{1/2}$). The PEDOT-NaCl Cl 2p region, Figure 3.3h, showed similar results to those of PEDOT-PBS with a characteristic spin-split doublet at 200.6 eV (Cl $2p_{3/2}$) and 202.2 eV (Cl $2p_{1/2}$) resulting from chloride contributions interacting with PEDOT's thiophene ring and other chlorine contributions, 196.8 eV (Cl $2p_{3/2}$) and 198.4 eV (Cl $2p_{1/2}$) at a lower binding energy attributed to Cl^-.[48] As seen previously, PEDOT bonding to Cl^- did cause shifts in binding energies from about 198.4 eV[45,47] to 200.6 eV. The correspondence between the Cl 2p peak positions in PEDOT-PBS and PEDOT-NaCl indicated that the primary anion source in PBS was NaCl.

3.3.4 Mixtures

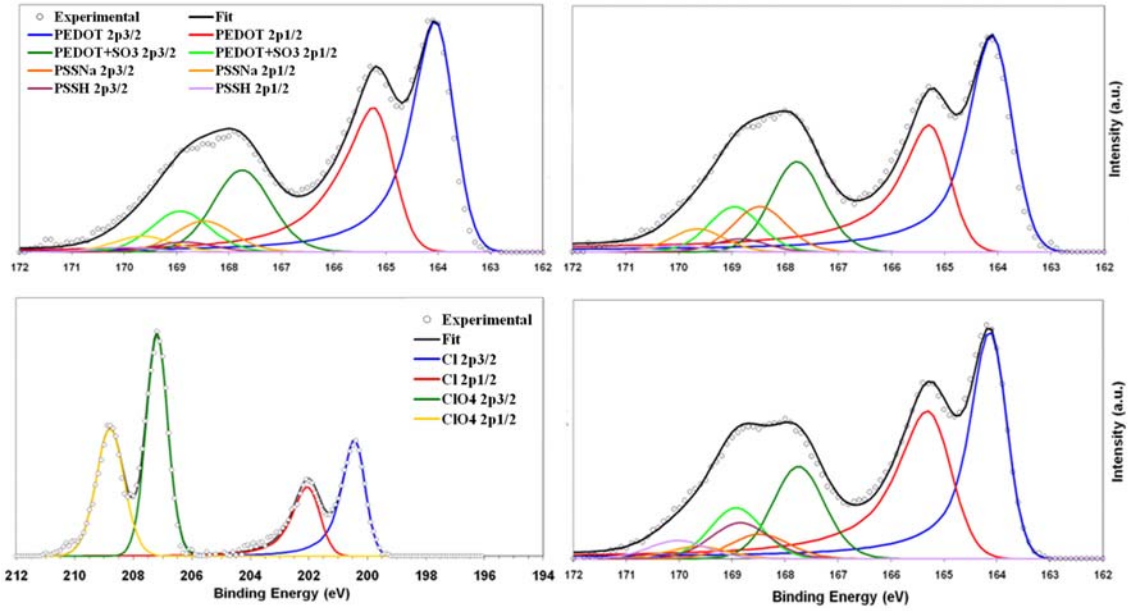

Figure 3.4 S 2p for PEDOT-PSS-$LiClO_4$ (top left), S 2p for PEDOT-PBS-PSS (top right), S 2p for PEDOT-PBS-$LiClO_4$ (bottom left), and Cl 2p for PEDOT-PBS-PSS-$LiClO_4$ (bottom right) characteristic spectra.

3.3.4.1 PEDOT-$LiClO_4$ vs. PEDOT-PSS

Different counter-ions have had different tendencies to incorporate into PEDOT as shown previously in the PBS case. In this section, the two best known and characterized counter-ions, PSS^- and ClO_4^-, were compared. Electrochemically polymerized PEDOT was polymerized in the presence of an equal amount of PSS^- and ClO_4^-. The resulting chemical bonding of the film was predominately characteristic of the PEDOT-PSS doping pathway, rather than doping with ClO_4^- (Figure 3.4). This can be seen from SO_3^- peaks in both the O 1s and S 2p regions. Trace amounts of perchlorate

were also detected in the survey spectra (not shown), but of insufficient quantities to obtain clear signal above the background. PSS was more likely to act as a counter-ion for PEDOT due to its poly-anionic nature: once one negative PSS^- site binds to $PEDOT^+$, the entire polymeric chain was attached as well, thus resulting in PSS signal. Since the poly-anionic chain was already attached to one site, the PSS can then quench the rest of the $PEDOT^+$ sites, resulting in blocking the anionic ClO_4^- from accessing PEDOT. This was confirmed by substituting sodium p-toluenesulfonate (TosNa) for PSS. The TosNa did not act as the counter-ion in all the mixture cases suggesting that the reason for the PSS acting as the counter-ion was due to the polymeric nature of PSS and not the SO_3^- group solely.

3.3.4.2 PEDOT-PBS vs. PEDOT-PSS

Since PSS was more likely to act as a counter-ion to PEDOT than ClO_4^-, will PSS also act as the counter-ion in a PBS-PSS mixture? As can be seen in Figure 3.4, the presence of an SO_3^- doublet in the S 2p region, clearly show that the PEDOT-PBS-PSS system, takes on primarily the character of PEDOT-PSS, rather than that of PEDOT-PBS. As with PEDOT-PSS-$LiClO_4$, the survey spectra does show a small amount of chlorine, which could be from either small amounts of Cl^- acting as counter-ions or chlorine trapped within the PEDOT-PBS-PSS structure. Once again, the poly-anionic nature of PSS lead to this being the preferred counter-ion even in the presence of PBS.

3.3.4.3 PEDOT-$LiClO_4$ vs. PEDOT-PBS

With the absence of poly-anionic PSS in the mixture, which ion(s), ClO_4^- or Cl^-, will act as counter-ion(s) to PEDOT? The C 1s and S 2p spectra for PEDOT-PBS-$LiClO_4$, Figure 3.4, were as expected since the peaks in these regions are solely attributed to PEDOT. The oxygen (not shown) and chlorine regions are where the differentiation can be drawn between the different counter-ions. The O 1s region contains two peaks, the PEDOT C-O-C and a C-O contribution. Since Cl^- from NaCl lacks a significant oxygen presence, the C-O contribution suggests that ClO_4^- acts as the counter-ion to PEDOT. Interestingly the chlorine spectra, Figure 3.4, from the mixture exhibited the presence of both the ClO_4^- Cl 2p and Cl^- 2p doublets at 207.2 eV and 208.8 eV and 200.4 eV and 202.1 eV respectively, indicating that both the ClO_4^- and Cl^- acted as counter-ions to PEDOT. Based upon the slightly higher intensity of the ClO_4^- doublet present in the Cl 2p region coupled with the appearance of oxygen in the O 1s region, ClO_4^- was a slightly more effective counter-ion than Cl^- . Taking into account the large concentration difference between NaC1 (0.15M) and ClO_4^- (0.01M) in the solution, it is believed that ClO_4^- more likely to act as a counter-ion in comparison to Cl^-. The weak hydration of ClO_4^- in the aqueous deposition solution, in comparison to Cl^- anions, might have caused the increase in ClO_4^- quantity.[49] According to the Hofmeister series,[49] the weaker hydration of ClO_4^- may enable it to interact with PEDOT more strongly in the solution, acting as the counter-ion during the electrochemical polymerization process more easily.

3.3.4.4 PSS vs. ClO_4^- vs. PBS

Is PSS still the dominant counter-ion when PEDOT is electrochemically polymerized in a mixture of PSS, PBS, and $LiClO_4$? As shown in Figure 3.4, the PEDOT-PBS-PSS-$LiClO_4$ mixture follows the PEDOT-PSS trends in all three characteristic regions with increased quantities of C-C/C-H and the appearance of SO_3^- peaks in both the O 1s and S 2p regions (Figure 3.4). Again, the survey spectra showed small amounts of chlorine.

3.3.5 General Characterization

3.3.5.1 Electrical Properties

Electrochemical impedance spectroscopy and cyclic voltammetry were used to characterize the electrical properties of the major types of films, PEDOT-PSS, PEDOT-$LiClO_4$, PEDOT-PBS, PEDOT-NaCl, and PEDOT-NaH_2PO_4 (Figure 3.5). PEDOT coatings have been known to lower impedance by as much as 1-2 orders of magnitude in the frequency range of 0.01-100 Hz in comparison to the bare electrode.[3,50,51] The impedance data ($|Z|$) , Figure 3.5, clearly shows the higher and more variable values for PEDOT-PBS in comparison to the lower, more consistent PEDOT-PSS and PEDOT-$LiClO_4$ values. The larger phase angle values suggests that PEDOT-PBS takes on more capacitive characteristics[35] at frequencies greater than 10 Hz in comparison to PEDOT-PSS and PEDOT-$LiClO_4$, while the reverse can be suggested at frequencies lower than 10 Hz. CV was used to compare the charge transfer capacity of the PEDOT films. As can be seen in Figure 3.5, the charge transfer capacity, defined as the area within the curve,

does not alter significantly for PEDOT-PSS and PEDOT-$LiClO_4$, whereas there was a decrease in charge transfer capacity for the PEDOT-PBS films.

The variation in the impedance and phase angle data for PEDOT-PBS, PEDOT-NaCl, and PEDOT-NaH_2PO_4 samples (large error bars) is probably a result of the film's instability. The PEDOT-PBS data follows the trends exhibited by PEDOT-NaCl both in EIS and CV results in comparison to the results from PEDOT-NaH_2PO_4. PEDOT-NaH_2PO_4, Figure 3.5, had a larger charge capacity than both PEDOT-PBS and PEDOT-NaCl. The charge capacities for PEDOT-PBS and PEDOT-NaCl were similar, offering further proof that Cl^- acted as the counter-ion to PEDOT as predicted with the XPS data.

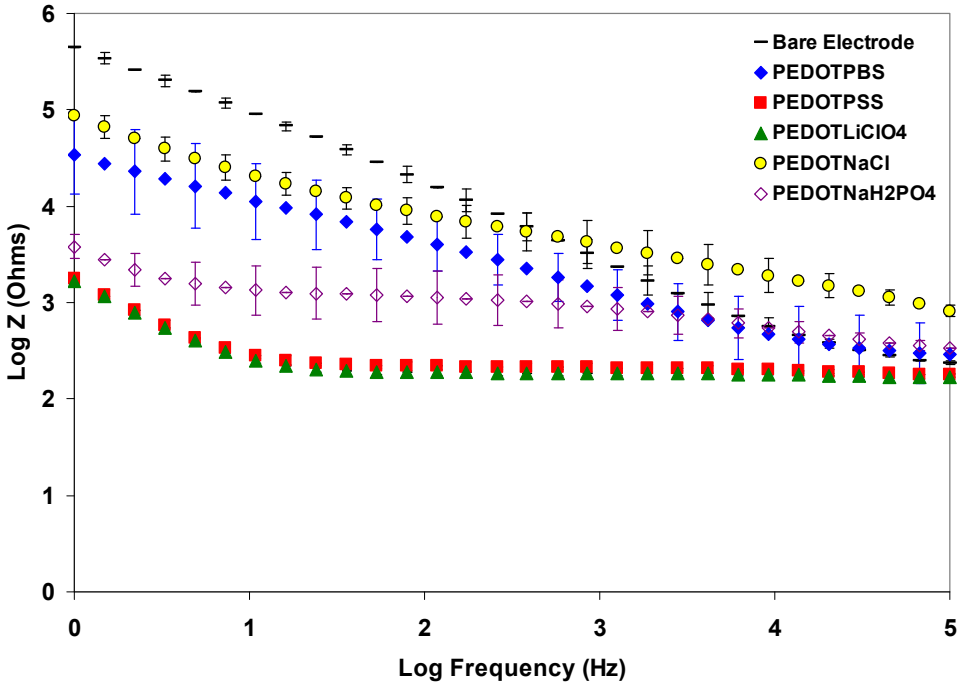

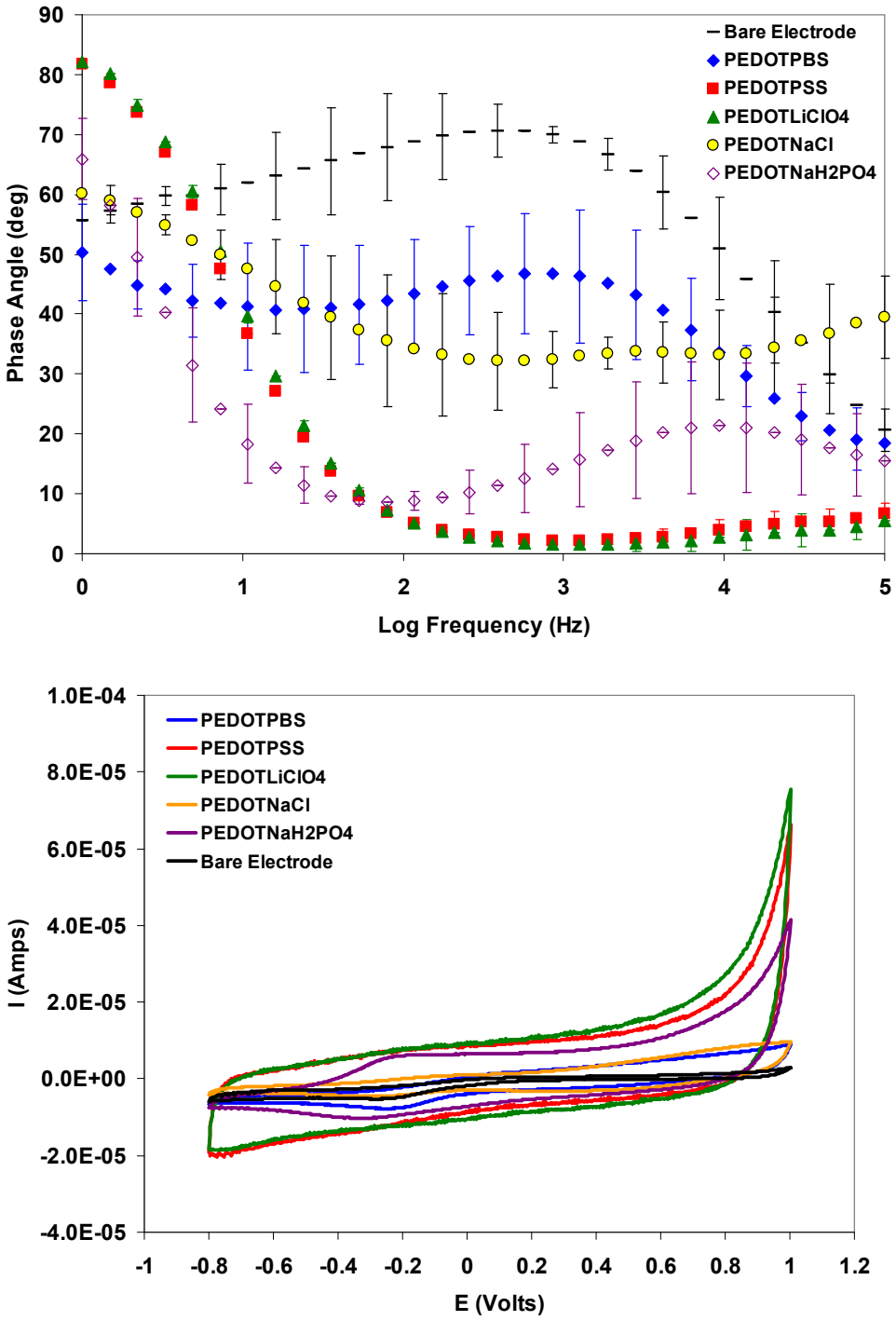

Figure 3.5 (Top) Impedance, (Middle) Phase Angle, and (Bottom) Cyclic voltammetry of PEDOT-PBS, PEDOT-PSS, PEDOT-$LiClO_4$, PEDOT-NaCl, and PEDOT-NaH_2PO_4

3.3.5.2 Scanning Electron Microscopy

Scanning electron micrographs, Figure 3.6, were also taken of PEDOT-PBS, PEDOT-NaCl, and PEDOT-NaH_2PO_4 in order to compare the resulting film's morphology. All three small anion types of PEDOT have a rough morphology with holes in the films. Both PEDOT-PBS and PEDOT-NaCl have large features with rough textures in comparison to the small, globular structures observed with PEDOT-NaH_2PO_4 films. This morphology observation reinforces the conclusion that NaCl within PBS acts as the counter-ion to PEDOT-PBS.

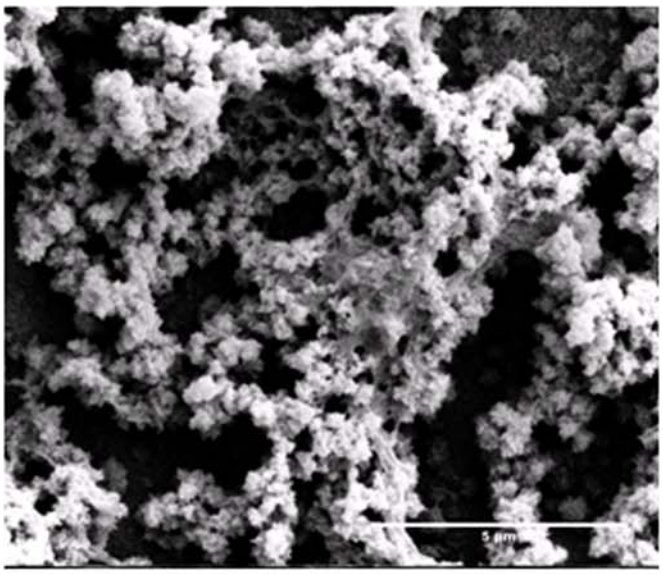
5 µm

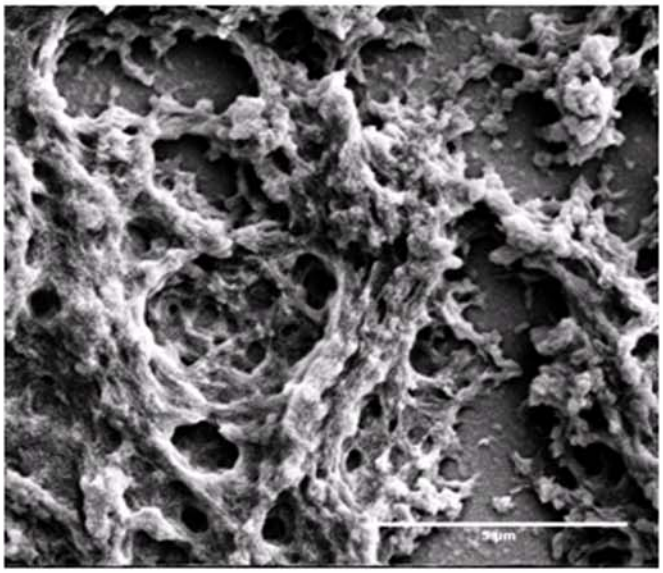
5µm

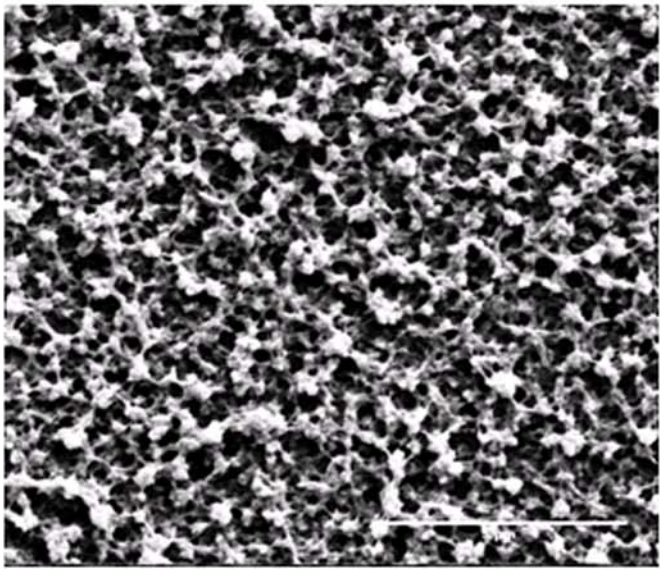

Figure 3.6 Scanning electron micrographs of (Top) PEDOT-PBS, (Middle) PEDOT-NaCl, and (Bottom) PEDOT-NaH_2PO_4. Scale bar equals 5 μm.

3.4 Conclusions

Previous studies had suggested that the electrochemically polymerized version of PEDOT-PSS had a greater relative amount of PEDOT present than in Baytron P. This was confirmed in this study by the greater quantities of C-O-C bonding in both the C 1s and O 1s regions coupled with the stronger PEDOT sulfur doublet in comparison to the SO_3 doublet.

Results from counter-ion mixtures study yielded PEDOT had an increased affinity for PSS than small anions. PSS was more likely to act as a counter-ion for PEDOT due to its poly-anionic nature. Since once poly-anionic chain is attached to one site, the PSS can then quench the rest of the $PEDOT^+$ sites resulting in blocking the smaller anionic ClO_4^- and Cl^- from quenching PEDOT. This has been confirmed by a control experiment substituting TosNa for PSS in the mixture to study counter-ion incorporation. The TosNa did not act as the counter-ion in all the mixture cases suggesting that the reason for the PSS acting as the counter-ion was due to the polymeric nature of PSS and not the SO_3^- group solely.

XPS results, coupled with EIS and SEM results, indicate that the primary counter-ion anion source in PBS was from the NaCl during PEDOT electrochemical polymerization. Understanding if and how counter-ions incorporate into PEDOT is important, especially in the presence of PBS, for future studies into PEDOT electrochemically polymerized in the presence of mixtures of ions and biological media.

3.5 References

1. Groenendaal, L.; Jonas, F.; Freitag, D.; Pielartzik, H.; Reynolds, J.R. *Adv. Mater.* **2000**, *12*, 481.

2. Kim, D.H.; Richardson-Burns, S.M.; Hendricks, J.L.; Sequera, C.; Martin, D.C. *Adv. Funct. Mater.* **2007**, *17*, 79.

3. Richardson-Burns, S.M.; Hendricks, J.L.; Foster, B.; Povlich, L.K.; Kim, D.H.; Martin, D.C. *Biomaterials* **2007**, *28*, 1539.

4. Barisci, J.N.; Hughes, D.; Minett, A.;G.G. Wallace, G.G. *Anal. Chim. Acta* **1998**, *371*, 39.

5. Campbell, T.E.; Hodgson, A.J.;Wallace, G.G. *Electroanalysis* **1999**, *11*, 215.

6. Gooding, J.J.; Wasiowych, C.; Barnett, D.; Hibbert, D.B.; Barisci, J.N.; Wallace, G.G. *Biosens. Bioelectron.* **2004**, *20*, 260.

7. Richardson, R. T.; Thompson, B.; Moulton, S.; Newbold, C.; Lum, M.G.; Cameron, A.; Wallace, G.; Kapsa, R.; Clark, G.; O'Leary, S. *Biomaterials* **2007**, *28*, 513.

8. Fabiano, S.; Minh, C.T.; Piro, B.; Dang, L.A.; Pham, M.C.; Vittori, O. *Mater. Sci. Eng., C* **2002**, *21*, 61.

9. Kros, A.; van Hövell, S.W.F.M.; Sommerdijk, N.A.J.M.; Nolte, R.J.M. *Adv. Mater.* **2001**, *13*, 1555.

10. Nien, P.C.; Tung, T.S.; Ho, K.C. *Electroanalysis* **2006**, *18*, 1408.

11. Piro, B.; Dang, L.A.; Pham, M.C.; Fabiano, S.; Minh, C.T. *J. Electroanal. Chem.* **2001**, *512*, 101.

12. Setti, L.; Fraleoni-Morgera, A.; Ballarin, B.; Filippini, A.; Frascaro, D.; Piana, C. *Biosens. Bioelectron.* **2005**, *20*, 2019.

13. Lock, J.P.; Im, S.G.; Gleason, K.K. *Macromolecules* **2006**, *39*, 5326.

14. Zotti, G.; Zecchin, S.; Schiavon, G.; Louwet, F.; Groenendaal, L.; Crispin, X.; Osikowicz, W.; Salaneck, W.R.; Fahlman, M. *Macromolecules* **2003**, *36*, 3337.

15. Beamson, G.; Briggs, D. *High Resolution XPS of Organic Polymers: The Scienta ESCA300 Database*; John Wiley & Sons: New York, New York, 1992.

16. Briggs, D.; Beamson, G. *Anal. Chem.* **1993**, *65*,1517.

17. Briggs, D. *Surface analysis of polymers by XPS and static SIMS*; Cambridge University Press: Cambridge, U.K.1998.

18. Siegbahn, K.; Nordling, C.; Fahlman, A.; Nordberg, R.; Hamrin, K.; Hedman, J.; Johansson, G.; Bergmark, T.; Karlsson, S.E.; Lindgren, I.; Lindberg, B. *ESCA: atomic, molecular and solid state structure studied by means of electron spectroscopy.* Uppsala: Uppsala,SWE, 1967.

19. Xing, K.Z.; Fahlman, M.; Chen, X.W.; Inganäs, O.; Salaneck, W.R. *Synth. Met.* **1997**, *89*, 161.

20. Greczynski, G.; Kugler, T.; Salaneck, W.R. *Thin Solid Films* **1999**, *354*, 129.

21. Greczynski, G.; Kugler, T.; Keil, M.; Osikowicz, W.; Fahlman, M.; Salaneck, W.R. *J. Electron Spectrosc. Relat. Phenom.* **2001**, *121*,1.

22. Crispin, X.; Marciniak, S.; Osikowicz, W.; Zotti, G.;Denier van der Gon, A.W.; Louwet, F.; Fahlman, M.; Groenendaal, L.; De Schryver, F.; Salaneck, W.R. *J. Polym. Sci., Part B: Polym. Phys.* **2003**, *41*, 2561.

23. Kim, T.Y.; Kim, J.E.; Suh, K.S. *Polym. Int.* **2006**, *55*, 80.

24. Lee, C.S.; Joo, J.; Han, S.; Koh, S.K. *Sens. Actuators, A* **2005**, *121*, 373.

25. Marciniak, S.; Crispin, X.; Uvdal, K.; Trzcinski, M.; Birgerson, J.; Groenendaal, L.; Louwet, F.; Salaneck, W.R. *Synth. Met.* **2004**, *141*, 67.

26. Tengstedt, C.; Kanciurzewska, A.; de Jong, M.P.; Braun, S.; Salaneck, W.R.; Fahlman, M. *Thin Solid Films* **2006**, *55*, 2085.

27. Denier van der Gon, A.W.; Birgerson, J.; Fahlman, M.; Salaneck, W.R. *Org. Electron.* **2002**, *3*, 111.

28. Wang, T.; Qi, Y.; Xu, J.; Hu, X.; Chen, P. *Appl. Surf. Sci.* **2005,** *250*,188.

29. Paczosa-Bator, B.; Peltonen, J.; Bobacka, J.; Lewenstam, A. *Anal. Chim. Acta* **2006**, *555*, 118.

30. Li, X.; Li, Y.; Tan, Y.; Yang, C.; Li, Y. *J. Phys. Chem. B* **2004**, *108*, 5192.

31. Khan, M.A.; Armes, S.P.; Perruchot, C.; Ouamara, H.; Chehimi, M.M.; Greaves, S.T.; Watts, J.T. *Langmuir* **2000**, *16*, 4171.

32. Jönsson, S.K.M.; Salaneck, W.R.; Fahlman, M. *J. Electron Spectrosc. Relat. Phenom.* **2004**, *137-140*, 805.

33. Nguyen, T.P.; de Vos, S.A. *Appl. Surf. Sci.* **2004**, *221*, 330.

34. Hong, K.H.; Oh, K.W.; Kang, T.K. *J. Appl. Polym. Sci.* **2005**, *97*, 1326.

35. Cui, X.; Hetke, J.K.; Wiler, J.A.; Anderson, D.J.; Martin, D.C. *Sens. Actuators, A* **2001**, *93*, 8.

36. Im, S.G.; Olivetti, E.A.; Gleason, K.K. *Surf. Coat. Technol.* **2007**, *201*, 9406.

37. Jönsson, S.K.M.; de Jong, M.P.; Groenendaal, L.; Salaneck, W.R.; Fahlman, M. *J. Phys. Chem. B* **2003**, *107*, 10793.

38. Gelius, U.; Allan, C.J.; Johansson, G.; Siegbahn, H.; Allison, D.A.; Siegbahn, K. *Phys. Scr.* **1971**, *3*, 237.

39. Jönsson, S.K.M.; Birgerson, J.; Crispin, X.; Greczynski, G.; Osikowicz, W.; Denier van der Gon, A.W.; Salaneck, W.R.; Fahlman, M. *Synth. Met.* **2003**, *139*, 1.

40. Kang, E.T.; Neoh, K.G.; Tan, K.L. *Phys. Rev. B: Condens. Matter Mater. Phys.* **1991**, *44***,** 10 461.

41. Riga, J.; Snauwaert, P.H.; DePryck, A.; Lazzaroni, R.; Boutique, J.P.; Verbist, J.J.; Brédas, J.L.; André, J.M.; Taliani, C. *Synth. Met.* **1987**, *21*, 223.

42. Wu, C.R.; Nilsson, J.O.; Inganäs, O.; Salaneck, W.R.; Österholm, J.E.; Brédas, J.L. *Synth. Met.* **1987**, *21*, 197.

43. Moulder, J.F.; Stickle, W.R.; Sobol, P.E.;K.D. Bomben, K.D. *Handbook of X-ray photoelectron spectroscopy: A reference book of standard spectra for identification and interpretation of XPS data.* Physical Electronics: Eden Prairie, MN, 1992.

44. Briggs, D.; Seah, M.P. *Practical Analysis: Volume 1 Auger and X-ray Photoelectron;* 2nd Ed. John Wiley & Sons: New York, 1990.

45. Morgan , W. E.; Van Wazer, J.R.; Stec, W.J. *J. Am. Chem. Soc.* **1973**, *95*, 751.

46. Heeg, J.; Kramer, C.; Wolter, M.; Michaelis, S.; Plieth, W.; Fischer, W.J. *Appl. Surf. Sci.* **2001**, *180*, 36.

47. Wren, A.G.; Phillips, R.W.; Tolentino, L.U. *J. Colloid Interface Sci.* **1979**, *70*, 544.

48. Kang, E.T.; Neoh, K.G.; Tan, T.C.; Khor, S.H.; Tan, K.L. *Macromolecules* **1990**, *23*, 2918.

49. Zhang, Y.; Cremer, P.S. *Curr. Opin. Chem. Biol*. **2006**, 10, 658.

50. Cui, X.; Martin, D.C. *Sens. Actuators, B* **2003**, *89*, 92.

51. Yang, J.Y.; Martin, D.C. *Sens. Actuators, A* **2004**, *113*, 204.

CHAPTER 4

X-RAY PHOTOELECTRON SPECTROSCOPY STUDY OF COUNTER-ION INCORPORATION IN POLY(3,4-ETHYLENEDIOXYTHIOPHENE) (PEDOT) 2: POLY-ANION EFFECT, TOLUENESULFONATE, AND SMALL ANIONS

4.1 Introduction

Previously we have studied the poly (3,4-ethylenedioxythiophene) (PEDOT) counter-ion incorporation in regards to the small anion mixture found in phosphate buffer solution and the effect of poly-anion mixtures with small anions, here we expand the study into different small anion mixtures as well as different poly-anionic mixtures in an effort to understand how different counter-ions affect both the polymer surface morphology and electrical properties of the PEDOT polymer film.[1,2] As in our previous research[1], X-ray photoelectron spectroscopy (XPS) was used as the chemical characterization technique[3-7] for this research.

As mentioned in the previous chapter, Zotti et al. previously studied the effects of different counter-ions on the electrical conductivity of PEDOT-PSSNa, PEDOT-PSSH, PEDOT-TosNa, and PEDOT-TosH films.[3] PEDOT-TosH was found to have higher conductivity than PEDOT-PSS due to a decrease in electron hopping distance. PSS increases the electron hopping distance leading to a decrease in conductivity. The effect of different cations (Na^+ verses H^+) on the poly-anion PSS^- and consequently on PEDOT conductivity was also studied. PSSH was found to have superior electrical conductivity

and to dope better in comparison to PSSNa.[3] The larger size of Na^+ verses that of H^+ was found to increase the electron hopping distance, thus decreasing the film's conductivity.

In this research, XPS was used to investigate different counter-ions incorporation during PEDOT electrochemical polymerization.

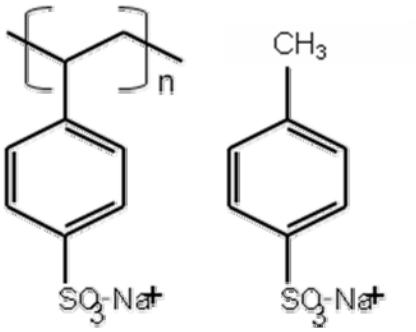

Figure 4.1 (Left) Poly(sodium 4-styrenesulfonate) (PSSNa) (Right) sodium p-toluenesulfonate (TosNa)

Previous research probed chemical composition differences between Baytron P, oxidatively polymerized PEDOT, and electrochemically polymerized PEDOT-PSS, PEDOT-$LiClO_4$, PEDOT-NaCl, PEDOT-NaH_2PO_4, and PEDOT-PBS.[1] In the case of PEDOT-PBS (phosphate buffer solution), the chlorine anion from sodium chloride was found to act as the counter-ion during PEDOT electrochemical polymerization in PBS solution. Results also found that the poly-anion, PSS^-, preferentially incorporated into the PEDOT in comparison to ClO_4^- and Cl^- anions when ion mixtures were used. PSS was believed to be more likely to act as a counter-ion for PEDOT due to its poly-anionic nature, which will be further examined in this study. The motivation driving the previous

research was to understand if and how counter-ions incorporate into PEDOT, especially in the presence of PBS, for future studies into PEDOT electrochemically polymerized in the presence of mixtures of ions and biological media.

In this current research, we continue to apply XPS to examine counter-ion incorporation to electrochemically polymerized PEDOT in a more systematic fashion. The following sections in this chapter are: (1) a study of sodium p-toluenesulfante (TosNa) versus poly (sodium styrenesulfonate) (PSSNa) in the presence of a mixture of small anions, (2) the effect of lithium bromide (LiBr) additions on PEDOT-PSS-LiBr and PEDOT-Poly (acrylic acid)-LiBr films, while (3) focused on PEDOT counter-ion affinity with anions which have a monovalent or divalent charges.

Previous studies examined incorporation of PSS, ions in PBS, and $LiClO_4$ into PEDOT, and found that PEDOT had an increased affinity for PSS over small anions in mixtures of PEDOT-PBS-PSS, PEDOT-PSS-$LiClO_4$, and PEDOT-PBS-PSS-$LiClO_4$.[1] The motivation behind the first section in this study was to understand whether the polymeric nature of PSSNa encourages counter-ion incorporation or whether simply the presence of the SO_3^- caused the dominance of PSSNa over the anions in phosphate buffer solution (PBS) and lithium perchlorate ($LiClO_4$). In order to accomplish this, sodium p-toluenesulfonate (TosNa) was substituted in the place of PSSNa to act as a monomer like version of PSSNa during electrochemical polymerization of PEDOT.[3] Therefore this work is a continuation of previous work in order to help elucidate the mechanisms that govern PEDOT counter-ion incorporation.

The second section is an extension towards understanding polymeric versus small anions as prospective PEDOT counter-ions; in this case LiBr additions were studied with

those already studied in a previous publication.[1] The third section of the study focuses on PEDOT counter-ion affinity of small anions. This section was divided into three sub-studies: the first was a continuation of the TosNa study expanded to include LiBr, the second contained anion mixtures with a monovalent negative charge, while the third focused on anions having divalent negative charges. Now the question becomes, given the same charge and anion concentration, whether there is a certain preferential anion PEDOT counter-ion incorporation affinity over other anions and what force (s) governs this affinity. In order to answer this question, mixtures of 3,4-ethylenedioxythiophene (EDOT) and various counter-ions, 0.01 M concentrations respectively, in de-ionized water were mixed and then electrochemically polymerized.

4.2 Experimental Methods

4.2.1 Chemicals

The monomer, 3,4-ethylenedioxythiophene (EDOT) was obtained from H.C. Starck. Lithium perchlorate ($LiClO_4$), lithium bromide (LiBr), sodium nitrate ($NaNO_3$), sodium thiosulfate ($Na_2S_2O_3$), sodium chloride (NaCl), sodium phosphate monohydrate (NaH_2PO_4 H_2O), sodium phosphate dibasic hepthydrate (Na_2HPO_4 $7H_2O$), sodium acetate trihydrate ($NaC_2H_3O_2$ $3H_2O$), sodium p-toluenesulfonate (TosNa), calcium carbonate ($CaCO_3$), sodium carbonate (Na_2CO_3), and poly (acrylic acid) (PAA) were ordered from Sigma-Aldrich. Poly(sodium 4-styrenesulfonate) (PSSNa) was purchased from Acros Organics. These chemicals were all used as received. Phosphate buffer solution (10x concentration), containing KH_2PO_4, NaCl, and Na_2HPO_4, was acquired

from Hyclone and then diluted to a 1x concentration (0.15 M NaCl, 0.0057 M NaH_2PO_4, and 0.001 M KH_2PO_4).

4.2.2 Electrochemical Polymerization

PEDOT electrochemical polymerization was performed using galvanostatic current from a 0.01M EDOT solution either polymerized in de-ionized water or 1x PBS solution with 0.01 M counter-ion concentration present. The XPS samples were deposited on Au/Pd sputter-coated barbell shaped electrodes (6 mm diameter) on polystyrene (PS) cover slips at 135 μA for 10 minutes. The samples were then rinsed in de-ionized water to remove excess counter-ion from the surface and allowed to air dry. Additional rinsing was not found to alter the quantity of incorporated counter-ion noticeably with the exception of PEDOT-LiBr. For PEDOT-LiBr, after soaking in de-ionized water for 24 hours, the amount of excess Br^- was found to reduce by at least half. XPS reference samples of $LiClO_4$, NaCl, and PBS were deposited from aqueous solution onto Au/Pd barbell electrodes and allowed to air dry. Solid samples, as received, of PSSNa, TosNa, $CaCO_3$, $Na_2S_2O_3$, LiBr, $NaC_2H_3O_2$ $3H_2O$, NaH_2PO_4 H_2O, Na_2HPO_4 $7H_2O$, and $NaNO_3$ were used as reference samples. Samples of PEDOT-TosNa, PEDOT-LiBr, PEDOT-$NaNO_3$, PEDOT-$CaCO_3$, PEDOT-Na_2CO_3, PEDOT-NaCl, PEDOT-$LiClO_4$, PEDOT-Na_2HPO_4, PEDOT-NaH_2PO_4, PEDOT-$Na_2S_2O_3$, and PEDOT-$NaC_2H_3O_2$ were also electrochemically polymerized and studied using XPS, as references for mixture studies.

4.2.3 X-Ray Photoelectron Spectroscopy

Initial survey scans were run using a pass energy of 160 eV, while characteristic region scans for C 1s, O 1s, N 1s, S 2p, Cl 2p, P 2p, and Br 3d were also collected utilized a pass energy of 20 eV with a step of 0.1 eV. All spectra were referenced using the C-C/C-H peak at 285 eV.

4.3 Results/ Discussion

4.3.1 Poly-Anion Effect: TosNa vs. PSSNa

First we hope to understand whether the monomeric version of PSSNa, TosNa, will be the dominant counter-ion when ion mixtures are used while electrochemically polymerizing PEDOT. The concentrations of SO_3^- in the mixtures of TosNa and other ions are the same as those in previous PSSNa mixtures investigated before. Therefore from this study we can understand whether the dominant incorporation of counter-ion PSS into PEDOT in the previous studied mixtures is due to the SO_3^- ions or the PSS polymeric nature.

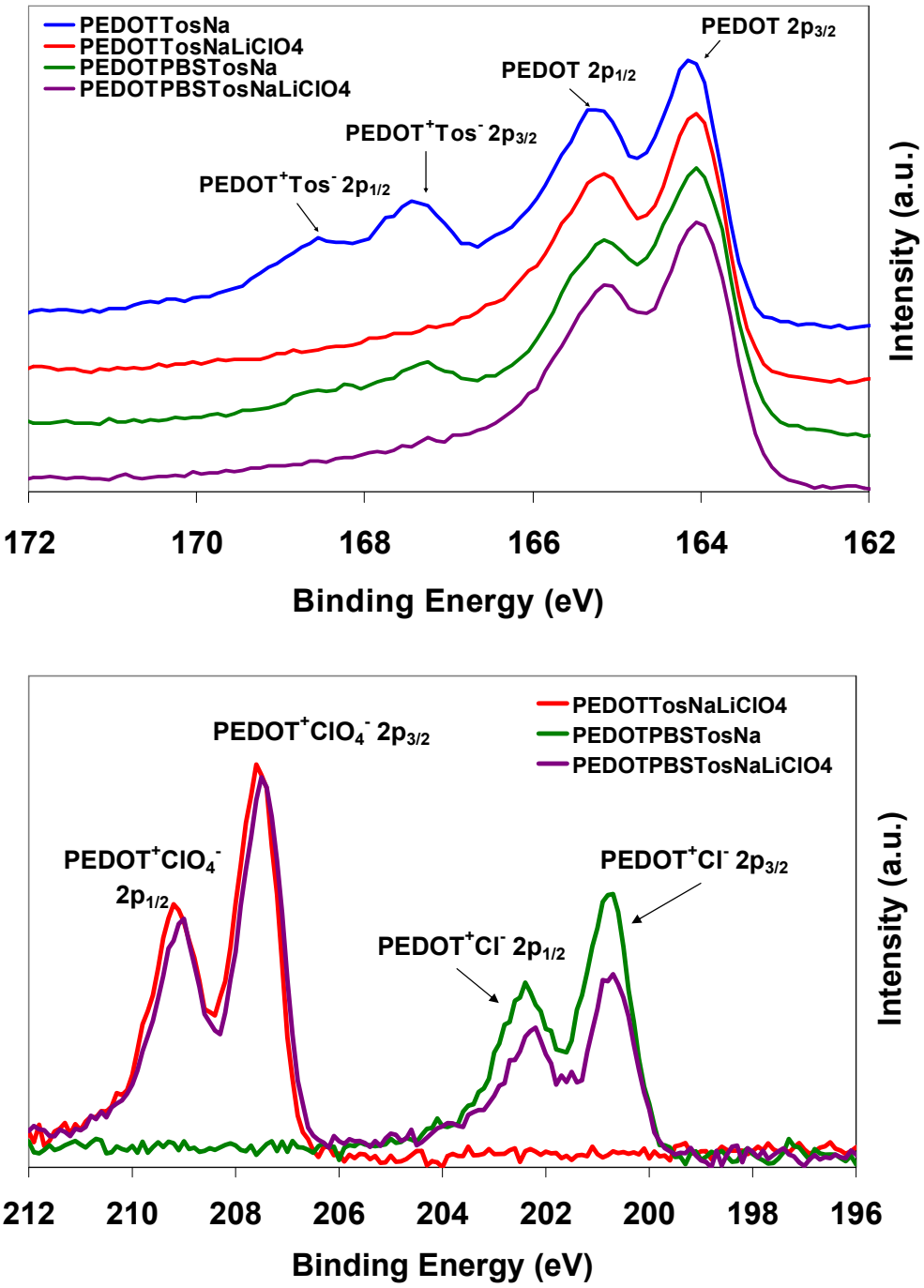

Figure 4.2 (Top) S 2p and (Bottom) Cl 2p characteristic regions for PEDOT-TosNa, PEDOT-TosNa-$LiClO_4$, PEDOT-PBS-TosNa, and PEDOT-PBS-TosNa-$LiClO_4$

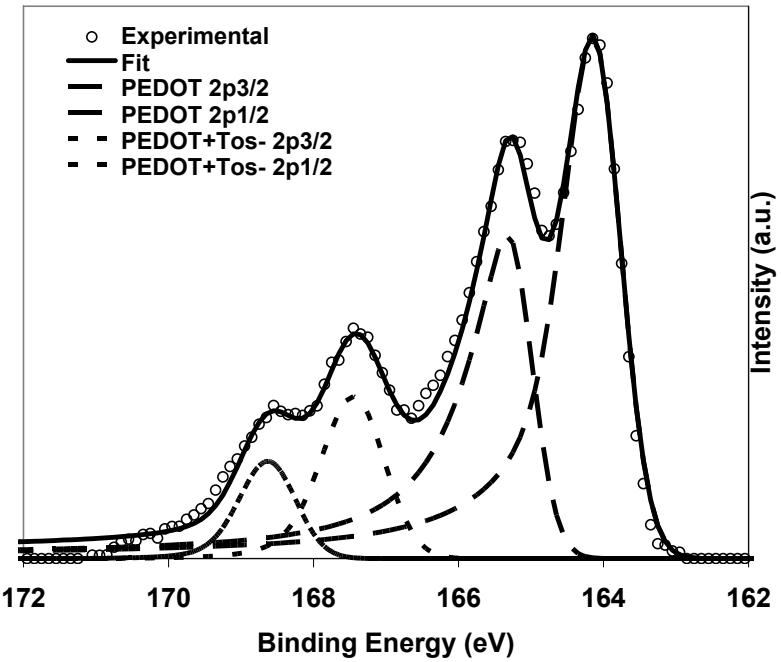

Figure 4.3 S 2p characteristic region for PEDOT-TosNa

Figure 4.2 depicts the characteristic XPS spectra in the S 2p and Cl 2p regions for the TosNa version of PEDOT-PBS-PSS, PEDOT-PSS-$LiClO_4$, and PEDOT-PBS-PSS-$LiClO_4$ found in the previous chapter.[1] The PEDOT spin-split sulfur coupling and $PEDOT^+Tos^-$ contributions were found at S $2p_{3/2}$ (~164.1 eV) and S $2p_{1/2}$ (~165.3 eV) and 167.4 eV and 168.6 eV (Figure 4.3) respectively with a separation between PEDOT $2p_{3/2}$ and $PEDOT^+Tos^-$ $2p_{3/2}$ of ~3.3 eV which roughly matches the results reported by Zotti *et. al.*.[3] All sulfur contributions had a characteristic separation between the $2p_{3/2}$ and $2p_{1/2}$ spin-split doublet of 1.18 eV.[8] The higher energy broad tail originated from positively charged sulfur within the thiophene ring (delocalization of π electrons).[3,9-11] This asymmetric tail was present in all XPS spectra in the S 2p regions for all combinations of PEDOT-counter-ion. Unlike dominant PSS, TosNa contributions were

only observed in PEDOT-PBS-TosNa and no contributions were observed in PEDOT samples when counter-ion solutions containing $LiClO_4$ were used.

In addition to the S 2p region, XPS spectra in the Cl 2p region were also investigated. The XPS spectra in the Cl 2p range show the perchlorate characteristic spin-split peaks at 207.5 eV (Cl $2p_{3/2}$) and 209.1 eV (Cl $2p_{1/2}$)[1] with a 1.6 eV separation.[8] It has been shown that Cl 2p PEDOT-PBS spectra have a $PEDOT^+Cl^-$ doublet at 200.8 eV (Cl $2p_{3/2}$) and 202.4 eV (Cl $2p_{1/2}$).[1] The observations in the XPS spectra in the Cl 2p region as well as the S 2p region discussed above suggest that in terms of PEDOT counter-ion affinity, ClO_4^- was preferable to TosNa, while minor contributions of $PEDOT^+Cl^-$ were also found in the Cl 2p characteristic region. The lack of TosNa dominance, Figure 4.2, in comparison to the PSSNa in comparable mixtures of PEDOT-PBS-PSS, PEDOT-PSS-$LiClO_4$, and PEDOT-PBS-PSS-$LiClO_4$ examined previously[1] indicates that that mechanism for counter-ion affinity was indeed due to the polymeric nature of PSSNa and not just the presence of the SO_3^- charge group that encourages counter-ion incorporation.

4.3.2 LiBr Behavior in Mixtures with Poly-Anions

As mentioned above, previous studies showed that PSS behaves as the dominant counter-ion in the electrochemically polymerized PEDOT when counter-ion mixtures of PSS, ClO_4^- and Cl^- are used. We proposed in the previous chapter (and further confirmed by the comparison on the studies of PSS and Tos here) that PSSNa can block the smaller anions ClO_4^- and Cl^- incorporation to PEDOT since once poly-anionic chain was attached to one site, the PSS can then quench the rest of the $PEDOT^+$ sites.[1] Based upon previous

results, it was expected that Br^-, which is also a small anion, should behave similarly to ClO_4^- and Cl^- when the mixture with PSSNa is used. Therefore, the addition of LiBr into a EDOT, PSSNa, and de-ionized water solution would not result in Br^- as a counter-ion. Surprisingly, as seen in Figure 4.4, both PSS^- and Br^- acted as counter-ions in electrochemically polymerized PEDOT. The S 2p spectrum showed PEDOT peaks at 164.2 eV (S $2p_{3/2}$) and 165.4 eV (S $2p_{1/2}$) and PSS peaks at 167.9 eV (S $2p_{3/2}$) and 169.0 eV (S $2p_{1/2}$) respectively, indicating that PSS anions were incorporated to PEDOT. At the same time, the characteristic $PEDOT^+Br^-$ spin-split doublet was observed around 70.9 eV (Br $3d_{5/2}$) and 71.9 eV (Br $3d_{3/2}$) (Figure 4.5) with a characteristic peak separation around 1.0 eV.[8]

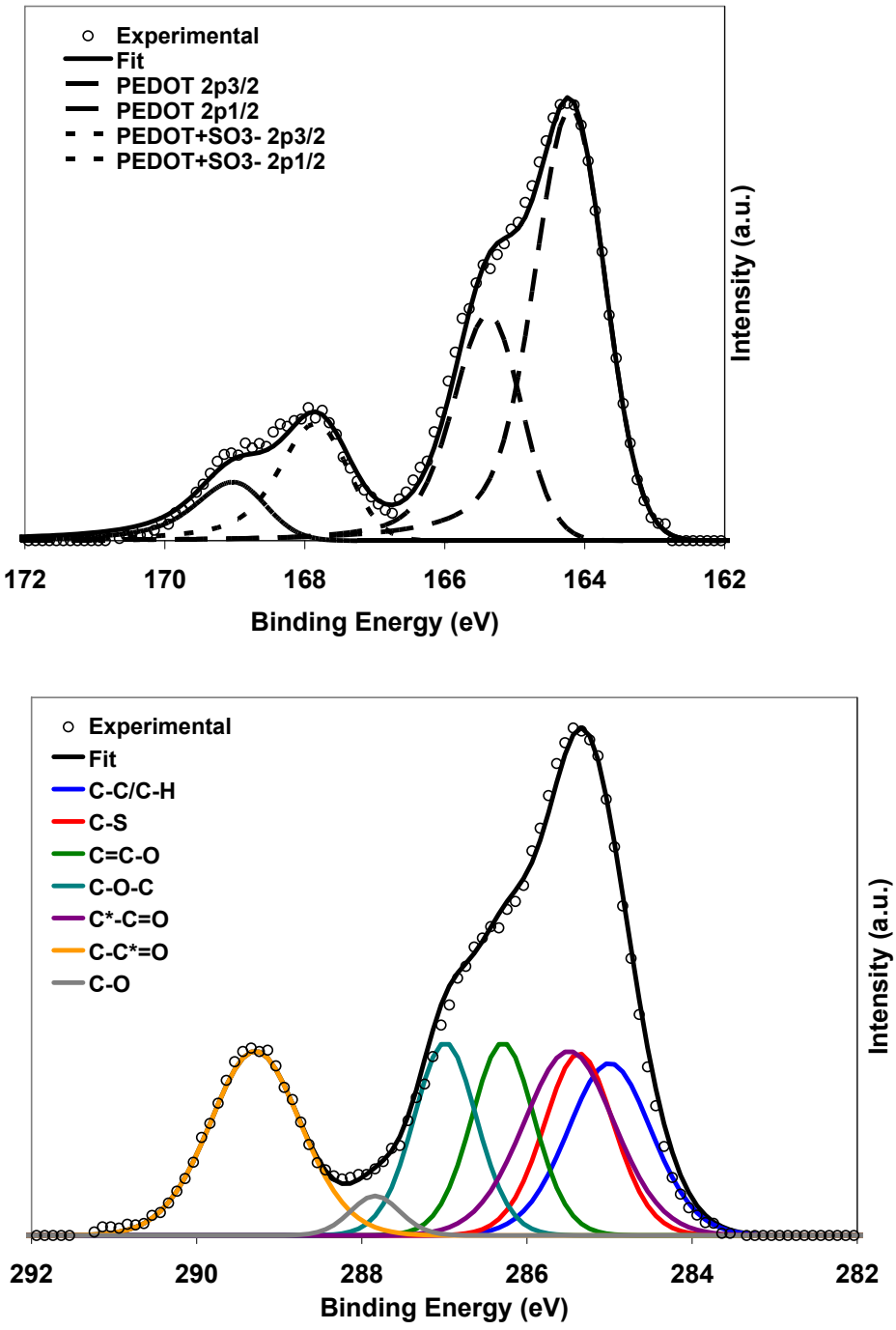

Figure 4.4 (Top) S 2p region for PEDOT-PSS-LiBr and (Bottom) C 1s region for PEDOT-PAA-LiBr

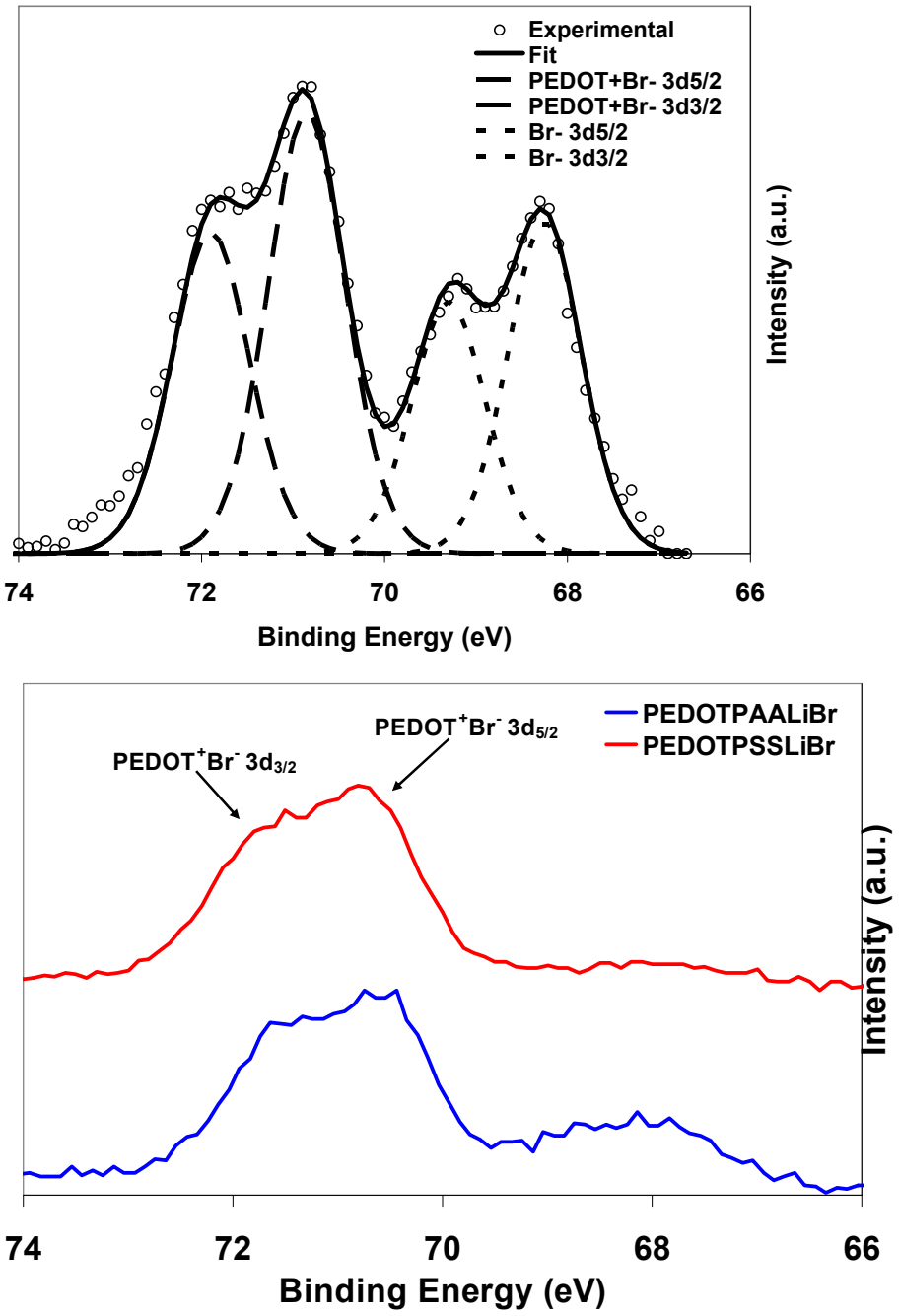

Figure 4.5 Br 3d characteristic region for (Top) PEDOT-LiBr and (Bottom) PEDOT-PSS-LiBr and PEDOT-PAA-LiBr

To examine whether the incorporation of Br^- as the counter-ion into PEDOT was just restricted to PSS, another poly anion, poly (acrylic acid)[2], was used as a substitute for PSS during PEDOT electrochemical polymerization. The PEDOT C 1s characteristic peaks, Figure 4.4, were C-S (285.3 eV) in the α position, C=C-O (286.2 eV) in the β position, and C-O-C (287 eV) bonding in the ethylene bridge, which were in agreement with values previously reported by Jönsson et al.[12] and Gelius et al.[13] in the PEDOT-PAA-LiBr sample. The characteristic PAA peaks were around 285 eV (C-C/C-H), 285.5 eV (C*CO) and 289.2 eV (CC*O) which were in agreement with Beamson et al..[4] The Br 3d region (Figure 4.5) showed $PEDOT^+Br^-$ signal indicating that the Br^- also acted as a counter-ion to PEDOT. Like the PSS-LiBr case, both Br^- and PAA act as counter-ions in PEDOT-PAA-LiBr system.

4.3.3 Mixture of TosNa and LiBr with Other Small Anions

In this section, we will study PEDOT counter-ion incorporation of mixtures containing TosNa and LiBr, both of which were investigated in the previous two sections. Our studies above indicated that Br^- can act as counter-ions even when mixed with poly anions PSS and PAA, while Tos does not act as the dominant counter-ion when mixed with $LiClO_4$ and PBS, different from its polymeric form PSS.

The results of TosNa with small counter-ion mixtures are listed in Table 4.1. PEDOT-TosNa-LiBr samples showed that both anions acted as counter-ions into PEDOT. The PEDOT-TosNa-NaCl-LiBr results showed that all the three anions, Tos^-, Br^-, and Cl^-, were incorporated as counter-ions during PEDOT electrochemical polymerization. We then replaced the NaCl in the mixture with PBS (now PBS-TosNa-

LiBr mixture). The PEDOT-PBS-TosNa-LiBr results were similar to that of the previous mixture of TosNa-NaCl-LiBr, where Tos^-, Br^- and Cl^- can act as counter-ions, which was to be expected due to the high NaCl concentration in phosphate buffer solution. A slight difference was detected, in comparison to PEDOT-TosNa-NaCl-LiBr, that more Br^- and Cl^- can be incorporated into PEDOT than Tos^-. For this mixture, no phosphate contributions were observed in the P 2p region (not shown), indicating that phosphate anions did not act as counter-ions for PEDOT in this instance.

PEDOT-CI	ClO_4^-	Br^-	Tos^-	Cl^-	HPO_4^{2-}/ $H_2PO_4^-$
TosNa-LiBr		**X**	**X**		
TosNa-NaCl-LiBr		**X**	**X**	**X**	
PBS-TosNa-LiBr		**XX**	**X**	**XX**	
PBS-TosNa-LiBr-$LiClO_4$	**XX**	**XX**		**X**	
TosNa-NaCl-LiBr-$LiClO_4$	**XX**	**XX**		**X**	
TosNa-LiBr-$LiClO_4$	**X**	**X**			
TosNa-NaCl-$LiClO_4$	**XX**			**X**	

Table 4.1 PEDOT counter-ion mixtures containing TosNa

When $LiClO_4$ was added to the above mixture of PBS-TosNa-LiBr, Br^- and ClO_4^- acted as the major counter-ions to PEDOT with some Cl^- anions contributions as well. No Tos- or phosphate anion incorporation was observed. The results differ from the previous three mixtures, where both Tos^- and Br^- can act as counter-ions. Here with the presence of $LiClO_4$, no Tos^- acted as counter-ions. When NaCl replaced PBS in the TosNa-NaCl-LiBr-$LiClO_4$ mixture, the results were the same as the previous mixture: Br^- and ClO_4^- act as the major counter-ions, some Cl^- anions were incorporated as well. No Tos^- ion

incorporation was observed. This confirmed that with the presence of $LiClO_4$ in the mixture, Tos^- does not act as the counter-ion. To further confirm this conclusion, a TosNa-LiBr-$LiClO_4$ mixture was examined. In this case, as predicted, only Br^- and ClO_4^- act as the counter-ions during electrochemical polymerization. For a comparison purpose, PEDOT-TosNa-NaCl-$LiClO_4$ was also studied. This mixture yielded a PEDOT film with ClO_4^- acting as the major counter-ion with some minor Cl^- anion contributions as well, but no Tos^- was observed.

The results of this section found that Br^- acted as the counter-ion during electrochemical polymerization. For all the mixtures studied here, as long as Br^- is present in the mixture, it always acted as a major counter-ion. Conversely, Tos^- did not always act as a PEDOT counter-ion though Tos^- can act as a counter-ion in the presence of PBS or Cl^-, but not ClO_4^-. Similar to the Br^- results, ClO_4^- incorporated into the PEDOT films in every mixture it was present, suggesting the high PEDOT affinity to ClO_4^-. Weak $PEDOT^+Cl^-$ signals indicated that Cl^- did act as a counter-ion, however, usually it did not act as a major counter-ion. No phosphate signal was observed in the P 2p region demonstrating that phosphate ions do not act as counter-ions. In summary, qualitatively, the perchlorate ClO_4^- and bromide Br^- anions were found to incorporate into the resulting PEDOT films more frequently, while smaller chloride Cl^- and Tos^- contributions were found less frequently, and no phosphate contributions were observed (Table 4.1). This trend in PEDOT counter-ion affinity will be further investigated below.

4.3.4 Monovalent Anion Mixtures

Since Br^-, ClO_4^-, and Cl^- have a monovalent negative charge, additional negatively monovalent charged anions were studied to obtain a more completed picture regarding the incorporation of counter-ions and PEDOT counter-ion affinity. The first mixture consisted of NaH_2PO_4, NaCl, $NaC_2H_3O_2$, LiBr, and $LiClO_4$ (denoted as -1 $LiClO_4$), while the second mixture was composed of NaH_2PO_4, NaCl, $NaC_2H_3O_2$, LiBr, and $NaNO_3$ (denoted as -1 $NaNO_3$). From previously obtained results, $H_2PO_4^-$ was not found to act as a counter-ion, while Br^-, ClO_4^-, and Cl^- can act as counter-ions. Here NO_3^- and $C_2H_3O_2^-$ were the only new anions included for in this study.

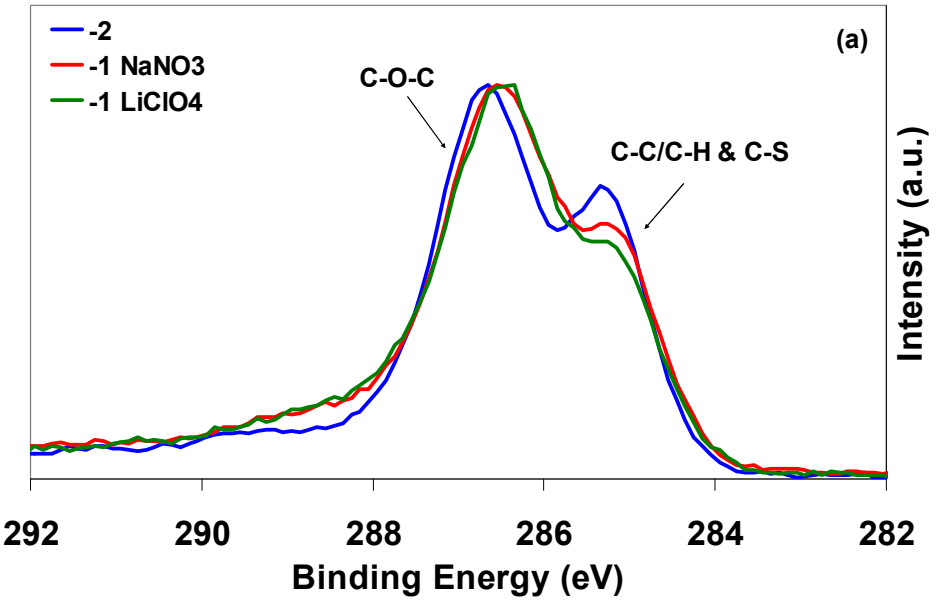

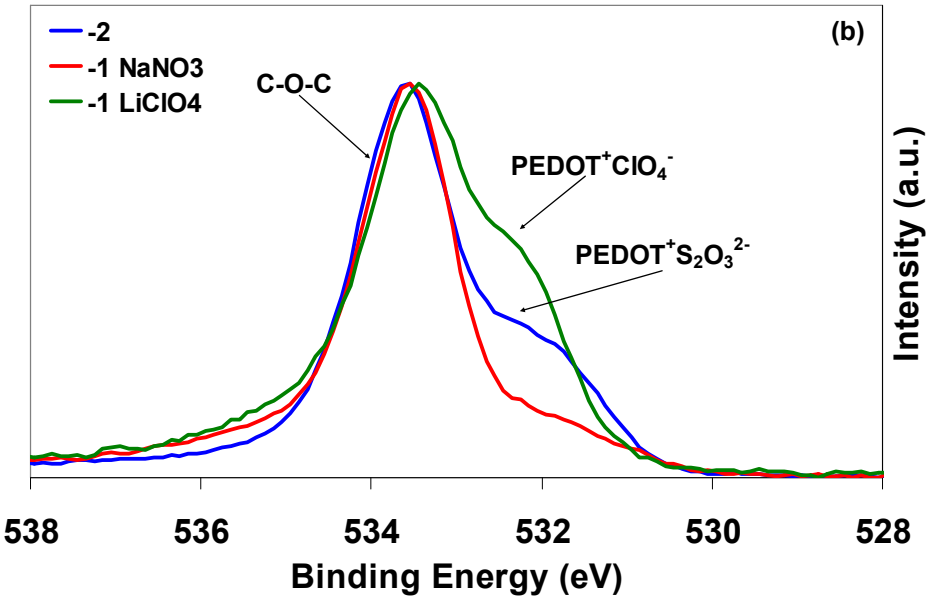
-2
-1 NaNO3
-1 LiClO4
(b)
C-O-C
PEDOT+ClO4-
PEDOT+S2O32-
Intensity (a.u.)
538
536
534
532
530
528
Binding Energy (eV)

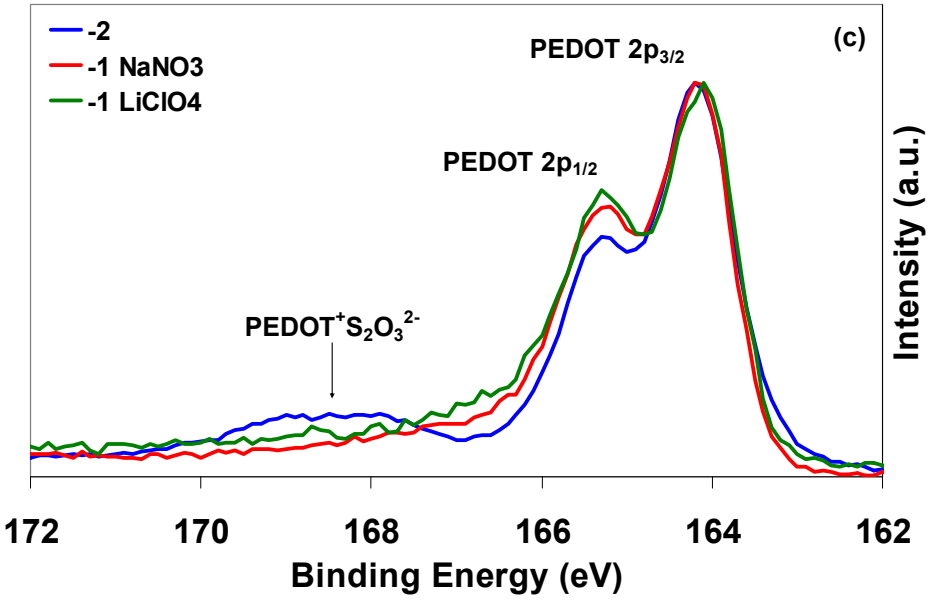
-2
-1 NaNO3
-1 LiClO4
(c)
PEDOT 2p3/2
PEDOT 2p1/2
PEDOT+S2O32-
Intensity (a.u.)
172
170
168
166
164
162
Binding Energy (eV)

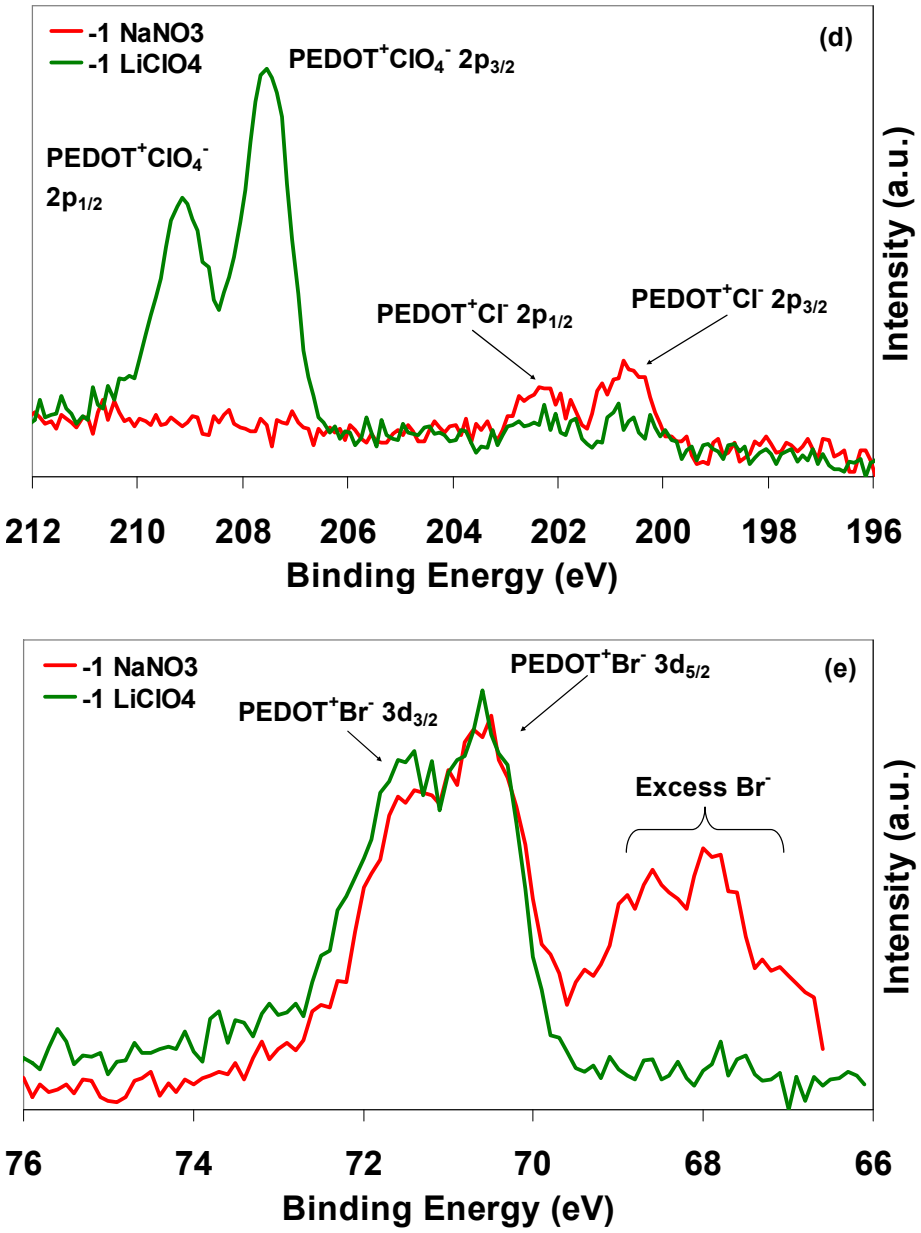

Figure 4.6 (a) C 1s, (b) O 1s, (c) S 2p, (d) Cl 2p, and (e) Br 3d characteristic regions for -1 $LiClO_4$ and-1 $NaNO_3$, and a mixture of anions of divalent negative charges.

Figure 4.6 displays XPS spectra in (a) C 1s, (b) O 1s, (c) S 2p, (d) Cl 2p, and (e) Br 3d regions for both -1 $LiClO_4$ and -1 $NaNO_3$ mixtures. For comparison purposes, XPS results for the mixture of divalent anions (denoted as -2) are also shown in Figure 4.6,

which will be discussed in the next section. The characteristic O 1s signal, Figure 4.6b, of PEDOT C-O-C was observed.[1] As expected no phosphate was detected, nor was acetate detected in the C 1s characteristic region, Figure 4.6a, eliminating both $H_2PO_4^-$ and COO^- as prospective counter-ions. The additional lower binding energy oxygen peak was from the $PEDOT^+ClO_4^-$ for the -1 $LiClO_4$ mixture, while no additional oxygen peak for the -1 $NaNO_3$ mixture was detected. This shows that in the -1 $LiClO_4$ mixture, ClO_4^- can act as a counter-ion, while NO_3^- did not act as a counter-ion in the -1 $NaNO_3$ mixture.

The S 2p region, Figure 4.6c, showed the expected PEDOT spin split doublet around 164.1 eV (S $2p_{3/2}$) and 165.3 eV (S $2p_{1/2}$). No additional sulfur signal was observed for -1 $LiClO_4$ and -1 $NaNO_3$ mixtures indicating no SO_2 signal from PEDOT degradation.[14] For the -1 $LiClO_4$ mixture, the Cl 2p region displayed the very strong characteristic $PEDOT^+ClO_4^-$ spin-split doublet at higher binding energies and smaller $PEDOT^+Cl^-$ contributions at lower binding energies, thus ClO_4^- acts as a major counter-ion with some Cl^- anion contributions (Figure 4.6d). These results also match those seen in the previous sections. For the -1 $NaNO_3$ mixture, a much weaker $PEDOT^+Cl^-$ signal, than that from $PEDOT^+ClO_4^-$ in the -1 $LiClO_4$ mixture was observed. The characteristic Br 3d region yielded a $PEDOT^+Br^-$ 3d spin-split doublet in both the -1 $LiClO_4$ and -1 $NaNO_3$ mixtures (Figure 4.6e). An excess amount of Br^-, the lower binding energy doublet, was found at lower binding energies in the -1 $NaNO_3$ mixture while none was observed in the -1 $LiClO_4$ mixture. For both the mixtures, the characteristic P 2p (not shown) displayed no phosphate signal, indicating phosphate did not act as a PEDOT counter-ion. Similarly, no $PEDOT^+NO_3^-$ signal was found in the N 1s region (not shown) either.

Here we hypothesize that anionic hydration can be the driving mechanism for PEDOT counter-ion affinity. The higher the anionic hydration, the less likely the anion is to leave the solution to act as a PEDOT counter-ion. The effect of anionic hydration in the precipitation of globulin from egg, isinglass, colloidal ferric oxide, and sodium oleate were first studied by Hofmeister in 1880's [15,16], and resulted in what is currently called the Hofmeister series: CO_3^{2-}, SO_4^{2-}, $S_2O_3^{2-}$, $H_2PO_4^-$, F^-, Cl^-, Br^-, NO_3^-, I^-, ClO_4^-, and SCN^-. The ions on the left are highly hydrated, and those on the right are less hydrated. If we only consider the anions with one negative charge, according to the general Hofmeister series[17] trends, the weaker hydration of ClO_4^- and Br^- may encourage PEDOT counter-ion affinity over the slightly more hydrated Cl^-, and strongly hydrated phosphate anions. This matches our observations in this study that ClO_4^- and Br^- like to act as major counter-ions, some Cl^- can be incorporated into PEDOT, while $H_2PO_4^-$ does not act as a counter-ion in PEDOT electrochemically polymerization. Apparently, NO_3^- is an exception in this study. Even though NO_3^- is weakly hydrated, but it does not act as a counter-ion.

4.3.5 Divalent Anion Mixture

Next mixtures of divalent anions were studied. The mixture was composed of Na_2HPO_4, $Na_2S_2O_3$, and $CaCO_3$. The S 2p region, Figure 4.6c, showed the expected PEDOT spin split doublet around 164.1 eV (S $2p_{3/2}$) and 165.3 eV (S $2p_{1/2}$), while a low, broad higher binding energy doublet occurred around 168.7 eV (S $2p_{3/2}$) and 169.9 eV (S $2p_{1/2}$) was seen, representative of $PEDOT^+S_2O_3^{2-}$ contributions (Figure 4.7).

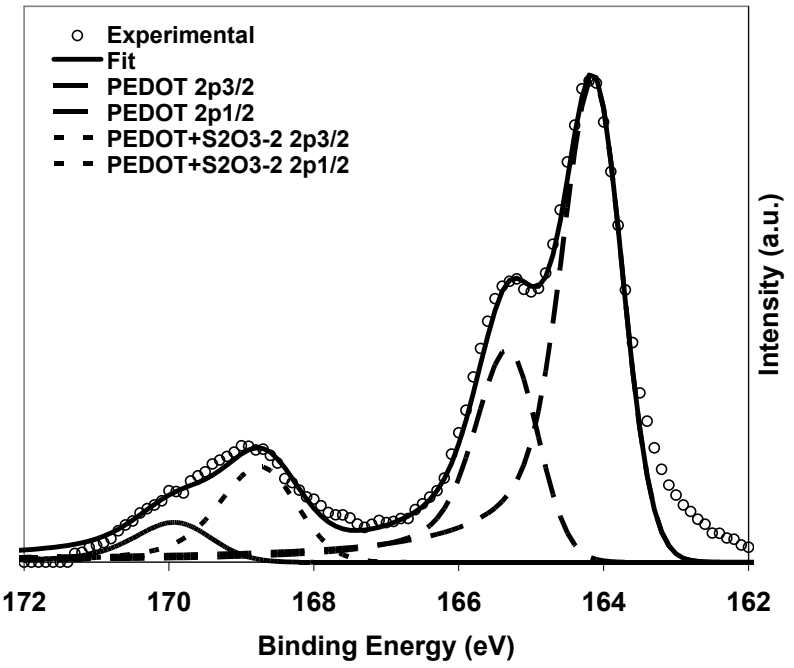

Figure 4.7 S 2p characteristic region for PEDOT-$Na_2S_2O_3$

In the O 1s region, Figure 4.6b, in addition to the PEDOT C-O-C peak, the lower binding energy peak was found to characteristic of PEDOT-$Na_2S_2O_3$, further reinforcing that $S_2O_3^{2-}$ acted as the PEDOT counter-ion. The -2 mixture was also studied with the more water soluble Na_2CO_3 carbonate version and the results did not alter from the $CaCO_3$ version. No HPO_4^{2-} contribution was observed in the P 2p region (not shown). Similar to the mixtures composed of anions with one negative charge, here for the divalent anion mixtures, we believe that the counter-ion incorporation to PEDOT is also mediated by the hydration of ions. Thiosulfate is less hydrated than both CO_3^{2-} and HPO_4^{2-}, thus it more likely acts as the counter-ion in the mixture of Na_2HPO_4, $Na_2S_2O_3$, and $CaCO_3$ (or Na_2CO_3). More ions will be included in the next chapter to test whether

the anionic hydration is the main determining factor for PEDOT incorporation during electrochemical polymerization.

4.4 Conclusions

Previous studies suggested PEDOT had an increased affinity for PSS over small anions when mixtures of anions are used in the PEDOT electrochemical polymerization process. The results found here indicate even with the same SO_3^- concentration in the anion mixture, Tos^- does not act as the dominant counter-ion to PEDOT. This shows that PSS dominates as the counter-ion due to its polymeric nature. In contrast to other small anions investigated previously, bromide anions were found to act as PEDOT counter-ions even in the presence of the polymeric anions PSS and PAA.

To obtain a more completed picture regarding PEDOT counter-ion incorporation, several other anion mixtures were investigated. The overall qualitative PEDOT counter-ion affinity for monovalent anions was: ClO_4^-, Br^- over smaller Cl^-, Tos^-, and COO^- (acetate), with no phosphate or NO_3^- contributions. As for the divalent anions, $S_2O_3^{2-}$ dominated over both carbonate and phosphate anions. The trends found in counter-ion affinity did loosely follow the general trend for anionic hydration suggested by the Hofmeister series. Anionic hydration in regards to PEDOT counter-ion incorporation will be further investigated more thoroughly in the next chapter.

4.5 References

1. Spanninga, S.A.; Martin, D.C.; Chen, Z. *J. Phys. Chem. C* **2009**, *113*, 5585.

2. Yang, J.; Lipkim, K.; Martin, D.C. *J. Biomater. Sci. Polymer Edn*., **2007**, *18*, 1075.

3. Zotti, G.; Zecchin, S.; Schiavon, G.; Louwet, F.; Groenendaal, L.; Crispin, X.; Osikowicz, W.; Salaneck, W.R.; Fahlman, M. *Macromolecules* **2003**, *36*, 3337.

4. Beamson, G.; Briggs, D. *High Resolution XPS of Organic Polymers: The Scienta ESCA300 Database*; John Wiley & Sons: New York, New York, 1992.

5. Briggs, D.; Beamson, G. *Anal. Chem.* **1993**, *65*,1517.

6. Briggs, D. *Surface analysis of polymers by XPS and static SIMS*; Cambridge University Press: Cambridge, U.K.1998.

7. Siegbahn, K.; Nordling, C.; Fahlman, A.; Nordberg, R.; Hamrin, K.; Hedman, J.; Johansson, G.; Bergmark, T.; Karlsson, S.E.; Lindgren, I.; Lindberg, B. *ESCA: atomic, molecular and solid state structure studied by means of electron spectroscopy.* Uppsala: Uppsala,SWE, 1967.

8. Moulder, J.F.; Stickle, W.R.; Sobol, P.E.;K.D. Bomben, K.D. Handbook of X-ray photoelectron spectroscopy: A reference book of standard spectra for identification and interpretation of XPS data. Physical Electronics: Eden Prairie, MN, 1992.

9. Greczynski, G.; Kugler, T.; Salaneck, W.R. *Thin Solid Films* **1999**, *354*, 129.

10. Greczynski, G.; Kugler, T.; Keil, M.; Osikowicz, W.; Fahlman, M.; Salaneck, W.R. *J. Electron Spectrosc. Relat. Phenom*. **2001**, *121*,1.

11. Kang, E.T.; Neoh, K.G.; Tan, K.L. *Phys. Rev. B: Condens. Matter Mater. Phys*. **1991**, *44*, 10 461.

12. Jönsson, S.K.M.; de Jong, M.P.; Groenendaal, L.; Salaneck, W.R.; Fahlman, M. *J. Phys. Chem. B* **2003**, *107*, 10793.

13. Gelius, U.; Allan, C.J.; Johansson, G.; Siegbahn, H.; Allison, D.A.; Siegbahn, K. *Phys. Scr*. **1971**, *3*, 237.

14. Marciniak, S.; Crispin, X.; Uvdal, K.; Trzcinski, M.; Birgerson, J.; Groenendaal, L.; Louwet, F.; Salaneck, W.R. *Synth. Met.* **2004**, *141*, 67.

15. Hofmeister, F. *Arch. Exp. Pathol. Pharmakol*. **1888**, *24*, 247.

16. Kunz, W.; Henle, J.; Ninham, B.W. *Curr. Opin. Colloid Interface Sci.* **2004**, *9*, 19.

17. Zhang, Y.; Cremer, P.S. *Curr. Opin. Chem. Biol*. **2006**, 10, 658.

CHAPTER 5

THE EFFECT OF ANIONIC HYDRATION ON COUNTER-ION INCORPORATION IN POLY(3,4-ETHYLENEDIOXYTHIOPHENE) (PEDOT): AN X-RAY PHOTOELECTRON SPECTROSCOPY STUDY

5.1 Introduction

In the last two chapters, we have previously demonstrated how the incorporation of various counter-ions into electrochemically polymerized PEDOT affected both the polymer surface morphology and electrical properties of the PEDOT polymer film.[1-3] In addition, we examined PEDOT counter-ion affinity in mixtures of monovalent anions and divalent anions. The findings suggest that PEDOT counter-ion incorporation "loosely" follows the hydration of the anions, although the details of this proposed correlation needed further examination.

Here we study the relationship between anion hydration in order to evaluate if this is indeed the primary driving force dictating PEDOT counter-ion incorporation. More specifically, the research in this chapter consists of three main components: (1) a systematic study of a series of anion mixtures with the gradual addition of more weakly hydrated anions; (2) an investigation of mixtures composed of two or three counter-ions, and (3) the examination of mixtures composed of four or five counter-ions. As in our previous studies, X-ray photoelectron spectroscopy (XPS) was used to deduce the respective PEDOT film's chemical composition. XPS is an ultra-high vacuum, surface

sensitive technique[4-7] that was used to investigate the differences in binding energy as a result of different counter-ion incorporation.

The anionic hydration has been studied according to what has become known as the Hofmeister series.[8,9] Franz Hofmeister first studied the effects of salts on protein precipitation in the 1880's. His research expanded from the precipitation of egg globulin to the precipitation of isinglass, colloidal ferric oxide, and sodium oleate utilizing different salts.[8,9] The efficiency of globulin precipitation caused by various ions are now known as the Hofmeister series. The precipitation efficiency was found to correlate to the hydration of the salt's anion. The Hofmeister Series was found (from lowest to highest precipitation efficiency, or from highest to lowest anionic hydration) to be: SO_4^{2-}, HPO_4^{2-}, $C_2H_3O_2^-$, $C_6H_5O_7^{3-}$, $C_4H_4O_6^{2-}$, CO_3^{2-}, CrO_4^{2-}, Cl^-, NO_3^-, and ClO_3^-.[8,9] Since the publication of Hofmeister's findings in the 1880's, the series has been modified and now taking a form similar to that was presented by Zhang *et al*[10]: CO_3^{2-}, SO_4^{2-}, $S_2O_3^{2-}$, $H_2PO_4^-$, F^-, Cl^-, Br^-, NO_3^-, I^-, ClO_4^-, and SCN^-. In addition to the experimental phenomenon seen with 'salting-out' processes in biological molecules, anionic hydration has also been studied rheologically through the use of the B coefficient in dilute salt solutions[11-14] and thermodynamically[12,15,16] amongst other ways.

Anionic hydration is normally divided into two categories: kosmotropes, water structure makers (strongly hydrated), or chaotropes, water structure breakers (weakly hydrated).[10,11] In general, a positive B coefficient (which deals with ion-solvent interactions) value suggests a kosmotrope, while a negative value suggests a chaotrope.[12,14] In terms of ΔG_{HB}, the effect on the solute of water's hydrogen bonded structure, the more negative value suggests water-structure-breaking ions, while the more

positive values suggest water-structure-making ions.[15,16] Table 5.1 gives information on the ionic radii, solubility, B coefficients, and ΔG_{HB} for the anions used in this research.

Cations	**Ionic Radii (pm)[15]**	**ΔG_{HB}[15]**	**B coefficient (dm^3/mol)[12]**
Ca^{2+}	100	0.34	0.284
Li^{+}	69	0.28	0.146
Na^{+}	102	-0.03	0.085
K^{+}	138	-0.52	-0.009
Anions			
$C_6H_5O_7^{3-}$			
CO_3^{2-}	178	0.028	0.294
$S_2O_3^{2-}$	250	-0.43	0.14, 0.16
HPO_4^{2-}	238	0.33	0.382
$H_2PO_4^{-}$	238	-0.10	0.340
$C_2H_3O_2^{-}$	190	0.12	0.246
Cl^{-}	181	-0.61	-0.005
Br^{-}	196	-0.80	-0.033
NO_3^{-}	200	-0.68	-0.043
ClO_4^{-}	240	-1.01	-0.058

Table 5.1 Ionic Radii, Solubility, B coefficient, and ΔG_{HB} information

The motivation behind this study was to understand whether anionic hydration is indeed the primary driving force for PEDOT counter-ion incorporation. The higher the anionic hydration, the more hydrogen-bonded water molecules surround the anion, the less likely the anion is to leave the solution to act as a PEDOT counter-ion. As stated above, in our previous study on several anion mixtures, we found that the PEDOT counter-ion incorporation followed the general trend predicted by the Hofmeister series, albeit with some exceptions.[17] Here, a more systematic study of 3,4-ethylenedioxythiophene (EDOT) with various differently hydrated anion mixtures from

the most to least hydrated anions, were mixed and a PEDOT film was then electrochemically deposited. If hydration was the sole mechanism for counter-ion affinity, then the electrochemically polymerized PEDOT film resulting from each mixture is expected to be dominated by the presence of the least hydrated anion.

Further studies into PEDOT counter-ion affinity were also carried out by utilizing mixtures of anions with different charges and different cations in two, three, four, and five counter-ion combinations. The motivation for this portion of the study was to augment the hydration study results to help deduce the PEDOT counter-ion driving mechanism.

5.2 Experimental Methods

5.2.1 Chemicals

The 3,4-ethylenedioxythiophene (EDOT) monomer was obtained from H.C. Starck. Sodium citrate tribasic dihydrate ($Na_3C_6H_5O_7$ $2H_2O$), potassium citrate tribasic monohydrate ($K_3C_6H_5O_7$ H_2O), sodium carbonate (Na_2CO_3), calcium carbonate ($CaCO_3$), sodium thiosulfate ($Na_2S_2O_3$), sodium acetate trihydrate ($NaC_2H_3O_2$ $3H_2O$), sodium phosphate dibasic hepthydrate (Na_2HPO_4 $7H_2O$), sodium phosphate monohydrate (NaH_2PO_4 H_2O), sodium chloride (NaCl), sodium bromide (NaBr), lithium bromide (LiBr), sodium perchlorate ($NaClO_4$), lithium perchlorate ($LiClO_4$), and sodium nitrate ($NaNO_3$) were purchased from Sigma-Aldrich. These chemicals were all used as received.

5.2.2 Electrochemical Polymerization

PEDOT electrochemical polymerization was performed using galvanostatic current from a 0.01 M EDOT aqueous solution with various counter-ions. The XPS samples were deposited on Au/Pd sputter-coated barbell shaped electrodes (6 mm diameter) on polystyrene (PS) cover slips at 135 μA for 10 minutes. All samples were polymerized in de-ionized water with 0.01 M counter-ion(s) concentration present. The samples were then rinsed in de-ionized water to remove excess counter-ion from the surface and allowed to air dry. Additional rinsing was not found to alter the quantity of incorporated counter-ion noticeably with the exception of PEDOT-LiBr or PEDOT-NaBr. In these two cases, after soaking in de-ionized water for 24 hours, the amount of excess Br^- was found to decrease. XPS reference samples of $Na_3C_6H_5O_7$ $2H_2O$, $K_3C_6H_5O_7$ H_2O, Na_2CO_3, $CaCO_3$, $Na_2S_2O_3$, $NaC_2H_3O_2$ $3H_2O$, Na_2HPO_4 $7H_2O$, NaH_2PO_4 H_2O, NaCl, NaBr, LiBr, $NaClO_4$, $LiClO_4$, and $NaNO_3$ were used as received. Samples of PEDOT-$K_3C_6H_5O_7$, PEDOT-$Na_3C_6H_5O_7$, PEDOT-$CaCO_3$, PEDOT-Na_2CO_3, PEDOT-$Na_2S_2O_3$, PEDOT- $NaC_2H_3O_2$, PEDOT-Na_2HPO_4, PEDOT-NaH_2PO_4, PEDOT-NaCl, PEDOT-LiBr, PEDOT-NaBr, PEDOT-$LiClO_4$, PEDOT-$NaClO_4$, and PEDOT-$NaNO_3$ were also electrochemically polymerized and utilized as comparison references.

5.2.3 X-Ray Photoelectron Spectroscopy

Initial survey scans were run using a pass energy of 160 eV, while characteristic region scans of the C 1s, O 1s, N 1s, S 2p, Cl 2p, P 2p, and Br 3d utilized a pass energy of 20 eV with a step of 0.1 eV. All spectra were referenced using the C-C/C-H peak at 285 eV.

5.3 Results and Discussion

5.3.1 Gradual Anionic Additions Following the Hofmeister Series

The rationale of this study was to examine anionic mixtures going from the most hydrated anion, citrate in this case, to the least hydrated, perchlorate. This was accomplished by adding one anion at a time, for example EDOT mixed with a most and a second most hydrated set of ions (e.g., $C_6H_5O_7^{3-}$ and CO_3^{2-}), and so on. More specifically, the following mixtures were studied: (1) PEDOT-$K_3C_6H_5O_7$, (1-2) PEDOT-$K_3C_6H_5O_7$- $CaCO_3$, (1-3) PEDOT-$K_3C_6H_5O_7$- $CaCO_3$- $Na_2S_2O_3$, (1-4) PEDOT-$K_3C_6H_5O_7$- $CaCO_3$- $Na_2S_2O_3$- $NaC_2H_3O_2$, (1-5) PEDOT-$K_3C_6H_5O_7$- $CaCO_3$- $Na_2S_2O_3$- $NaC_2H_3O_2$- Na_2HPO_4, (1-6) PEDOT-$K_3C_6H_5O_7$- $CaCO_3$- $Na_2S_2O_3$- $NaC_2H_3O_2$- Na_2HPO_4- NaH_2PO_4, (1-7) PEDOT-$K_3C_6H_5O_7$- $CaCO_3$- $Na_2S_2O_3$- $NaC_2H_3O_2$- Na_2HPO_4- NaH_2PO_4-NaCl, (1-8) PEDOT-$K_3C_6H_5O_7$- $CaCO_3$- $Na_2S_2O_3$- $NaC_2H_3O_2$- Na_2HPO_4- NaH_2PO_4-NaCl-LiBr, (1-9 $NaNO_3$) PEDOT-$K_3C_6H_5O_7$- $CaCO_3$- $Na_2S_2O_3$- $NaC_2H_3O_2$- Na_2HPO_4- NaH_2PO_4-NaCl-LiBr-$NaNO_3$, (1-9 $LiClO_4$) PEDOT-$K_3C_6H_5O_7$- $CaCO_3$- $Na_2S_2O_3$- $NaC_2H_3O_2$- Na_2HPO_4- NaH_2PO_4-NaCl-LiBr-$LiClO_4$.

If hydration is the primary mechanism for PEDOT counter-ion affinity, the expected results would show that for each mixture, the anion acting as the PEDOT counter-ion should be dominated by the least hydrated anion present in the mixture. So the above solutions (1), (1-2), (1-3), (1-4), (1-5), (1-6), (1-7), (1-8), (1-9 $NaNO_3$), and (1-9 $LiClO_4$), should have been dominated by $C_6H_5O_7^{3-}$, CO_3^{2-}, $S_2O_3^{2-}$, $C_2H_3O_2^{-}$, HPO_4^{2-}, $H_2PO_4^{-}$, Cl^{-}, Br^{-}, NO_3^{-}, and $LiClO_4^{-}$, respectively. XPS was then utilized to study the resulting electrochemically polymerized PEDOT films.

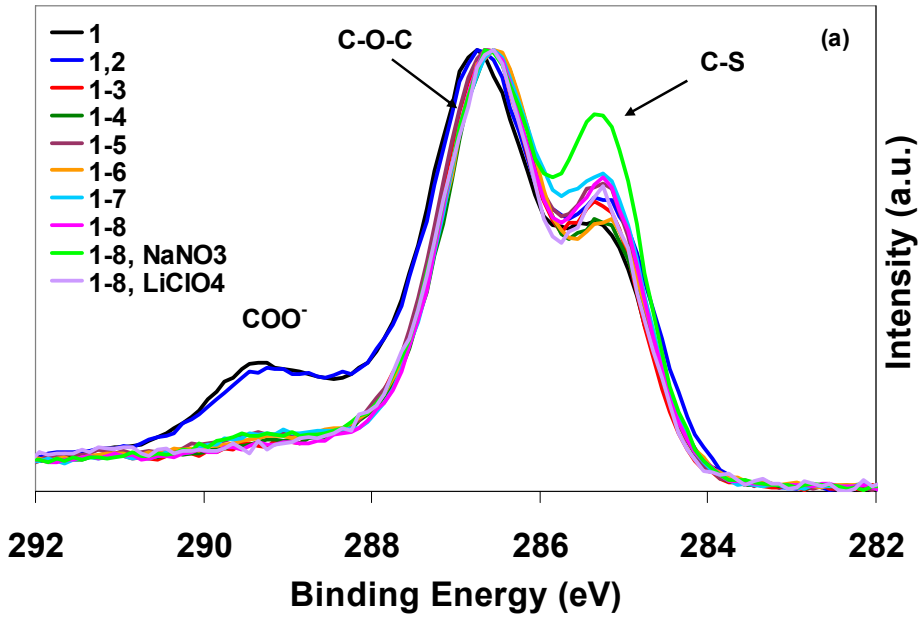
1
1,2
1-3
1-4
1-5
1-6
1-7
1-8
1-8, NaNO3
1-8, LiClO4
C-O-C
C-S
COO-
(a)
Intensity (a.u.)
292
290
288
286
284
282
Binding Energy (eV)

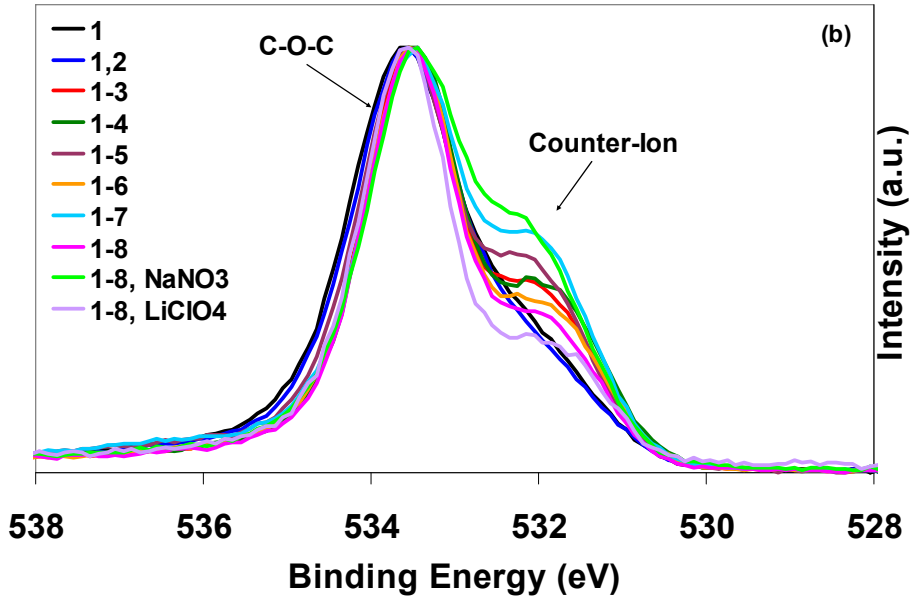
1
1,2
1-3
1-4
1-5
1-6
1-7
1-8
1-8, NaNO3
1-8, LiClO4
C-O-C
Counter-Ion
(b)
Intensity (a.u.)
538
536
534
532
530
528
Binding Energy (eV)

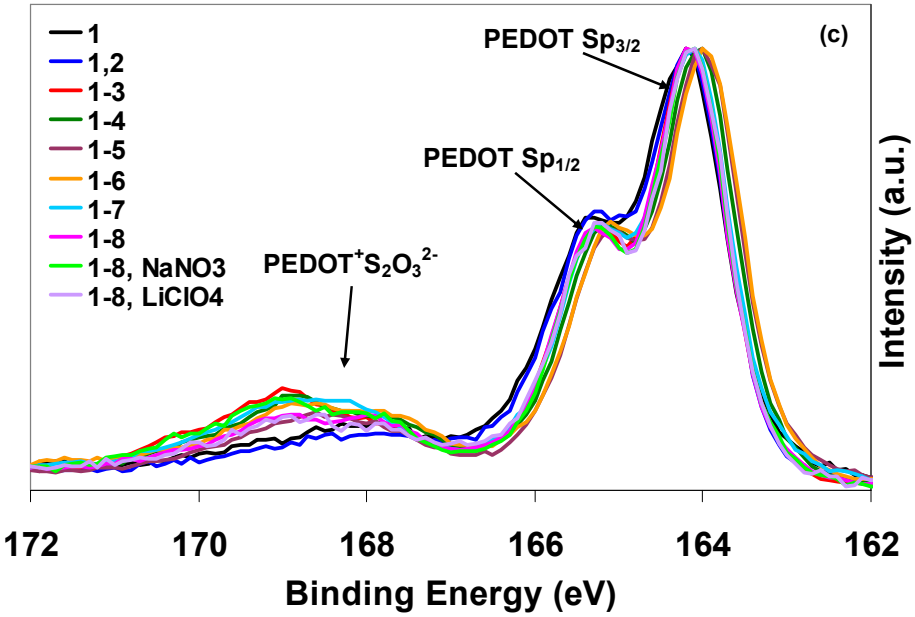

Figure 5.1 (a) C 1s, (b) O 1s, and (c) S 2p characteristic regions for gradual anionic additions following the Hofmeister Series

The C 1s characteristic XPS spectrum is shown in Figure 5.1a. The results in Figure 5.1a demonstrate that before the addition of $Na_2S_2O_3$ to the mixture, for samples (1) and (1-2), there was a peak around 289 eV which was characteristic of COO^- or CO_3^{2-} contributions (note that there was spectral overlap between COO^- (in $C_6H_5O_7^{3-}$) and CO_3^{2-})[18-20] demonstrating that COO^- (in $C_6H_5O_7^{3-}$) and/ or CO_3^{2-} act as counter-ions. Once the addition of $Na_2S_2O_3$ was made, in sample (1-3) and thereafter, the characteristic COO^- or CO_3^{2-} contributions disappeared in the C 1s region. In the O 1s spectral region, Figure 5.1b, the appearance of various lower binding energy shoulder intensities suggests that multiple oxygen components are present and thus possibly various counter-ion components as well.

In the S 2p spectral region (Figure 5.1c), a low, broad S 2p spin-split doublet from $PEDOT^+S_2O_3^{2-}$ appeared indicating that thiosulfate acts as the dominate counter-ion and not citrate or carbonate. Interestingly, with the addition of more weakly hydrated ions into the mixture, the $PEDOT^+S_2O_3^{2-}$ low, broad S 2p spin-split doublet could always be observed in the XPS spectra. It was found that $S_2O_3^{2-}$ ions was dominant over all the other anions regardless of their anionic hydration state in the rest of the samples. The lack of $PEDOT^+CO_3^{2-}$ (~289 eV) and $PEDOT^+COO^-$ (~289 eV) signals in C 1s, phosphate signal (133.7 eV) in the P $2p^1$ (not shown), $PEDOT^+ClO_4^-$ (Cl $2p_{3/2}$ at 207.4 eV) and $PEDOT^+Cl^-$ (Cl $2p_{3/2}$ at 200.6 eV) signals in the Cl $2p^1$, $PEDOT^+Br^-$ (Br $3d_{5/2}$ ~70.9 eV) signal in the Br 3d (not shown), and $PEDOT^+NO_3^-$ (~406.4 eV) in the N 1s (not shown) in these samples eliminates the possibility of other counter-ions such as, $CaCO_3$, $NaC_2H_3O_2$, Na_2HPO_4, NaH_2PO_4, NaCl, LiBr, $NaNO_3$, and $LiClO_4$, acting as PEDOT counter-ions. Thus, based on the thiosulfate dominance over all other anions, we conclude that anionic hydration was not the sole driving force for PEDOT counter-ion incorporation. The fact that no other anions were incorporated as counter-ions indicates that another type of interaction was taking place, in addition to anionic hydration effects. Perhaps the dominant incorporation of $S_2O_3^{2-}$ into electrochemically polymerized PEDOT is because of some specific favorable interactions between EDOT and $S_2O_3^{2-}$, details of which are not yet known.

5.3.2 Mixtures with Two or Three Anions

To further understand the anion hydration effect on the PEDOT counter-ion affinity, especially when $S_2O_3^{2-}$ is absent in the mixture, PEDOT counter-ion

incorporation was investigated with different mixtures including two, three, four, and five anions. In this section, we focus on the mixtures with two or three anions. Mixtures with four or five anions will be investigated in the next section. The goal of this further mixture study was to determine PEDOT counter-ion affinity within the different mixtures and to also deduce whether the number of different anions in the mixtures contributed to determining PEDOT counter-ion affinity.

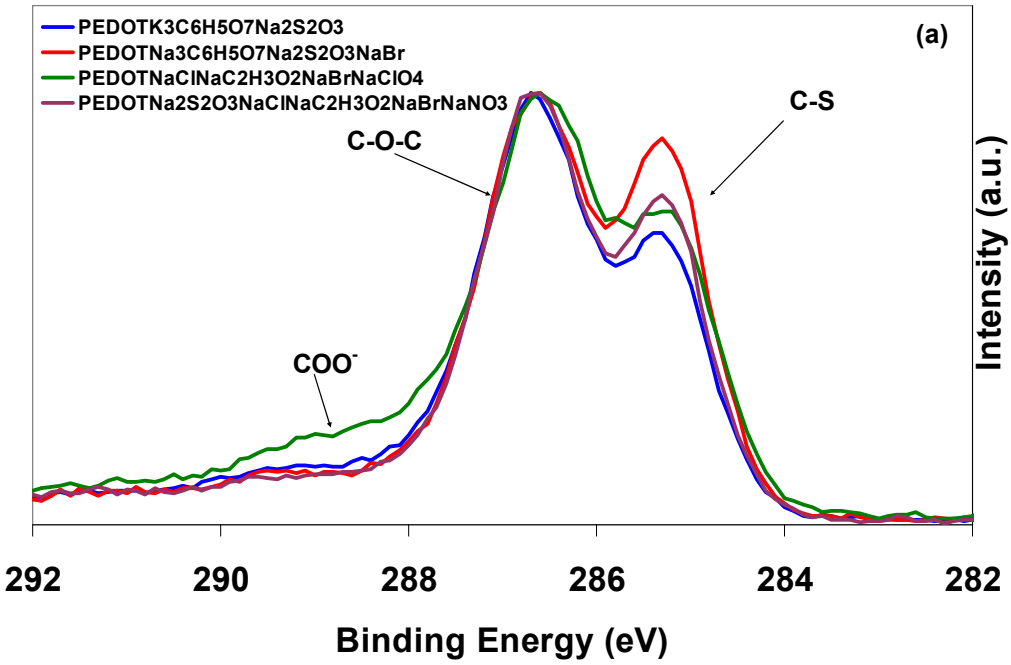

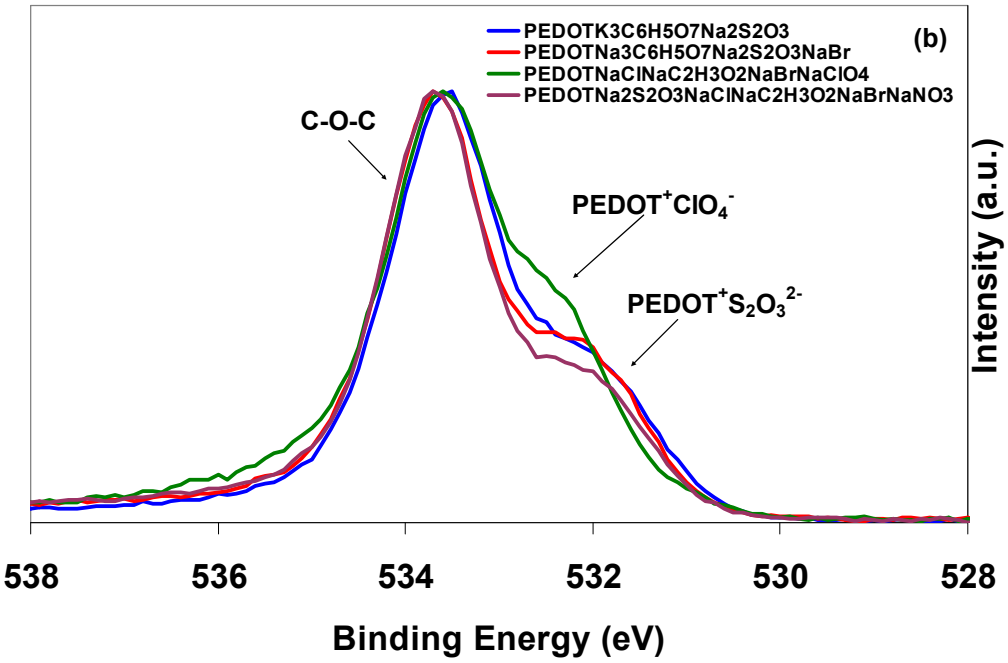
PEDOTK3C6H5O7Na2S2O3
PEDOTNa3C6H5O7Na2S2O3NaBr
PEDOTNaClNaC2H3O2NaBrNaClO4
PEDOTNa2S2O3NaClNaC2H3O2NaBrNaNO3
(b)
C-O-C
PEDOT+ClO4-
PEDOT+S2O32-
Intensity (a.u.)
538
536
534
532
530
528
Binding Energy (eV)

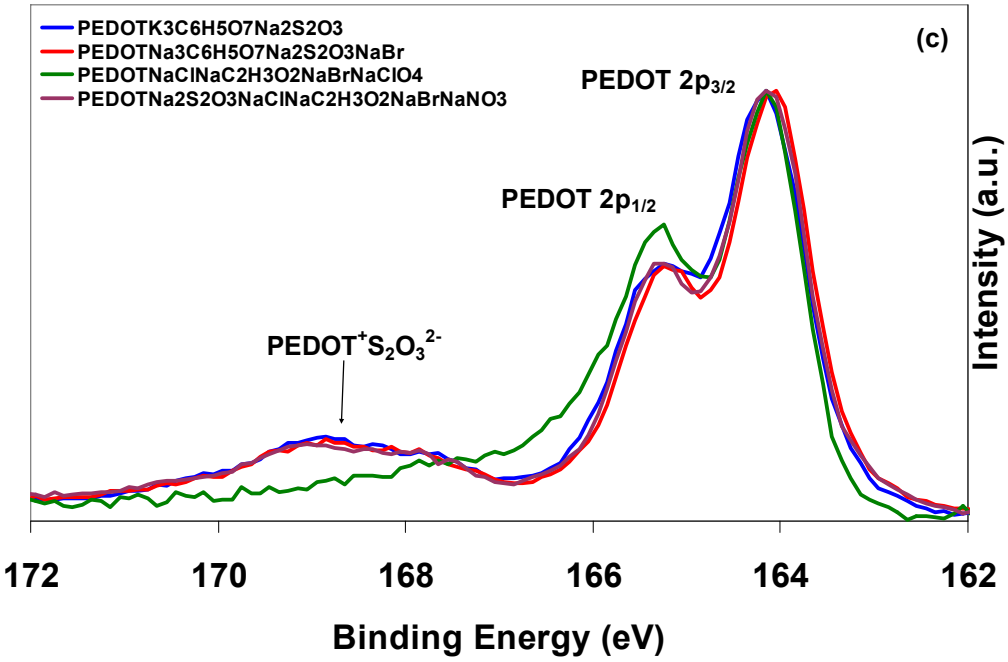
PEDOTK3C6H5O7Na2S2O3
PEDOTNa3C6H5O7Na2S2O3NaBr
PEDOTNaClNaC2H3O2NaBrNaClO4
PEDOTNa2S2O3NaClNaC2H3O2NaBrNaNO3
(c)
PEDOT 2p3/2
PEDOT 2p1/2
PEDOT+S2O32-
Intensity (a.u.)
172
170
168
166
164
162
Binding Energy (eV)

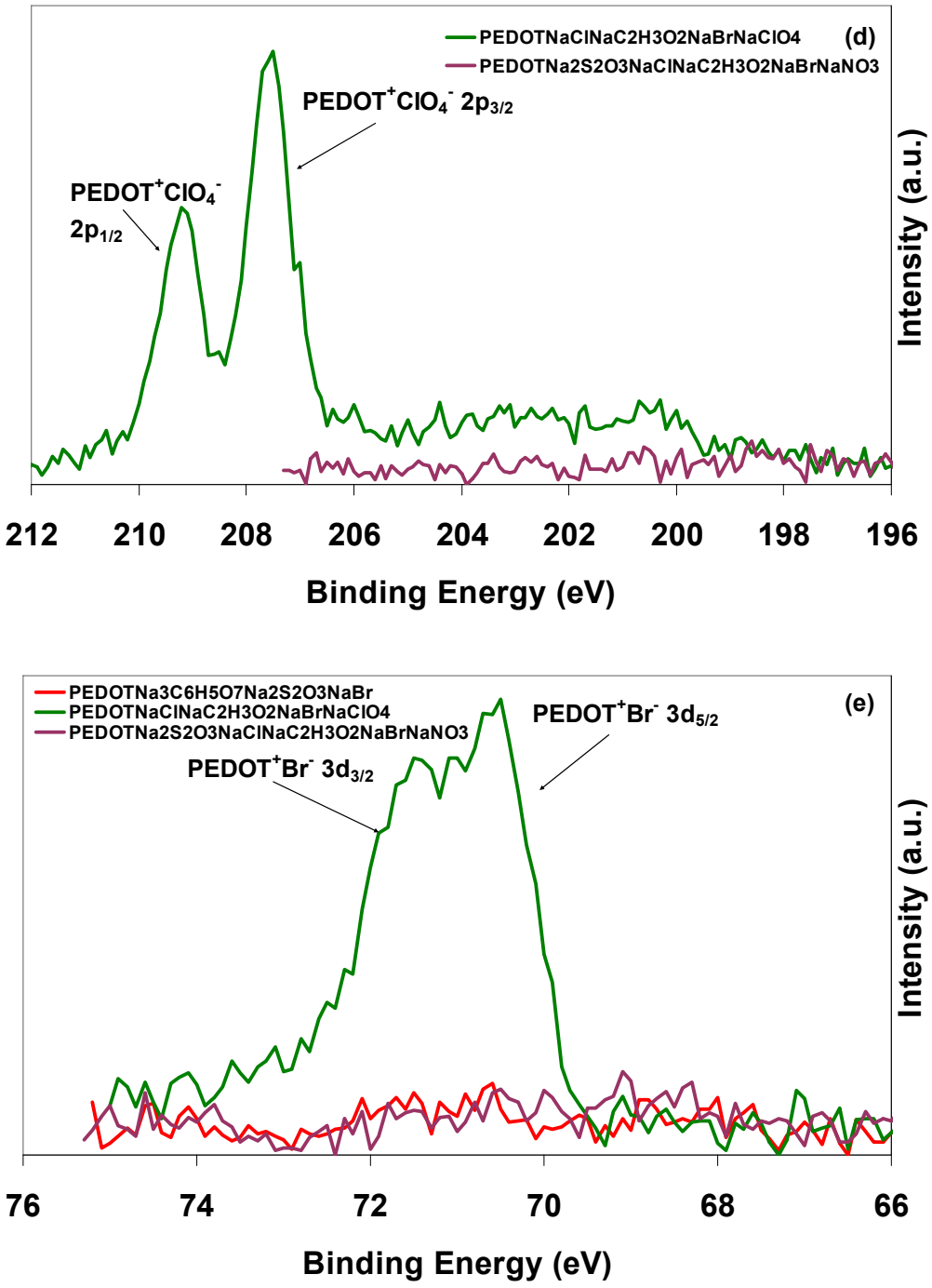

Figure 5.2 Examples of XPS spectra of PEDOT electrochemically polymerized with anion mixtures of two, three, four, and five anion mixtures: (a) C 1s, (b) O 1s, (c) S 2p, (d) Cl 2p, and (e) Br 3d

XPS spectra were collected of PEDOT films electrochemically polymerized using anion mixture solutions with two or three anions. To simplify the discussion, only one example of each two, three, four, and five anion mixtures, Figure 5.2, are shown here. As can be seen in the C 1s region, the higher binding energy contribution for PEDOT-NaCl-$NaC_2H_3O_2$-NaBr-$NaClO_4$ could be from COO^-, while the PEDOT-$K_3C_6H_5O_7$-$Na_2S_2O_3$, PEDOT-$Na_3C_6H_5O_7$-$Na_2S_2O_3$-NaBr, and PEDOT-$Na_2S_2O_3$-NaCl-$NaC_2H_3O_2$-NaBr-$NaNO_3$ did not have higher carbon binding energy contributions but did have a low, broad higher binding energy contribution from $PEDOT^+S_2O_3^{2-}$ in the S 2p region indicating that thiosulfate acts as a PEDOT counter-ion during electrochemical polymerization. The O 1s shows that the lower binding enery shoulder contribution from different caount-ions varies in the intensity and peak shape. The appearance of perchlorate signal in the Cl 2p region indicates ClO_4^- was acting a counter-ion for the PEDOT-NaCl-$NaC_2H_3O_2$-NaBr-$NaClO_4$, though there was no $PEDOT^+Cl^-$ signal observed for either PEDOT-NaCl-$NaC_2H_3O_2$-NaBr-$NaClO_4$ or PEDOT-$Na_2S_2O_3$-NaCl-$NaC_2H_3O_2$-NaBr-$NaNO_3$ indicating Cl^- did not act a PEDOT counter-ion for either mixture. In the Br 3d region, a characteristic $PEDOT^+Br^-$ spin-split doublet could be observed for the PEDOT-NaCl-$NaC_2H_3O_2$-NaBr-$NaClO_4$ sample, but not for either PEDOT-$Na_3C_6H_5O_7$-$Na_2S_2O_3$-NaBr or PEDOT-$Na_2S_2O_3$-NaCl-$NaC_2H_3O_2$-NaBr-$NaNO_3$ indicating that bromide did not act as PEDOT counter-ions for either of these mixtures. The N 1s region was not shown, but there was no nitrate contribution for the PEDOT-$Na_2S_2O_3$-NaCl-$NaC_2H_3O_2$-NaBr-$NaNO_3$ sample. The qualitative summarized results are listed in Table 5.2 for ease. Some quantitative results (atomic percentages) from selected samples are shown in Table 5.5.

PEDOT-CI	$C_6H_5O_7^{3-}$	$H_2PO_4^-$ /HPO_4^{2-}	$S_2O_3^{2-}$	CO_3^{2-}	Cl^-	$C_2H_3O_2^-$	Br^-	ClO_4^-	NO_3^-
$Na_3C_6H_5O_7$ -$Na_2S_2O_3$	X		XX						
$K_3C_6H_5O_7$-NaCl	XX				X				
$Na_3C_6H_5O_7$ -Na_2CO_3	X			X					
$K_3C_6H_5O_7$-LiBr	X						X		
$Na_3C_6H_5O_7$ -NaBr	X						X		
$K_3C_6H_5O_7$-$LiClO_4$	X							X	
$Na_3C_6H_5O_7$ -$NaClO_4$	X							X	
$K_3C_6H_5O_7$-$NaNO_3$	X								
$Na_3C_6H_5O_7$ -$NaNO_3$	X								
Na_2HPO_4-$Na_2S_2O_3$			X						
Na_2HPO_4-LiBr		X					X		
Na_2HPO_4-$LiClO_4$								X	
Na_2HPO_4-$NaNO_3$		X							
$Na_2S_2O_3$-$CaCO_3$			X						
$Na_2S_2O_3$-NaCl			X						
$Na_2S_2O_3$-LiBr			X						
$Na_2S_2O_3$-$LiClO_4$			X						
$Na_2S_2O_3$-$NaNO_3$			X						
Na_2CO_3-NaBr				X			XX		
Na_2CO_3-$NaClO_4$				X				XX	
Na_2CO_3-$NaNO_3$				XX					X
NaCl-$NaC_2H_3O_2$					X	X			
NaCl-LiBr					X		X		
NaCl-NaBr					X		XX		
NaCl-					X			XX	

$NaClO_4$									
NaCl-$NaNO_3$					X				X
$NaC_2H_3O_2$-LiBr						X	X		
$NaC_2H_3O_2$-NaBr						X	XX		
$NaC_2H_3O_2$-$LiClO_4$						X		XX	
$NaC_2H_3O_2$-$NaClO_4$						X		XX	
$NaC_2H_3O_2$-$NaNO_3$						X			X
LiBr-$LiClO_4$							X	X	
NaBr-NaClO4							X	XX	
LiBr-$NaNO_3$							X		
NaBr-$NaNO_3$							X		

Table 5.2 Summary of XPS results on PEDOT electrochemically polymerized with two anions mixtures (XX denotes higher quantity)

As seen in the previous section, when present in the mixture, $S_2O_3^{2-}$ always dominated as the major PEDOT counter-ion. Table 5.2 also shows the dominance of citrate, when without the presence of thiosulfate in the mixture, as the PEDOT counter-ion. This is true even for the $C_6H_5O_7^{3-}$-$S_2O_3^{2-}$ mixture, where citrate still can act as a counter-ion, despite the fact that the $S_2O_3^{2-}$ is dominating. In citrate mixtures, other anions can also act as counter-ions with the exception of nitrate, which does not incorporate. In all the mixtures containing Br^- or ClO_4^-, when $S_2O_3^{2-}$ is not present, these two anions can always act as major counter-ion contributors. In contrast, NO_3^- only acts as a counter-ion in limited cases, such as with CO_3^{2-}, $C_2H_3O_2^-$, and Cl^-.

PEDOT-CI	$C_6H_5O_7^{3-}$	$H_2PO_4^-$ /HPO_4^{2-}	$S_2O_3^{2-}$	CO_3^{2-}	Cl^-	$C_2H_3O_2^-$	Br^-	ClO_4^-	NO_3^-
NaCl-LiBr-$LiClO_4$							X	X	
NaCl-NaBr-$NaClO_4$					X		XX	XX	
NaCl-NaBr-$NaNO_3$					X		XX		
$NaC_2H_3O_2$-NaBr-$NaClO_4$							X	X	
$Na_3C_6H_5O_7$-$Na_2S_2O_3$-NaBr	X		XX						
NaH_2PO_4-$Na_2S_2O_3$-Na_2CO_3			XX	X					
NaH_2PO_4-NaCl-NaBr					X		XX		
NaH_2PO_4-NaCl-$NaNO_3$					X				
NaCl-$NaC_2H_3O_2$-$NaClO_4$					X			XX	

Table 5.3 Summary of XPS results on PEDOT electrochemically polymerized with three anions mixtures (XX denotes higher quantity)

Similar trends can also be observed in three anion mixtures (Table 5.3). When a mixture contains $S_2O_3^{2-}$, it is always the dominant counter-ion. Br^- and ClO_4^- act as the dominant counter-ions when $S_2O_3^{2-}$ is absent. Chloride acts as a counter-ion in many cases, but only as a minor role. Nitrate and phosphates do not like to act as PEDOT counter-ions at all. By combining these results with those found with the two anion

mixtures the following general qualitative trend of PEDOT counter-ion affinity was determined (from strongest to weakest): $S_2O_3^{2-}$ > COO^- (citrate), Br^-, ClO_4^- > Cl^-, COO^- (acetate), CO_3^{2-}, NO_3^-, $H_2PO_4^-$/HPO_4^{2-}. These results do not follow the Hofmeister Series rigidly, but some of the general trends were present such as the dominance of Br^- and ClO_4^- in all mixtures not containing thiosulfate. The dominance of the $S_2O_3^{2-}$ (hydrated) and citrate COO^- (strongly hydrated) as well as the lack of NO_3^- (weakly hydrated) contributions are the major points of deviation from the Hofmeister series, suggesting that anion hydration is only one factor in determining PEDOT counter-ion affinity.

5.3.3 Mixtures with Four and Five Anions

Next mixtures of four or five anions were studied using XPS. Examples of four and five anion mixtures are displayed in Figure 5.3 as well. The summary of results is shown in Table 5.4. The four anion mixture results, $S_2O_3^{2-}$>ClO_4^-, Br^->CO_3^{2-}, Cl^-, COO^-, closely resemble those of the two and three anion mixtures reported in the previous section, though once five prospective counter-ions were added together, the results resembled those found in the multiple anionic mixtures found in Section 5.3.1 (Table 5.4). Thiosulfate was found to dominate as a PEDOT counter-ion over all other anions. Citrate contributions were found to be the second most dominant. Contributions from the other anions used were only seen when neither thiosulfate nor citrate were present. The lack of all other counter-ion signals in their respective characteristic regions further indicates that other interactions besides anionic hydration were also occurring, possibly amongst the anions in solution.

PEDOT-Cl	$C_6H_5O_7^{3-}$	$H_2PO_4^-$ /HPO_4^{2-}	$S_2O_3^{2-}$	CO_3^{2-}	Cl^-	$C_2H_3O_2^-$	Br^-	ClO_4^-	NO_3^-
$Na_3C_6H_5O_7$-$Na_2S_2O_3$-NaCl-NaBr	X		XX						
NaH_2PO_4-NaCl-$NaC_2H_3O_2$-NaBr		X			X	X	X X		
NaH_2PO_4-$Na_2S_2O_3$-NaCl-NaBr			XX				X		
NaH_2PO_4-NaCl-NaBr-$NaClO_4$					X		X X	XX	
NaH_2PO_4-NaCl-NaBr-$NaNO_3$					X		X X		
$Na_2S_2O_3$-NaCl-$NaC_2H_3O_2$-NaBr			XX			X	X		
$Na_2S_2O_3$-NaCl-NaBr-$NaClO_4$			XX				X	X	
$Na_2S_2O_3$-NaCl-NaBr-$NaNO_3$			X						
Na_2CO_3-NaCl-NaBr-$NaClO_4$				X			X X	XX	
Na_2CO_3-NaCl-NaBr-$NaNO_3$				X			X		
NaCl-$NaC_2H_3O_2$-NaBr-$NaClO_4$						X	X X	XX	
NaCl-$NaC_2H_3O_2$-NaBr-$NaNO_3$					X	X	X X		
$Na_3C_6H_5O_7$-$Na_2S_2O_3$-NaCl-NaBr-$NaClO_4$	X		XX						
$Na_3C_6H_5O_7$-$Na_2S_2O_3$-NaCl-NaBr-	X		XX						

$NaNO_3$									
NaH_2PO_4-NaCl-$NaC_2H_3O_2$-NaBr-$NaNO_3$					X	X	X X		
$Na_2S_2O_3$-NaCl-$NaC_2H_3O_2$-NaBr-$NaClO_4$			X						
$Na_2S_2O_3$-NaCl-$NaC_2H_3O_2$-NaBr-$NaNO_3$			X						

Table 5.4 Summary of XPS results on PEDOT electrochemically polymerized with four and five anions mixtures (XX denotes higher quantity)

PEDOT-CI	**$C_6H_5O_7^{3-}$**	**$H_2PO_4^-$ /HPO_4^{2-}**	**$S_2O_3^{2-}$**	**CO_3^{2-}**	**Cl^-**	**$C_2H_3O_2^-$**	**Br^-**	**ClO_4^-**	**NO_3^-**
NaCl-NaBr					0.41		3.7		
NaCl-$NaClO_4$					0.35			1.91	
NaCl-NaBr-$NaNO_3$					1.77		2.65		
NaCl-$NaC_2H_3O_2$-$NaClO_4$					0.19			1.16	
NaH_2PO_4-NaCl-NaBr-$NaNO_3$					0.39		3.11		

Table 5.5 Examples of quantitative atomic percentages values for the PEDOT counter-ion mixtures

5.3.4 Further Discussion

The domination of the thiosulfate was unexpected especially when given the experimental dominance of ClO_4^- and Br^- seen previously, which was expected due to them being weakly hydrated anions (Table 5.1). An additional unexpected observation found was that in two to three anion combinations containing Br^-, the appearance of

excess Br^- at lower binding energies seemed to be determined by the other counter-ion(s) present in the mixture. This observation was also found to be dependent upon whether the source of Br^- was either LiBr or NaBr. The excess Br^- signature tended to appear with NaCl, Na_2CO_3, $NaNO_3$, and H_2PO_4 mixtures, and with the NaBr and $NaC_2H_3O_2$ mixture. This observation coupled with the lack of other anions acting as PEDOT counter-ions suggests that perhaps an ion-ion interaction is occurring in the water media.

The use of the different cations with the same anion did not generally have a significant impact on the mixture results. This was to be expected because all of the cations used in this study were kosmotropes (from most to least hydrated: Ca^{2+}> Li^+> Na^+> K^+) with the exception of K^+ which is a weak chaotrope.[12,16] The solubility of the salts was not an issue because all the salts used are soluble in aqueous media, except $CaCO_3$ which is weakly soluble. There was also no observed anionic charge dominance trend (i.e. whether monovalent charged anions dominate over multi-valent ones or vice versa).

Ionic size could be another factor to consider. The ionic sizes for anions are listed in Table 5.1. The largest anions, used in this study, were thiosulfate, citrate, and perchlorate, which correlate well with dominance of these species suggesting that ionic size could account for the PEDOT counter-ion affinity order. However, this trend does not account for either the dominance of bromide or the lack of nitrate and phosphate contributions which would be expected if the counter-ion affinity was based soley on ionic size. Overall, the PEDOT counter-ion affinity appears to be based on a variety of variables such as anionic hydration, size, and possibly ion-ion interactions in the aqueous media. Unfortunately, narrowing the variables further is beyond the scope of this study.

5.4. Conclusions

In this study, we investigated PEDOT counter-ion incorporation during the electrochemical polymerization using XPS. Different mixtures with two, three, four, and five anions were investigated to characterize the PEDOT counter-ion affinity in each mixture. A series of anion mixtures varying from one to nine anions by gradually adding one more anion at a time from most highly to most weakly hydrated were also examined. Thiosulfate was found to be dominant over all other anions acting as a PEDOT counter-ion, indicating that PEDOT counter-ion incorporation did not precisely follow the anionic hydration seen in the Hofmeister Series. Thus anionic hydration was not found to be the sole driving force for PEDOT counter-ion incorporation. For every mixture that it was present in, the thiosulfate was found to be the dominant PEDOT counter-ion incorporated regardless of the anionic charge, cation, or anionic hydration in the mixture study.

In the absence of the thiosulfate, $C_6H_5O_7^{3-}$, Br^-, and ClO_4^- were found to act as major counter-ions. Phosphate and nitrate anions were not found to act as PEDOT counter-ions in many circumstances. Since nitrate is weakly hydrated, the expected results would be that nitrate has a similar dominance to that of bromide and perchlorate, but since this result did not occur, another driving force must also be occurring. It is obvious that the number of anions in solution also affect PEDOT counter-ion affinity indicating possible ion-ion interactions in the solution. Using XPS, this study determined the PEDOT counter-ion affinity during the electrochemical polymerization. The general PEDOT counter-ion affinity trend is (from strongest to weakest): $S_2O_3^{2-} > COO^-$ (citrate), Br^-, $ClO_4^- > Cl^-$, COO^- (acetate), CO_3^{2-}, NO_3^-, $H_2PO_4^-/HPO_4^{2-}$. We believe that this

understanding of ion incorporation will aid in the design of electrochemically polymerized PEDOT films to optimize film properties.

5.5 References

1. Spanninga, S.A.; Martin, D.C.; Chen, Z. *J. Phys. Chem. C* **2009**, *113*, 5585.

2. Yang, J.; Lipkim, K.; Martin, D.C. *J. Biomater. Sci. Polymer Edn*., **2007**, *18*, 1075.

3. Zotti, G.; Zecchin, S.; Schiavon, G.; Louwet, F.; Groenendaal, L.; Crispin, X.; Osikowicz, W.; Salaneck, W.R.; Fahlman, M. *Macromolecules* **2003**, *36*, 3337.

4. Beamson, G.; Briggs, D. *High Resolution XPS of Organic Polymers: The Scienta ESCA300 Database*; John Wiley & Sons: New York, New York, 1992.

5. Briggs, D.; Beamson, G. *Anal. Chem.* **1993**, *65*,1517.

6. Briggs, D. *Surface analysis of polymers by XPS and static SIMS*; Cambridge University Press: Cambridge, U.K.1998.

7. Siegbahn, K.; Nordling, C.; Fahlman, A.; Nordberg, R.; Hamrin, K.; Hedman, J.; Johansson, G.; Bergmark, T.; Karlsson, S.E.; Lindgren, I.; Lindberg, B. *ESCA: atomic, molecular and solid state structure studied by means of electron spectroscopy.* Uppsala: Uppsala,SWE, 1967.

8. Hofmeister, F. *Arch. Exp. Pathol. Pharmakol*. **1888**, *24*, 247.

9. Kunz, W.; Henle, J.; Ninham, B.W. *Curr. Opin. Colloid Interface Sci.* **2004**, *9*, 19.

10. Zhang, Y.; Cremer, P.S. *Curr. Opin. Chem. Biol*. **2006**, *10*, 658.

11. Collins, K.D. *Biophys. J*. **1997**, *72*, 65.

12. Jenkins, H.D.B.; Marcus, Y. *Chem. Rev*. **1995**, *95*, 2695.

13. Jones, G.; Dole, M. *J. Am. Chem. Soc*. **1929**, *51*, 2950.

14. Ru, M.T.; Hirokane, S.Y.; Lo, A.S.; Dordick, J.S.; Reimer, J.A.; Clark, D.S. *J. Am. Chem. Soc*. **2000**, *122*, 1565.

15. Marcus, Y. *J. Soln. Chem*. **1994**, *23*, 831.

16. Marcus, Y. *Chem. Rev*. **2009**, *109*, 1346.

17. Spanninga, S.A.; Martin, D.C.; Chen, Z. (submitted)

18. Dennis, A.M.; Howard, R.A.; Kadish, K.M.; Bear, J.L.; Brace, J.; Winograd, N. *Inorg. Chem. Acta* **1980**, *44*, L139.

19. Gelius, U.; Heden, P.F.; Hedman, J.; Lindberg, B.J.; Manne, R.; Nordberg, C.; Nordling, C.; Siegbahn, K. *Phys. Scr*. **1970**, *2*, 70.

20. Tselesh, A.S. *Thin Solid Films* **2008**, *516*, 6253.

CHAPTER 6

PEDOT-BASED BIOSENSORS

6.1 Introduction

The ability to sense biologically relevant chemical quantities is important both scientifically and for improving the quality of life. Biosensors have already been demonstrated to improve the quality of life for those affected by improper biochemistry conditions. Enzyme-based biosensors are of special interest since by utilizing the natural function of an enzyme, substances in the body may be quantitatively measured, while minimizing the amount of foreign materials introduced. Physical immobilization of the enzyme within a polymer matrices have become popular as interfacing agents with tissue due to their favorable physical properties, such as softness, low impedance, and high surface area.

In biosensors, biologically active molecules, such as proteins, enzymes, and antibodies, act as the sensing components. Biosensors can be grouped into two major types based on the method by which the biologically active component is immobilized: chemical and physical immobilization. Within each of the two major type of fabrication, there are multiple methods that can be employed to immobilize the sensing component to improve overall performance.

Physical immobilization is the direct entrapment of the biological component, in this case an enzyme, usually within a matrix material. Enzyme based biosensors take advantage of the reduction-oxidation (redox) reactions occurring within the redox center of the enzyme for their ability to sense. The electrons given off during this reaction are transported to the electrode and detected using amperometry. The proximity of the redox center to the outside of the enzyme aids in the determination of the electron transfer mechanism. In order to optimize biosensor performance, the enzyme should be immobilized in such a way to offer the least resistance in the electron path from the redox center to the electrode. A direct connection between the enzyme and the electrode to maximize the electron transfer and minimize the transfer distance would be the most preferable condition and forms the basis for enzyme based conductive polymer biosensors.[1]

Biosensors based upon electron transfer also tend to utilize diffusional mediators to increase electron transfer rates and efficiency to the electrode. Unfortunately, many common mediators are toxic, therefore prohibiting their use within the human body. In order for efficient electron transfer to occur, the mediator must have an electron transfer rate equal to or greater than that of the substrate to enzyme.[1]

Poly (3,4-ethylenedioxythiophene) (PEDOT) has been used to fabricate biosensors using similar methods to those employed for polypyrrole (PPy) to achieve a superior biosensor. Researchers in the Wallace Group, as well as others, have shown that PPy can successfully incorporate biological materials such as antibodies[2-4], enzymes[5,6], and even whole red blood cells[7] into a biosensor by electrochemical polymerization. Electrochemical polymerization of the PPy acts to both trap and immobilize the

biological material as well as using its conductive nature to detect environmental changes. These environmental changes, such as the presence of an antigen, were detected by either a difference in resistance, in the reduction-oxidation positions in the cyclic voltammetry curves, or by chrono-amperometry.

Some of the ionically and conductive polymers which have or could act as biosensor matrix materials are PPy, PEDOT, and potentially melanin. Both PPy and PEDOT have been extensively electrically tested and characterized. Polypyrrole has a more extensive history in terms of biological applications, including its use in the fabrication of biosensors.[5,6,8-12] In contrast to both PEDOT and PPy, melanin is a natural alternative to synthetic polymers, but further research must be conducted on its properties before it can be considered for future application uses.

The incorporation of the enzyme, glucose oxidase, during electrochemical polymerization has already been used to fabricate glucose biosensors.[9,12-17] PEDOT based sensors were found to have better life-time[12] and less degradation[9] than their PPy counter-parts. To maximize the quantity of enzyme incorporated, many studies have either used chemically modified glucose oxidase[16], put in additives such as surfactants[13,15,16], or positively charged polymers[14] to attract the negatively charged enzyme. In order to improve charge carrying efficiency a mediator, such as ferrocene, is commonly used.[8,9,14-17]

In the current study, we prepared PEDOT-based biosensors by physical entrapment of glucose oxidase (GOx), l-lactate dehydrogenase (LDH), glutamate oxidase (GLOD), and Tyrosinase during the electrochemical polymerization of an aqueous solution onto indium tin oxide (ITO) or Pt/Ir cochlear ball electrodes. Glucose oxidase

was the first enzyme used in the fabrication and underwent parameter optimization. Fabrication parameters such as enzyme concentration, the presence of a counter-ion(s), and electrochemical polymerization deposition conditions were optimized. L-lactate dehydrogenase, tyrosinase and glutamate oxidase biosensors followed the successful fabrication of glucose oxidase biosensors.

Enzyme concentration and deposition parameters were optimized using ITO electrodes for ease in both chemical and physical characterization. Initial attempts began with EDOT-enzyme based aqueous solution, followed by the introduction of PEDOT counter-ions (such as PSS) to optimize sensor performance, then the addition of a mediator to increase electron transfer mobility, and finally by trying to maximize the quantity of enzyme at the surface. The goal during fabrication was to maximize the amount of exposed enzyme at the surface, in conjunction with trying to minimize the amount buried within the polymer matrix. These conditions were favored in order to decrease the amount of substrate diffusion required to reach the enzyme's active site. In order to accomplish this, a layering technique was utilized. Following parameter optimization, platinum/iridium (Pt/Ir) wire cochlear ball electrodes were used to minimize the quantities of enzyme concentrated solution that were required for deposition.

Three different categories of characterization; chemical, biosensor performance, and physical; were used to determine enzyme entrapment, sensitivity, and selectivity. In this study, the presence of the enzyme will be verified using X-ray photoelectron spectroscopy (XPS) for chemical confirmation, electrical properties will be determined with electrochemical impedance spectroscopy (EIS) and cyclic voltammetry (CV) for

electrical properties. Enzyme functionality, sensitivity, and selectivity were tested using chrono-amperometry.

6.2 Experimental

6.2.1 Materials

The 3,4-ethylenedioxythiophene (EDOT) monomer was obtained from H.C. Starck. Glucose Oxidase from Aspergillus niger (GOx) (EC 1.1.3.4) (Type II 15,000-50,000 units/g, 160 kDa), L-Lactic Dehydrogenase from Bovine heart (EC 1.1.1.27) (Type III, ammonium sulfate suspension, > 500 units/mg), L-Glutamate Oxidase from Streptomyces (EC 1.4.3.11) (>5 units/mg, 140 kDa), Tyrosinase (EC 1.14.18.1) (>1000 unit/mg, ~120 kDa), D-(+)-glucose, sucrose, D-(-) fructose, D-(+) galactose, heparin sodium salt, sodium pyruvate, 3,4-Dihydroxy-L-phenylalanine (L-dopa), L-glutamic acid, and ferrocene were obtained from Sigma-Aldrich. Beta-Nicotinamide adenine dinucleotide disodium salt (NADH) and poly(sodium 4-styrenesulfonate) (PSS) was obtained from Acros Organics. These chemicals were all used as received. Phosphate buffer solution (10x concentration), containing KH_2PO_4, NaCl, and Na_2HPO_4, was obtained from Hyclone and then diluted to a 1x concentration. Indium tin oxide (7x10 mm at 4-8 ohms) was obtained from Delta Technologies Limited. Platinum/ Iridium cochlear ball electrodes (0.0078 cm^2) made in house from 90/10 Pt/Ir teflon coated wire from A-M Systems, Inc.

6.2.2 Electrochemical Polymerization, Impedance Spectroscopy, Cyclic Voltammetry, and Chrono-Amperometry

PEDOT electrochemical polymerization was performed using galvanostatic current to a 0.01 M EDOT aqueous solution with 0.01 M PSS and 1000 units/ml (47.2 mg/ml) GOx. The samples were deposited on indium tin oxide (ITO) electrodes (7 x 10 mm) at 30 μA. Based on preliminary experiments, a layer of PEDOT-PSS was deposited for 3 minutes and then another layer of PEDOT-PSS-GOx was deposited for 2 minutes. The same experiment conditions were used for LDH and PEDOT-Heparin-GOx, except Heparin was substituted for PSS, sensors. Conentrations of 1000 units/ml were used in the LDH and Heparin deposition solution concentrations. PEDOT-Tyrosinase sensors were deposited for 10 minutes at 30 μA on ITO electrodes (7x10 mm). PEDOT-GLOD sensors were deposited on Pt/Ir electrodes for 10 minutes at 30 μA. The samples were then rinsed in de-ionized water to remove excess counter-ion from the surface and allowed to air dry.

The impedance range was 1-100,000 Hz while a range of -1 V to +1 V was used for CV at a scan rate of 0.1 V/s for three cycles. Chrono-amperometry utilized a potential of 0.7 versus a SCE in 1x PBS with 0.3 mM ferrocene under continuous stirring.

6.2.3 X-Ray Photoelectron Spectroscopy (XPS)

Initial survey scans were run using a pass energy of 160 eV, while characteristic region scans of the C 1s, O 1s, S 2p, N 1s, and Si 2p utilized a pass energy of 20 eV with a step of 0.1 eV. All spectra were referenced using the C-C/C-H peak at 285 eV.

6.3 Results and Discussion

6.3.1 PEDOT-PSS-Glucose Oxidase

Glucose oxidase (EC 1.1.3.4) is classified as an oxidoreducatase enzyme undergoing oxidation-reduction reactions on the CH-OH group of the donor with O_2 as an acceptor by the following reaction:

B-D-Glucose+O_2+H_2O→D-Glucono-1,5-Lactone+H_2O_2

Glucose oxidase has been used extensively in previous research in glucose biosensor fabrication[9,12-17] for diabetes applications.

Glucose sensing can take place through two possible pathways (Figure 6.1). The first involves directly reading the electron given off from the enzyme's redox center to the electrode or by the electron being transferred to the ferrocene, the ferrocene goes through a redox reaction, then the electron is transferred to the electrode. The second pathway involves reading the electron given off from H_2O_2, a byproduct of the enzyme reaction, when $O_2+2H^+ +2e^- \Leftrightarrow H_2O_2$. The H_2O_2 pathway is possible because the standard potential needed for this to occur, 0.454 V vs. SCE, is within the 0.7 V potential applied to the system.[18]

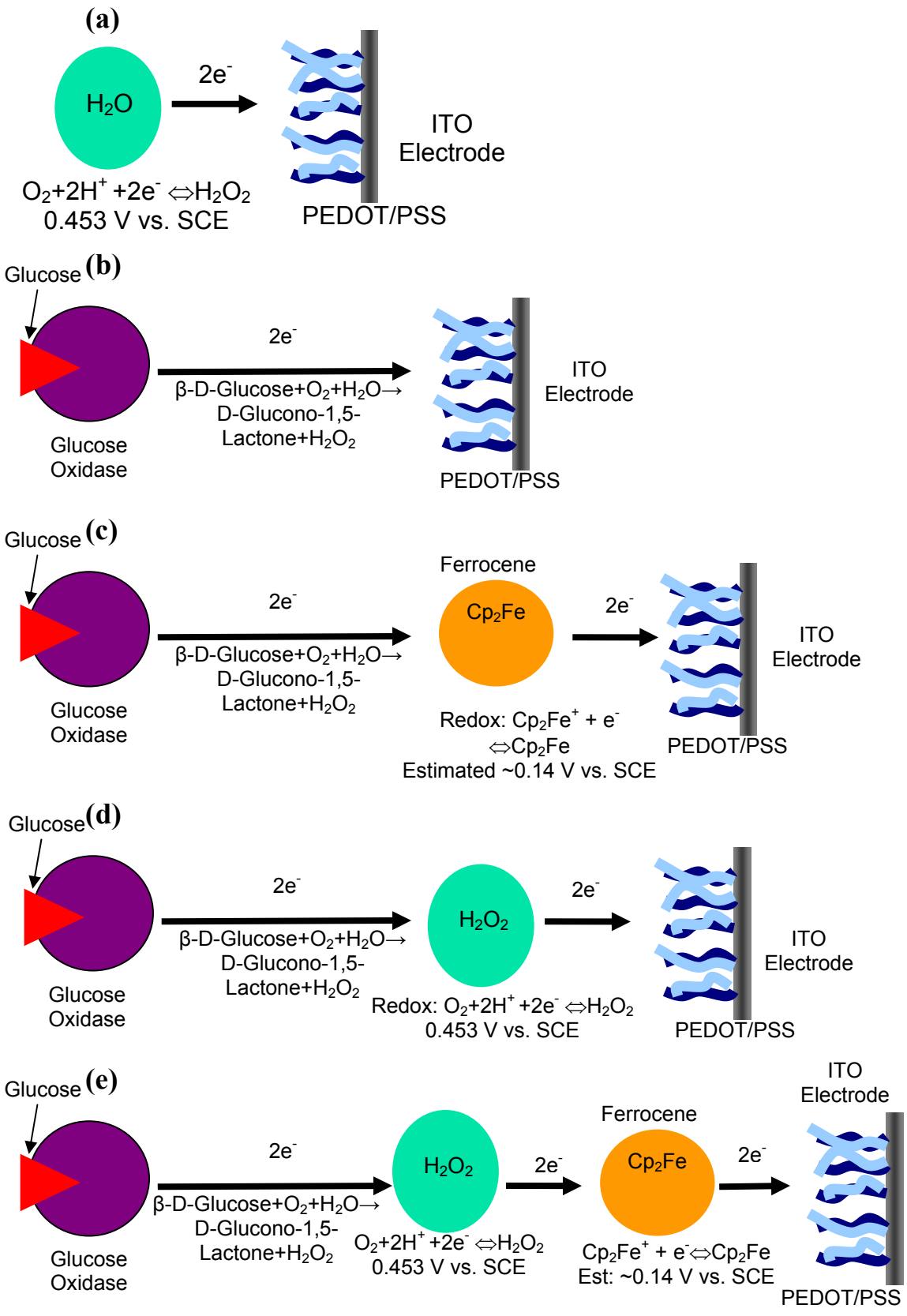
(a)
H_2O
2e⁻
ITO
Electrode
$O_2+2H^+ +2e^- \Leftrightarrow H_2O_2$
0.453 V vs. SCE
PEDOT/PSS
Glucose
(b)
2e⁻
β-D-Glucose+O_2+H_2O→
D-Glucono-1,5-
Lactone+H_2O_2
ITO
Electrode
Glucose
Oxidase
PEDOT/PSS
Glucose
(c)
Ferrocene
Cp_2Fe
2e⁻
2e⁻
β-D-Glucose+O_2+H_2O→
D-Glucono-1,5-
Lactone+H_2O_2
ITO
Electrode
Glucose
Oxidase
Redox: $Cp_2Fe^+ + e^-$
$\Leftrightarrow Cp_2Fe$
Estimated ~0.14 V vs. SCE
PEDOT/PSS
Glucose
(d)
2e⁻
H_2O_2
2e⁻
β-D-Glucose+O_2+H_2O→
D-Glucono-1,5-
Lactone+H_2O_2
ITO
Electrode
Glucose
Oxidase
Redox: $O_2+2H^+ +2e^- \Leftrightarrow H_2O_2$
0.453 V vs. SCE
PEDOT/PSS
Glucose
(e)
ITO
Electrode
Ferrocene
2e⁻
H_2O_2
2e⁻
Cp_2Fe
2e⁻
β-D-Glucose+O_2+H_2O→
D-Glucono-1,5-
Lactone+H_2O_2
Glucose
Oxidase
$O_2+2H^+ +2e^- \Leftrightarrow H_2O_2$
0.453 V vs. SCE
$Cp_2Fe^+ + e^- \Leftrightarrow Cp_2Fe$
Est: ~0.14 V vs. SCE
PEDOT/PSS

Figure 6.1 Glucose sensing pathways (a) H_2O_2 sensing, (b) Direct electron sensing, (c) Sensing through ferrocene mediated pathway, (d) H_2O_2 Sensing from GOx, and (e) H_2O_2 Sensing from GOx through ferrocene mediated pathway

6.3.1.1 Electrical Characterization

EIS and CV (Figure 6.2) were used to characterize the electrical properties of the films with various glucose oxidase concentrations in the deposition solution. Figure 6.2 showed only slight changes in the impedance, phase angle, and cyclic voltammetry plots when compared to the PEDOT-PSS film grown under the same conditions for 5 minutes, this was likely because the films take on the characteristics of PEDOT-PSS films since the first layer was composed entirely of PEDOT-PSS and the second layer was also composed of PEDOT-PSS components along with the glucose oxidase.

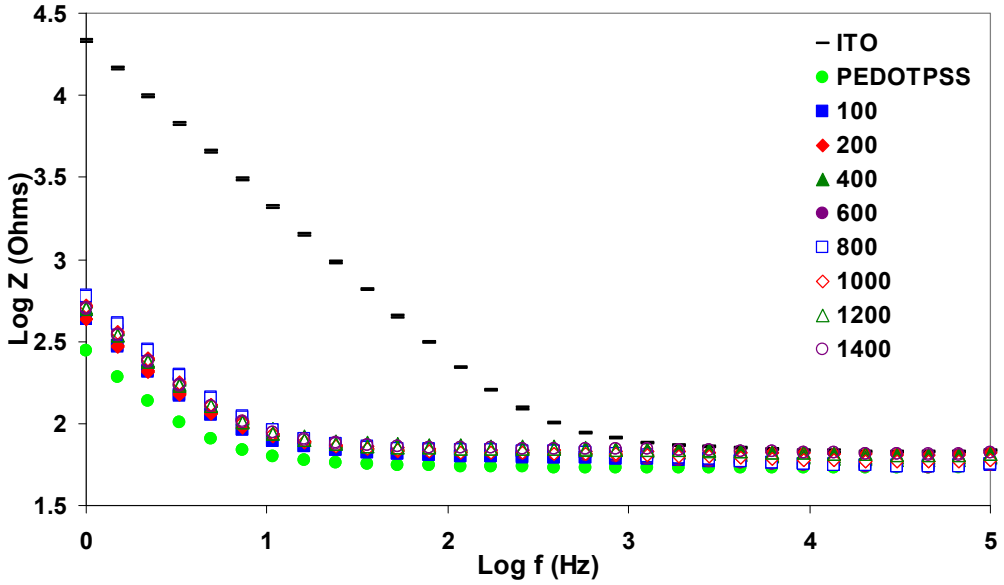

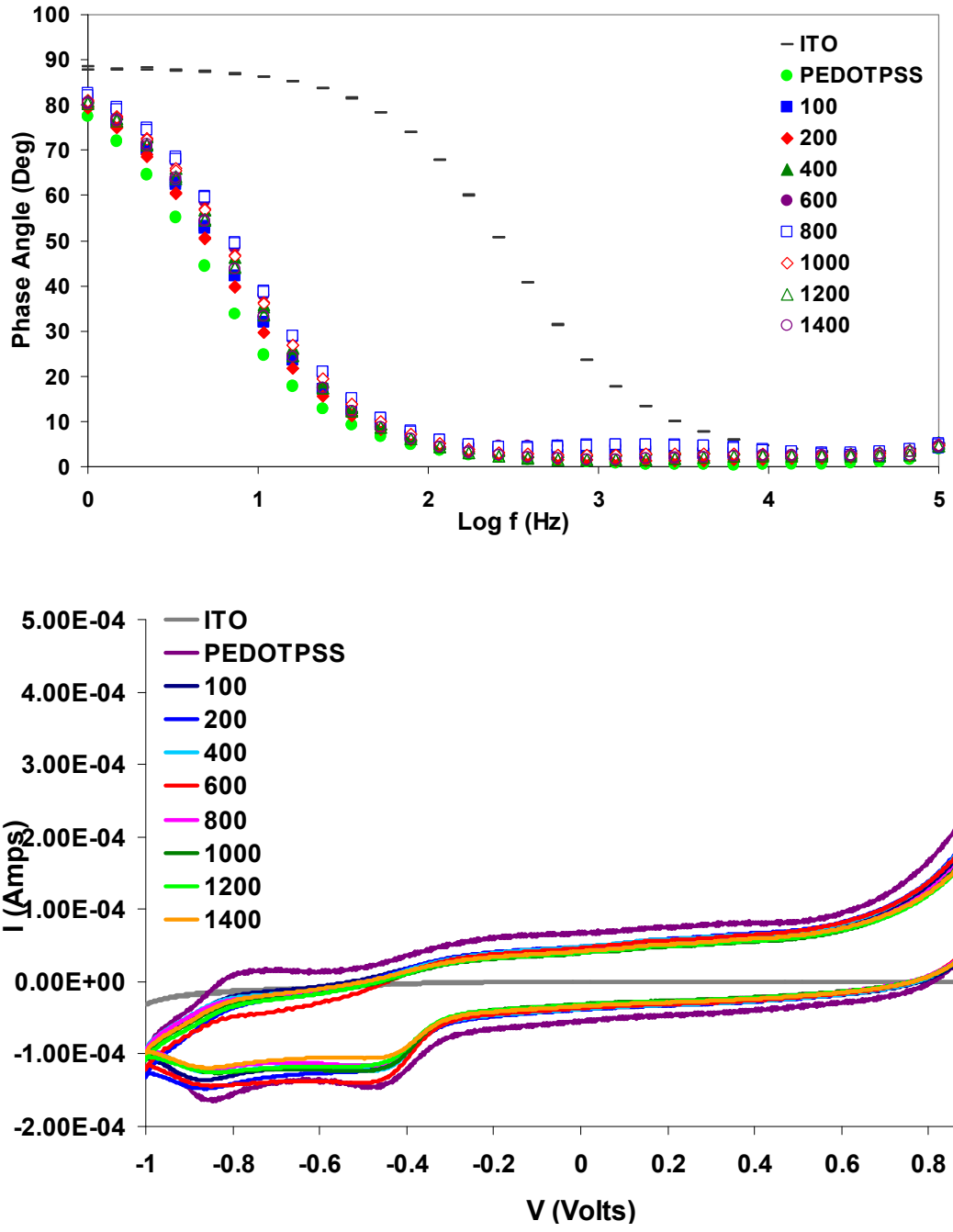

Figure 6.2 (top) Impedance spectra, (middle) Phase Angle spectra, and (bottom) Cyclic voltammetry of PEDOT-PSS 3 + PEDOT-PSS-GOx 2 minute biosensors with different Glucose Oxidase concentrations (units/ml)

6.3.1.2 Chemical Analysis

Figure 6.3 show the characteristic C1s, S 2p and N 1s regions for PEDOT-PSS 3+ PEDOT-PSS-GOx 2 biosensors respectively. The characteristic C 1s region, Figure 6.3a, displays peaks at 285 eV (C-C/C-H), 285.3 eV(C-S), 286.3 eV (C=C-O), 287 eV (C-O-C)[19], and ~288. 5 eV (amidic N-CH-C*=O).[20] While the C-C/C-H, C-S, C=C-O, C-O-C, and C-SO_3 contributions were from both PEDOT and PSS respectively, the additional C-C/C-H bonding and the presence of the amidic N-CH-C*=O peak were indictative of the enzyme GOx. The verification of the enzyme's presence was seen in the characteristic N 1s spectra, Figure 6.3c, with the appearance of the amidic N-H peak at ~400.5 eV.

The characteristic S 2p region, Figure 6.3b, was interesting because it clearly showed that as the glucose oxidase concentration in the deposition solution increased; the characteristic PEDOT sulfur spin-split doublet (S $2p_{3/2}$ ~164 eV) decreased suggesting that the glucose oxidase was covering the PEDOT. The PSS sulfur doublet (SO_3 $2p_{3/2}$~168 eV) also decreased, but only slightly in comparison to the PEDOT. This decrease was likely due to the PSS only being partially covered by the glucose oxidase. Figure 6.4 compares the decreasing PEDOT $2p_{3/2}$ with the increasing GOx N-H peak intensities. The results show that by a concentration of 1400 units/ml, only ~17% of the orginal PEDOT signal is present indicating extensive GOx surface coverage.

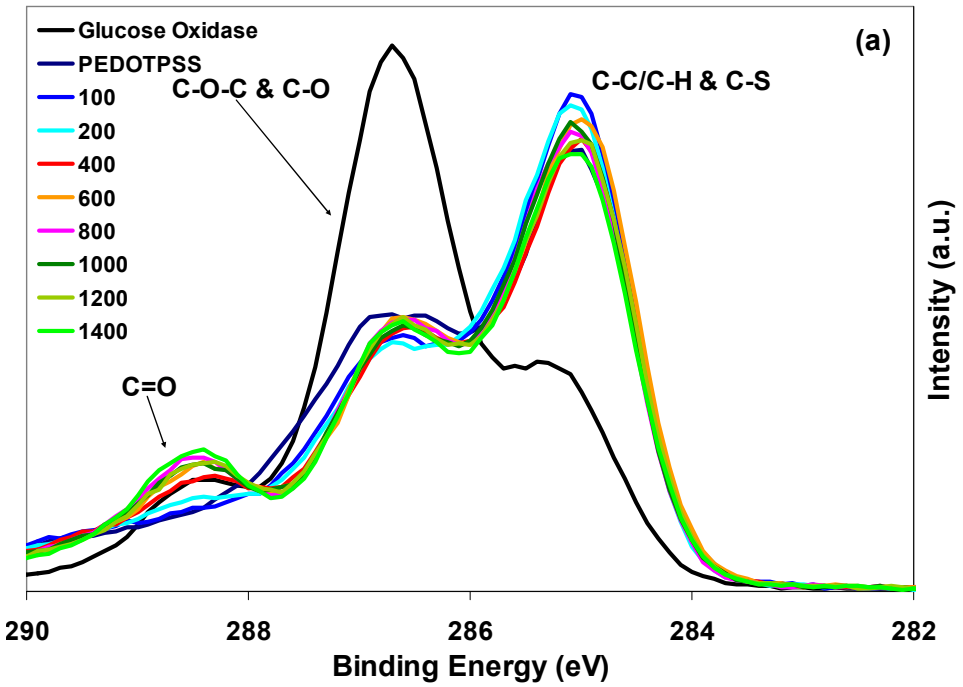
Glucose Oxidase
PEDOTPSS
100
200
400
600
800
1000
1200
1400
(a)
C-O-C & C-O
C-C/C-H & C-S
C=O
Intensity (a.u.)
290
288
286
284
282
Binding Energy (eV)

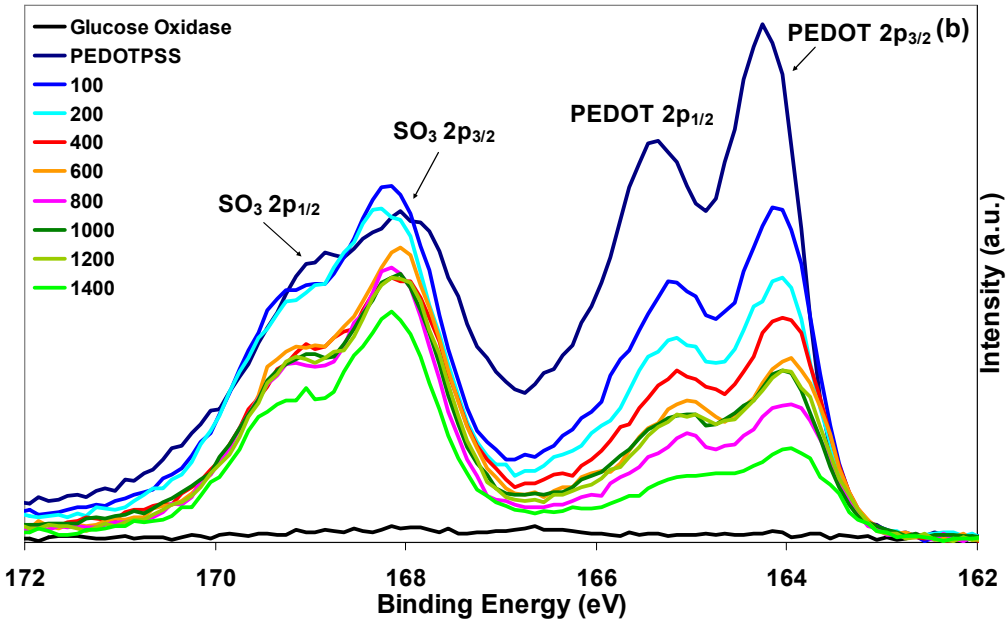
Glucose Oxidase
PEDOTPSS
100
200
400
600
800
1000
1200
1400
PEDOT 2p3/2 (b)
PEDOT 2p1/2
SO3 2p3/2
SO3 2p1/2
Intensity (a.u.)
172
170
168
166
164
162
Binding Energy (eV)

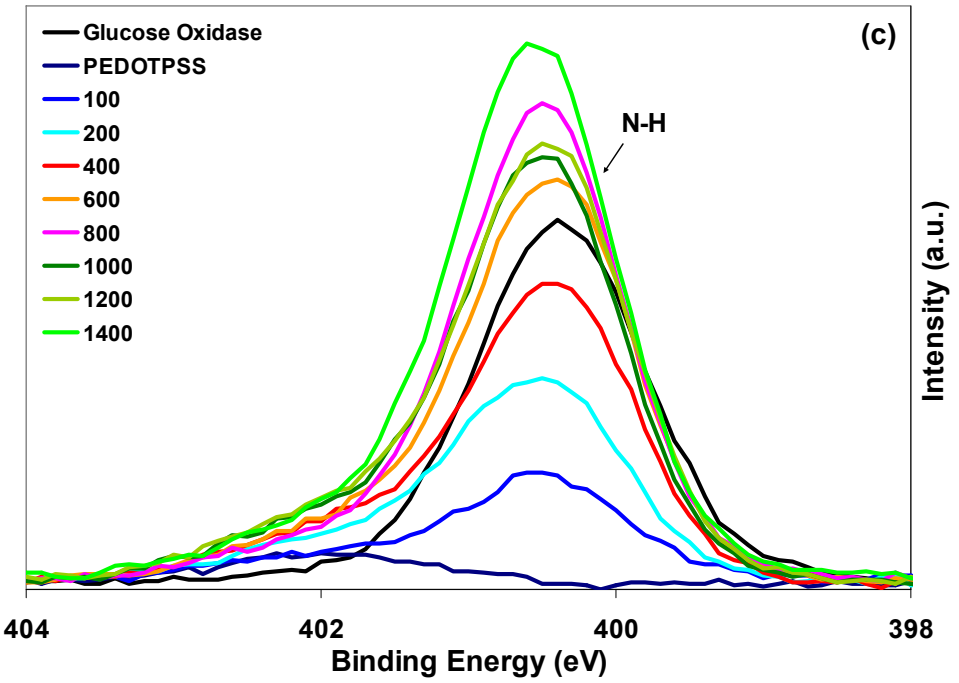

Figure 1.3 (a) C 1s, (b) S 2p, and (c) N 1s characteristic regions of PEDOT-PSS 3 + PEDOT-PSS-GOx 2 minute biosensors with different Glucose Oxidase concentrations (units/ml)

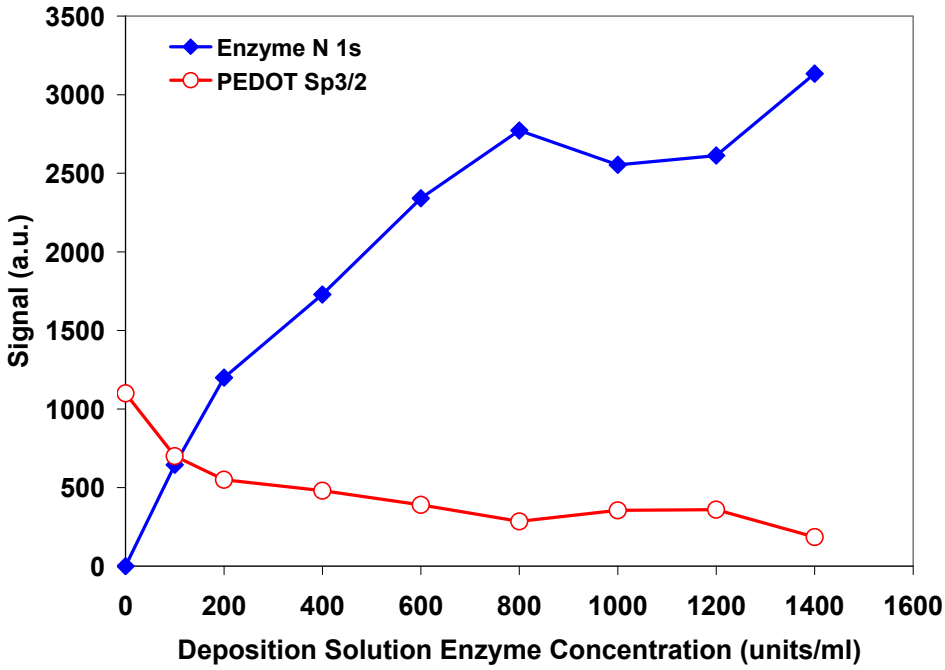

Figure 6.4 PEDOT and Glucose Oxidase Signal as a function of enzyme deposition solution concentration

6.3.1.3 Sensitivity

The ability to sense hydrogen peroxide as depicted in Figure 6.1a diagram was tested by adding H_2O_2 to the bath in the presence of a PEDOT-PSS-GOx deposited for 10 minutes on ITO (Figure 6.5). The results show that H_2O_2 sensing was possible as would be expected at a potential of 0.7 V.

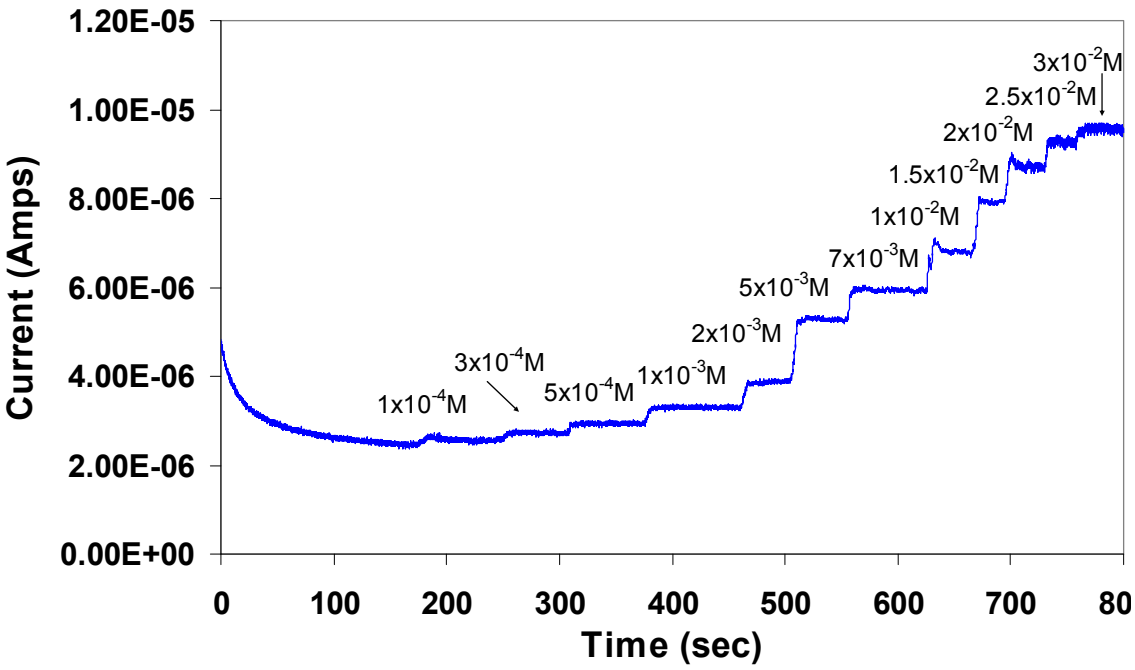

Figure 6.5 Hydrogen peroxide sensing in the presence of a PEDOT-PSS-GOx film.

After the hydrogen peroxide control was tested, glucose sensing without a mediator with a PEDOT-PSS 3 minute + PEDOT-PSS- GOx 2 minute films was completed (Figure 6.6). Since no mediator was present the possible sensing pathways are limited to Figures 6.1a and 6.1b. PEDOT-PSS 3+PEDOT-PSS-GOx 2 minute films were tested in 1x PBS as well as in the presence of 0.3 mM ferrocene in 1x PBS both with and without glucose additions ($1x10^{-4}$, $3x10^{-4}$, $5x10^{-4}$, $1x10^{-3}$, $2x10^{-3}$, $5x10^{-3}$, $7x10^{-3}$, $1x10^{-2}$, $1.5x10^{-2}$, $2x10^{-2}$, $2.5x10^{-2}$, and $3x10^{-2}$ M) occurred approximately every 50 seconds at ~25°C. As can be see, even without a mediator present, there was sensing but the sensing was not sensitive to glucose concentration.

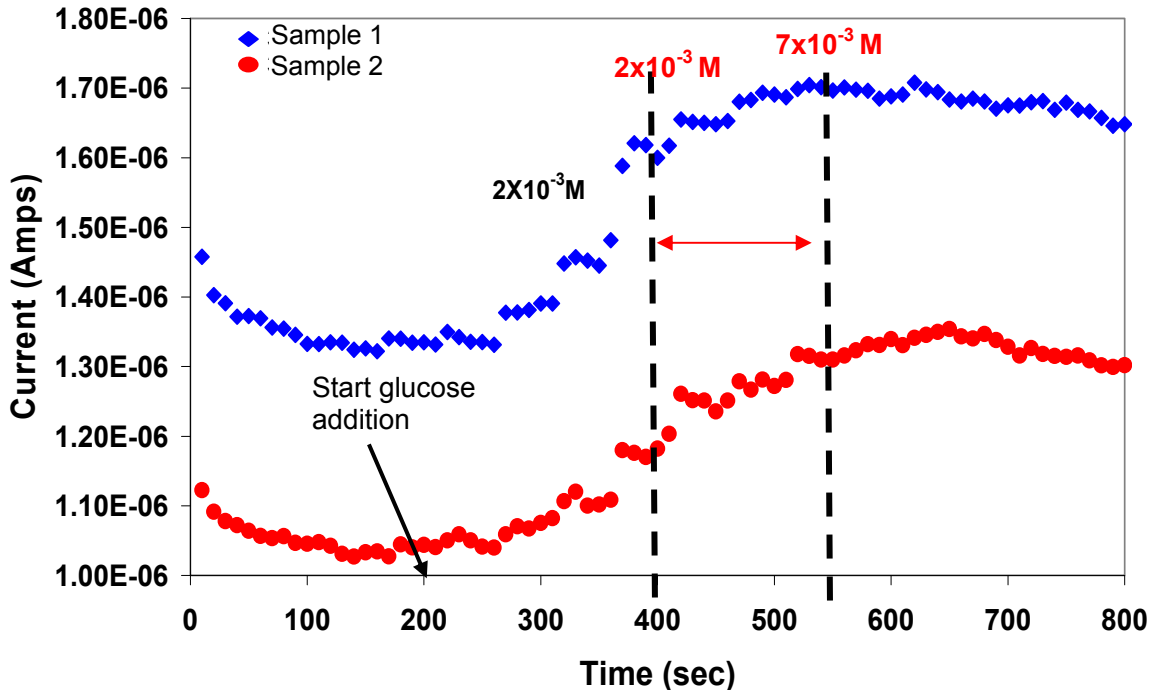

Figure 6.6 Glucose sensing using a 3+2 PEDOT-PSS-GOx sensor without the presence of a mediator

Figure 6.7 demonstrates the sensing ability with clear and defined step-like responses to glucose additions of a PEDOT-PSS 3+PEDOT-PSS-GOx 2 minute biosensor in the presence of ferrocene indicates that electron transfer via ferrocene is occurring either by the Figure 6.1c or 6.1e pathways. The minimum amount of glucose detected was ~$5x10^{-4}$M glucose.

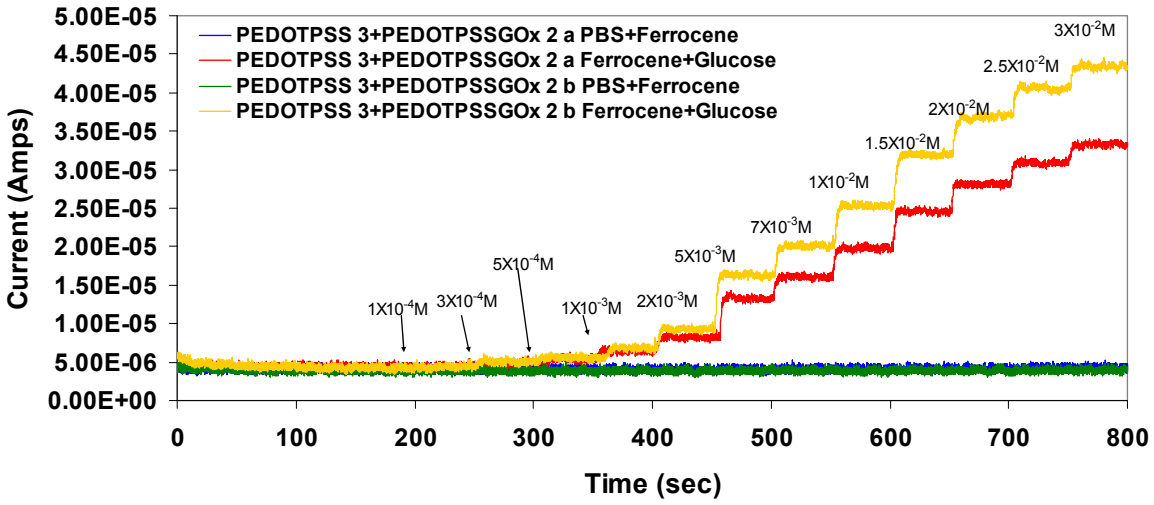

Figure 6.7 Chrono-amperometry of PEDOT-PSS 3 + PEDOT-PSS-GOx 2 minute biosensors

The current response as a function of glucose addition concentration for sensors with different enzyme deposition solution concentrations is shown in Figure 6.8. The basic data trend suggests that with increased amounts of glucose oxidase present, there was a larger current response per glucose addition. This would be expected because the higher the GOx surface concentration would result in larger amount of electrons given off through direct transfer and/or through the H_2O_2 pathway and a higher probability that those electrons would be transferred to the electrode. A concentration of 1000 units/ml GOx was chosen because it had a significant current response with all the glucose additions. In terms of detection, a larger enzyme concentration would imply easier detection.

The 800 units/ml samples had higher current responses. This was likely caused by the deposited enzymes having a more favorable orientation (i.e. not buried within the film). Since the orientation can not be controlled during this type of physical

immobilization, the only way to correct this is by chemical immobilization using a non-prevalent amino acid on the enzyme's surface. By using a non-prevalent amino acid, essentially the enzyme's orientation on the surface is able to be directed. Judging from previously published data[15], the current response was supposed to be linear with glucose addition. This did not occur, at this time it is not know why there are slope deviations occurring around the 0.005 M and 0.007 M glucose additions.

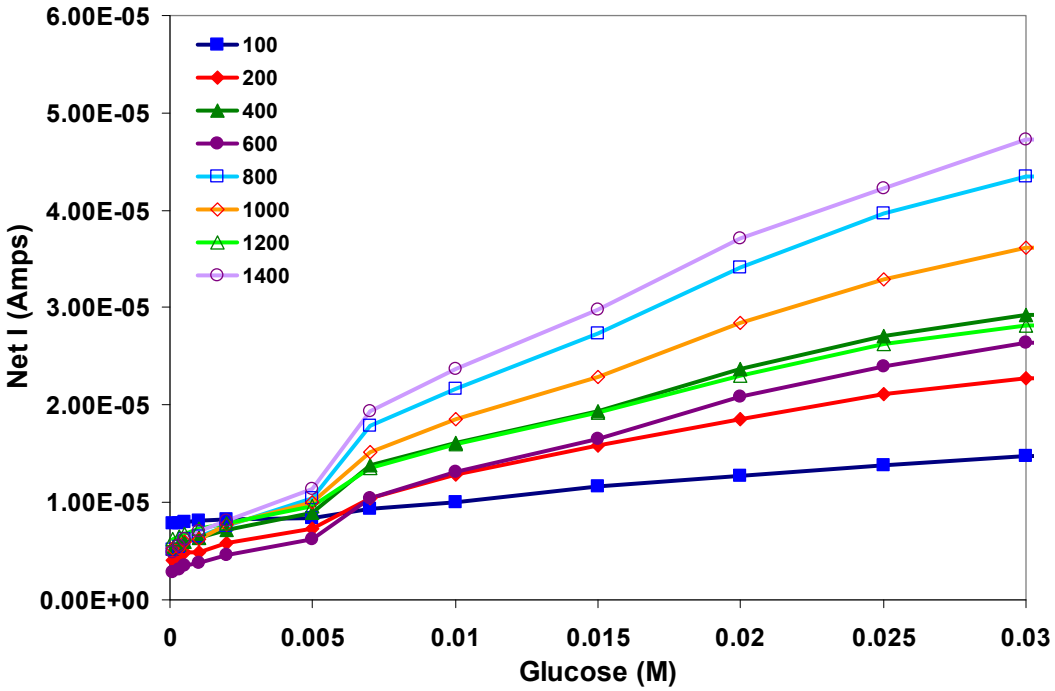

Figure 6.8 Current response as a function of glucose addition concentrations of PEDOT-PSS 3 + PEDOT-PSS-GOx 2 minute biosensors with different Glucose Oxidase concentrations (units/ml)

6.3.1.4 Selectivity

In order to test the selectivity, PEDOT-PSS 3+PEDOT-PSS-GOx 2 minute biosensors were also tested with sucrose, fructose, and galactose (Figure 6.9) additions using the concentrations as used with glucose additions. Where fructose and galactose are isomers of glucose and sucrose is a disaccharide verses glucose which is a monosaccharide. The biosensors only detected glucose and not sucrose, fructose, or galactose. This confirms that the natural specificity and selectivity of glucose oxidase is toward only glucose.

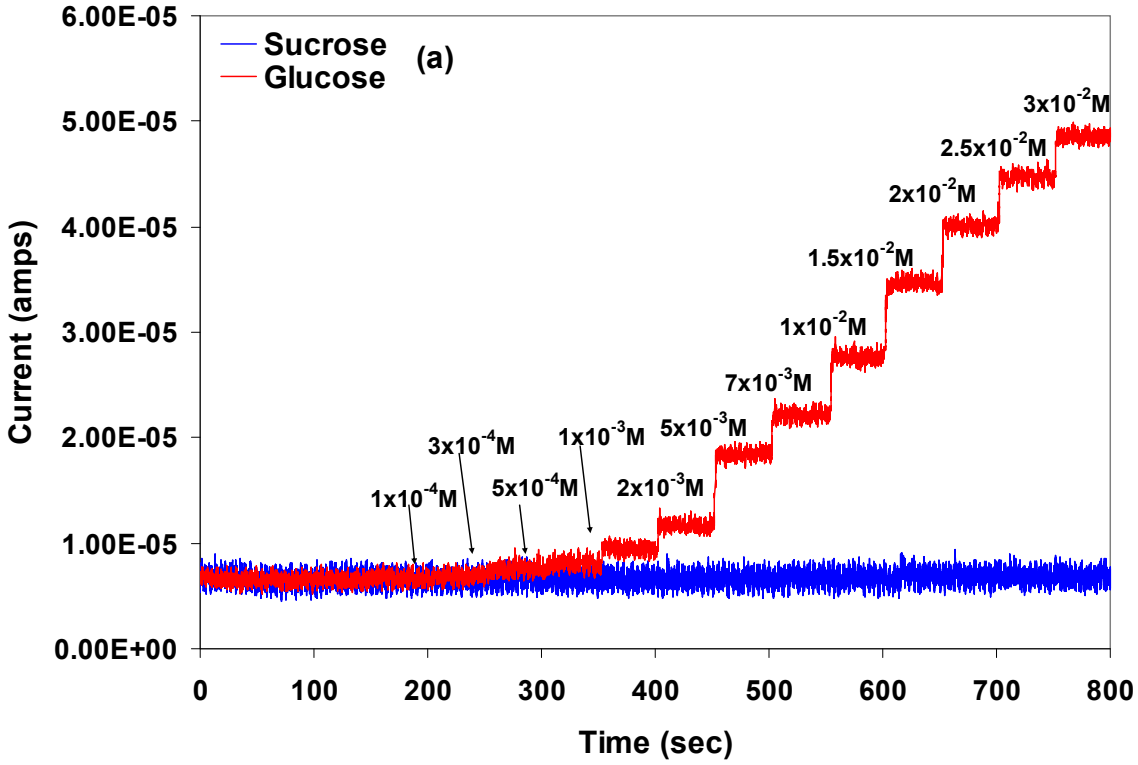

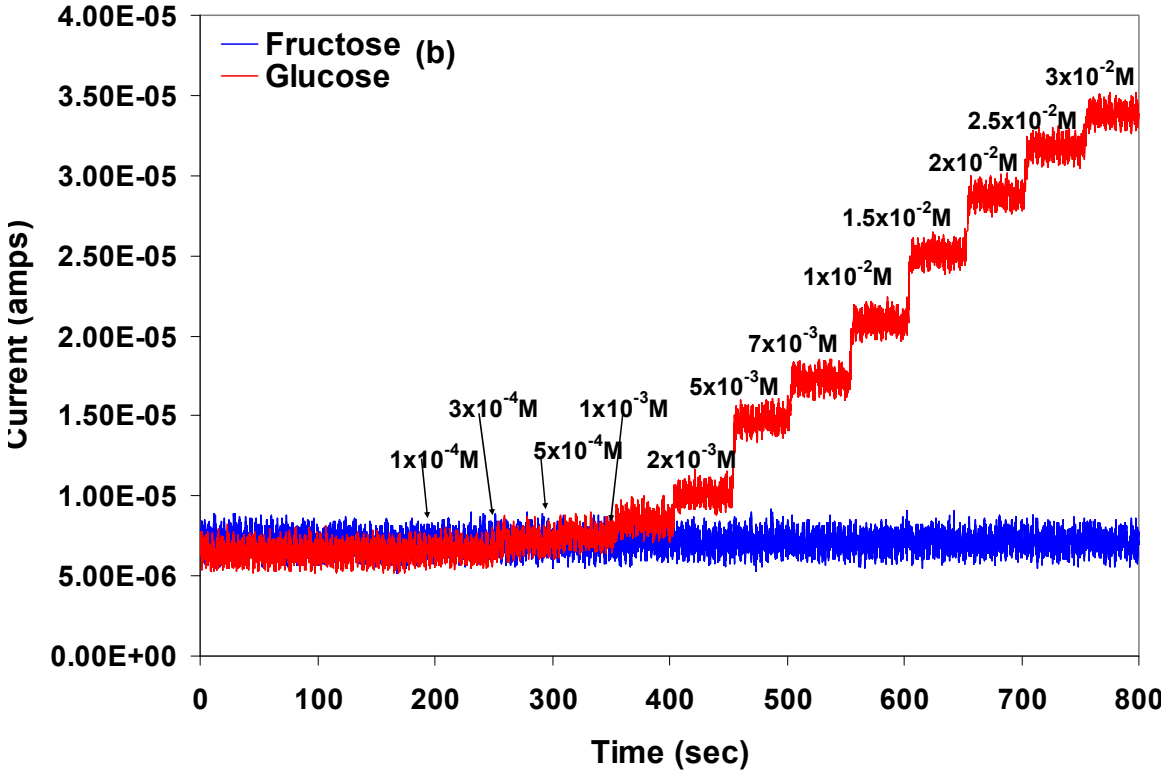
Fructose
Glucose
(b)
Current (amps)
Time (sec)
4.00E-05
3.50E-05
3.00E-05
2.50E-05
2.00E-05
1.50E-05
1.00E-05
5.00E-06
0.00E+00
0
100
200
300
400
500
600
700
800
1x10-4M
3x10-4M
5x10-4M
1x10-3M
2x10-3M
5x10-3M
7x10-3M
1x10-2M
1.5x10-2M
2x10-2M
2.5x10-2M
3x10-2M

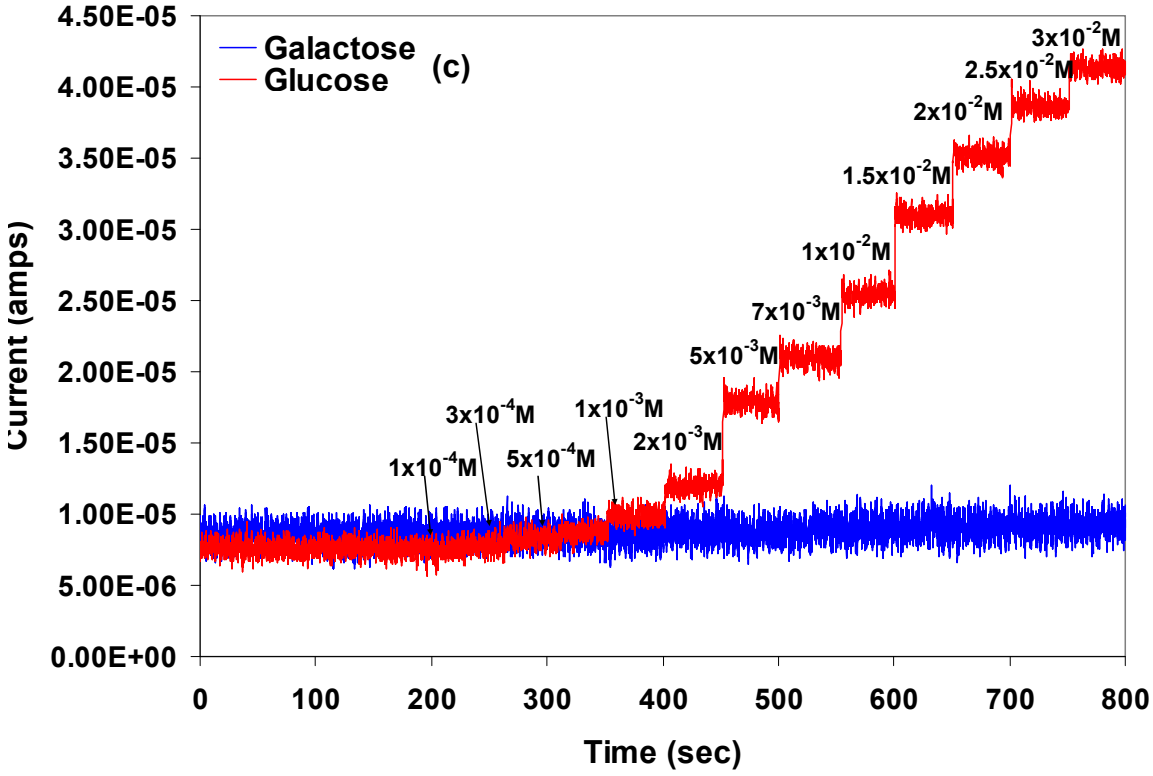
Galactose
Glucose
(c)
Current (amps)
Time (sec)
4.50E-05
4.00E-05
3.50E-05
3.00E-05
2.50E-05
2.00E-05
1.50E-05
1.00E-05
5.00E-06
0.00E+00
0
100
200
300
400
500
600
700
800
1x10-4M
3x10-4M
5x10-4M
1x10-3M
2x10-3M
5x10-3M
7x10-3M
1x10-2M
1.5x10-2M
2x10-2M
2.5x10-2M
3x10-2M

Figure 6.9 (a) Sucrose, (b) Fructose, and (c) Galactose selectivity study of PEDOT-PSS 3 + PEDOT-PSS-GOx 2 minute biosensors

6.3.1.5 Performance

In order to test the sensor's life time, the sensors were tested only once a day using chrono-amperammetry until no current activity was detected. When not being tested, the sensors were stored in 1x PBS solution in the refrigerator. Another sensor made at the same time as the sensors used in the life time study was just stored in 1x PBS solution and then tested after the life time sensors expired to determine whether the sensor was still viable after storage.

The biosensors lost their sensitivity within 8 days, leaving only residue sensing ability up to 30 days (Figure 6.10 top). The ability to sense after 31 days in storage, Figure 6.10 bottom, suggested that the enzyme does not denature or was lost when stored.

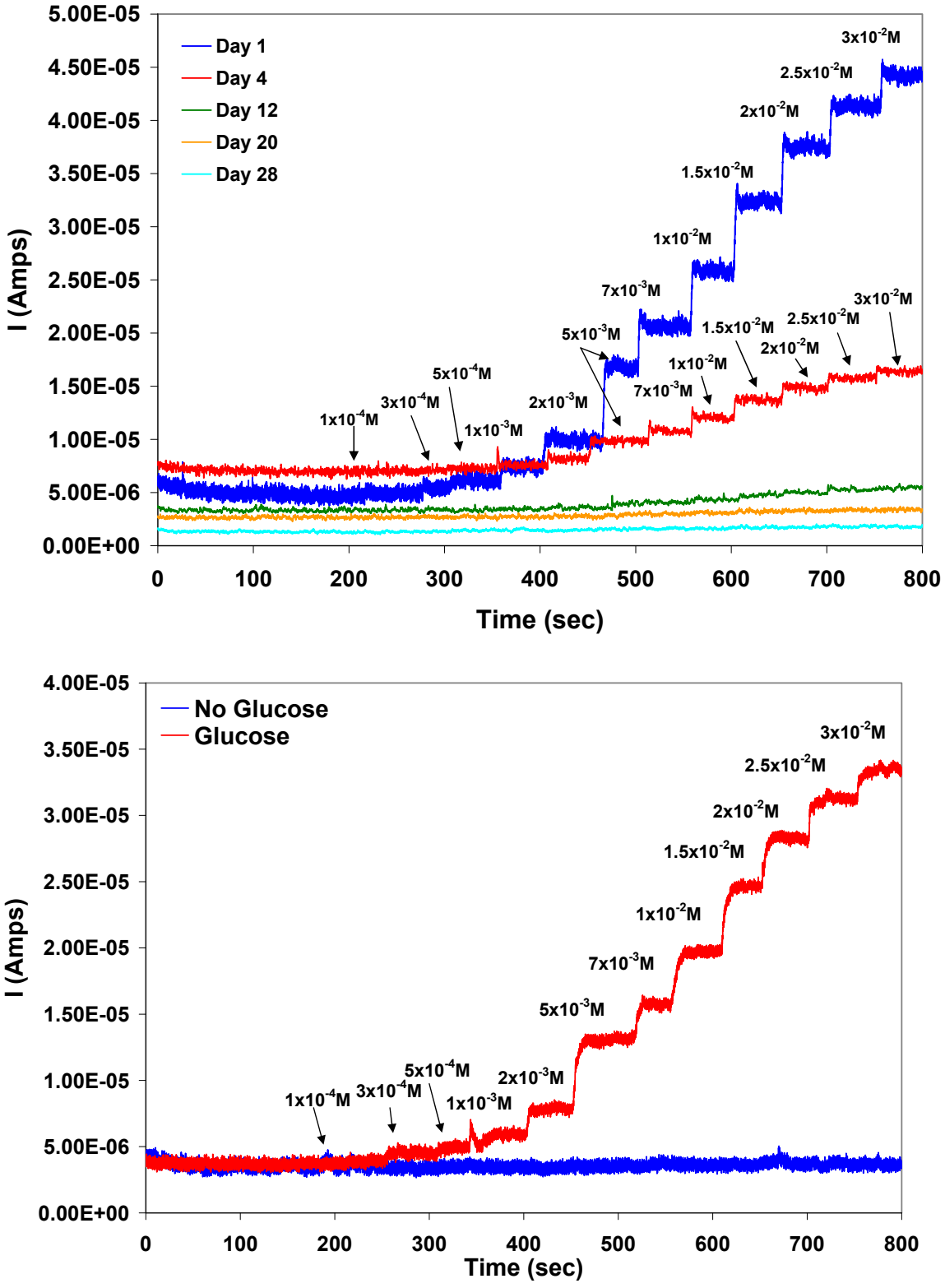

Figure 6.10 (top) Biosensor life time study and (bottom) Biosensor storage in 1x PBS study of PEDOT-PSS 3 + PEDOT-PSS-GOx 2 minute biosensor

6.3.1.6 Failure Analysis

The preliminary failure analysis used EIS, CV, and XPS to study the films after the sensors no longer functioned. By eye, the films looked like they delaminated from the ITO surface. Figure 6.11 below shows the impedance, phase angle, and CV data of some of the sensors. As can be seen, the PEDOT-PSS 3 minute+PEDOT-PSS-GOx 2 minute sensors a-d (denoted as 3+2) did not have the characteristic reduction in impedance usually seen with the presence of a PEDOT film, like in sample 3+2e. The sample 3+2e is the sample which sat in storage for 31 days. Both the impedance and phase angle data with their similarities to the bare electrode suggested that the film was removed. The slight increase in the film's (3+2a-d) charge capacity suggests a residue amount of PEDOT film on the surface.

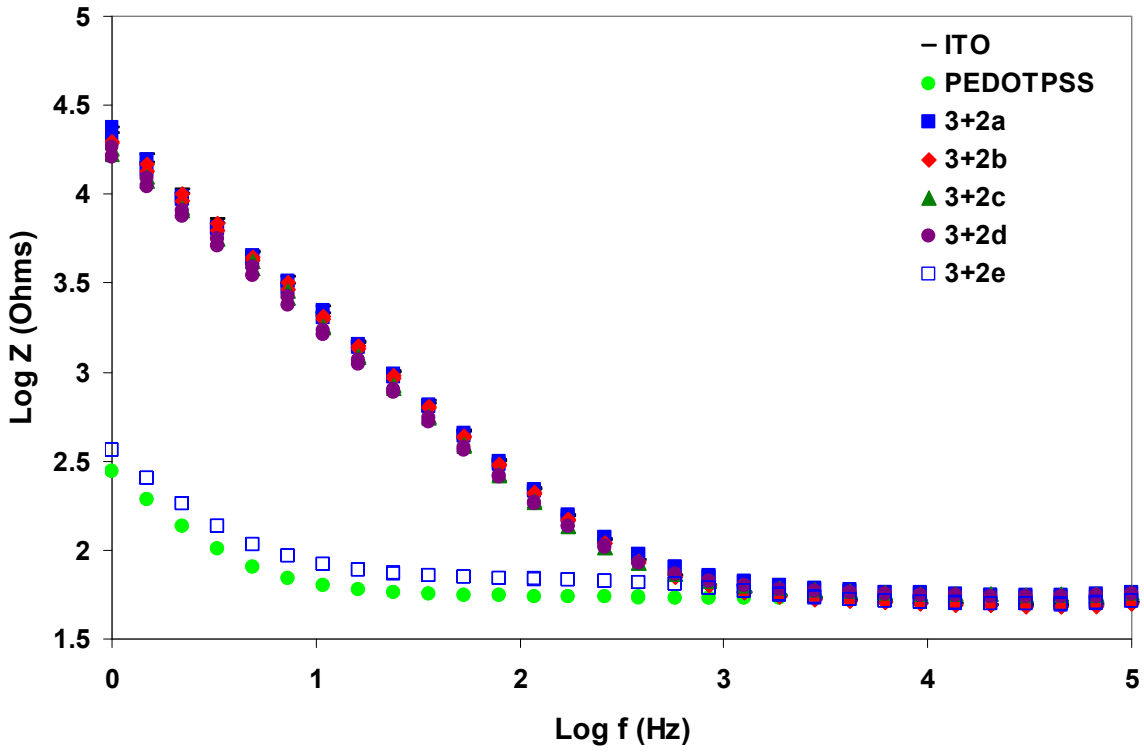

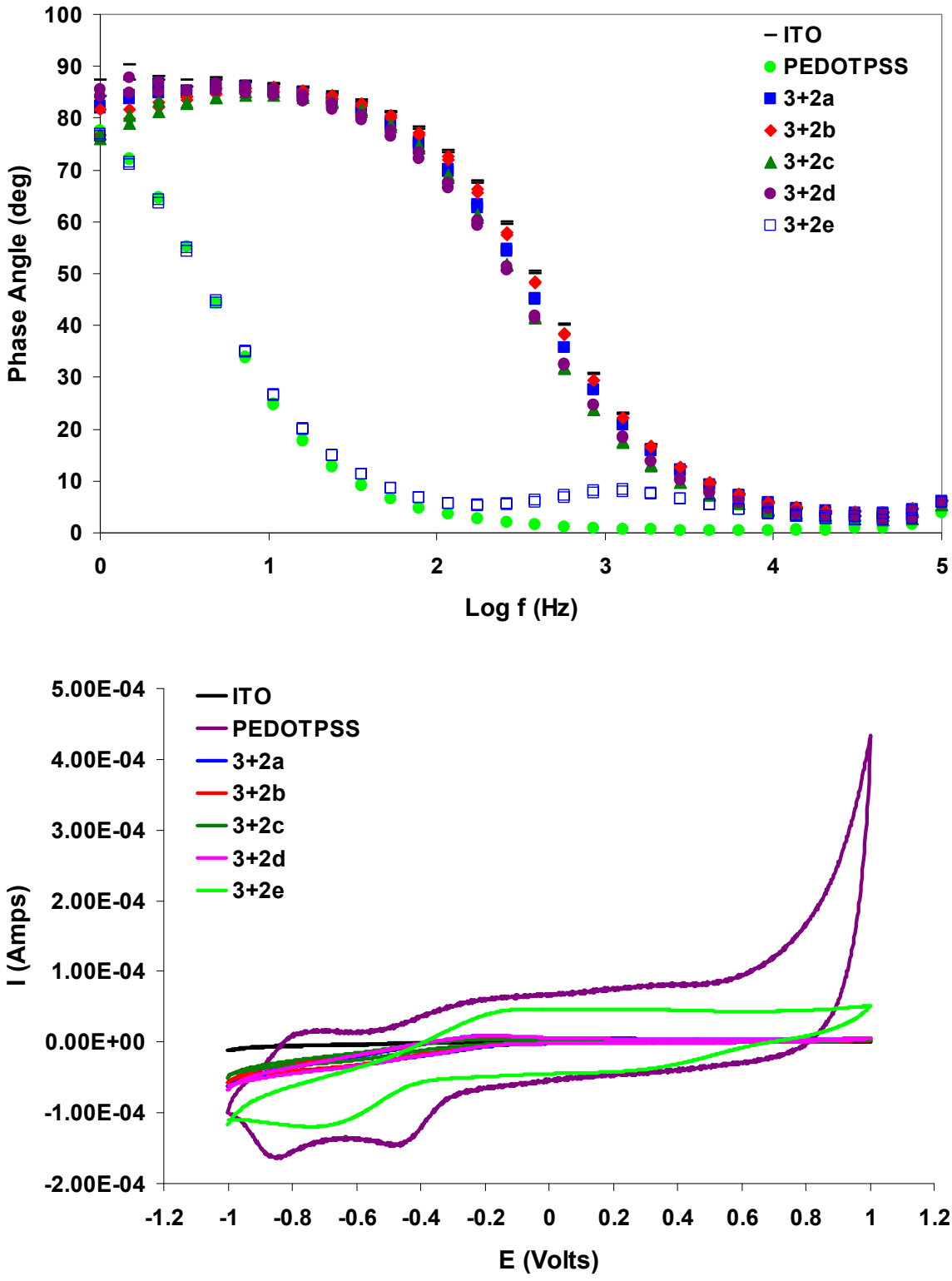

Figure 6.11 (top) Impedance, (middle) Phase Angle, and (bottom) CV for failed PEDOT-PSS 3 +PEDOT-PSS-GOx 2 minute biosensors

Figure 6.12 depicts the same group of sensors seen above in Figure 6.10. The appearance of the characteristic PEDOT and PSS peaks in the C 1s (Figure 6.12a) and S 2p (Figure 6.12b) regions confirms the presence of a PEDOT film still on the surface. The presence of GOx was also detected in the N 1s region, Figure 6.12c. The XPS analysis also suggests that there is at some residual amount of PEDOT film left as suggested by the CV results. Overall, the reduction in C 1s, S 2p, and N 1s signals with the failed sensors coupled with the EIS and CV findings suggested that a significant portion of the film was removed.

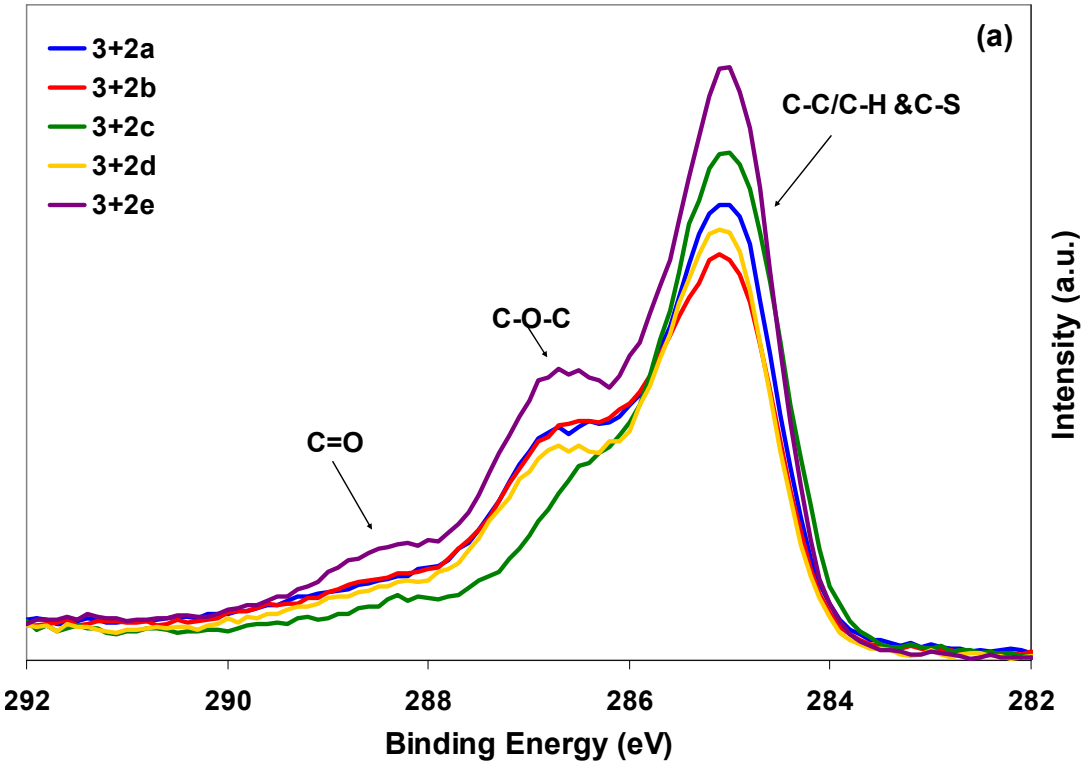

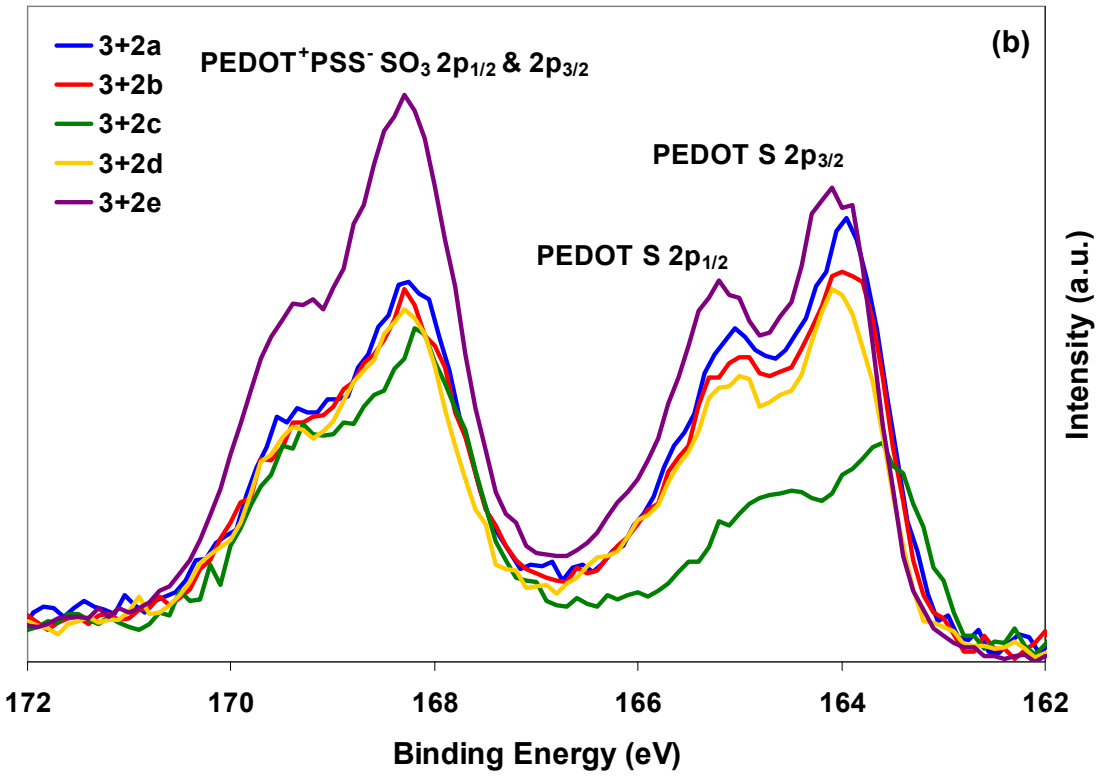
3+2a
3+2b
3+2c
3+2d
3+2e
PEDOT+PSS- SO3 2p1/2 & 2p3/2
PEDOT S 2p3/2
PEDOT S 2p1/2
(b)
Intensity (a.u.)
172
170
168
166
164
162
Binding Energy (eV)

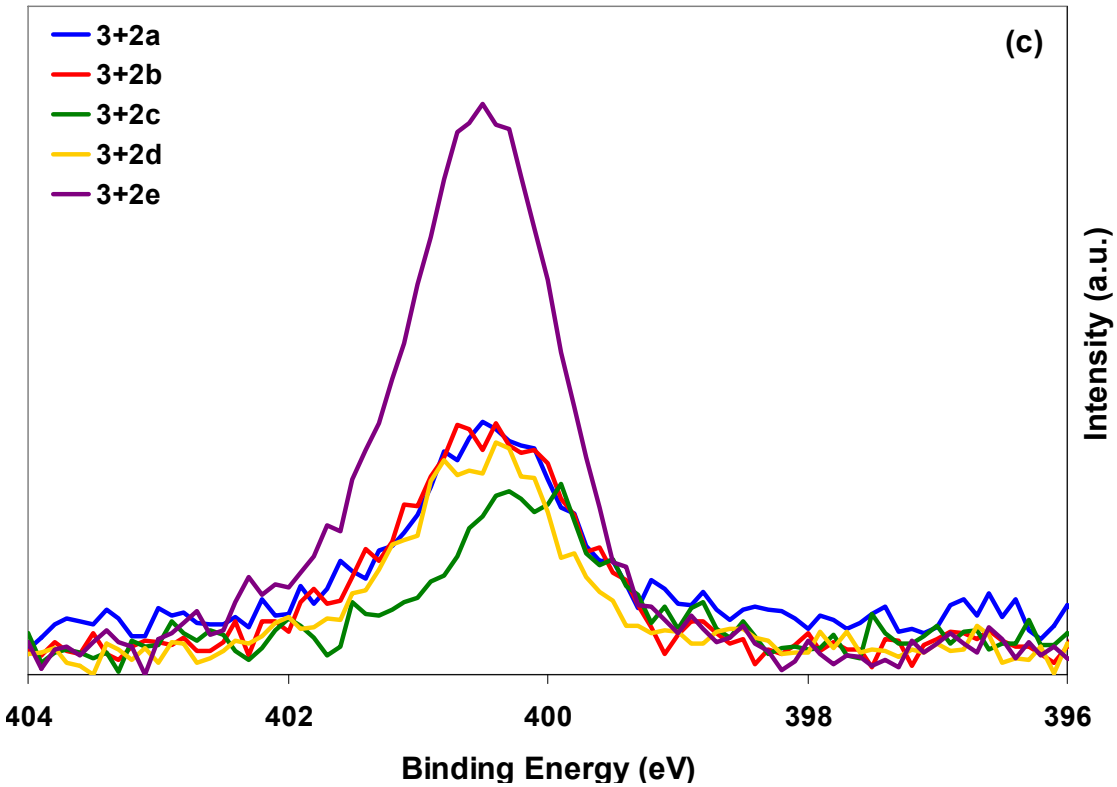
3+2a
3+2b
3+2c
3+2d
3+2e
(c)
Intensity (a.u.)
404
402
400
398
396
Binding Energy (eV)

Figure 6.12 (a) C 1s, (b) S 2p, and (c) N 1s characteristic regions for failed PEDOT-PSS 3 +PEDOT-PSS-GOx 2 minute biosensors

6.3.1.6 Electrode Size Reduction

Once the general functional PEDOT enzyme electrode proof of principle study was demonstrated with large area electrodes (0.7 cm^2) biosensors, the electrode size was reduced to 0.0078 cm^2 (Pt/Ir cochlear ball electrodes). Figure 6.13 shows a functional PEDOT-GOx biosensor fabricated using the Pt/Ir ball electrode.

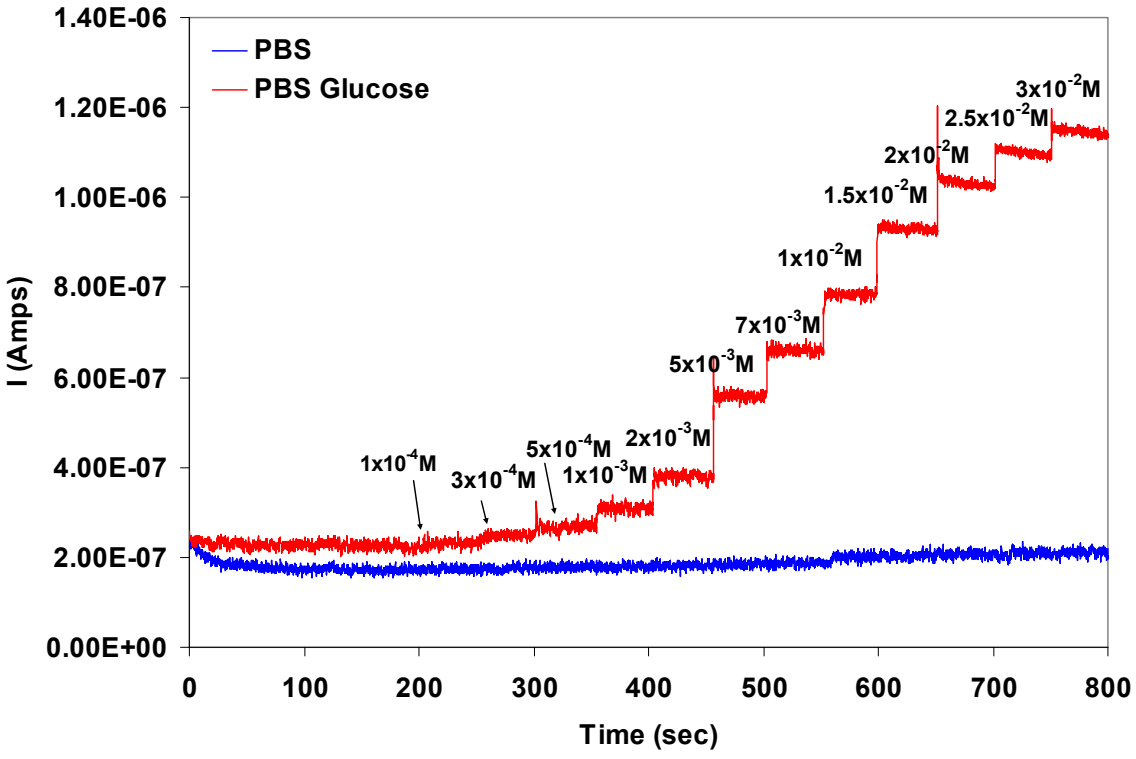

Figure 6.13 Electrode reduction study of a PEDOT-GOx 10 minute biosensor (area: 0.0078 cm^2)

6.3.2 PEDOT-Heparin-GOx

A variation of the PEDOT-glucose oxidase biosensor was also fabricated by replacing the PSS counter-ion with heparin. The motivation was to use a more natural counter-ion than PSS.

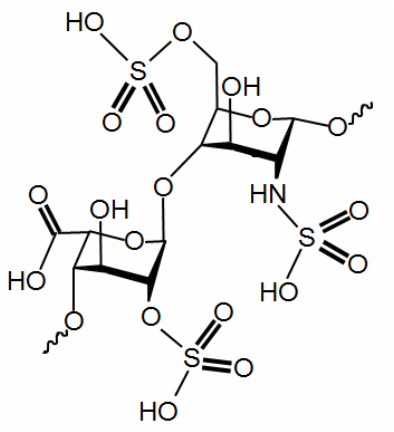

Figure 6.14 Heparin sodium salt structure

6.3.2.1 Electrical Characterization

EIS and CV (Figures 6.15) were used to characterize the electrical properties of both PEDOT-Heparin and PEDOT-Heparin 3 minute + PEDOT-Heparin-GOx 2 minute films. Figures 6.15 showed only slight changes in impedance, phase angle, or cyclic voltammetry plots of PEDOT-Heparin 3 minute + PEDOT-Heparin-GOx 2 minute films in comparison to the PEDOT-Heparin film grown under the same conditions for 5 minutes. The impedance results and CV results of PEDOT-Heparin films show the same trends as those seen with PEDOT-PSS with a lowering of the impedance and an increase in film charge capacity.

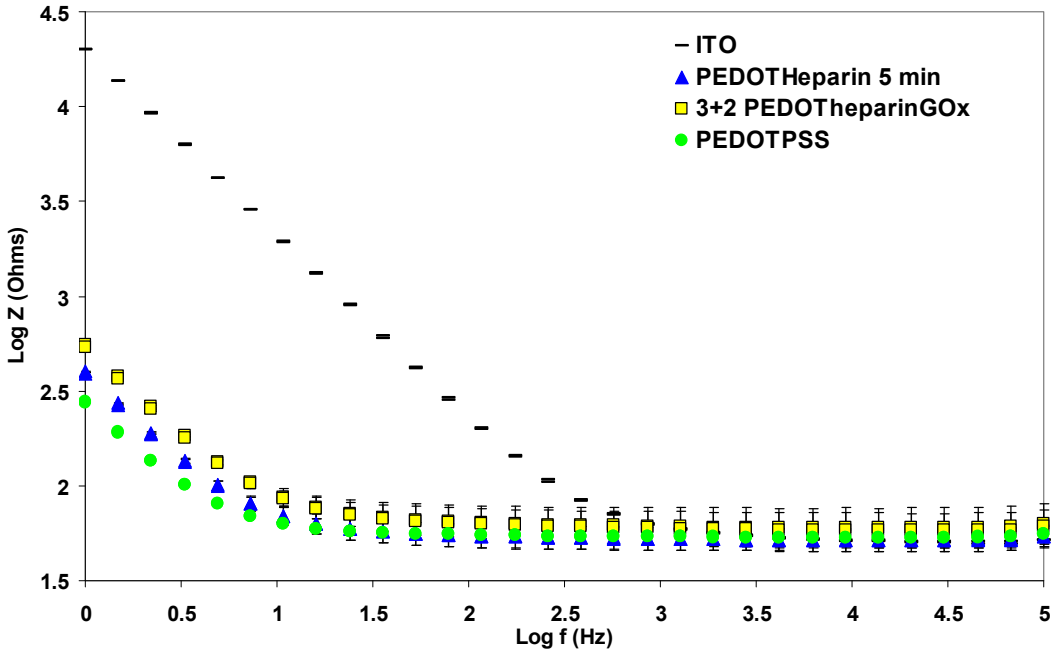
ITO
PEDOTHeparin 5 min
3+2 PEDOTheparinGOx
PEDOTPSS
Log Z (Ohms)
Log f (Hz)
4.5
4
3.5
3
2.5
2
1.5
0
0.5
1
1.5
2
2.5
3
3.5
4
4.5
5

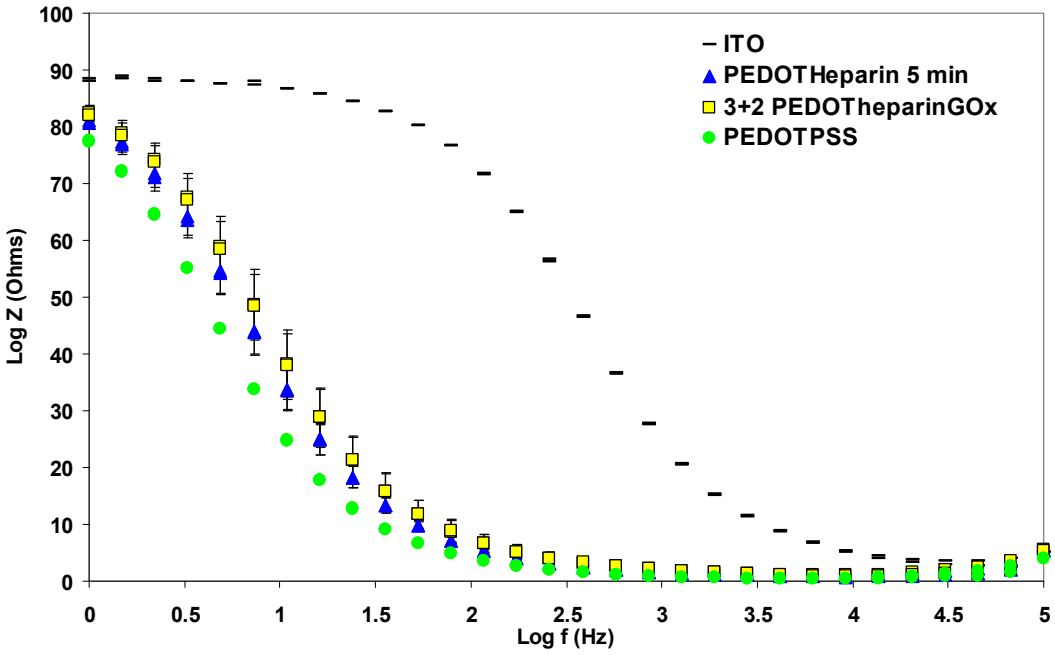
ITO
PEDOTHeparin 5 min
3+2 PEDOTheparinGOx
PEDOTPSS
Log Z (Ohms)
Log f (Hz)
100
90
80
70
60
50
40
30
20
10
0
0
0.5
1
1.5
2
2.5
3
3.5
4
4.5
5

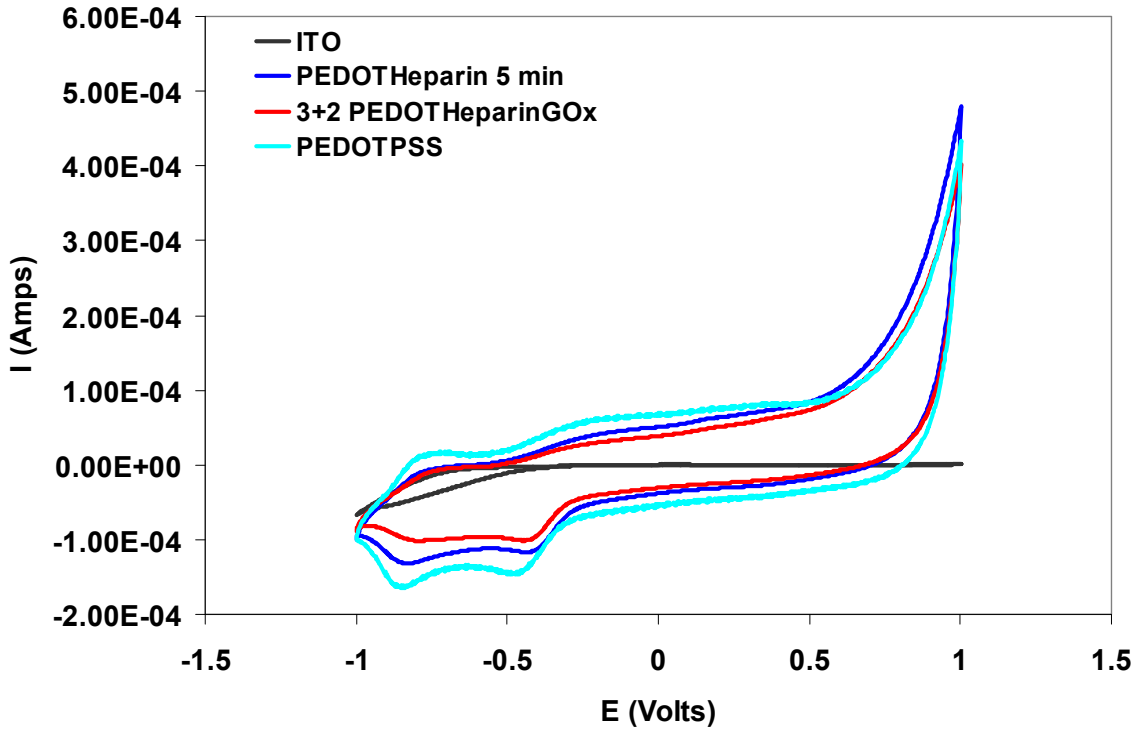

Figure 6.15 (top) Impedance, (middle) Phase Angle, and (bottom) Cyclic Voltammetry Data for PEDOT-Heparin 5 min and PEDOT-Heparin 3 minute + PEDOT-Heparin-GOx 2 minute biosensors

6.3.2.2 Chemical Analysis

The C 1s (Figure 6.16a), O 1s (Figure 6.16b), and N 1s (Figure 6.16d) characteristic regions all contained the characteristic PEDOT peaks similar to those seen above with PEDOT-PSS 3 minute + PEDOT-PSS-GOx 2 minute biosensors without the presence of the C-SO_3 and SO_3 peaks in the C 1s and O 1s from the PSS counter-ion respectively. Again the presence of the glucose oxidase was confirmed with the appearance of the amidic N-CH-C*=O peak ~288.5 eV and the N-H bonding peak in the N 1s, which is only present in glucose oxidase. The characteristic S 2p region, Figure 6.16c, differs in both in the overall and in the higher binding energy intensity region from

that of PEDOT-PSS based sensors due to the lower SO_3 content within heparin in comparison to the poly-anionic PSS.

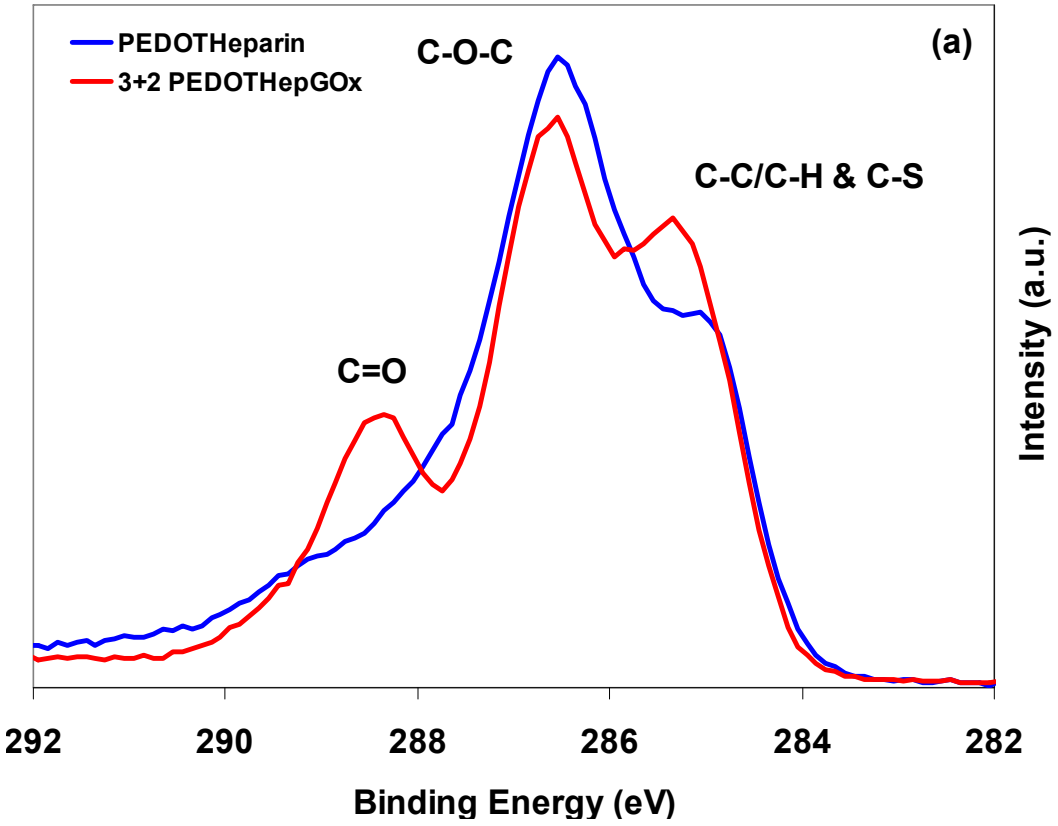

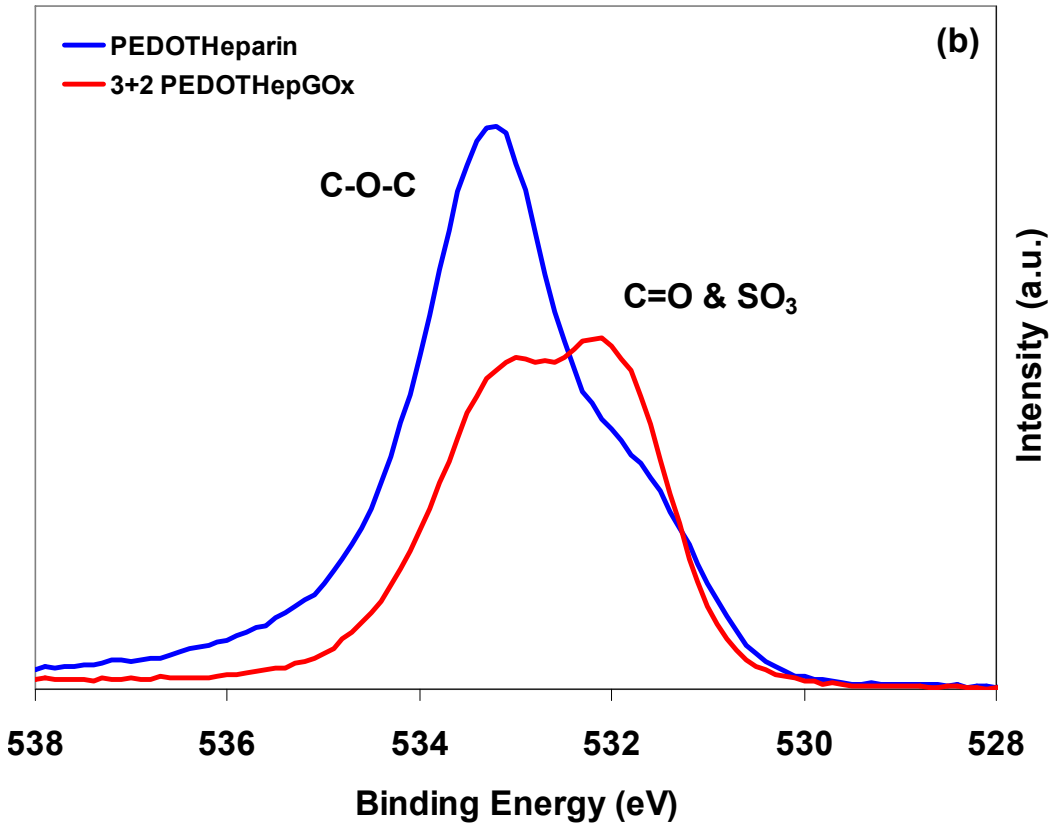
PEDOTHeparin
3+2 PEDOTHepGOx
(b)
C-O-C
C=O & SO3
Intensity (a.u.)
538
536
534
532
530
528
Binding Energy (eV)

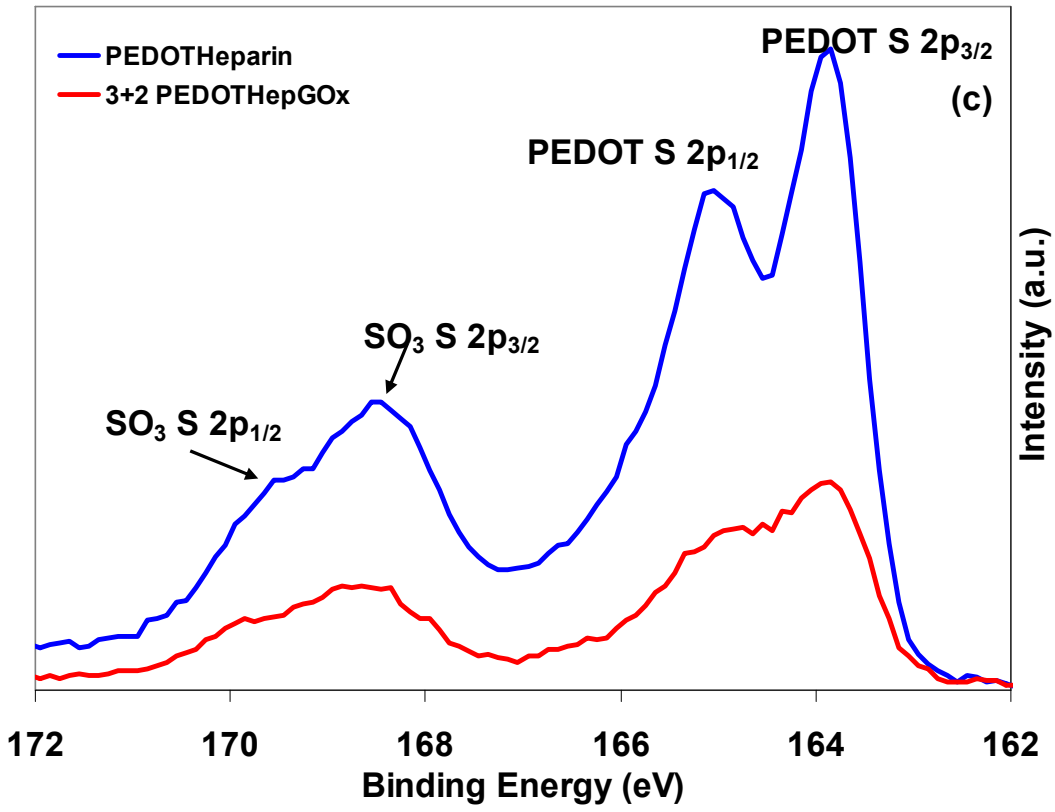
PEDOTHeparin
3+2 PEDOTHepGOx
PEDOT S 2p3/2
(c)
PEDOT S 2p1/2
SO3 S 2p3/2
SO3 S 2p1/2
Intensity (a.u.)
172
170
168
166
164
162
Binding Energy (eV)

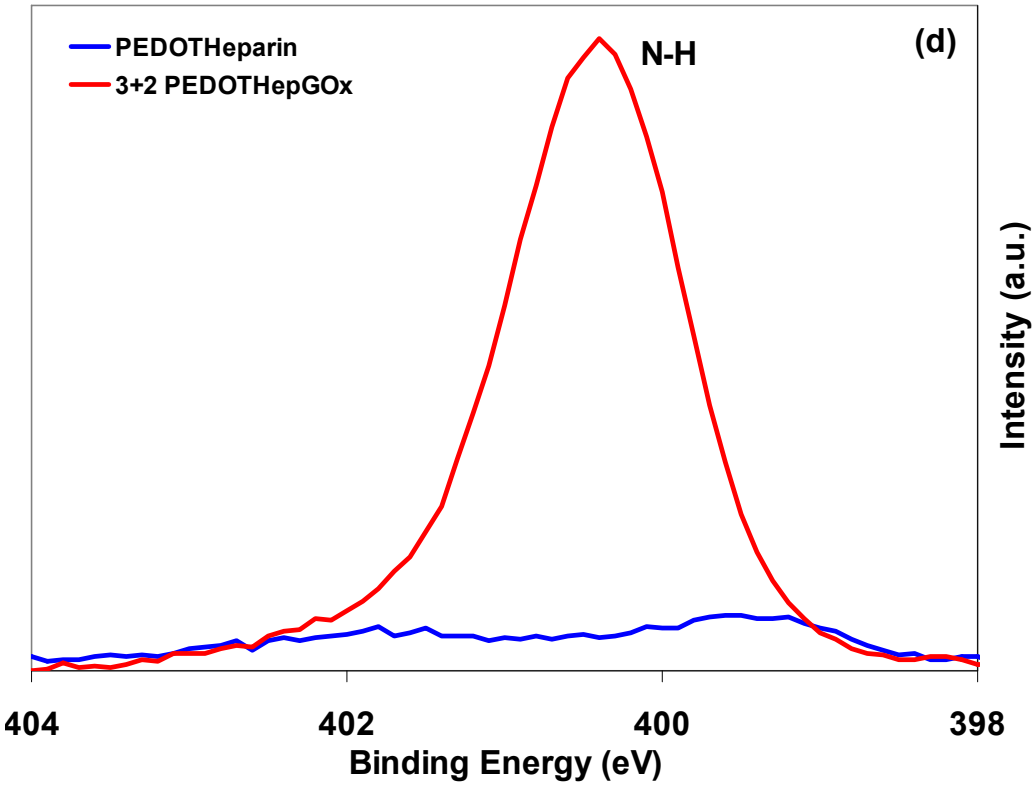

Figure 6.16 (a) C 1s, (b) O 1s, (c) S 2p, and (d) N 1s characteristic region for PEDOT-Heparin and PEDOT-Heparin 3 + PEDOT-Heparin-GOx 2 minute sensors

6.3.2.3 Sensitivity

Figure 6.17 demonstrates the PEDOT-Heparin-GOx sensors were indeed functional and were able to detect at a minimum glucose concentration of $5x10^{-4}$M. This was to be expected because the sensing component, GOx, was the same was with the PEDOT-PSS 3+PEDOT-PSS-GOx 2 minute biosensors. The ability to sense indicated that the heparin did not impede the glucose from being able to diffuse to the glucose oxidase's redox center and that the GOx was still functional.

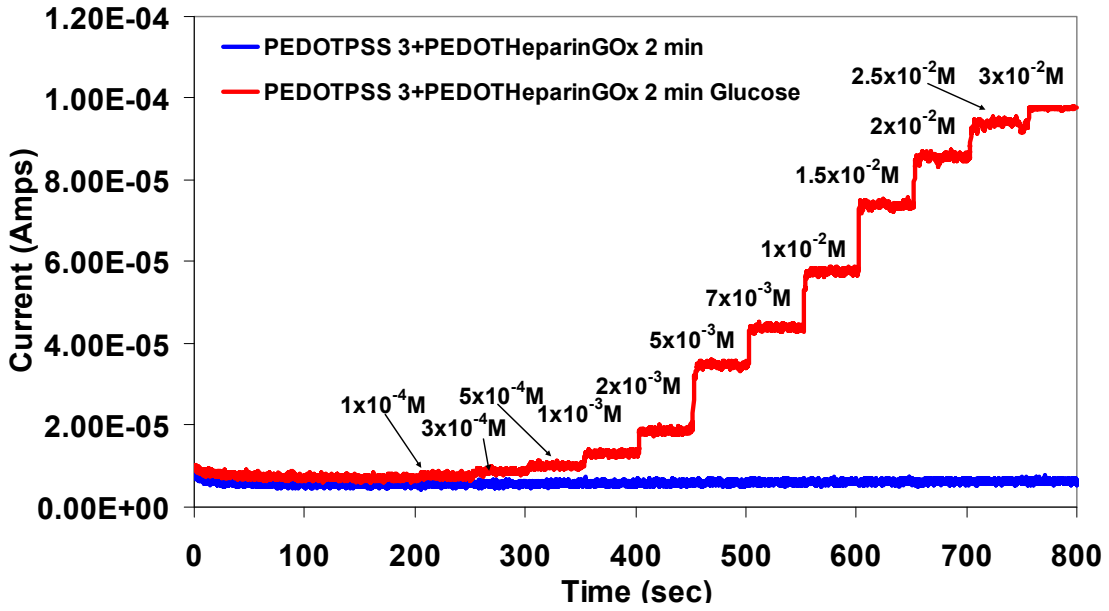

Figure 6.17 Chrono-Amperometry of PEDOT-Heparin-GOx 10minute biosensors

6.3.3 PEDOT-PSS-L-Lactate Dehydrogenase

L-lactate dehydrogenase (EC 1.1.1.27), which is used in glycolysis, is also classified as an oxidoreductatase enzyme. LDH undergoes redox reactions on the CH-OH group of the donor with NAD acting as an acceptor[21]:

Pyruvate+β-NADH→L-lactate+β-NAD

L-lactate dehydrogenase has been used in lactic acid detection.[22,23] Since LDH does not produce H_2O_2, this experiment helped to determine whether the detection route occurring with the GOx sensors was actually direct electron transfer via ferrocene to the electrode or the detection of the H_2O_2 reaction.

6.3.3.1 Electrical Characterization

EIS and CV (Figures 6.18) were used to characterize the electrical properties of PEDOT-PSS 3 minute + PEDOT-PSS-LDH 2 minute films. Figures 6.18 showed only slight changes in either impedance, phase angle, or cyclic voltammetry plots compared to the PEDOT-PSS film grown under the same conditions for 5 minutes, this was likely because the films take on the characteristics of PEDOT-PSS films since the first layer was composed entirely of PEDOT-PSS and the second layer was also composed of PEDOT-PSS components.

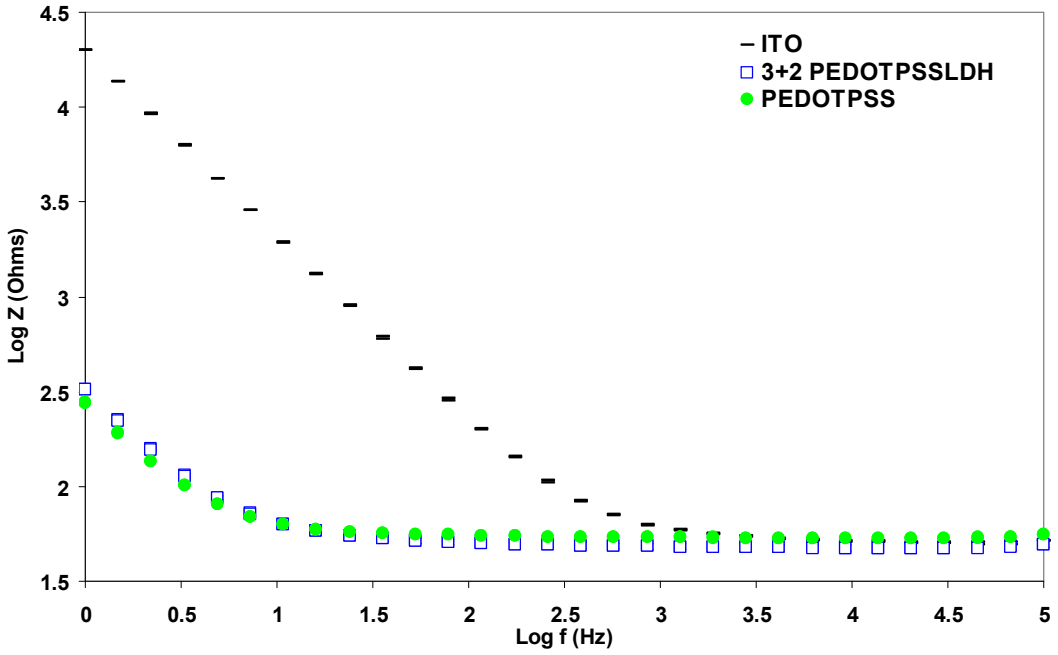

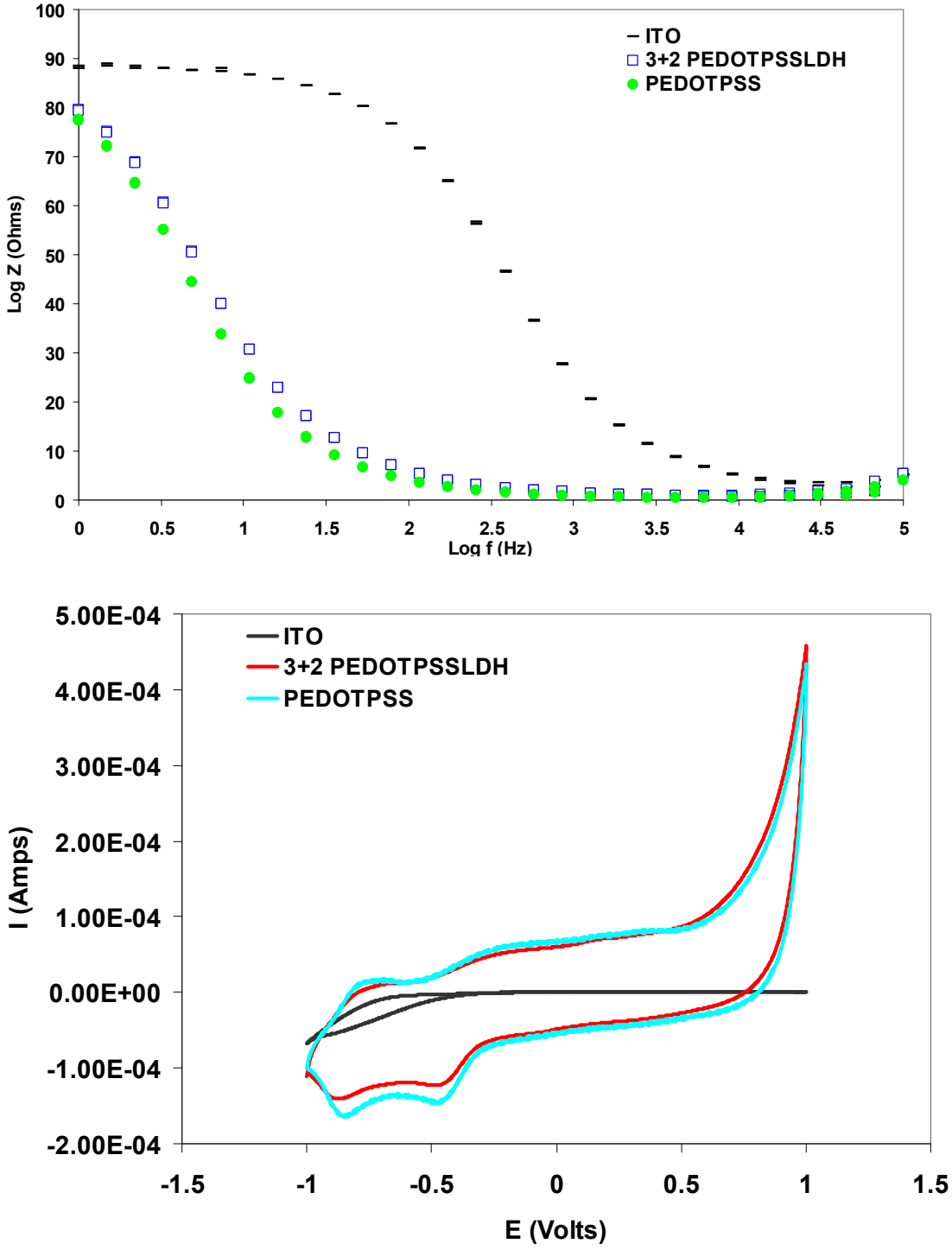

Figure 6.18 (top) Impedance, (middle) Phase Angle, and (c) Cyclic Voltammetry Data for PEDOT-PSS 3 minute + PEDOT-PSS-LDH 2 minute biosensors

6.3.3.2 Chemical Analysis

As seen previously with glucose oxidase based sensors, the C 1s (Figure 6.19a) and S 2p (Figure 6.19c) regions all exhibited the characteristic PEDOT and PSS peaks. The O 1s, Figure 6.19c, did differ from the PEDOT-glucose oxidase biosensors with a large C=O and SO_3 intensity ~532 eV. The detection of LDH was confirmed with the amidic C=O in the C 1s region, the increased C=O signal in the O 1s region, and the N-H in the N 1s region (Figure 6.19d). The appearance of a higher SO_3 from PSS intensity than that of the PEDOT spin split doublet in the S 2p region was likely caused by the enzyme covering the PEDOT, like the results observed previously with the PEDOT-PSS 3+PEDOT-PSS-GOx 2 minute biosensors.

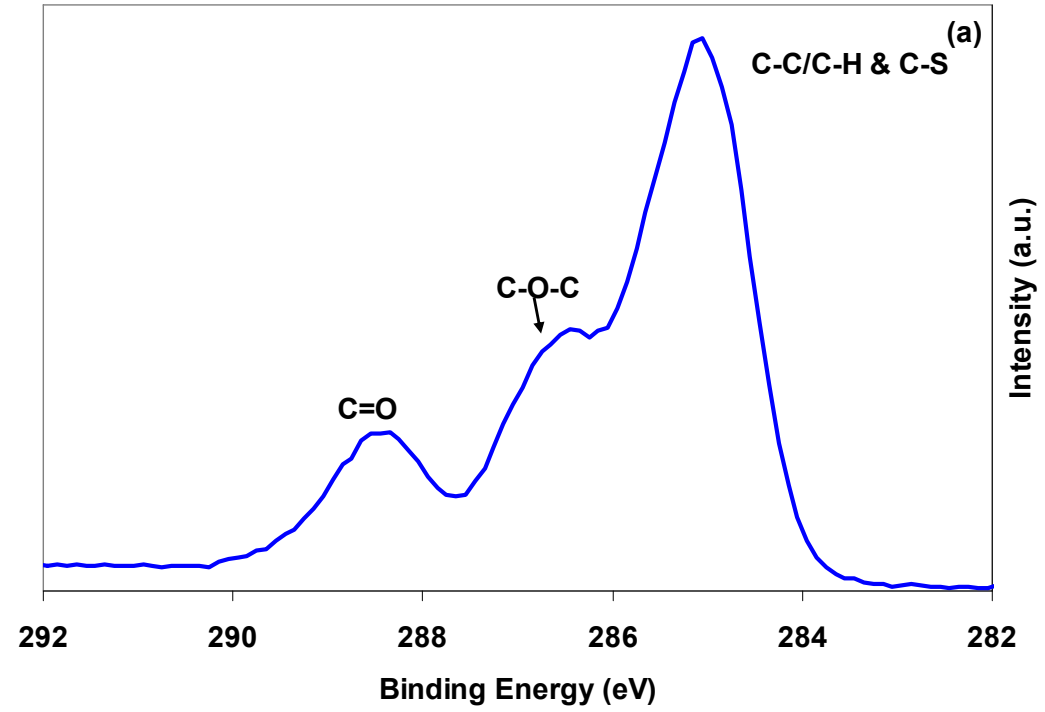
(a)
C-C/C-H & C-S
C-O-C
C=O
Intensity (a.u.)
292
290
288
286
284
282
Binding Energy (eV)

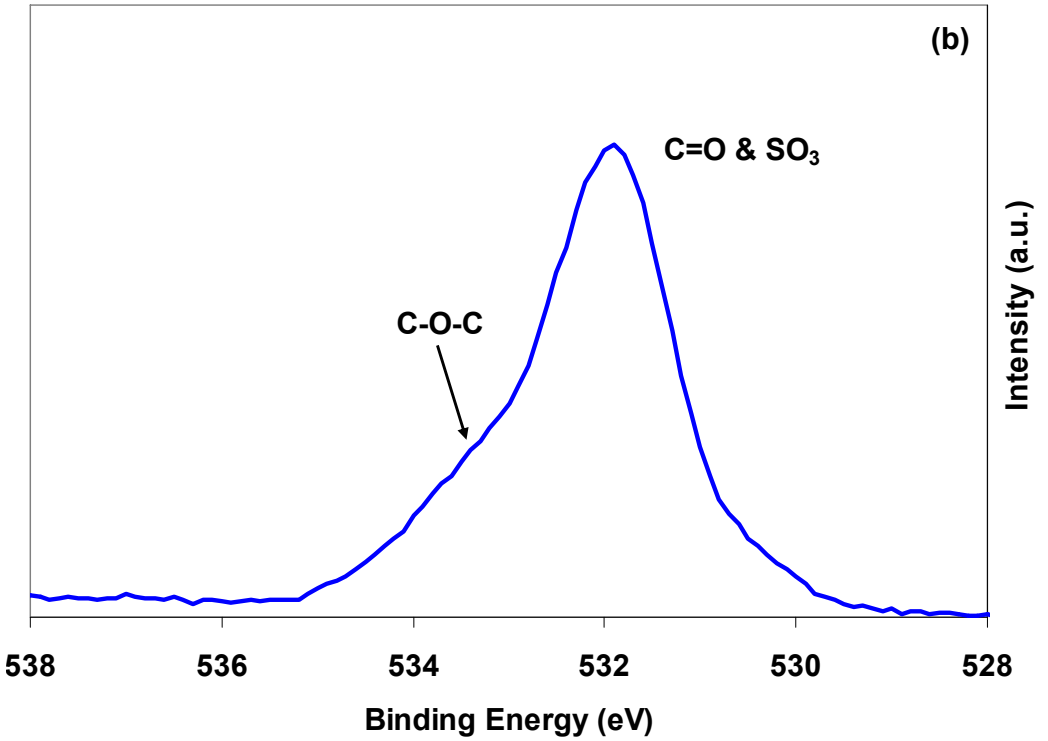
(b)
C=O & SO3
C-O-C
Intensity (a.u.)
538
536
534
532
530
528
Binding Energy (eV)

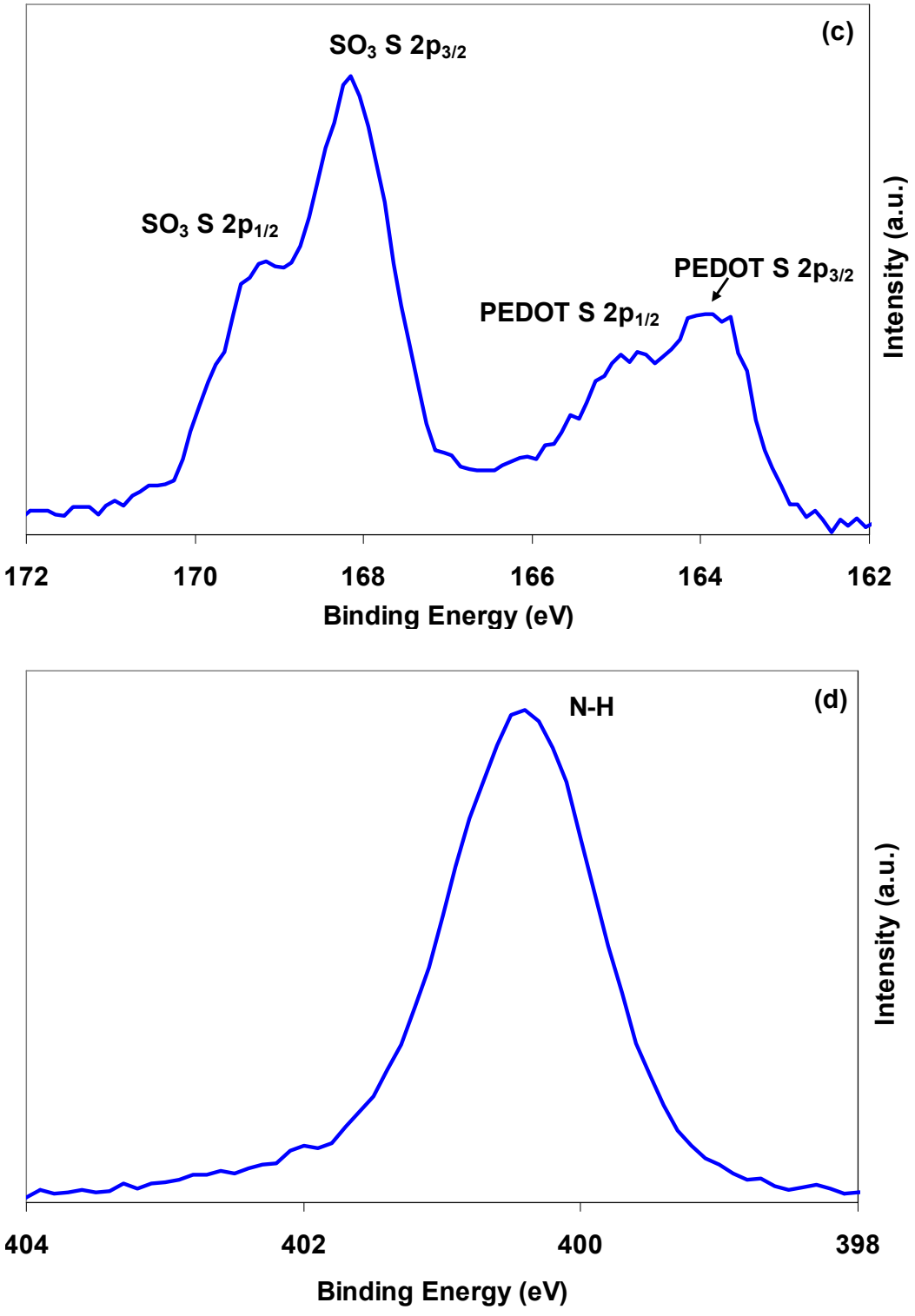

Figure 6.19 (a) C 1s, (b) O 1s, (c) S 2p, and (d) N 1s characteristic regions for PEDOT-PSS 3 + PEDOT-PSS-LDH 2 minute biosensors

6.3.3.3 Performance

Chrono-amperometry was used to deduce the sensitivity of the LDH biosensors, unfortunately the Beta-Nicotinamide adenine dinucleotide disodium salt (NADH) could be detected with just ITO and without the PEDOT-PSS-LDH film present. Figures 6.21 and 6.22 depict NADH sensing with NADH additions. This occurred because the electron being detected came from the NADH undergoing its own redox reaction, $NADH \rightarrow NAD^+ + H^+ + 2e^-$, instead of the electron given off from the enzyme's redox center (Figure 6.20).[24] The oxidation potential for NADH is known to be effected by the type of electrode[25] and/or whether the surface is modified.[24,26-28] In the case of a PEDOT modified electrode, the NADH oxidation potential has been shown to decrease to 0.2 V for an ITO electrode with PEDOT-PSS-Au nanoparticles[24] or 0.46 V for PEDOT electrochemically grown on a glassy carbon electrode[28], both within the 0.7 V potential used in these experiments allowing for the oxidation of the NADH to occur. Figure 6.21 shows an increase in the current response with the presence of a PEDOT-PSS film at the surface at this time it is unknown why this occurred.

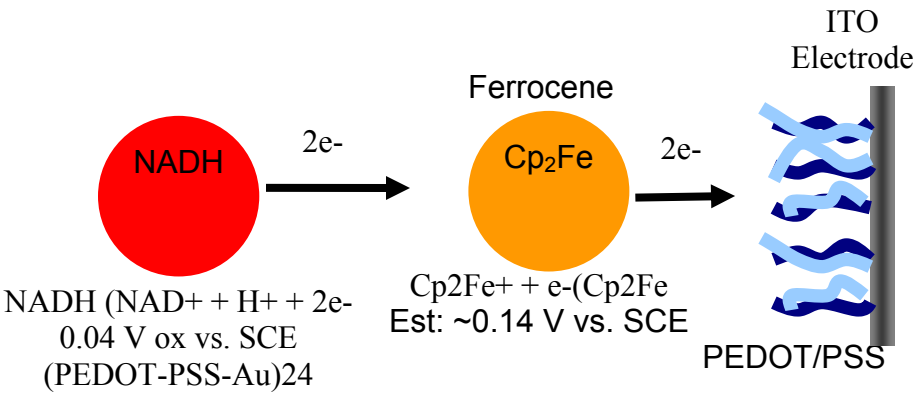

Figure 6.20 Diagram of the NADH sensing pathway

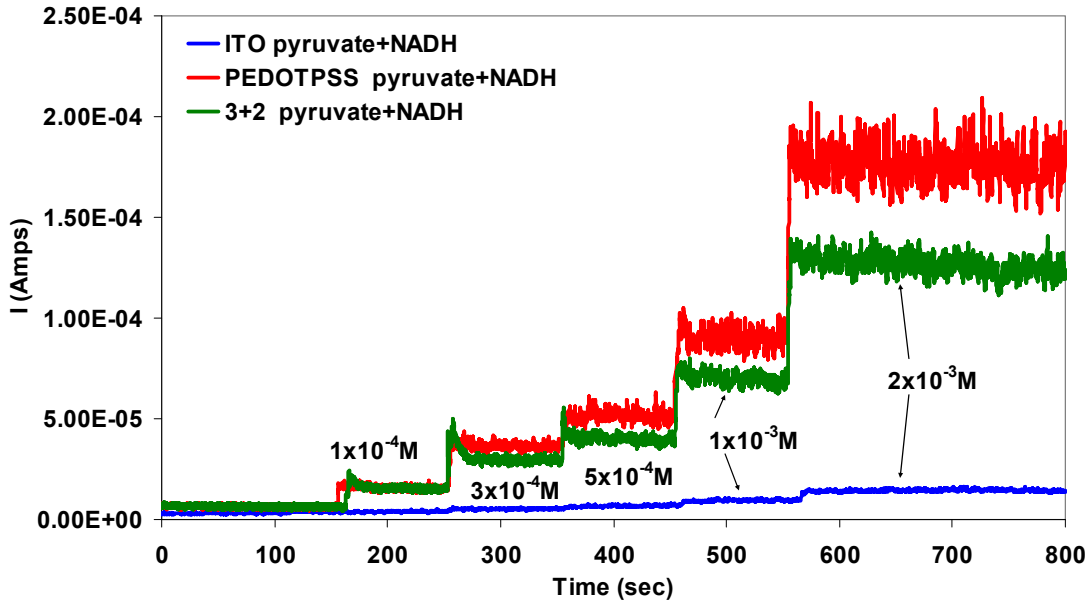

Figure 6.21 Chrono-Amperometry Data of PEDOT-PSS-LDH biosensor Controls

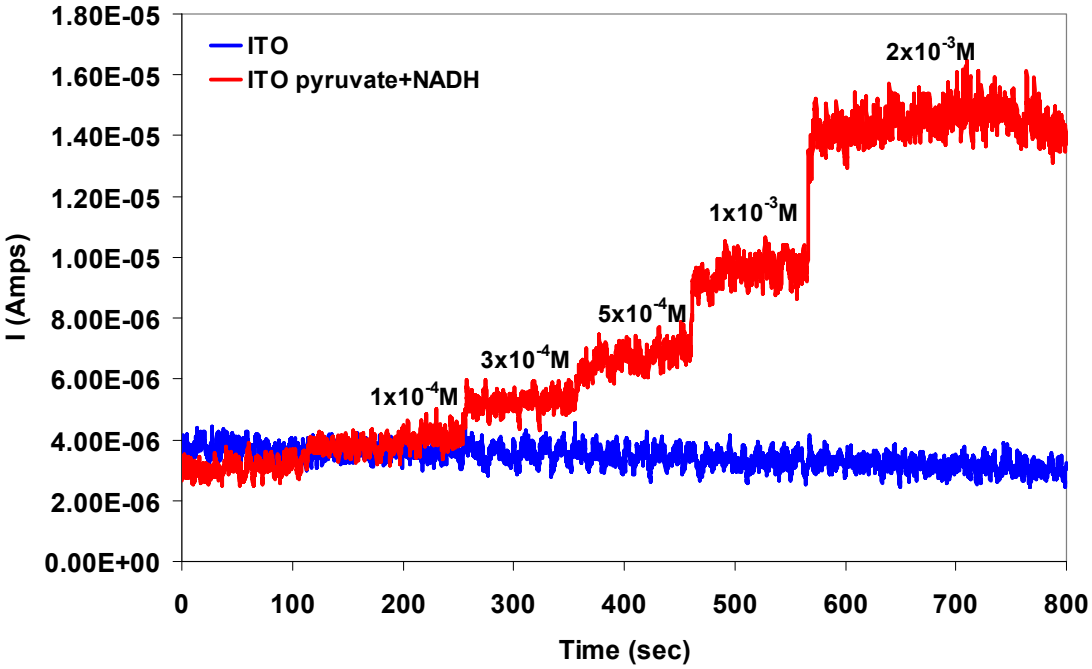

Figure 6.22 Chrono-Amperometry Data of ITO with pyruvate and NADH Controls

6.3.4 PEDOT-Tyrosinase

Tyrosinase (EC 1.14.18.1), which is used in melanin production, is also classified as an oxidoreductatase enzyme.

L-tyrosine + L-dopa + O_2 = L-dopa + dopaquinone + H_2O

Tyrosinase was incorporated into a PEDOT film in the hopes of using the enzyme for future use to grow melanin directly onto an existing PEDOT film. In this case, Tyrosinase was used as the PEDOT counter-ion due to it's negative charge in order to ensure incorporation and to maximize the enzymatic amount.

6.3.4.1 Electrical Characterization

EIS and CV (Figures 6.23) were used to characterize the electrical properties of PEDOT-Tyrosinase 10 minute films. The results show that the PEDOT-Tyrosinase films follow the same electrical characteristic as the ITO substrates. This result was not really surprising because the films do not deposit homogenously on the ITO substrates.

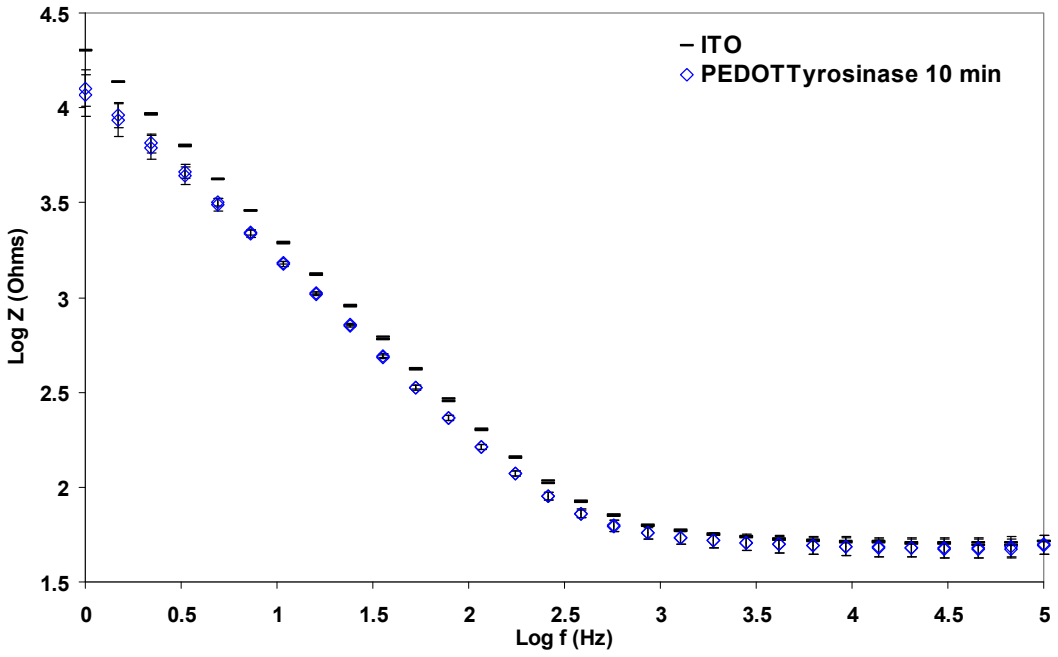

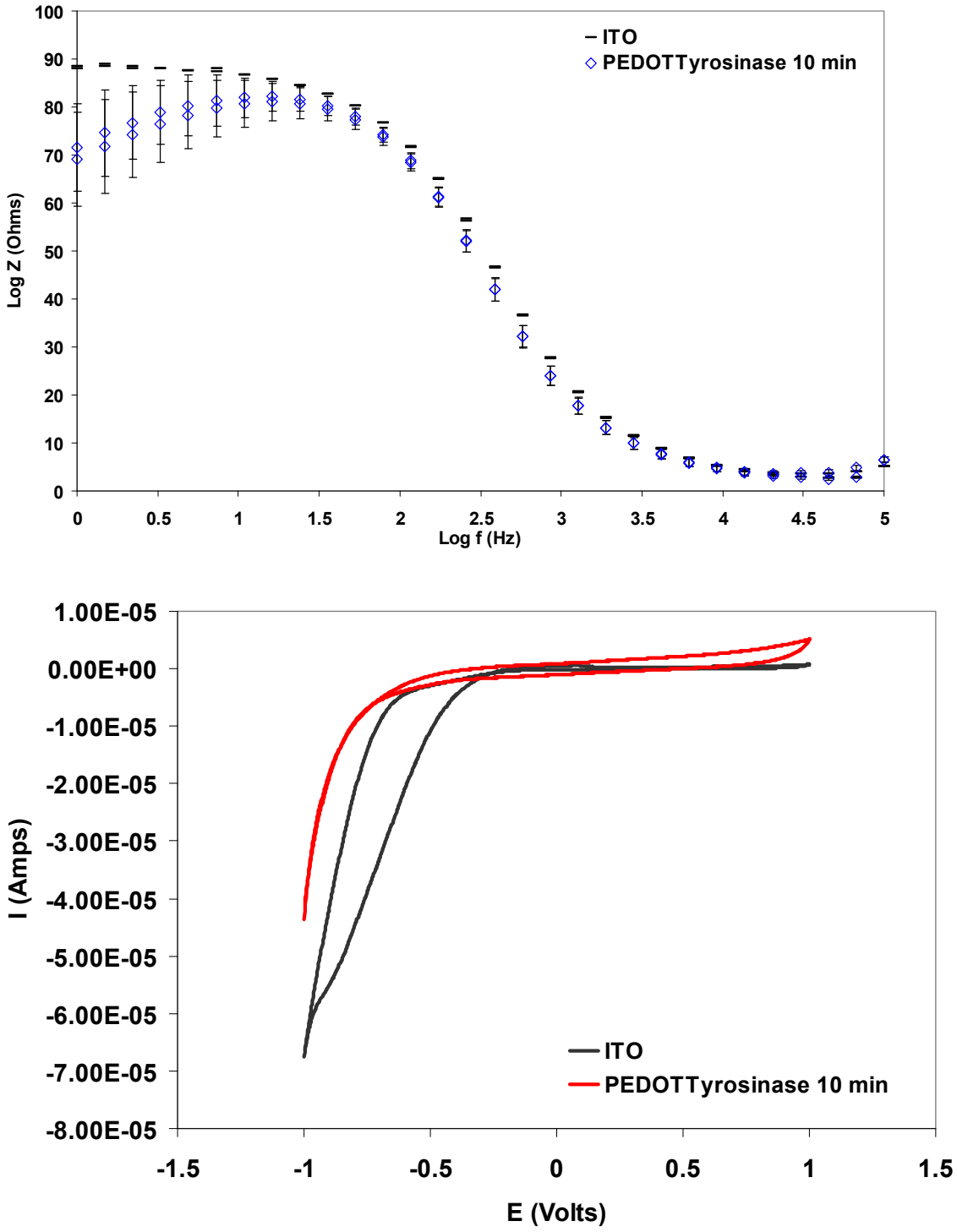

Figure 6.23 (top) Impedance, (middle) Phase Angle, and (bottom) Cyclic Voltammetry Data for PEDOT-Tyrosinase 10 minute biosensors

6.3.4.1 Chemical Analysis

As observed previously with both GOx and LDH, the presence of a C=O peak in both the C 1s and O 1s characteristic regions, Figures 6.24a and 6.24b, respectively as well as in the presence of a N-H peak in the N 1s region (Figure 6.24d) indicated that the enzyme was indeed incorporated into the film. The existence of PEDOT was confirmed with the PEDOT characteristic sulfur spin split (Figure 6.24c) peak at ~163.8 eV (S $2p_{3/2}$) and 164.8 eV (S $2p_{1/2}$). The higher energy contributions in the sulfur region are likely caused by SO_2 from PEDOT over oxidation/ partial degradation.[29]

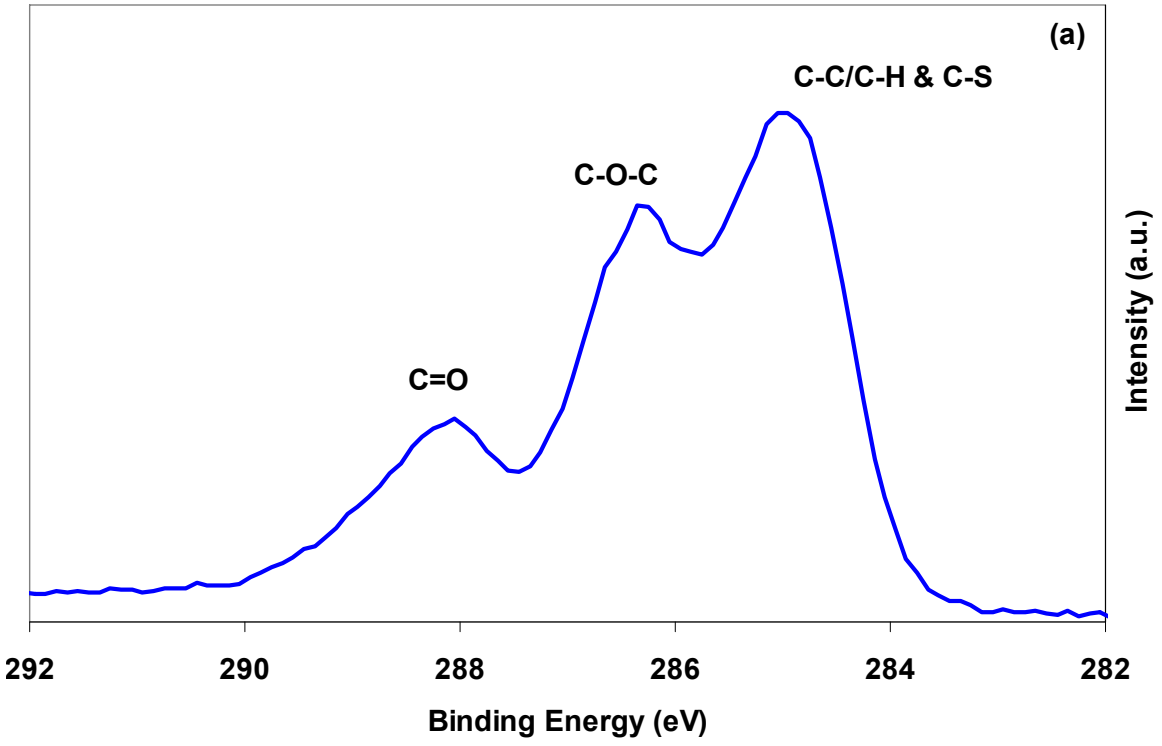

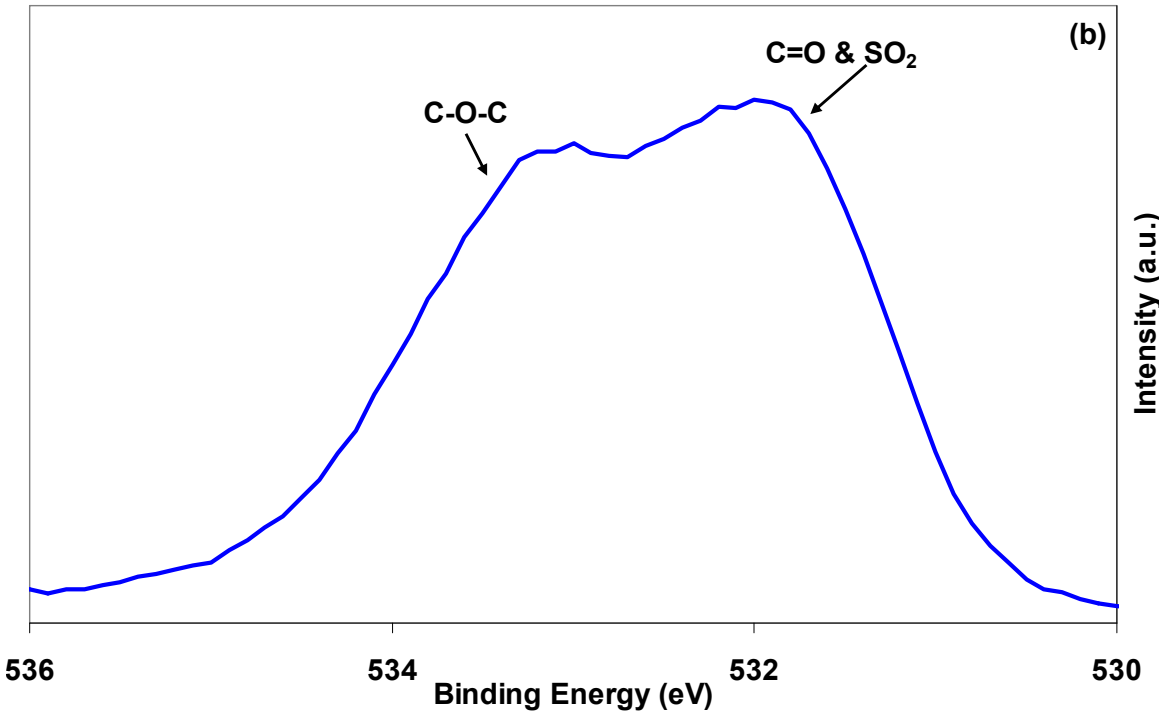
(b)
C=O & SO2
C-O-C
Intensity (a.u.)
536
534
532
530
Binding Energy (eV)

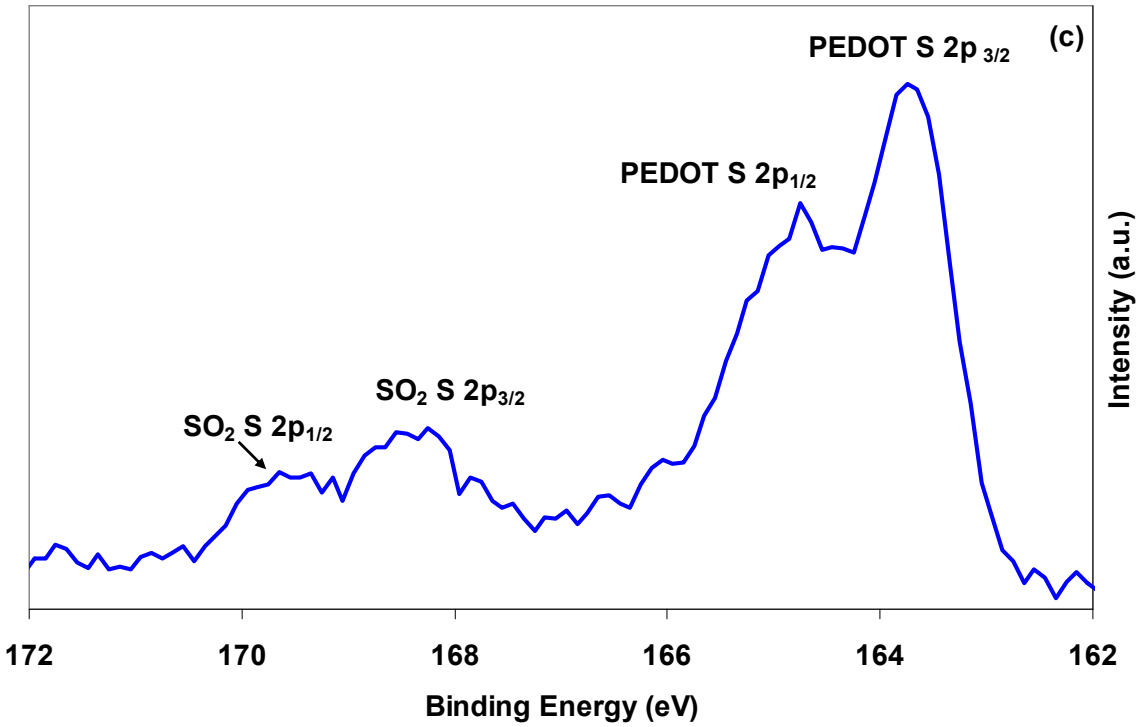
(c)
PEDOT S 2p 3/2
PEDOT S 2p1/2
SO2 S 2p3/2
SO2 S 2p1/2
Intensity (a.u.)
172
170
168
166
164
162
Binding Energy (eV)

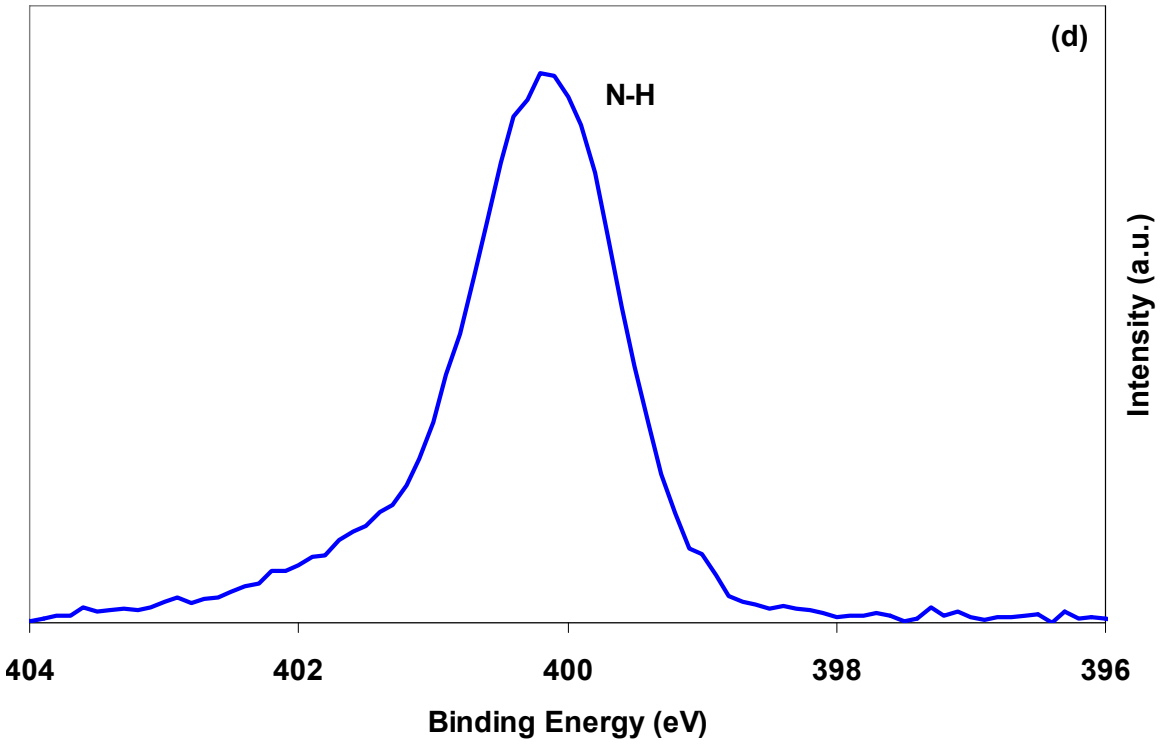

Figure 6.24 (a) C 1s, (b) O 1s, (c) S 2p, and (d) N 1s characteristic regions for PEDOT-Tyrosinase 10 minute biosensors

6.3.4.3 Performance

Unfortunately just like the LDH biosensors, the ITO electrode could detect the l-dopa without the presence of the PEDOT-Tyrosinase film. Figure 6.26 actually depicts the ITO sensing the l-dopa additions and not the Tyrosine. Like the previous situation with NADH, l-dopa (oxidation potential ~0.2-0.3 V) also underwent a redox reaction, l-dopa→dopaquione + $2H^+$ +$2e^-$ (Figure 6.25), upon addition to the PBS bath resulting in the electrons being detected during chrono-amperammetry.[30,31]

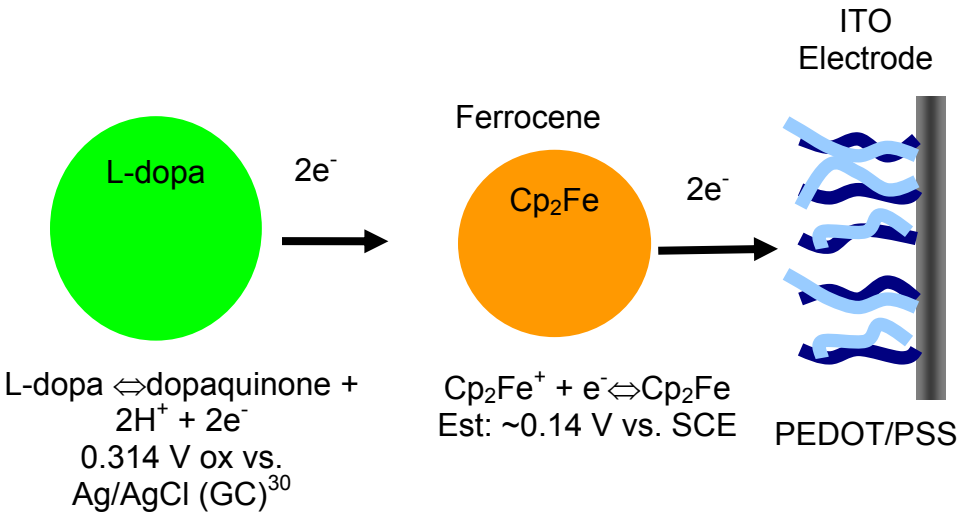

Figure 6.25 Diagram of L-dopa sensing

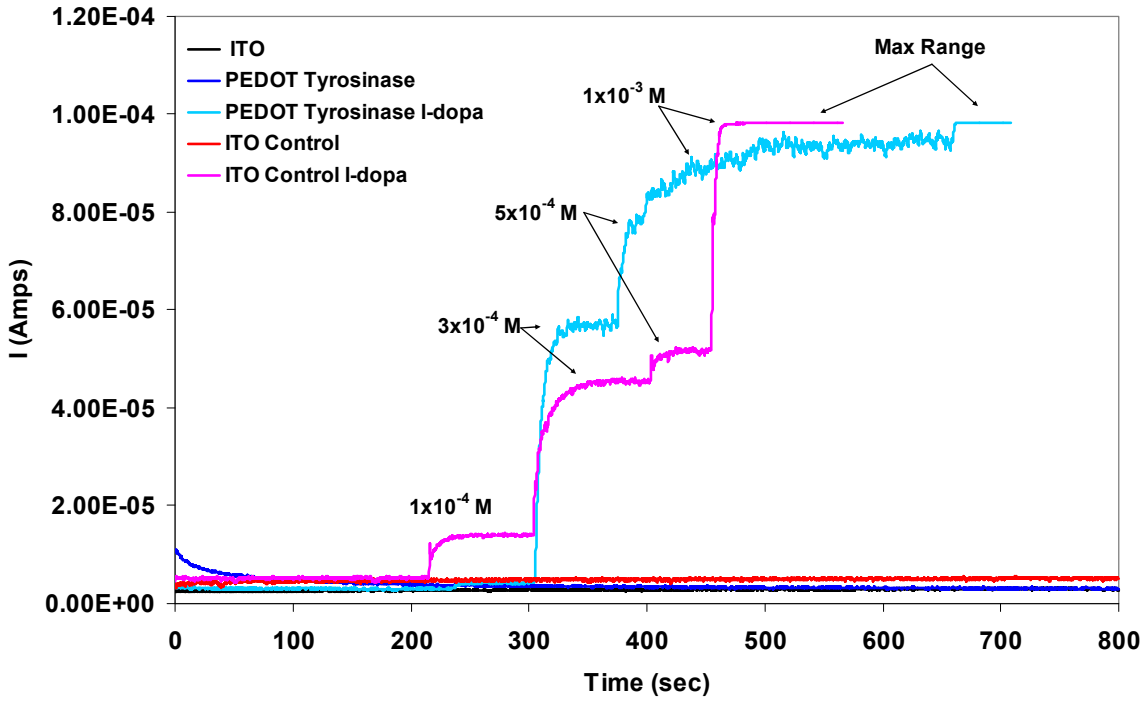

Figure 6.26 Chrono-Amperometry for PEDOT-Tyrosinase 10 minute biosensors

6.3.5 PEDOT-Glutamate Oxidase

Glutamate oxidase (EC 1.4.3.11) is an oxidoreductase acting on the CH-NH_2 group of the donor with O_2 as an acceptor:

L-glutamate+O_2+H_2O→α-ketoglutaric acid+NH_3+H_2O_2

Glutamate has multiple uses in human biochemistry, such as an amino acid and precursor to α-ketoglutaric acid, but it is the use an excitory neurotransmitter[21] that is of interest in this research. The glutamate oxidase films were deposited onto Pt/Ir cochlear ball electrodes and using the glutamate oxidase as the PEDOT counter-ion in an effort to minimize the amount of enzyme needed in the deposition solution and to increase the amount of enzyme in the film respectively.

6.3.5.1 Initial PEDOT-Glutamate Oxidase Experiments

6.3.5.1.1 Electrical Characterization

The decrease in impedance and phase angle data like those found with PEDOT films, Figures 6.27, suggests the presence of a PEDOT film at the electrodes surface. The cyclic voltammetry, Figure 6.27, data also suggests the presence of a film with a slight increase in the film's charge capacity.

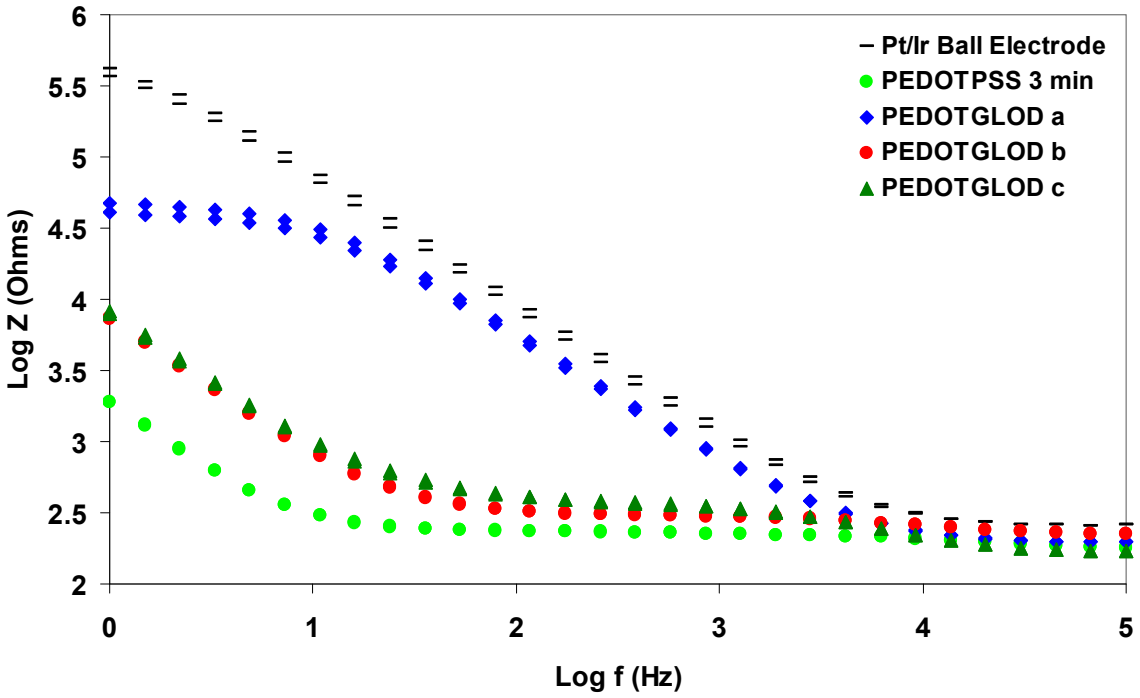
Log Z (Ohms)
Log f (Hz)
Pt/Ir Ball Electrode
PEDOTPSS 3 min
PEDOTGLOD a
PEDOTGLOD b
PEDOTGLOD c

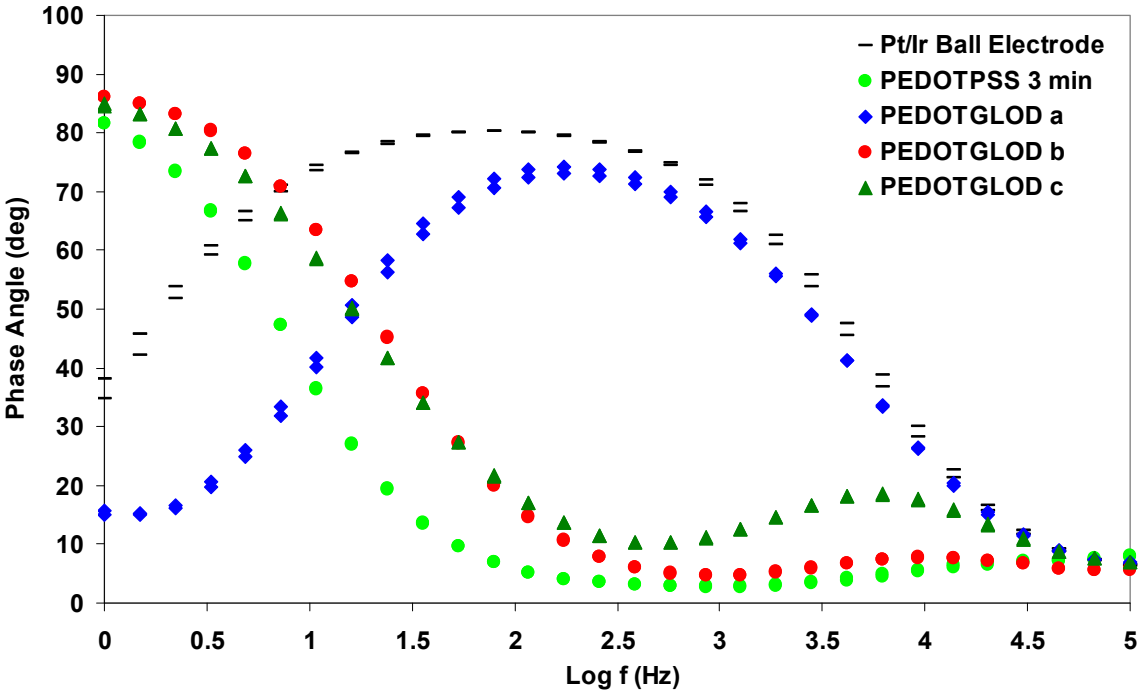
Phase Angle (deg)
Log f (Hz)
Pt/Ir Ball Electrode
PEDOTPSS 3 min
PEDOTGLOD a
PEDOTGLOD b
PEDOTGLOD c

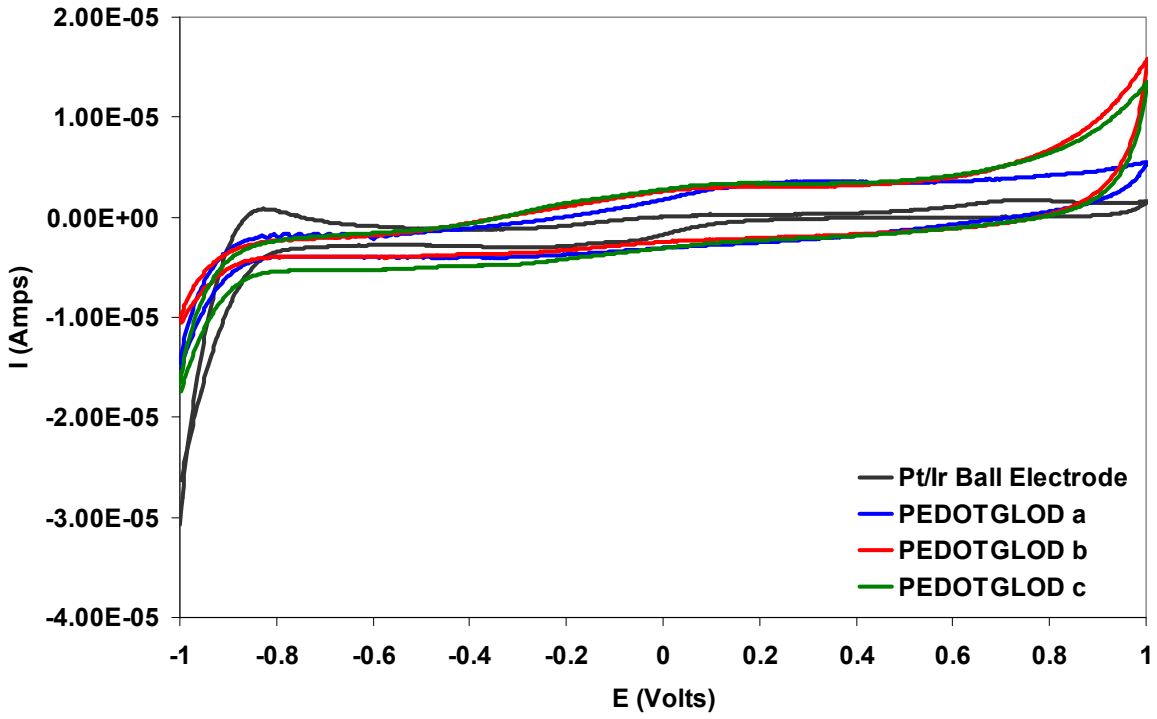

Figure 6.27 (top) Impedance, (middle) Phase Angle, and (bottom) Cyclic voltammetry data for PEDOT-GLOD 5 minute biosensors

6.3.5.1.2 Sensitivity

Glutamate additions of the following concentrations were added: $1x10^{-4}$, $3x10^{-4}$, $5x10^{-4}$, $1x10^{-3}$, $2x10^{-3}$, $5x10^{-3}$, $7x10^{-3}$, $1x10^{-2}$, $1.5x10^{-2}$, $2x10^{-2}$, $2.5x10^{-2}$, and $3x10^{-2}$ M, to test glutmate sensing. The optimum results are shown in Figure 6.28, but these results were by no means conclusive. Attempts at optimization included increasing the deposition time (no sensing), decreasing the deposition current to 10 μA to lower the deposition voltage (no sensing), increasing the deposition solution current (no sensing), and depositing a PEDOT-PSS initial layer to increase the film's mechanical stability to avoid delamination (no sensing). The lack of sensing was likely caused by the low enzyme concentration, ~20 units/ml, when compared to the enzyme concentrations used

with glucose oxidase, 100-1000 units/ml. As seen in Figures 6.29 and 6.30, there was no glucose sensing at enzyme concentrations comparable to those of GLOD and two times that of GLOD suggesting that the enzyme concentration was the major obstacle to sensing.

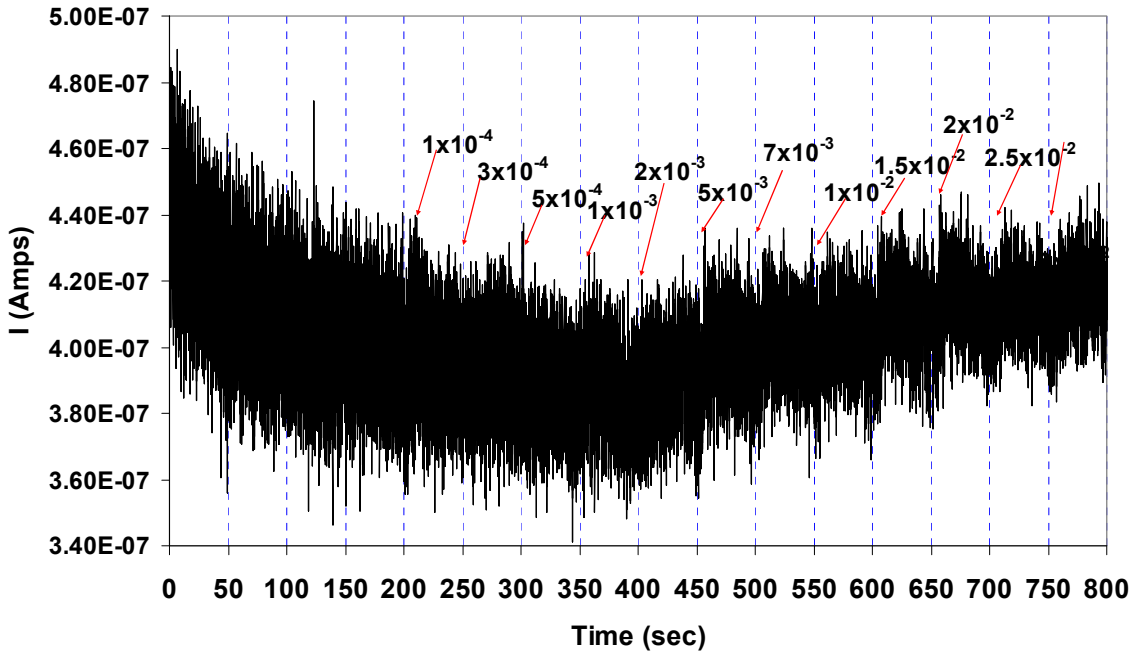

Figure 6.28 Chrono-Amperommetry for PEDOT-GLOD 10 minute biosensors

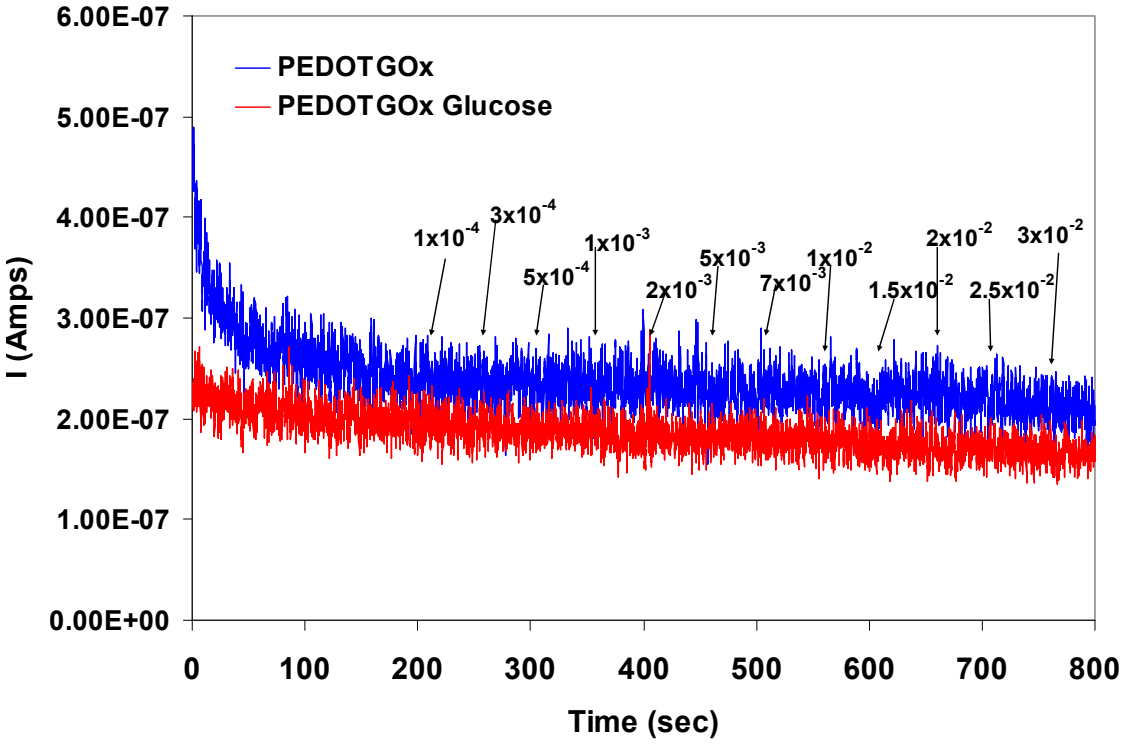

Figure 6.29 Chrono-Amperommetry for PEDOT-GOx 10 minutes (10 units/ml Glucose Oxidase) biosensors

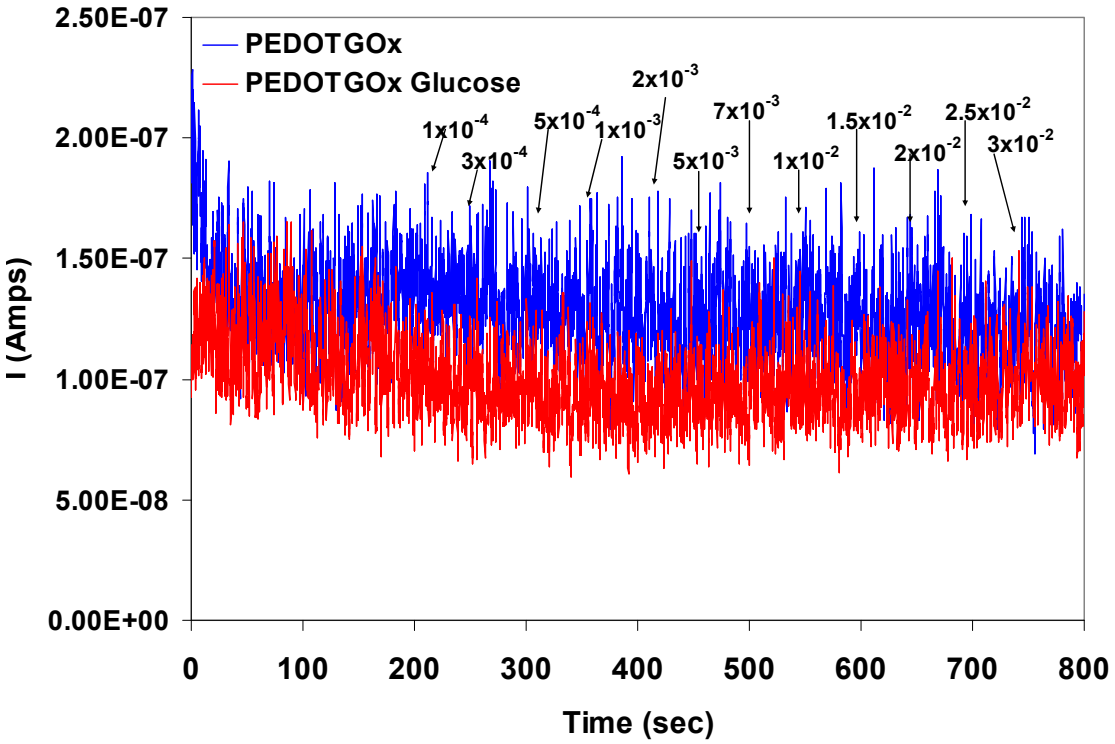

Figure 6.30 Chrono-Amperometry for PEDOT-GOx 10 minutes (40 units/ml Glucose Oxidase) biosensors

6.3.5.2 Chemical Immobilization of Glutamate Oxidase

Since physical entrapment of GLOD did not yield a functioning sensor, chemical immobilization was used to secure GLOD (via silane and lysine bonding)[23] to the surface of a Si wafer in order to test whether a functioning glutamate sensor could be fabricated in this manner. XPS was used to determine whether the enzyme was immobilized and then chrono-amperometry was used to test sensing ability.

6.3.5.2.1 Chemical analysis

The samples analyzed consisted of one sample of Si wafer with silane (step 1), one sample of Si wafer with silane and glutaraldehyde (step 2), and three samples of Si wafer with silane and glutaraldehyde and GLOD (step 3).[23] Two spots, denoted a and b, were taken on each sample, but only one spot was shown for simplicity.

Figures 6.31 display the XPS data for the C 1s, N 1s, and Si 2p characteristic regions respectively. The appearance of C=O (~288 eV) in Figure 6.31a, which was present only in the enzyme samples, suggests that GLOD did chemically immobilize on the surface. This was further suggested with the significant presence of nitrogen for the enzyme samples (Figure 6.31b) and the reduction of Si 2p signal indicating some sort of surface coverage in Figure 6.31c.

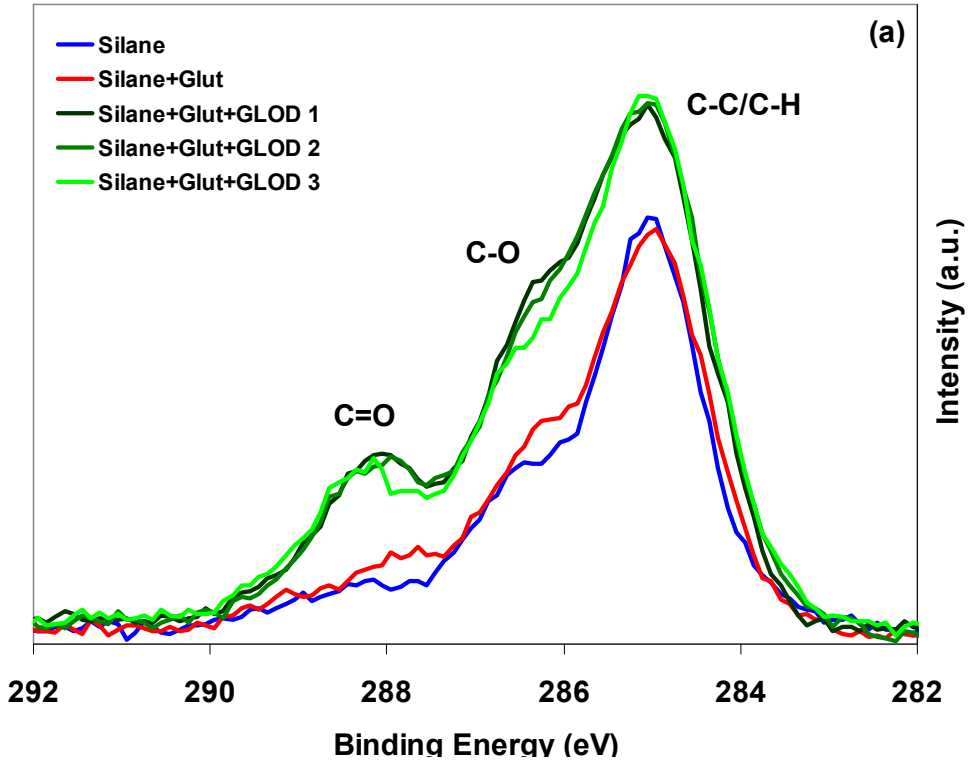
(a)
Silane
Silane+Glut
Silane+Glut+GLOD 1
Silane+Glut+GLOD 2
Silane+Glut+GLOD 3
C-C/C-H
C-O
C=O
Intensity (a.u.)
292
290
288
286
284
282
Binding Energy (eV)

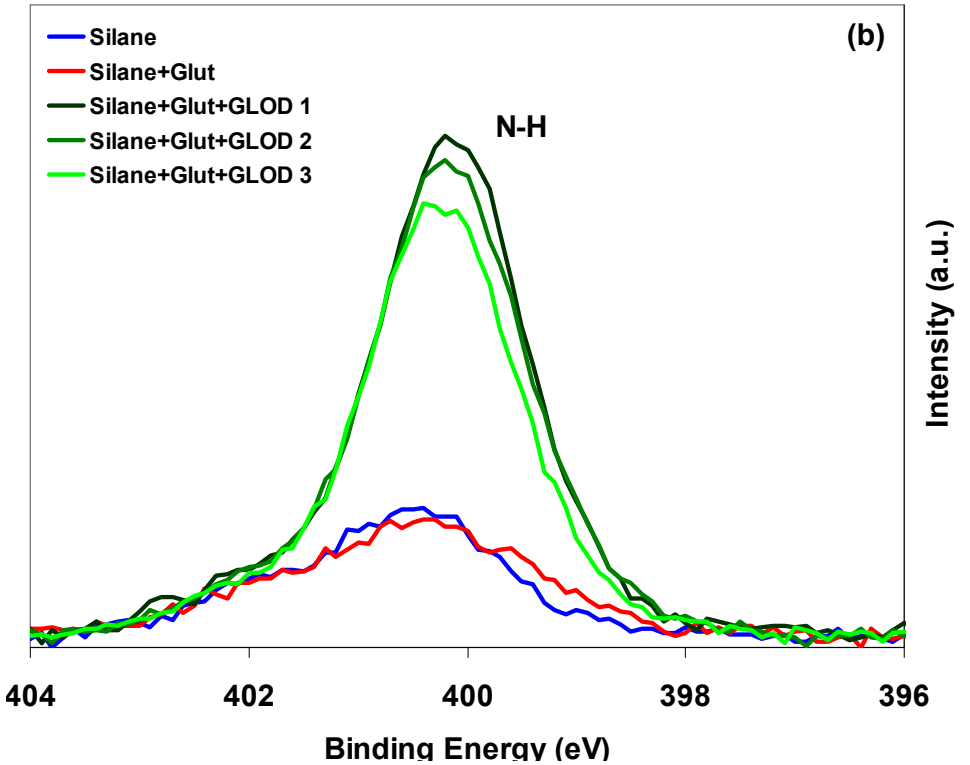
(b)
Silane
Silane+Glut
Silane+Glut+GLOD 1
Silane+Glut+GLOD 2
Silane+Glut+GLOD 3
N-H
Intensity (a.u.)
404
402
400
398
396
Binding Energy (eV)

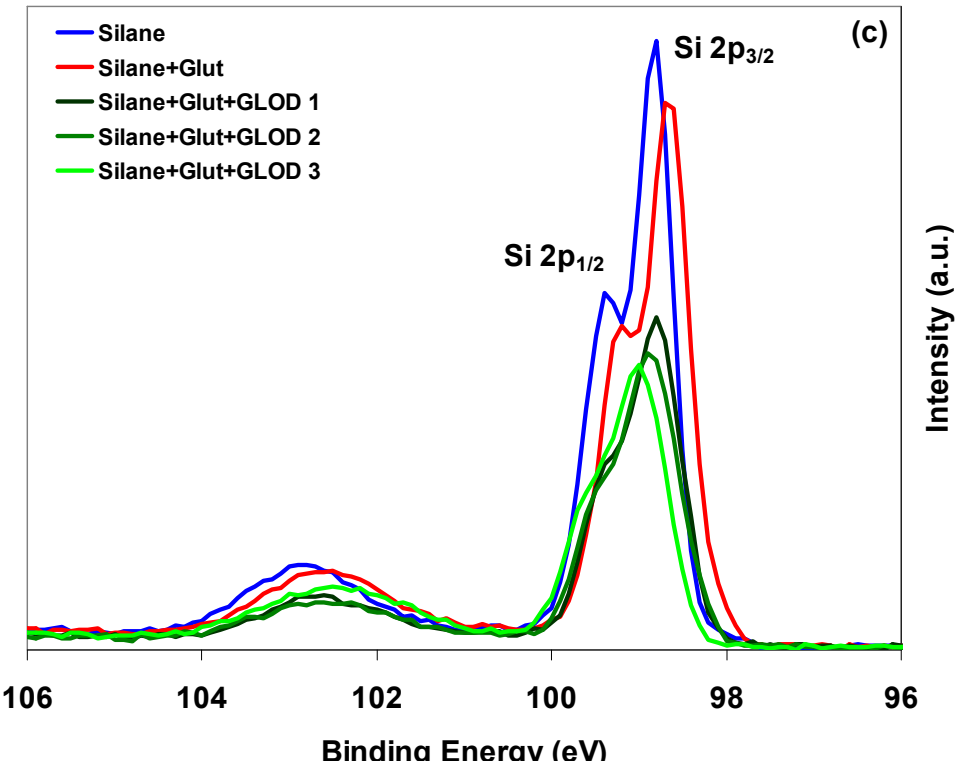

Figure 6.31 (a) C 1s, (b) N 1s, and (c) Si 2p characteristic regions for chemically immobilized GLOD

6.3.5.2.3 Sensitivity

A different batch of samples from the XPS samples were prepared for chrono-amperometry testing. The chemical immobilization process used was the same as that for the XPS samples. The experimental chrono-amperometry parameters used were the same as for the glucose oxidase based sensors (0.7V potential, PBS + ferrocene bath, glutamate additions every 50 seconds starting at ~200 seconds).

Figures 6.32 is an example of a chemically immobilized glutamate oxidase sensors. The lack of a step like response or even any kind of response indicates no

sensing was present. The jumps in the curves represent the pipette tip touching the liquid surface, the bath being disturbed, and/or Autolab instability.

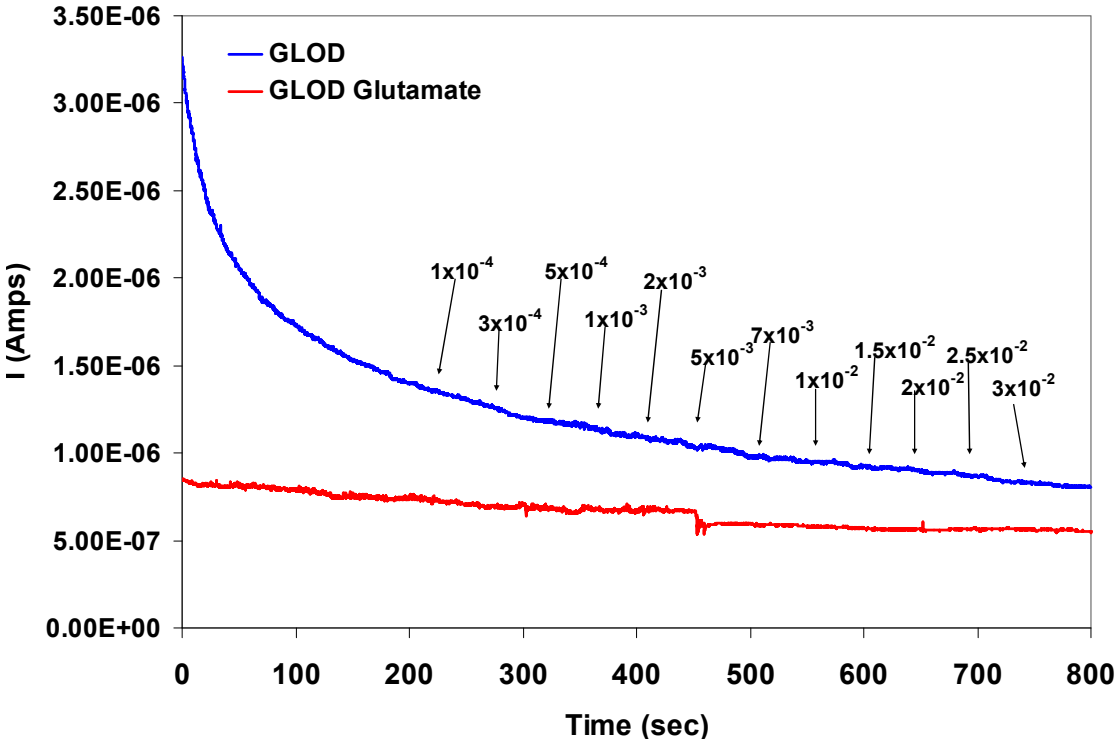

Figure 6.32 Chrono-Amperometry data for chemically immobilized GLOD sensor

6.4 Conclusions

Functional PEDOT-based glucose biosensors were fabricated using physical immobilization of the enzyme glucose oxidase within a PEDOT counter-ion matrix. These biosensors were fabricated using either PSS or heparin as the counter-ion. Enzyme entrapment was verified using X-ray photoelectron spectroscopy. The electrical properties of the resulting film were found to be very similar to those of PEDOT-PSS. The minimum glucose concentration that was detected for both PEDOT-PSS and PEDOT-Heparin counter-ion based sensors was found to be ~$5x10^{-4}$ M using chrono-

amperometry. Preliminary PEDOT-PSS biosensor life time results suggest that the films have the ability to sense up to 8 days and that storage does not affect the films up to 31 days. The primary failure mechanism appears to be the physical removal of the film from the substrate.

Further enzyme entrapment was also proven with LDH, Tyrosinase, and chemically immobilized GLOD, but biosensor functionality could not be proven at this time. Electrical characterization results of the LDH sensors were found to be very similar to PEDOT-PSS films. The impedance and cyclic voltammetry data for PEDOT-Tyrosinase biosensors were found to follow the ITO substrate trends. This was likely caused by a non-homogenous film coverage. As for GLOD based biosensors, the impedance data and cyclic voltammery data suggests the presence of a film after electrochemical polymerization, but at this time GLOD sensing can not be proven.

6.5 References

1. Heller, A. *J. Phys. Chem.* **1992**, *96*, 3579.

2. Barisci, J.N.; Hughes, D.; Minett, A.;G.G. Wallace, G.G. *Anal. Chim. Acta* **1998**, *371*, 39.

3.Gooding, J.J.; Wasiowych, C.; Barnett, D.; Hibbert, D.B.; Barisci, J.N.; Wallace, G.G. *Biosens. Bioelectron.* **2004**, *20*, 260.

4. Minett, A.I.; Barisci, J.N.; Wallace, G.G. *Anal. Chim. Acta* **2003**, *475*, 37.

5. Adeloju, S.B.; Barisci, J.N.; Wallace, G.G. *Anal. Chim. Acta* **1996**, *332*, 145.

6. Morrin, A.; Ngamna, O.; Killard, A.J.; Moulton, S.E.; Smyth, M.R.; Wallace,G.G. *Electroanalysis* **2005**, *17*, 423.

7. Campbell, T.E.; Hodgson, A.J.; Wallace, G.G. *Electroanalysis* **1999**, *11*, 215.

8. Foulds, N.C.; Lowe, C.R. *J. Chem. Soc., Faraday Transactions 1* **1986**, *82*, 1259.

9. Kros, A.; Sommerdijk, N.A.J.M.; Nolte, R.J.M. *Sens. Actuators B* **2005**, *106*, 289.

10. Lewis, T.W.; Wallace, G.G.; Smyth, M.R.. *Analyst* **1999**, *124*, 213.

11. Wallace, G.G.; Smyth, M.; Zhao, H. *Trends Anal. Chem.* **1999**, *18***,** 245.

12. Yamato, H.; Ohwa, M.; Wernet, W. *J. Electroanal. Chem.* **1995**, *397***,** 163.

13. Fabiano, S.; Minh, C.T.; Piro, B.; Dang, L.A.; Pham, M.C.; Vittori, O. *Mater. Sci. Eng., C* **2002**, *21*, 61.

14. Kros, A.; van Hövell, S.W.F.M.; Sommerdijk, N.A.J.M.; Nolte, R.J.M. *Adv. Mater.* **2001**, *13*, 1555.

15. Nien, P.C.; Tung, T.S.; Ho, K.C. *Electroanalysis* **2006**, *18*, 1408.

16. Piro, B.; Dang, L.A.; Pham, M.C.; Fabiano, S.; Minh, C.T. *J. Electroanal. Chem.* **2001**, *512*, 101.

17. Setti, L.; Fraleoni-Morgera, A.; Ballarin, B.; Filippini, A.; Frascaro, D.; Piana, C. *Biosens. Bioelectron.* **2005**, *20*, 2019.

18. Bard, A.J.; Faulkner, L.R. *Electrochemical Methods: Fundamentals and Applications*. 2nd Ed. John Wiley & Sons: New York, 2001.

19. Spanninga, S.A.; Martin, D.C.; Chen, Z. *J. Phys. Chem. C* **2009**, *113*, 5585.

20. Curulli, A; Cusma, A.; Kaciulis, S.; Padeletti, G.; Pandolfi, L.; Valentini, F.; Viticoli, M. *Surf. Int. Anal.* **2006**, *38*, 478.

21. Garrett, R.H.; Grisham, C.M. *Biochemistry*. 2nd Ed. Harcourt College Publishers: New York, 1999.

22. Chaubey, A.; Pande, K.K.; Singh, V.S.; Malhotra, B.D. *Anal. Chim. Acta* **2000**, *407*, 97.

23. Liu, X.; Tan, W. *Mikrochim. Acta* **1999**, *131*, 129.

24. Manesh, K.M.; Santhosh, P.; Gopalan, A.; Lee, K.P. *Talanta* **2008**, *75*, 1307.

25. Moiroux, J.; Elving, P.J. *Anal. Chem*. **1978**, *50*, 1056.

26. Balamurugan, A.; Chen, S.M. *Sens. Actuators B* **2008**, *129*, 850.

27. Barzegar, A.; Moosavi-Movahedi, A.A.; Ganjali, M.R. *J. Appl. Electrochem*. **2009**, *39*, 1111.

28. Vansantha, V.S.; Chen, S.M. *Electrochim. Acta* **2006**, *52*, 665.

29. Marciniak, S.; Crispin, X.; Uvdal, K.; Trzcinski, M.; Birgerson, J.; Groenendaal, L.; Louwet, F.; Salaneck, W.R. *Synth. Met.* **2004**, *141*, 67.

30. Liu, X.; Zhang, Z.; Cheng, G.; Dong, S. *Electroanalysis* **2003**, *15*, 103.

31. Robinson, G.M; Iwuoha, E.I.; Smyth, M.R. *Electrochim. Acta* **1998**, *43*, 3489.

CHAPTER 7

CONCLUSIONS

7.1 Conclusions

The first part of this study utilized sum frequency generation vibrational spectroscopy to determine the orientation of the phenyl ring in the commercially available form of PEDOT:PSS (Baytron P). For the para-substituted PSSNa phenyl ring, the tilt and twist angles were found to be 46° ± 2° and 57° ± 4° respectively. The Baytron P tilt and twist angles were found to be 47° ± 2° and 64° ± 3° respectively. The similarity between PSSNa and the PSSNa in Baytron P in both the tilt and twist angles was to be expected because a significant portion of the signal likely resulted from the excess PSSNa (1 PEDOT: 2.5 PSSNa) present in Baytron P. The minor differences between PSSNa and Baytron P twist angle values could be attributed to the fact that some of PSSNa in Baytron P acts as the counter-ion to PEDOT, affecting the phenyl ring orientation.

The second research section focused on the chemical composition of PEDOT with various counter-ions. X-ray photoelectron spectroscopy(XPS) was used to determine the film's chemical composition. The XPS work began with a comparison between Baytron P and electrochemically polymerized form of PEDOT-PSS. Previous studies had suggested that the electrochemically polymerized version of PEDOT-PSS has a greater relative amount of PEDOT present than in Baytron P. This was confirmed by the greater

quantities of C-O-C bonding in both the C 1s and O 1s regions coupled with the stronger PEDOT sulfur doublet in comparison to the SO_3 doublet found in the S 2p spectra.

Preliminary results from poly-anionic versus small anion counter-ion mixtures study yielded PEDOT had an increased affinity for PSS than small anions. PSS was more likely to act as a counter-ion for PEDOT due to its poly-anionic nature. Since once poly-anionic chain is attached to one site, the PSS can then quench the rest of the $PEDOT^+$ sites resulting in blocking the smaller anionic ClO_4^- and Cl^- from quenching PEDOT. This has been confirmed by a control experiment substituting TosNa for PSS in the mixture to study counter-ion incorporation. The TosNa did not act as the counter-ion in all the mixture cases suggesting that the reason for the PSS acting as the counter-ion was due to the polymeric nature of PSS and not the SO_3^- group solely. In contrast to ClO_4^- and Cl^-, bromide anions were found to act as PEDOT counter-ions even in the presence of the polymeric anions PSS and PAA.

The XPS study then moved onto mixtures composed of small anions and the driving force for PEDOT counter-ion incorporation. Phosphate buffer solution was first investigated due to its importance for future biological applications. XPS results indicate that the primary PBS counter-ion anion source was from the NaCl during PEDOT electrochemical polymerization.

To obtain a more completed picture regarding PEDOT counter-ion incorporation, several other anion mixtures were investigated in regards to the counter-ion charge, anionic hydration, and number of anions in a mixture. The PEDOT counter-ion affinity for anions with the same charge was first tested. The overall qualitative PEDOT counter-ion affinity for monovalent anions was: ClO_4^-, Br^- over smaller Cl^-, Tos^-, and COO^-

(acetate), with no phosphate or NO_3^- contributions. As for divalent anions, $S_2O_3^{2-}$ dominated over both carbonate and phosphate anions. The trends found in counter-ion affinity did loosely follow the general trend for anionic hydration suggested by the Hofmeister series.

Anionic hydration was then systematically tested. A series of anion mixtures varying from one to nine anions by gradually adding one more anion at a time from most highly to most weakly hydrated was examined. Thiosulfate was found to be dominant over all other anions acting as a PEDOT counter-ion, indicating that PEDOT counter-ion incorporation did not precisely follow the anionic hydration seen in the Hofmeister Series. Thus anionic hydration was not found to be the sole driving force for PEDOT counter-ion incorporation. For every mixture that it was present in, the thiosulfate was found to be the dominant PEDOT counter-ion incorporated regardless of the anionic charge, cation, or anionic hydration in the mixture study.

Different mixtures with two, three, four, and five anions were investigated to characterize the PEDOT counter-ion affinity in each mixture. In the absence of the thiosulfate, $C_6H_5O_7^{3-}$, Br^-, and ClO_4^- were found to act as major counter-ions. Phosphate and nitrate anions were not found to act as PEDOT counter-ions in many circumstances. Since nitrate is weakly hydrated, the expected results would be that nitrate has a similar dominance to that of bromide and perchlorate, but since this result did not occur, another driving force must also be occurring. It is obvious that the number of anions in solution also affect PEDOT counter-ion affinity indicating possible ion-ion interactions in the solution. The general PEDOT counter-ion affinity trend is (from strongest to weakest): $S_2O_3^{2-} > COO^-$ (citrate), Br^-, $ClO_4^- > Cl^-$, COO^- (acetate), CO_3^{2-}, NO_3^-, $H_2PO_4^-/HPO_4^{2-}$.

Fabrication of PEDOT-enzyme based biosensors was also completed in this research. Functional PEDOT-based glucose biosensors were fabricated using physical immobilization of the enzyme glucose oxidase within a PEDOT counter-ion matrix. These biosensors were fabricated using either PSS or heparin as the counter-ion. The impedance and CV properties were very similar to PEDOT-PSS. Enzyme entrapment was verified using XPS. The minimum glucose concentration that was detected for both PEDOT-PSS and PEDOT-Heparin counter-ion based sensors was found to be ~$5x10^{-4}$ M using chrono-amperometry. Preliminary PEDOT-PSS biosensor life time results suggest that the films have the ability to sense up to 8 days and that storage does not affect the films up to 31 days. The primary failure mechanism appears to be the physical delanmination of the film from the substrate.

Further enzyme entrapment was also proven with LDH, Tyrosinase, and chemically immobilized GLOD, but biosensor functionality could not be proven at this time. Electrical characterization results of the LDH sensors were found to be very similar to PEDOT-PSS films. The impedance and cyclic voltammetry data for PEDOT-Tyrosinase biosensors were found to follow the ITO substrate trends. This was likely caused by a non-homogenous film coverage. As for GLOD based biosensors, the impedance data and cyclic voltammery data suggests the presence of a film after electrochemical polymerization, but at this time GLOD sensing cannot be conclusively proven.

7.2 Future Work

In terms of the biosensor section, chemical immobilization of the glutamate oxidase using a non-prevalent amino acid so as to control the enzyme's deposition orientation should be tried. This should help to eliminate the enzyme's redox center being buried within the film and hopefully adhere the enzyme to the surface to prevent enzyme loss and thus failure. XPS imaging, for sample positioning, could also be used to obtain chemical information for the PEDOT-GLOD sensors. The LDH and Tyrosinase biosensors should be tried below the respective oxidation potentials of NADH and l-dopa to prevent signal overlap with the electrons given off by enzyme's redox center. First CV needs to be run for both NADH and l-dopa using an ITO electrode with an electrochemically grown PEDOT film to determine the exact oxidation potentials for NADH and l-dopa under these specific experimental conditions. Ultimately, PEDOT could be replaced with melanin to fabricate an even more biologically friendly biosensor.

For the XPS analysis, the valence data should be analyzed along with the impedance data already collected for PEDOT with single counter-ions to see whether there are any trends between ionic size and electrical conductivity. Since $S_2O_3^{2-}$ is so dominate, it would be interesting to see the affinity trend when compared to PSS or PAA. XPS imaging might be able to be used to see whether there are chemical compositional differences the PEDOT-Br films and the crystal structures growing within the films.

Further SFG analysis needs to be done to figure out the alpha helix and beta sheet orientation of GOx and LDH from the data already collected of enzyme solution in contact with PMMA, PS, and ~35% sulfonated PS. Successful SFG signal needs to be

collected from chemically immobilized enzymes in the hopes of comparing the physical absorption to the chemically immobilized enzyme's orientation.